CONJUGATED POLYMERS AND DESIGNED INTERFACES: CONFORMATIONAL ANALYSIS AND APPLICATIONS

by

Byungjin Koo

B.S., Materials Science and Engineering, *summa cum laude*
Seoul National University, 2012

Submitted to the Department of Materials Science and Engineering
in Partial Fulfillment of the Requirements for the Degree of

DOCTOR OF PHILOSOPHY IN MATERIALS SCIENCE AND ENGINEERING
at the
MASSACHUSETTS INSTITUTE OF TECHNOLOGY

June 2017

Signature of Author: _____
Department of Materials Science and Engineering
May 10, 2017

Certified by: _____
Timothy M. Swager
John D. MacArthur Professor of Chemistry
Thesis Supervisor

Certified by: _____
Michael F. Rubner
TDK Professor of Polymer Materials Science and Engineering
Thesis Reader

Accepted by: _____
Donald R. Sadoway
John F. Elliott Professor of Materials Chemistry
Chairman, Departmental Committee on Graduate Studies

Dedicated to My Loving Family:

Kyungsool, Chaesoon, and Hyunjoo

CONJUGATED POLYMERS AND DESIGNED INTERFACES: CONFORMATIONAL ANALYSIS AND APPLICATIONS

by

Byungjin Koo

Submitted to the Department of Materials Science and Engineering on May 10, 2017
in Partial Fulfillment of the Requirements for the Degree of
Doctor of Philosophy in Materials Science and Engineering

ABSTRACT

The conformations of conjugated polymers can be altered by nearby environments. The intrapolymer conformation and interpolymer assemblies have a crucial impact on a variety of properties such as absorption, energy migration, and fluorescence. In this dissertation, the conformational changes and their effects on photophysics in different environments will be discussed. In Chapter 1, the basic principles to understand this thesis will be reviewed, including the processes of absorption and emission, exciton migration, the Langmuir–Blodgett technique, and interfacial phenomena. In Chapter 2, the conformational control and alignment of conjugated polymers at the air–water interface and how this alignment of polymers can lead to new emissive aggregates will be presented. The emission has the characteristics of excimers with the improved fluorescence quantum yields. The transfer of the aligned aggregates to glass substrates is attempted and these excimer films undergo reorganization upon exposure to solvent vapors, which triggers the fluorescence color change from yellow to cyan, leading to fluorescence-based chemical sensors. In Chapter 3, exciton migration to low-energy emissive traps at amphiphilic interfaces will be discussed. This chapter will deliver the design of interfaces and how the exciton migration can occur at the air–water interface and the hydrocarbon–water interface in lyotropic liquid crystals. To expand this interfacial exciton migration to more generalizable interfaces, Chapter 4 will show the fabrication of oil-in-water emulsions and how exciton migration in oil-in-water emulsion can produce distinct fluorescences between solution and interfaces. Chapter 5 will discuss the structural variations of novel functional conjugated polymers and how substituents can change the conformation of the polymer backbones. Additionally, how this conformational change affects the electronic and optical properties of polymers will be examined.

Thesis Supervisor: Timothy M. Swager
Title: John D. MacArthur Professor of Chemistry

Table of Contents

List of Figures

List of Schemes

List of Tables

Chapter 1

Introduction and Backgrounds

Abstract: This chapter will describe the concepts of photophysics, the chemistry and properties of poly(phenylene ethynylene)s (PPEs), energy transfer, and interfacial phenomena, all of which are central to understand this dissertation. Photophysics (absorption and emission) is an essential optical method to analyze the conformation and aggregation states of conjugated polymers. Fundamentals of vibrational transitions along with the Franck–Condon principles will be reviewed, which determines the shapes of absorption and emission spectra. The synthesis of PPEs with Sonogashira cross-couplings will be discussed. Exciton migration, a central topic of this dissertation, will be dealt based on the fundamental mechanisms, Förster and Dexter energy transfer. In the section of interfacial phenomena, pressure–area isotherms, micellization, and emulsion fabrication will be discussed.

1.1 Photophysics of π-Conjugated Polymers and Conformational Analysis

Photophysics deals with the interaction between light and matter (a molecule) with no structural change of a molecule, as opposed to photochemistry which results in the change of a chemical structure.[1] Photophysics commonly refers to the process of absorption and emission of light in a molecule. The absorption of light causes an electron to be excited, called excitation where an electron is transferred from its ground-state (low-energy) to excited-state (high-energy). This process can be described in the following equation.

$$A + h\nu \rightarrow A^*$$

where A and A* represent a molecule in a ground-state and an excited-state, respectively. Figure 1.1 shows the singlet ground state (S_0) and singlet first-excited state (S_1) with the vibrational energy levels ν, assuming there are only three vibrational states. The excitation of an electron starts from the S_0 ($\nu = 0$), and the transitions from S_0 ($\nu = 0$) to different vibrational states in S_1 ($\nu = 0, 1, 2$) are possible. These transitions are indicated as 0–0, 0–1, 0–2 absorption transitions, respectively (Figure 1.1).

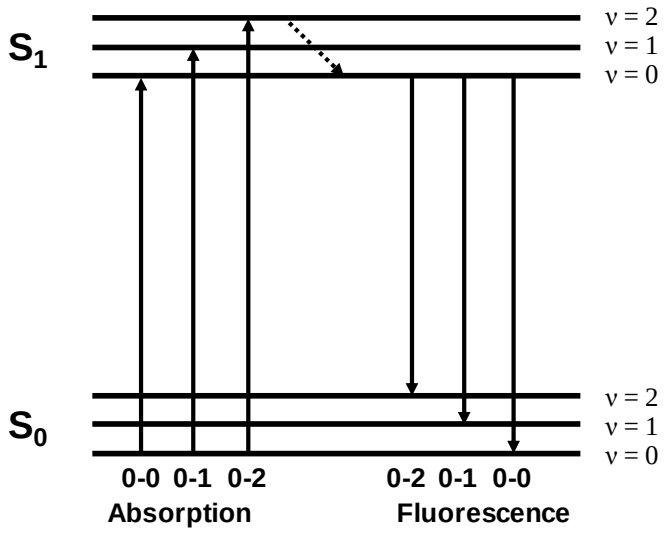

Figure 1.1. Absorption and fluorescence with different vibrational transitions.

The probability of relative vibrational transitions are determined by the Franck–Condon principle. The principle states that during the radiative transition of an electron, nuclei do not change their positions and geometry. From the classical mechanics point of view, nuclei are much heavier than electrons, so the nucleus vibrations take 10^{-13} – 10^{-14} s, whereas the electron vibrations take 10^{-15} – 10^{-16} s. That is, at an instant time, excitation is only seen from electron, while nuclei are stationary. Quantum mechanically, the principle states that the most probable transition takes place between the closely resembling wave functions of the initial and final vibrational states.[2] When the potential energy curve of the exited-state is vertically placed from the one of the ground-state (Figure 1.2a), 0–0 transition is the Franck–Condon-allowed transition, whereas 0–2 transition is weak. The Franck–Condon principle states that the position of the potential curve cannot be moved horizontally since the nuclei are stationary during the transition. In the case where the excited-state structure is significantly different from the ground-state (Figure 1.2b), the potential energy curve of the excited-state is moved horizontally, meaning that from the diagram of Figure 1.2b, the most probable transition is 0–2, and the least is 0–0. In both cases, the expected absorption spectra are shown in Figure 1.2. The emission spectra are mirror images each other since once again, from the result of the Franck–Condon principle, if the 0–0 absorption is most probable, so is the 0–0 emission. So far, it is assumed the emission begins from the lowest excited-state (S_1, $\nu = 0$). This is generally true because the electron in the higher vibrational energies undergoes fast relaxation to the lowest excited-state energy level ($\nu = 0$), following the Kasha's rule (dotted arrow in Figure 1.1).[3] This relaxation is much faster than any other process such as intersystem crossing or fluorescence.

π-Conjugated molecules generally interact with light ranging from untraviolet (UV) and visible to near-infrared (NIR) and therefore have a variety of technological applications such as

solar cells,[4,5] luminescence materials,[6,7] and fluorescent chemical sensors.[8,9] The interaction with UV–NIR range of light takes place because the frontier molecular orbitals (HOMO, highest

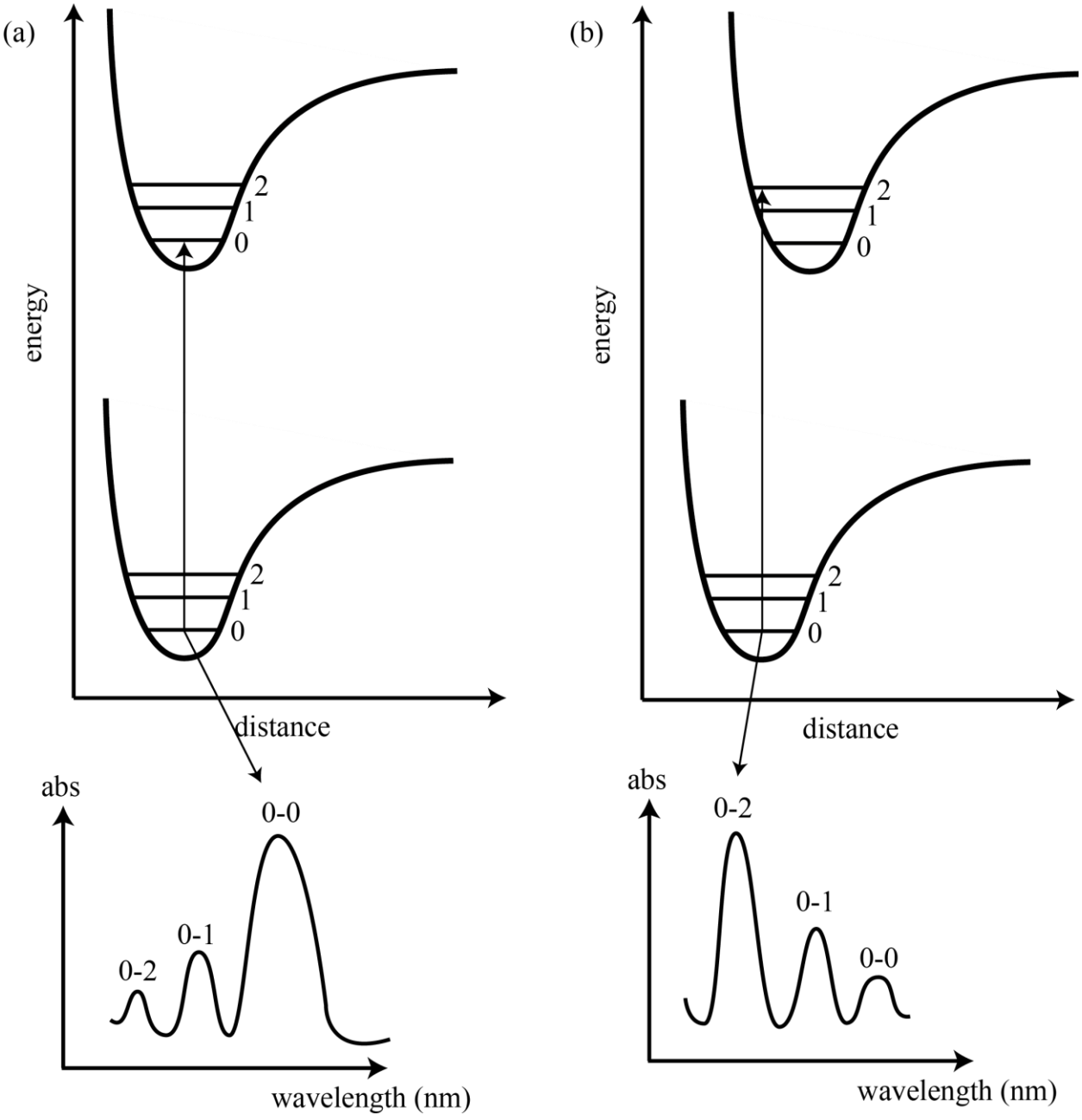

Figure 1.2. Potential energy curves where (a) ground-state and excited-state geometries are similar and (b) excited-state geometry is different from the ground-state geometry and thus horizontally shifted. The most probable Franck–Condon transition is (a) 0–0 and (b) 0–*n* (here 0–2). Expected absorption spectra are shown in the bottom. Fluorescence curves are expected to be mirror images of absorption spectra.

occupied molecular orbital, and LUMO, lowest unoccupied molecular orbital) of π-conjugated molecules have similar energy levels with UV, visible, and near-infrared light, in contrast to σ-molecular orbitals where the difference between boning and antibonding orbitals are higher as a result of their greater orbital overlap and stabilization compared to π-orbitals.

π-Conjugated polymers are a special type of π-conjugated molecules where (1) polymer backbone should be π-conjugated and (2) molecular weights are typically more than 3,000 Da. Changing chemical structures of polymers, molecular weights, and processing conditions (solution or solid-states) can alter photophysical properties of conjugated polymers. First, the changes of chemical structures include attaching electron-rich or electron-poor functional groups. More electrons that participate in π-conjugation leads to the decrease in HOMO–LUMO gap and red-shift of absorption and emission spectra. Donor–acceptor type conjugated polymers have also been increasingly investigated as low bandgap materials.[10-12] Second, molecular weights affect the conjugation length, and generally increasing molecular weights lead to the red-shift of absorption spectra. However, it is known that expanding the molecular weight infinitely does not necessarily result in the infinite red-shift of spectra. Effective conjugation length (ECL) is defined as the minimum length, typically expressed as n_{ECL} where n is the repeat unit, of aromatic bonds wherein optical and electronic properties are converged. That means that at a certain length the red-shift of absorption spectra would be saturated. The ECL even exists in a very high molecular weight polymer without any defects[13] and was reported in many different types of conjugated polymers including poly(phenylene vinylene)s (n_{ECL} = 11),[13] poly(phenylene ethynylene)s (n_{ECL} = 5),[13] poly(*p*-phenylene)s (n_{ECL} = 9),[13] polythiophenes (n_{ECL} = 17[13] or higher[14]), polypyrroles (n_{ECL} = 13),[13] polyfluorenes (n_{ECL} = 11),[15] and pentiptycene-drived oligo(*p*-phenylene ethynylene)s (n_{ECL} = 4.5).[16] Computational results also support the concept of ECL and the experimental results.[17]

Third, processing conditions alter photophysical properties. In solution with a sufficiently diluted concentration, polymers behave individually and possess relatively random conformations, whereas in thin films they are stretched and planarized, leading to the red-shift of optical properties. Interpolymer interactions and aggregations are possible in the solid-state. The absorption spectra in solution are usually broad, whereas the solid-state absorption generally shows more sharp spectra. This is because in solution a variety of random conformations or ensemble absorb all different wavelengths of light, as opposed to solid-state polymers which have limited conformations whose segments absorb narrow range of light.

A 2D plane can serve as the intermediate state between solution and thin films. When polymers are on the plane, if they are far apart, they may exist individually, but if they are close together, they may exist in a collective way. On a 2D plane, they are presumably slightly more stretched than solution because of spatial constraints, but not as much as the solid-state. We can think of a 2D planar interface as a platform to study the conformations and assemblies of conjugated polymers depending on the interpolymer distances, along with any changes in properties such as absorption and fluorescence.

In order to address conformation–photophysics relationships in conjugated polymers, we will utilize the Langmuir–Blodgett method where a planar 2D interface is given. A detailed review on the Langmuir–Blodgett technique was reported,[18] and a brief concept will be discussed in this Chapter and Chapter 1.4. Figure 1.3 shows the schematics and pictures of the Langmuir–Blodgett instrument. The instrument is composed of a trough that contains water and two bars that are placed on top of the trough. Two bars serve as compressing and expanding the surfactant monolayers (or multilayer). The aligned monolayers can be transferred to a substrate (either hydrophobic or

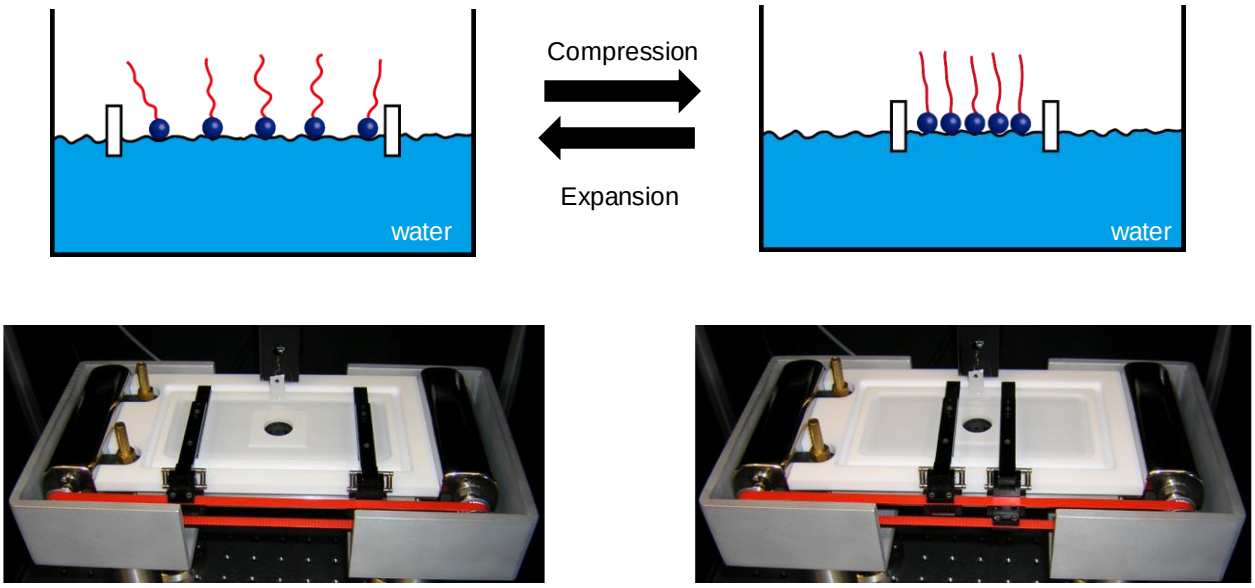

Figure 1.3. Schematic representation and pictures of the Langmuir–Blodgett instrument. Surfactants can be deposited on top of water and their intermolecular distance can be altered by compression and expansion of the two bars.

hydrophilic). Using this method, highly anisotropic films were previously fabricated for energy transfer studies.[19,20]

1.2 Poly(Phenylene Ethynylene)s

The most parts of my thesis are mainly using poly(phenylene ethynylene)s (PPEs) (Chapter 2–4), and thus the chemistry and properties of these polymers are introduced in this chapter. The details on PPEs are reviewed in the literature.[21] Polythiophenes (Chapter 5) are also utilized for new synthetic methodology and conformational studies, but the introductory statement on polythiophenes will be delivered in Chapter 5.1.

PPEs are synthesized by a Sonogashira cross-coupling reaction (Scheme 1.1) wherein a terminal acetylene and an aryl halide are coupled to form a C_{sp}–C_{sp2} bond in the presence of palladium (0), copper (I), and a base.[22] Palladium (II) can also be used, but should be reduced in

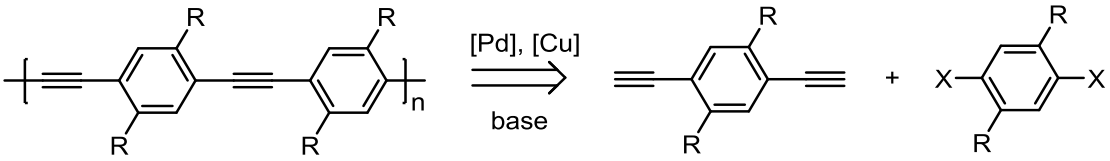

Scheme 1.1. Retrosynthetic analysis of PPEs.

the reaction. To make a polymer, diacetylene and dihalide monomers are employed with the reaction temperature around 50–70 °C. Hence, the polymerization is an AA and BB type polycondensation reaction and thus follow step–growth polymerization kinetics. $Pd(PPh_3)_4$ (Pd(0)) or $Pd(PPh_3)_2Cl_2$ (Pd(II)) are commonly used, but the latter one should be reduced to Pd(0) for an oxidative addition reaction. CuI (I) is used for the copper (I) source, and the amine bases such as

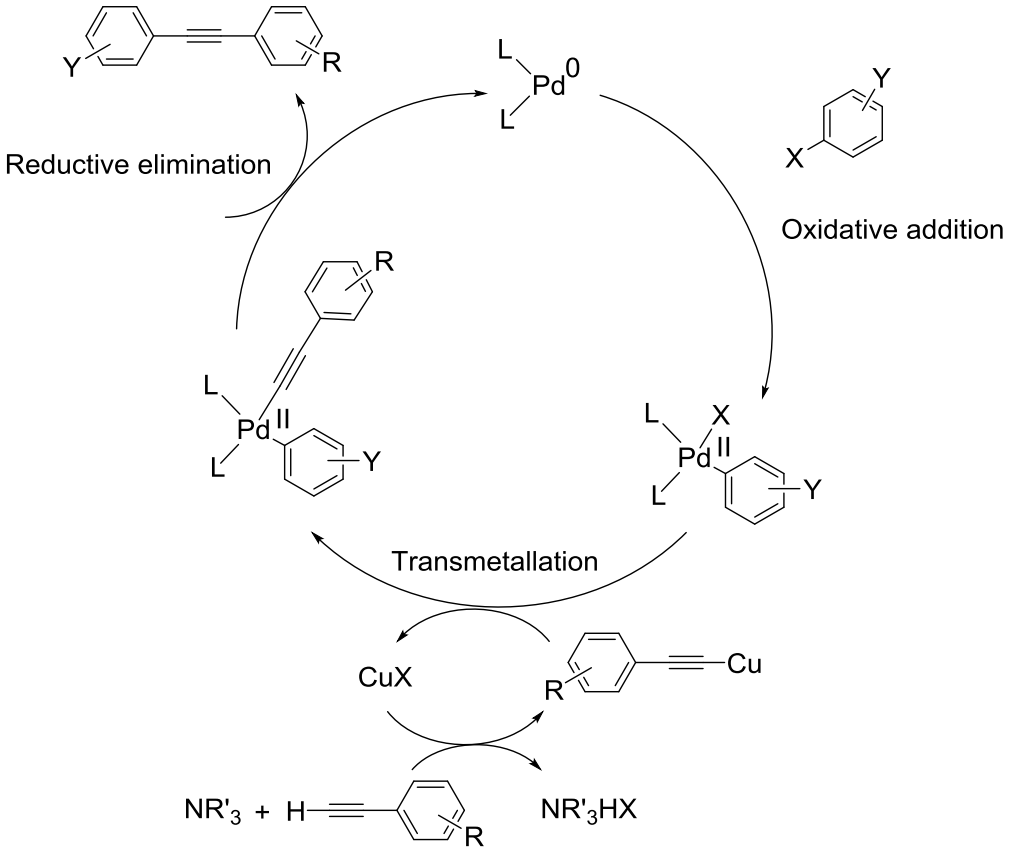

Scheme 1.2. Catalytic cycle of the Sonogashira cross-coupling reaction.

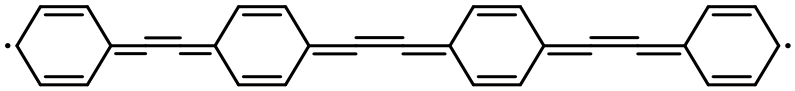

Scheme 1.3. Excited-state structure of the PPE repeat unit.

triethylamine or diisopropylamine are used. The catalytic cycle is shown in Scheme 1.2. The first step is the oxidative addition of aryl halide (aryl iodide or aryl bromide is common) to Pd(0), which is oxidized to Pd(II). Then transmetallation with a Cu(I)-acetylene, which is made from a terminal alkyne, CuI, and a base, takes place, followed by the reductive elimination of Pd(II) to Pd(0), releasing the coupling product.

PPEs are highly fluorescent polymers and have been utilized as fluorescence indicators.[8] The fluorescence quantum yields are around 50% in most cases and up to unity.[21] The high quantum yields would be related to their highly rigid excited-state structure, which is butatriene-like planar structure (Scheme 1.3).[23] This means that in the excited-state electrons undergo less nonradiative pathways such as phonon vibrations. Another factor that makes PPEs as promising fluorescence markers is their signature cyan emission (460 – 480 nm) wherein the lowest perception concentration by human eyes is 0.1 μg/ml $CHCl_3$.[23] Therefore, their fluorescence is sensitive to human eyes.

One interesting feature that makes PPEs as sensory materials is that the rotational barrier of C_{sp}–C_{sp2} between acetylene and phenyl group (red in Scheme 1.4) is weak and thus sensitive to

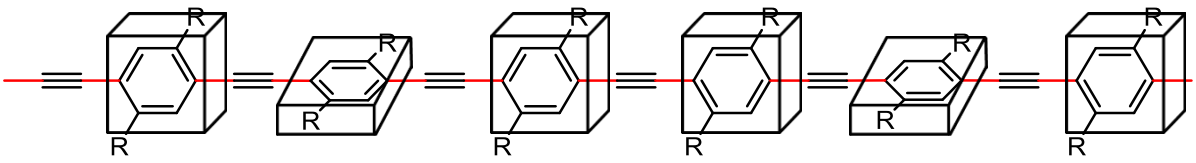

Scheme 1.4. Conformation of PPEs. The rotational barrier of the red bond is low (< 1 kcal/mol), suggesting that they could be responsive to environmental stimuli.

environmental stimuli. The barrier is less than 1 kcal/mol,[24,25] indicating that at room temperature about 20% of the bonds are freely-rotating (consider the Boltzmann factor exp(-E/kT)). Therefore, environmental stimuli could facilitate conformational changes. Since the absorption and emission are dependent on the effective conjugation lengths as discussed in Chapter 1.1, their photophysics can be varied depending on whether they are in a highly stretched conformation (red-shift) or random conformation (blue-shift), which can be triggered from the stimuli. This also changes the exciton migrations to low-energy traps, which will be discussed in the next section.

1.3 Energy Transfer

Energy transfer, or exciton migration, is the diffusion of an exciton (excited electron/hole pair) to low-energy sites. Conjugated polymers undergo facile energy transfer in the presence of low-energy traps.[26] Our group has exploited this strategy to produce signal-amplified chemical sensors.[27-29] Herein the mechanism of energy transfer will be reviewed and how this can be related to the photophysics of conjugated polymers.

Two mechanisms[30] explain energy transfer as shown in Figure 1.4. Förster[31] energy transfer takes place between two weakly interacting dipoles, or called a dipole–dipole interaction. This happens through space and thus it is not necessary to have the direct orbital overlap which is significant in the Dexter energy transfer. Furthermore, Förster transfer operates in a relatively long-range (up to 100 Å). The transfer rate k_{ET} is shown as follows.

$$k_{ET} = \frac{\kappa^2 J \times 8.8 \times 10^{-28}\, mol}{n^4 \tau_0 {R_{DA}}^6}$$

where n is the refractive index of the medium, τ_0 is the donor lifetime, R_{DA} is the distance between the donor and the acceptor, and J is the spectral overlap between the donor emission and the

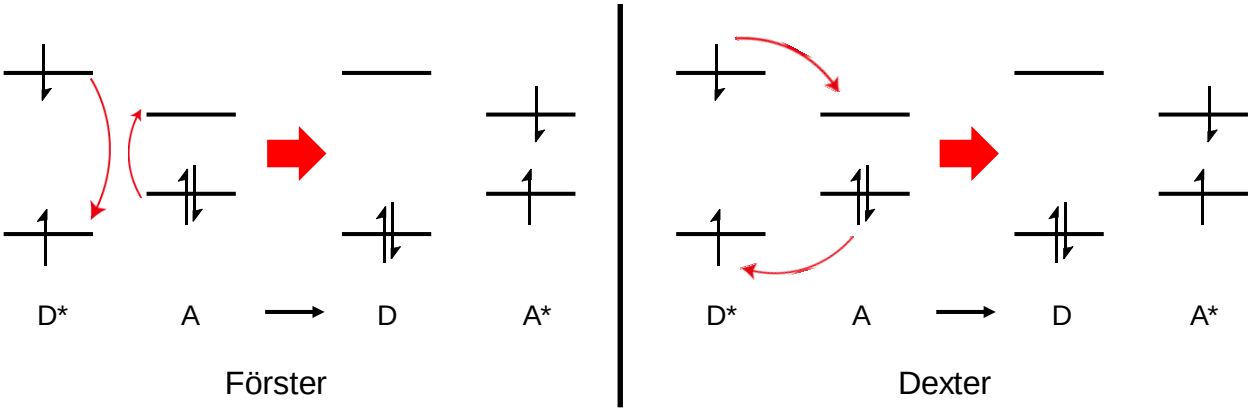

Figure 1.4. Two energy transfer mechanisms.

Figure 1.5. Examples of the orientation factor in Förster energy transfer. A head-to-tail type alignment (left) shows the highest orientation value, whereas an orthogonal alignment (right) produces the zero value.

acceptor absorption. The orientation factor κ is related to the relative orientation of transition dipoles. Figure 1.5 shows the examples of the orientation factor wherein the maximum value is observed in a head-to-tail alignment of the donor and acceptor dipoles.

Dexter energy transfer[32] is referred as electron–exchange as shown in Figure 1.4. Direct wavefunction overlap is a necessary condition for the Dexter transfer and therefore the donor and acceptor should be in closer proximity than Förster energy transfer. In this sense, it occurs when dipoles are strongly coupled usually within the distance of 10 Å. The rate of Dexter transfer is shown as follows.

$$k_{ET} = \frac{KJ}{Exp\,(\frac{2R_{DA}}{L})}$$

where K is the specific orbital interactions and L is the van der Waals radii between the donor and the acceptor. The exponential relationship between the rate and the distance demonstrates that Dexter energy transfer is indeed highly effective when they are very close each other.

Energy transfer in conjugated polymers is facilitated when the interpolymer distance is small. That means in solution where polymer chain exists individually, energy transfer is not facile. In thin films, however, higher energy transfer to low-energy sites is observed. This may results from the combination of Dexter (improved π-orbital overlap from planarization) and Förster energy transfer. In addition, in the solid-states exciton hoppings can happen through 3-dimension, whereas in solution it could happen along intrapolymer chain (1-dimension), which indicates that the solid-states may provide improved statistical movement of excitons (a shortcut for excitons). It is believed that energy transfer is usually facile in the solid-states, which is an important point to understand the phenomena discussed in this thesis.

1.4 Phenomena at Interfaces

Hydrophobic–hydrophilic interfaces play a pivotal role in many scientific and technological systems such as colloids and membranes. Colloids are metastable dispersion of one phase in a continuous phase and have significance in from medicine and food to petroleum recovery. Membranes are the materials that separate two phases and are central components especially in biology where protein activities and essential cell signaling can occur. From thermodynamic point of view, these interfaces have excess (Gibbs) free energy because two phases with the disparate nature meet each other.[33] Surfactants are the surface-active components that stabilize these interfaces. In this Chapter 1.4, three interface systems (air–water interface, micellization, and oil-in-water emulsions) and their preparation, thermodynamics, and applications

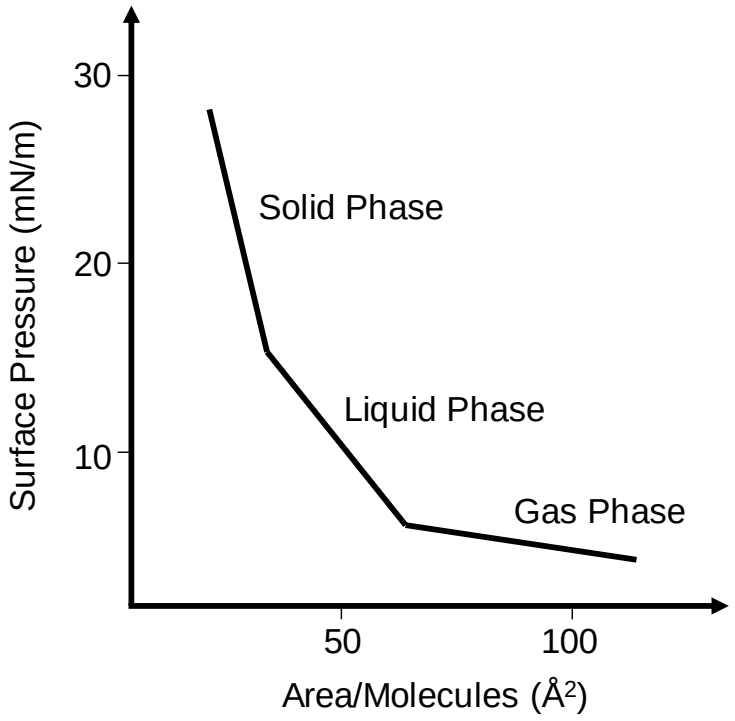

Figure 1.6. Example of pressure–area isotherm. The numbers on *x*- and *y*-axis are arbitrary but represent the order-of-magnitude in ordinary measurements.

are briefly discussed. Surfactant-type conjugated polymers and their applications in these interfaces are the main subjects of the Chapter 2, 3, and 4.

Langmuir–Blodgett provides a 2D planar interface (air–water interface) and the operation principle is introduced in Chapter 1.1 with Figure 1.3. The development and applications of Langmuir–Blodgett was reviewed recently.[18] In this chapter, the concept of pressure–area isotherm will be discussed and how that related to the conformation of simple surfactants, which can also be extended to polymer cases. Pressure–area isotherms are recorded during the compression and expansion cycles and exhibit how the effective interfacial tension is varied depending on the intermolecular distances. An example pressure–area isotherm is shown in Figure 1.6. It is often misleading that the *y* axis indicates the absolute surface tension. However, the values of *y*-axis are

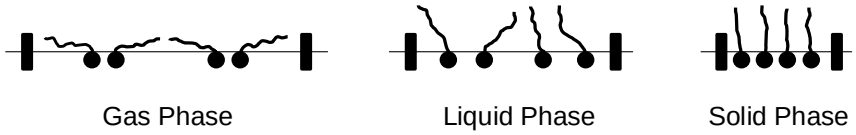

Figure 1.7. Conformation of surfactants in each phase in Langmuir monolayers.

obtained by subtracting 72.8 mN/m (surface tension of water) from the absolute surface pressure, which is also given as follows.

$$\text{absolute surface pressure} = 72.8 - \text{y}$$

Therefore, the increase of the *y*-axis value does not mean that absolute surface tension between water and air is increasing; rather, absolute surface tension is decreasing because the surfactant density is increasing and serves as stronger stabilizing agents. The values of *x*-axis are calculated by dividing the actual area by the number of molecules added.

Pressure–area isotherms are generally divided three regions for simple surfactant molecules (such as stearic acid), which are a gas phase, a liquid phase, and a solid phase.[34] The molecular snapshot in each phase is given in Figure 1.7. In a gaseous phase, the area per molecules is large and the tail of a surfactant does not interact one another, and therefore it has random conformations. Since they do not interact, a two dimensional ideal gas law holds, which is $\pi A = kT$ where surface pressure (π) is approaching to zero and thus the area (A) becomes infinite. When surfactants are compressed, it enters into a liquid phase. For stearic acids, this transition occurs around 24 $Å^2$.[34] The alkyl chain of the surfactant is now interacting and the absolute value of the slope is increased (steeper). Further compression leads to a solid phase (20 $Å^2$ for stearic acid)[34] and the tail becomes closely packed and highly anisotropic.

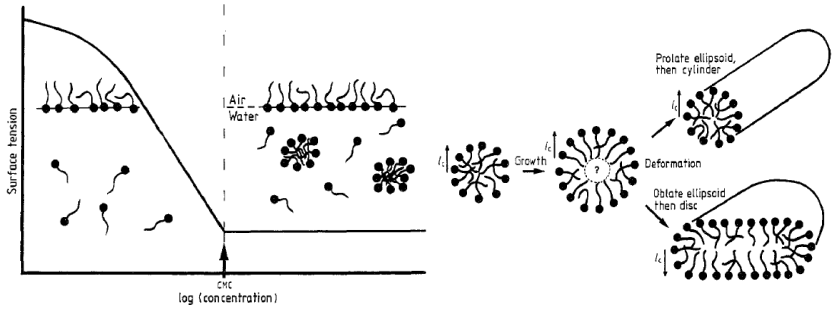

Figure 1.8. Schematic of micellization processes (Reference 35).

Micellization can also provide an interface between hydrocarbon and water. Micelles are a type of surfactant aggregates in water which can be generated above critical micellar concentration (CMC). Figure 1.8 indicates the micellization processes.[35] Surface tension becomes decrease as increasing the concentration of surfactants and will be saturated at CMC at which micelles begin to form. Micelles are initially spherical. However, the further addition of surfactants induce the transformation of micelles into rod or disk shapes, and the entire solution becomes anisotropic. This anisotropic solution is called lyotropic liquid crystals (LLCs, and further discussion in Chapter 3) and specific liquid crystalline textures can be observed in an optical microscope equipped with cross polarizers.

Emulsions are dispersion of two (or more) immiscible liquids where one phase is dispersed in a continuous phase in the presence of surfactants. Some review papers on microemulsion and nanoemulsions are reported.[36-39] Many different combinations can be possible, and herein the discussion is restricted to oil-in-water emulsions where oil is a dispersed phase (usually less than 10 vol%) and water is a continuous phase. Depending on the surfactants, the droplet sizes and numbers can be controlled. In order to stabilize the droplets, a stronger surfactant is necessary which is the difference between micelles (thermodynamically stable) and emulsions (microemulsions are thermodynamically stable but our focus is on macroemulsions which are

thermodynamically unstable but kinetically weakly stable). In Chapter 4 where conformation and exciton migration of conjugated polymers in emulsions are discussed, we will show a design principle to synthesize strongly hydrophilic surfactant-type conjugated polymers.

1.5 Objectives

The title of this thesis is "Conjugated Polymers and Designed Interfaces: Conformational Analysis and Applications". As it says, the primary purpose is to provide an understanding of how the conformations of conjugated polymers can be altered in interfaces (Chapter 2, 3, and 4) or structurally varied environments (Chapter 5), as well as how their photophysical outcome will be. Chapter 2 discusses the relative conformational changes of PPEs to the air–water surface, which results in the new emissive excimeric aggregates, referred as incline–stack conformation. It is observed that the exciton migration to the excimer bands occurs, and their application to solvent vapor sensing will be displayed. Chapter 3 exhibit the exciton migration at the air–water interface in the presence of low-energy emissive end-groups. Compared to Chapter 3 which uses 2D planar interface, Chapter 4 deals with the exciton migration in oil–water emulsions, which has curved, spherical interfaces. Conjugated polymers with stronger surface-active properties are required for emulsion fabrication. In contrast to Chapter 2–4, Chapter 5 discusses the functionalized polythiophenes with different substituents and how their conformations can be varied depending on the substituents. Novel postpolymerization modification methodology using lithium–bromine exchange reactions will be discussed.

1.6 References

(1) Anslyn, E. V.; Dougherty, D. A. *Modern Physical Organic Chemistry*; University Science Books: Sausalito, California, 2006.

(2) Turro, N. J.; Ramamurthy, V.; Scaiano, J. C. *Modern Molecular Photochemistry of Organic Molecules*; University Science Books: Sausalito, California, 2010.

(3) Kasha, M. *Discuss. Faraday. Soc.* **1950**, *9*, 14.

(4) Li, G.; Zhu, R.; Yang, Y. *Nat Photon* **2012**, *6*, 153.

(5) Günes, S.; Neugebauer, H.; Sariciftci, N. S. *Chem. Rev.* **2007**, *107*, 1324.

(6) Burroughes, J.; Bradley, D.; Brown, A.; Marks, R.; Mackay, K.; Friend, R.; Burns, P.; Holmes, A. *Nature* **1990**, *347*, 539.

(7) Friend, R. H.; Gymer, R. W.; Holmes, A. B.; Burroughes, J. H.; Marks, R. N.; Taliani, C.; Bradley, D. D. C.; Santos, D. A. D.; Bredas, J. L.; Logdlund, M.; Salaneck, W. R. *Nature* **1999**, *397*, 121.

(8) McQuade, D. T.; Pullen, A. E.; Swager, T. M. *Chem. Rev.* **2000**, *100*, 2537.

(9) Thomas, S. W.; Joly, G. D.; Swager, T. M. *Chem. Rev.* **2007**, *107*, 1339.

(10) Müllen, K.; Pisula, W. *J. Am. Chem. Soc* **2015**, *137*, 9503.

(11) Jenekhe, S. A.; Lu, L.; Alam, M. M. *Macromolecules* **2001**, *34*, 7315.

(12) Beaujuge, P. M.; Amb, C. M.; Reynolds, J. R. *Acc. Chem. Res.* **2010**, *43*, 1396.

(13) Meier, H.; Stalmach, U.; Kolshorn, H. *Acta Polym.* **1997**, *48*, 379.

(14) Izumi, T.; Kobashi, S.; Takimiya, K.; Aso, Y.; Otsubo, T. *J. Am. Chem. Soc.* **2003**, *125*, 5286.

(15) Klaerner, G.; Miller, R. *Macromolecules* **1998**, *31*, 2007.

(16) Yang, J. S.; Yan, J. L.; Lin, C. K.; Chen, C. Y.; Xie, Z. Y.; Chen, C. H. *Angew. Chem. Int. Ed.* **2009**, *48*, 9936.

(17) Ma, J.; Li, S.; Jiang, Y. *Macromolecules* **2002**, *35*, 1109.

(18) Ariga, K.; Yamauchi, Y.; Mori, T.; Hill, J. P. *Adv. Mater.* **2013**, *25*, 6477.

(19) Levitsky, I. A.; Kim, J.; Swager, T. M. *J. Am. Chem. Soc.* **1999**, *121*, 1466.

(20) Kim, J.; McQuade, D. T.; Rose, A.; Zhu, Z.; Swager, T. M. *J. Am. Chem. Soc.* **2001**, *123*, 11488.

(21) Bunz, U. H. F. *Chem. Rev.* **2000**, *100*, 1605.

(22) Chinchilla, R.; Najera, C. *Chem. Soc. Rev.* **2011**, *40*, 5084.

(23) Bunz, U. H. In *Conjugated Polymers: Theory, Synthesis, Properties, and Characterization*; CRC Press: 2006.

(24) Okuyama, K.; Hasegawa, T.; Ito, M.; Mikami, N. *J. Phys. Chem.* **1984**, *88*, 1711.

(25) Seminario, J. M.; Zacarias, A. G.; Tour, J. M. *J. Am. Chem. Soc.* **1998**, *120*, 3970.

(26) Swager, T. M.; Gil, C. J.; Wrighton, M. S. *J. Phys. Chem.* **1995**, *99*, 4886.

(27) Zhou, Q.; Swager, T. M. *J. Am. Chem. Soc.* **1995**, *117*, 12593.

(28) Yang, J.-S.; Swager, T. M. *J. Am. Chem. Soc.* **1998**, *120*, 11864.

(29) Rochat, S.; Swager, T. M. *ACS Appl. Mater. Interfaces* **2013**, *5*, 4488.

(30) Rose, A.; Tovar, J. D.; Yamaguchi, S.; Nesterov, E. E.; Zhu, Z.; Swager, T. M. *Phil. Trans. R. Soc. A* **2007**, *365*, 1589.

(31) Förster, T. *Discuss. Faraday. Soc.* **1959**, *27*, 7.

(32) Dexter, D. L. *J. Chem. Phys.* **1953**, *21*, 836.

(33) Roberts, G. *Langmuir-blodgett films*; Springer Science & Business Media, 2013.

(34) Ulman, A. *An Introduction to Ultrathin Organic Films: From Langmuir--Blodgett to Self--Assembly*; Academic press, 2013.

(35) Chevalier, Y.; Zemb, T. *Rep. Prog. Phys.* **1990**, *53*, 279.

(36) Schwuger, M.-J.; Stickdorn, K.; Schomaecker, R. *Chem. Rev.* **1995**, *95*.

(37) Bibette, J.; Calderon, F. L.; Poulin, P. *Rep. Prog. Phys.* **1999**, *62*, 969.

(38) Mason, T.; Wilking, J.; Meleson, K.; Chang, C.; Graves, S. *J. Phys.: Condens. Matter* **2006**, *18*, R635.

(39) Gupta, A.; Eral, H. B.; Hatton, T. A.; Doyle, P. S. *Soft Matter* **2016**, *12*, 2826.

Chapter 2

Conformational Control and Supramolecular Assemblies of Conjugated Polymers for Emissive Excimers and Chemical Sensors

Abstract: Interactions between π-conjugated polymers are known to create ground-state aggregates, excimers, and exciplexes. With few exceptions, these species exhibit decreased fluorescence quantum yields relative to the isolated polymers in liquid or solid solutions. Herein, we report a method to assemble emissive conjugated polymer excimers and demonstrate their applicability in the detection of selected solvent vapors. Specifically, poly(phenylene ethynylene)s (PPEs) with amphiphilic side chains are organized in a Langmuir monolayer at the air−water interface. Compression of the monolayer results in the reversible conversion from a face-on organization of the π-system relative to the water to what appears to be an incline-stack conformation. The incline-stack organization creates a bright yellow emissive excimeric state with increases of 28% in relative fluorescence quantum yields to the face-on monolayer conformation. Multilayers can be transferred onto the glass substrate via a Langmuir−Blodgett method with preservation of the excimer emission. These films are metastable and the fluorescence reverts to a cyan color similar to the spectra obtained in solution and spin-cast films after exposure to selected solvent vapors. This behavior has practical utility as a fluorescence-based indicator for selected volatile organic compounds.

Parts of this chapter were adapted and reprinted with permission from Koo, B.; Swager, T. M. "Highly Emissive Excimers by 2D Compression of Conjugated Polymers" *ACS Macro Lett.* **2016**, 5, 889.

2.1 Introduction

Understanding and controlling the structure and electronic couplings of semiconductive polymers in the solid state is central to their utility in photonic and organic electronic technologies.[1,2] Intrapolymer conformation and relevant physical properties have been investigated by conventional spectroscopy and by single-molecule spectroscopy.[3] Studying and understanding interpolymer couplings is complicated by a virtual continuum of conformations that depend on sample composition, deposition, and annealing. To this end, there has been considerable focus on modulating intrinsic polymer properties such as molecular weight, side-chain structure/density, and processing conditions that produce film morphologies with largely empirically optimized transport properties[4] and organizations.[5] However, presently the critical solid-state properties of transport (carriers and excitons) are limited by interpolymer interactions, and hence new methods are needed for the continued development of organic electronics.

The Langmuir-Blodgett method[6] remains as a preferred technique for the fabrication and study of highly ordered films from surfactants. For π-conjugated polymers, Langmuir monolayers at the air-water interface and transferred films have provided definitive information regarding correlations between conformation and π-stacking.[7,8] These conclusions were made possible by in situ absorption and emission spectroscopic measurements. These previous studies revealed that depending upon the structure poly(phenylene ethynylene)s display highly emissive phases with planarized or twisted conformations and π-stacked (H-type) organizations with highly quenched emission. The latter is understood to be the reason for the low solid-state emission quantum yields of organic polymers that lack steric blocking groups.

Interpolymer interactions most often give rise to ground-state aggregates with low quantum yields[9] and excimers that similarly have low emission.[10] Ground-state aggregates typically have

cofacial π-π stacking, with spectroscopic properties similar to the edge-on conformation at the air-water interface (Figure 2.1b). With the associated aggregation-caused quenching, they display characteristic red-shifted absorption peaks.[7,8,11-13] Excimers (excited-state dimers: M*+M → [MM]*)[14,15] have red-shifted and broad emissions with increased lifetimes. Both ground-state aggregates and excimers are generally considered to be species that should be avoided as a result of their nonradiative decay channels that give lower the quantum yields.[16,17] As a result, many electrooptic polymers accommodate groups that block cofacial π-π stacking,[18] large disordered side chains[19] or hyperbranched copolymers[20] to generate amorphous films.

Although excimers of conjugated polymers are considered to be less emissive and are thus to be avoided, there are cases wherein excimers of small molecules are highly emissive.[21,22] We report herein emissive excimers of conjugated polymers[23] that are organized at the air-water interface by compression of a film with face-on (Figure 2.1a) organization to give a proposed incline-stack (Figure 2.1c) with π-π interactions. The incline-stack model that we propose is achieved as a result of the strong anchoring at the water interface that prevents cofacial polymer aggregates (vide infra).

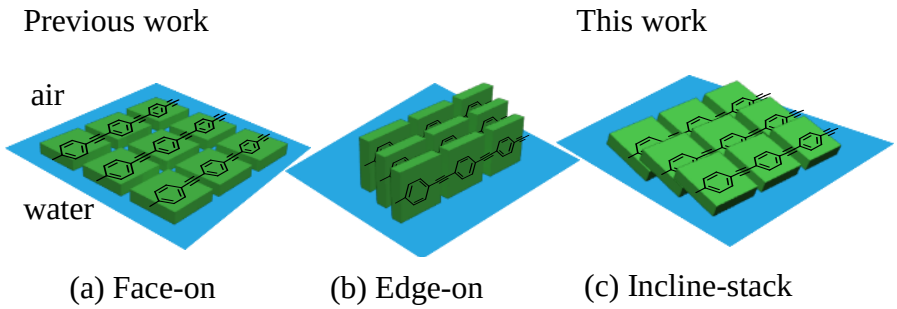

Figure 2.1. Polymer conformations at the air-water interfaces. Planes of phenyl repeat units are (a) parallel (face-on) and (b) perpendicular (edge-on) to the surface of water, respectively, reported in the literature. (c) Incline-stack is proposed in this work where the face of phenyl is inclined and stacked to form bright excimers.

2.2 Results and Discussion

We synthesized homopolymer **P1** (Figure 2.2a), a derivative of poly(phenylene ethynylene) (PPE), with amphiphilic side chains at 1,4-position. Related polymers had been previously demonstrated to give sufficiently strong anchoring at water/organic interfaces to be incorporated in lyotropic liquid crystals.[24] **P1** was synthesized through Sonogashira-type polymerization (procedures in the Chapter 2.4 Experimenal Details) and after purification has a molecular weight (GPC) of 33 kDa (degree of polymerization (n) ~ 22) and polydispersity of 1.40. Consistent with previous designs, **P1's** equilibrium structure is a face-on organization at the air-water interface (Figure 2.2b, top). An extrapolated area per one phenylene ethynylene unit is about 170 Å^2 obtained from the pressure-area isotherm (Figure 2.3) and is consistent with the expected face-on conformation.[7] Upon compression of the Langmuir monolayer, the cyan emission of the face-on

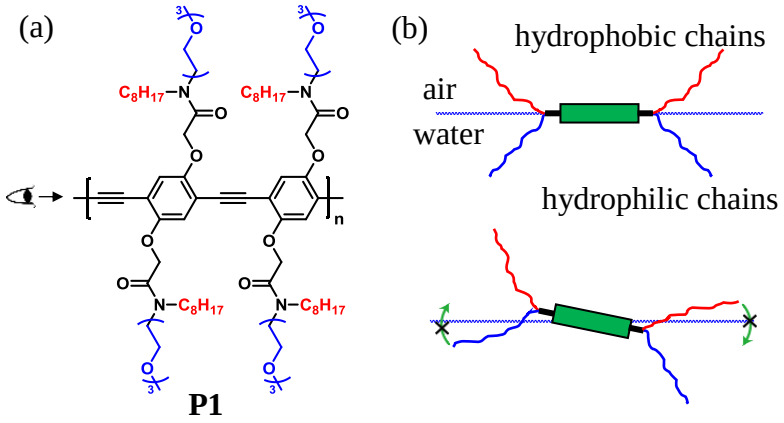

Figure 2.2. (a) The structure of the polymer **P1** (33 kDa, Đ 1.40) with amphiphilic side chains functionalized in a symmetric fashion. (b) The possible conformation depending on the presence of the external surface pressure. The green rectangle is a phenylethynylene repeat unit seen from the end of the axis of the backbone. With surface pressures less than 25 mN/m (top), a face-on structure is present. At higher surface pressures (bottom), the strong anchoring of side chains to the water prevents the perpendicular orientation of the backbone and result in the proposed incline-stack conformation.

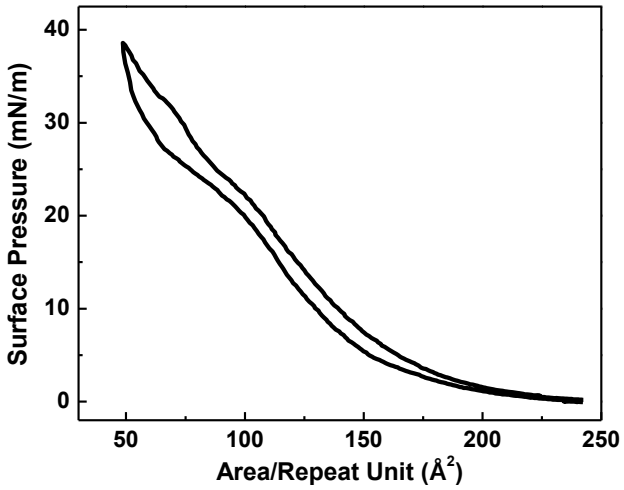

Figure 2.3. Pressure-area isotherm of **P1** with the small amount of sample loading to observe the onset point. The isotherm with the higher amount of sample loading is shown in Figure 2.4d.

state (Figure 2.4a, top) transforms to give a yellow emission that is visibly observed under a hand-held black light (Figure 2.4a, bottom, and see the SI for a video in the following publication: Koo, B.; Swager, T. M. *ACS Macro Lett.* **2016**, 5, 889). We propose that the yellow emission results from incline-stack conformation, which is formed by strong anchoring to the water (Figure 2.2b, bottom) that would be lost if the system adopted an edge-on compressed conformation.

In situ absorption and photoluminescence (PL) spectroscopy (Figure 2.4b,c) were performed to determine the origin of emission changes. At 8 mN/m, the absorption (466 nm) and emission (475 nm) maxima are red-shifted when compared to the solution spectra shown in Figure 2.5 (439 nm for absorption and 471 nm for emission), which indicates the planarized conformation at the air-water interface. Initial compression promotes a very slight blue shift in the absorption spectra from 466 nm (8 mN/m) to 464 nm (21 mN/m) owing to disorder of π-system from the equilibrium face-on structure[7] and similarly small changes in the emission. The pressure-area isotherm (Figure 2.4d) is relatively linear from 8 mN/m (black circle) to 21 mN/m (green circle),

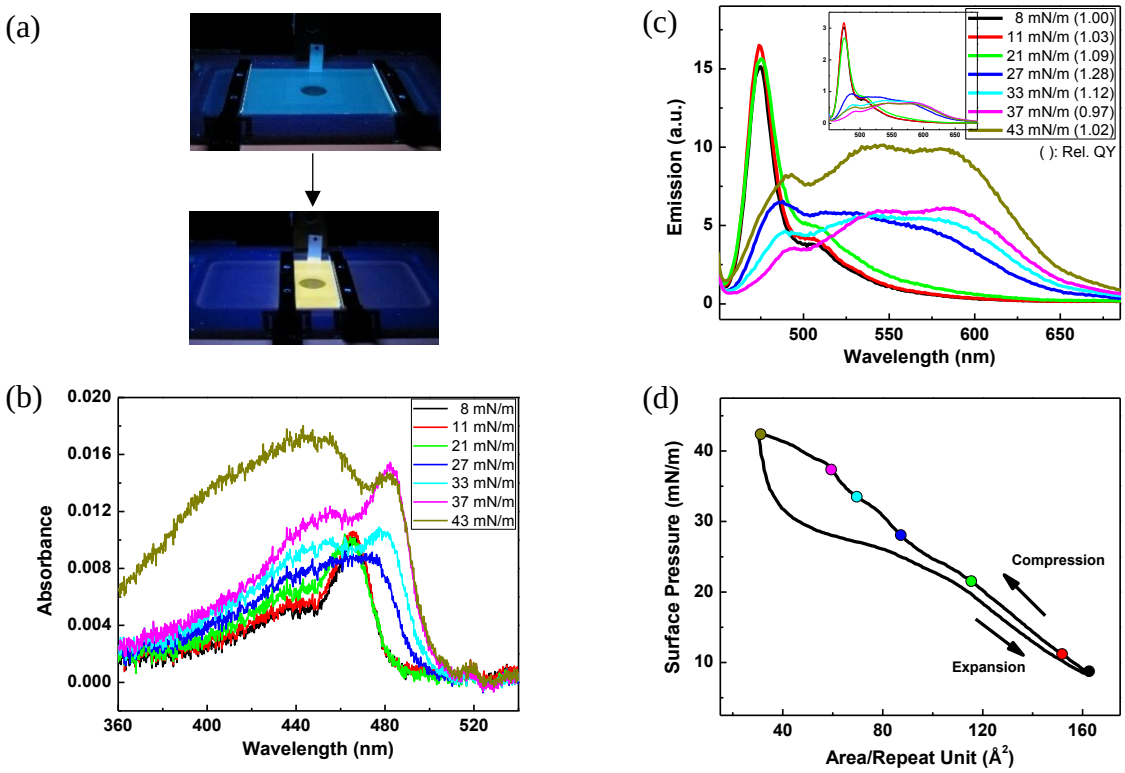

Figure 2.4. (a) Compression-induced bright yellow excimers of **P1**. Pictures are taken under 365 nm hand-held UV lamp from the fixed position. The areas upon expansion (top) and compression (bottom) are ca. 77 cm^2 (11 × 7 cm) and 18 cm^2 (2.6 × 7 cm), respectively. (b) In situ absorption spectra depending on the surface pressure. Increased planarization is observed from 27 mN/m to 37 mN/m with a new peak around 480 nm. All spectra (except multilayer at 43 mN/m) shows identical shape with the increased absorbance as a result of the decreased surface area. (c) In situ PL spectra recorded depending on the applied surface pressure with excitation at 435 nm. Broad, structureless, red-shifted emission bands from 475-650 nm are the characteristics of excimers. Relative quantum yields are shown in the parenthesis. The inset is the modified spectra calculated based on the same absorption at 435 nm in each surface pressure. (d) Pressure-area isotherm of the **P1** monolayer. Here the repeat unit on the x-axis is considered as one phenylene ethynylene unit. The inflection point at 25 mN/m is the point where the transition of the conformation from face-on to incline-stack occurs. Another transition observed at ca. 38 mN/m exhibits the multilayer formation.

which suggests the absence of a phase transition. At 25 mN/m, we observe an inflection point in the pressure-area isotherm and large changes in the absorption and emission spectra. The absorption spectrum at 27 mN/m gains a new sharp red-shifted peak (475 nm) that is typical of

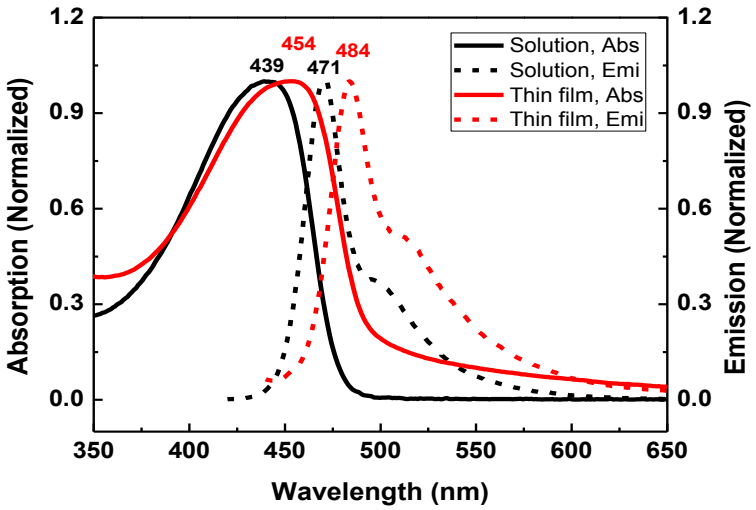

Figure 2.5. Spectra of solution and thin films of **P1** that do not display emissive excimers. Absorption (solid) and emission (dotted) spectra in solution (black) and thin films (red) are obtained. Thin films show no excimeric emission.

chain-chain interactions of planar polymers[25] which further red-shifts (483 nm at 37 mN/m) at higher pressures. The PL spectrum shows the red-shifted, broad, featureless emission extending from 475 to 650 nm. There are two broad emission bands at 545 and 585 nm (ΔE = 1260 cm^{-1}),

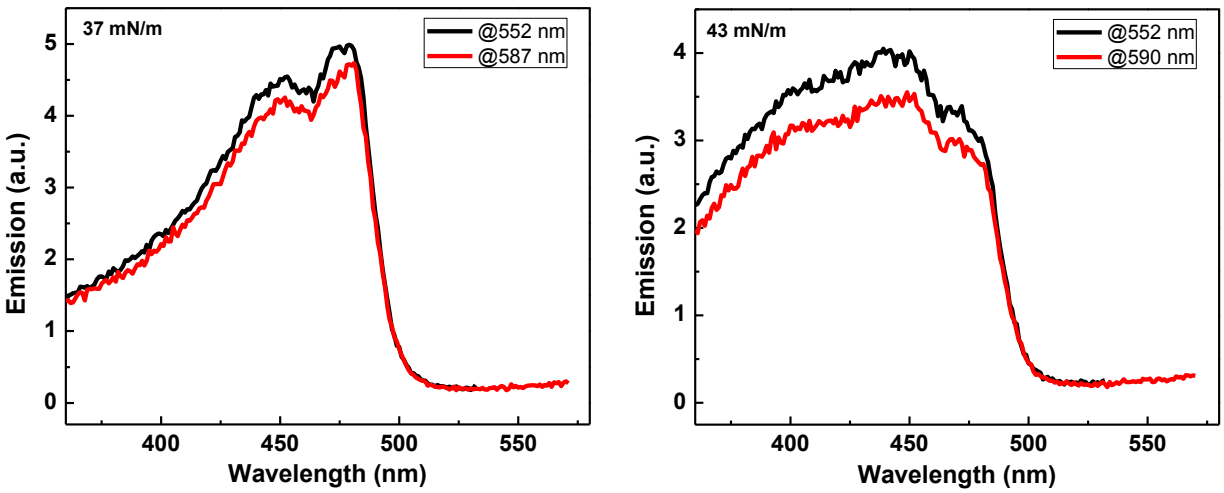

Figure 2.6. Excitation spectra at 37 mN/m (left) and 43 nm (right) of the **P1** monolayer at the air-water interface.

the relative intensities of which vary with pressure, suggesting two slightly different emissive states, although the excitation spectra (Figure 2.6) cannot distinguish them. The new emissions have classic broad exciplex features. The strong anchoring of the hydrophilic side-chains in the water prevents eclipsed stacking of the backbones and we suggest that the excimer emission and the new sharp feature in the absorption are associate with an incline-stack organization. The fact that the repeating unit area (one phenylene ethynylene unit) of the incline-stack transition (ca. 90 $Å^2$) is between the face-on (170 $Å^2$) and the previously reported edge-on (30 – 40 $Å^2$)[8] further implies the intermediate conformational features of the incline-stack between face-on and edge-on. With this area of 90 $Å^2$, one Ph-CC unit length of 7 Å provides the average interpolymer distance of 13 Å, which is in the similar range of pyrene excimer distance of ~ 10 Å. At 27 mN/m, the quantum yield increases by 28% (Figure 2.4c parentheses) relative to the uncompressed face-on conformation (8 mN/m). The slight decreases in the relative quantum yields after 27 mN/m are attributed to unstructured ground-state interactions, which typically give rise to self-quenching. Multilayer formation is observed above 38 mN/m from the pressure-area isotherm and the vivid yellow emission is maintained at 43 mN/m. In the multilayers, the observed broader absorption is perhaps attributed to the fact that some of the layers lack anchoring to the water and therefore may have more random conformations. The subsequent expansion from 43 mN/m entails the rapid decrease of the surface pressure and a different isotherm shape from compression, which may indicate the fast relaxation of the compressed multilayers (discussed later). The isotherms are highly reversible (Figure 2.7).

In order to confirm that the preorganization (planarization and alignment) at the air-water interface is key to forming emissive excimers, we investigated emission obtained from different sample preparations (Figure 2.5 and 2.8). Spin-cast films of **P1** on glass substrates display an

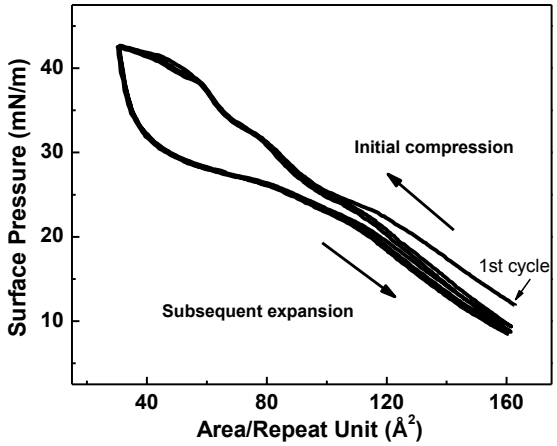

Figure 2.7. The pressure-area isotherms of the first three cycles for mechanical annealing, supplemental to Figure 2.4d. The consistent shapes indicate the reversible and reproducible formation of incline-stack conformation. The first cycle is slightly off from the equilibrium, implying that the mechanical annealing indeed helps the polymers pack each other after one compression-expansion cycle.

emission maximum at 484 nm that is red-shifted from λ_{max} of the solution with no evidence of the broad excimer emission (Figure 2.5). Aggregates generated in solution by the addition of hexane (a poor solvent for the polymer) results in aggregation-induced quenching without excimeric emission (Figure 2.8).

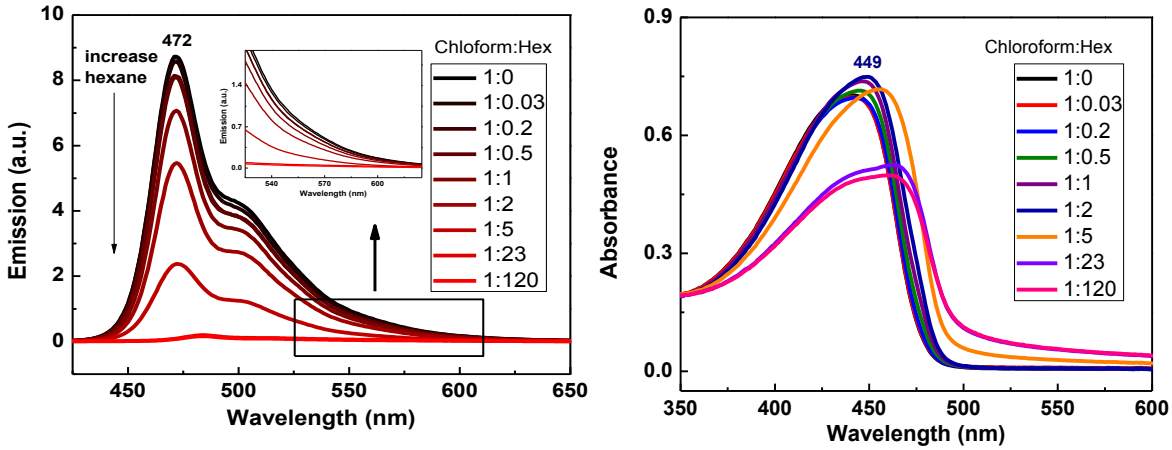

Figure 2.8. Emission spectra (left) of solution aggregates of **P1** that do not display emissive excimers. Aggregate dispersions by adding a poor solvent (hexane) are generated. The increased amount of hexane triggers the self-quenching as a result of cofacial ground-state aggregates (see absorption spectra (right)). The enlarged spectra in inset confirm the absence of excimers. Absorption spectra (right) of solution aggregates of **P1** in varying ratio of hexane to chloroform.

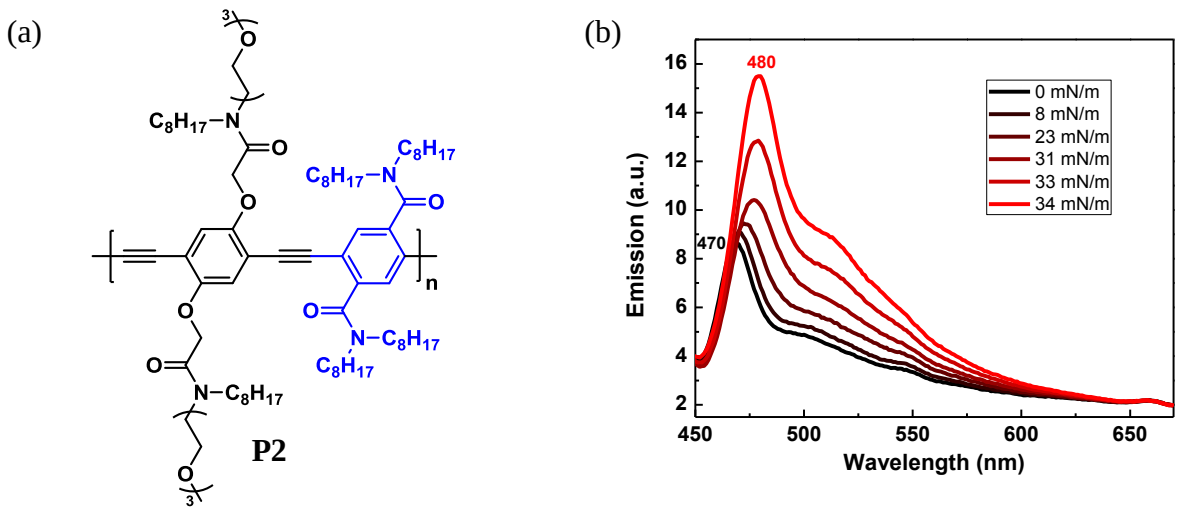

Figure 2.9. A hetero-type PPE, **P2**, showing the absence of excimer formation. (a) The structure of **P2** (23 kDa, Đ 1.51) where bis(*N*,*N*-dioctylamide)benzene in blue is introduced as a co-monomer. (b) The in situ emission spectra of **P2** at the air-water interface. No excimer emission was observed.

To probe the role of chemical structure on excimer formation, we designed and synthesized an alternating copolymer, **P2** (Figure 2.9a). Following the synthesis from the literature,[24] a molecular weight of 23 kDa with the polydispersity of 1.51 was obtained which was similar to **P1**. **P2** also forms Langmuir monolayers but the PL spectra (Figure 2.9b) exhibit no evidence of excimer formation. This sustained shape of **P2's** PL spectra, its extrapolated area (155 $Å^2$ per one phenyl ethynylene unit), and absence of aggregation-induced quenching suggest that the conformation of the **P2** is face-on at pressures below folding into multilayers (pressure-area isotherm in Figure 2.10).

The ability of **P1** to form excimers with compression suggests their utility as a chemical indicator. To accomplish this, we first transferred **P1** in its compressed multilayer excimer form that shows intense yellow emission (43 mN/m) to a hydrophilic glass slide (treated with nitric acid and sodium hydroxide solution) using the Langmuir-Blodgett (LB) method with an upstroke. The

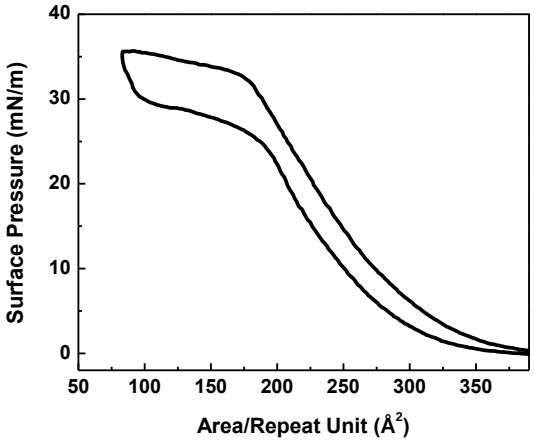

Figure 2.10. Pressure-area isotherm of hetero-type PPE (**P2**). The repeat unit on the x-axis contains two phenylene ethynylenes.

films are highly emissive (Figure 2.11a, inset) and the absorption spectrum (Figure 2.11a, black solid line) is analogous to those of cyan emitting spin-coated films, implying there are no new ground-state interactions among polymer chains. The sharp absorption peak at 482 nm that existed

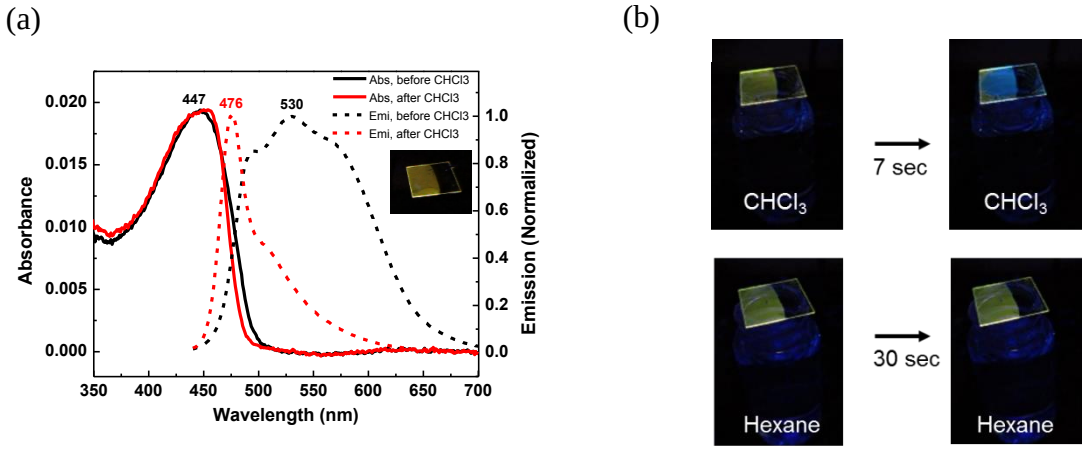

Figure 2.11. Transfer of the compressed multilayer onto the glass substrate using Langmuir-Blodgett method and solvent vapor detection. (a) Absorption (solid) and emission spectra (dotted) of the transferred **P1** films and before (black) and after (red) exposure to chloroform. The inset picture is the film under 365 nm irradiation. (b) Solvent vapor sensing is demonstrated wherein good solvents (chloroform, methanol, acetone, and THF) induce the reorganization of the aligned polymers, reverting to cyan emission in a few seconds. In contrast, prolonged exposure to poor solvents (hexane and water) produces no response.

at the air-water interface that was attributed to a highly planarized slipped stacked structure is lost presumably as a result reorganization of multilayers. However, the emission spectrum of the transferred film still displays a broad featureless excimer emission (Figure 2.11a, black dotted line). The fluorescence lifetime of the film (4.9 ns) is longer than that in solution (0.64 ns) and spin-cast films (0.11 ns) and is consistent with excimer emission.

The proposed incline-stack organization on glass substrates is metastable. The organization is thermally robust and is not changed with heating to 70 °C for 15 min. However, the cyan emission can be generated by exposure to solvents that have sufficient interactions with the polymer to facilitate reorganization. Specifically, exposing the excimer films to vapors from vials of chloroform, methanol, acetone, and THF results in the rapid (seconds) transformation of the yellow emission to cyan (Figure 2.11b and 2.12, and see the SI for a video in the following publication: Koo, B.; Swager, T. M. *ACS Macro Lett.* **2016**, 5, 889). The emission spectrum after exposure to $CHCl_3$ in Figure 2.11a (red dotted line) exhibits the disappearance of yellow excimeric emission and generation of the cyan emission. No significant changes are observed in absorption

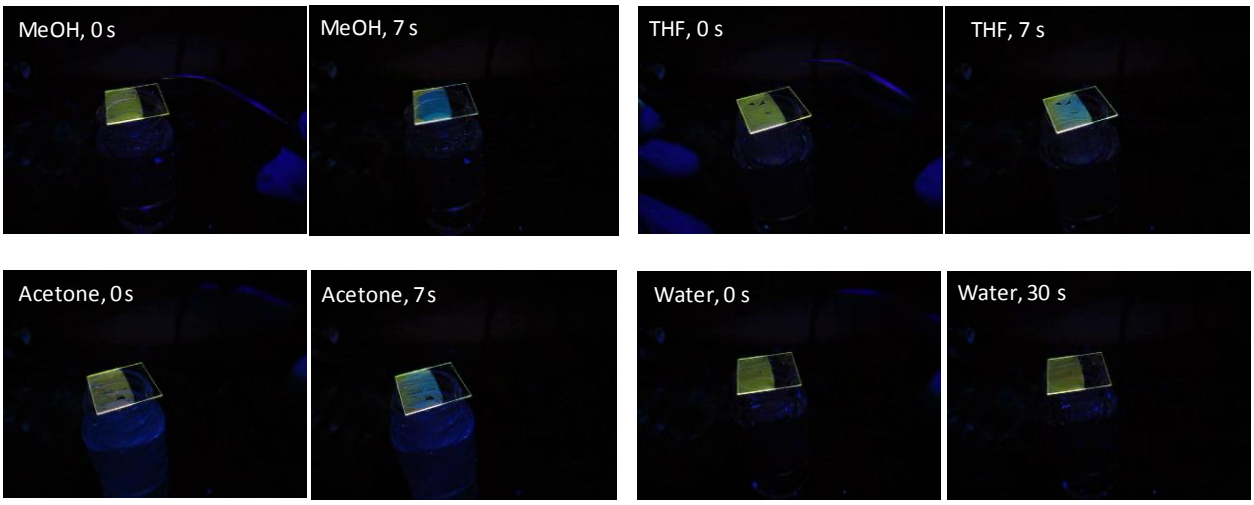

Figure 2.12. Excimer films that are exposed to different solvent vapors. Overall, they are responsive to good solvents (chloroform, methanol, THF, and acetone) and not responsive to poor solvents (hexane and water).

spectra. In contrast, exposure of LB films to poor solvents (hexane and water) produces no reduction in the yellow emission (Figure 2.11b and 2.12, and see the SI for a video in the following publication: Koo, B.; Swager, T. M. *ACS Macro Lett.* **2016**, 5, 889).

2.3 Conclusions

We used molecular design and conformational control at the air-water interface to form structured semiconductive polymer monolayers and multilayers that possess photophysical characteristics consistent with excimer formation with 28% increase in the relative fluorescence quantum yield. Based on this work and established models for the organization of semiconductive polymers at the air-water interface, we propose an incline-stack conformation generated from the 2D compression of the polymer nematic phases. The structured multilayers transferred onto glass substrates maintain the excimer emission and strongly interacting solvents trigger a rapid change in the emission from yellow to cyan. This effect has utility for chemical indicators of solvent exposures, which could be used for occupational safety applications. Although excimers have often been considered as parasitic species, this work demonstrates that, with conformational control, polymeric excimers can be brightly emissive. The broad emission of excimers offers the prospects for new applications.

2.4 Experimental Details

2.4.1 General

Chemicals were purchased from Aldrich, Alfa Aesar, and TCI America without further purification unless noted otherwise. All reactions were carried out under argon with standard Schlenk techniques. Compound **1**, **2**, and **P2** were synthesized by following the literature

procedures.[24] All ^{1}H NMR spectra are reported in ppm on a Bruker Avance-400. ^{1}H NMR is referenced to a chloroform peak (δ = 7.26 ppm). The multiplicity is reported as follows: s = singlet, d = doublet, t = triplet, m = multiplet or unresolved, br = broad. ^{13}C NMR is referenced to a 1,1,2,2-tetrachloroethane peak (δ = 73.78 ppm). Coupling constants J are reported in Hz. Elemental analyses were carried out by Robertson Microlit Laboratories, Ledgewood, NJ (USA).

THF Gel Permeation Chromatography (GPC) was performed with a concentration of 0.5 mg/ml on an Agilent 1260 Infinity system, calibrated with monodisperse polystyrene standards. UV-vis spectra were recorded on Agilent Cary 4000 or Cary 5000 spectrometer at room temperature. Fluorescence measurements were performed at room temperature with a Horiba Jobin Yvon SPEX Fluorolog-τ3 fluorimeter (model FL-321, 450 W Xenon lamp) using right-angle conformation for solution and Langmuir monolayers and front-face conformation for thin films. Lifetime measurements were carried out on a Horiba Jobin Yvon MF2 lifetime spectrometer equipped with a 365 nm laser diode via frequency modulation. POPOP in ethanol was used as a reference lifetime sample (τ = 1.35 ns). For sample preparations of photophysics measurements, the solutions were prepared in chloroform with 10^{-5} M – 10^{-6} M. The solid-state films were prepared on glass by spin-coating 1000 rpm for 60 seconds from the solution in chloroform (5 mg/ml) and annealed at 70 °C for 15 min in ambient atmosphere.

The in situ UV/PL measurements on Langmuir monolayers were carried out with fiber optic cables that are connected with the Agilent spectrometer and the Horiba fluorimeter. The Langmuir monolayers were prepared from the polymer in chloroform solution (1 mg/mL) on 102 M trough from NIMA Technology equipped with a fused quartz window, using purified water with > 18 MΩ·cm as subphase. After drying the chloroform for ca. 15 min, the monolayers were mechanically annealed with 3 compression-expansion cycles and photophysics data were recorded.

For the transfer of the monolayers to glass substrates, NIMA 602 M equipped with a vertical dipper was used where the Langmuir monolayers were deposited in the same way as NIMA 102 M. 18×18 mm glass microscope cover slides were sonicated using a detergent solution for 20 min, rinsed with the purified water (> 18 MΩ·cm) three times, and sonicated with the purified water for 20 min, followed by vacuum drying. For hydrophilic surfaces, the washed glass slides were sonicated with concentrated nitric acid for 20 min, rinsed with the purified water three times, sonicated with 10% sodium hydroxide solution for 20 min, and finally rinsed with the purified water three times, followed by vacuum drying.

For sensing experiments, a solvent of interest is contained in a scintillation vial with a cap being closed so that the inside of the vial is saturated with the solvent vapor. The cap is open and the LB film is placed on top of the vial under a hand-held UV lamp with 365 nm.

2.4.2 Polymerization Procedure for P1

1 (1.00 eq, 0.100 mmol, 79.0 mg), **2** (1.05 eq, 0.105 mmol, 104.4 mg), $Pd(PPh_3)_4$ (5 mol%, 5.8 mg), and CuI (10 mol%, 1.9 mg) are added into a flame-dried flask equipped with a magnetic stirrer bar. Then the flask containing reagents was evacuated and back-filled with argon for 5 times. The mixture of dry toluene:diisopropylamine (3:1 v/v) was degassed with nitrogen for 30 min. 4 mL of the mixture was added to the flask. The reaction mixture was stirred for 30 min at room temperature to completely dissolve all the materials. Temperature was increased into 65 °C and stirred for 7 h, followed by increasing the temperature into 75 °C and stirring for additional 22 h. After cooling down to room temperature, the solvents in the reaction mixture was evaporated under reduced pressure, and the contents are dissolved in dichloromethane (DCM). The mixture was filtered through a short plug of silica gel and eluted with excess amount of DCM. The filtrate was evaporated under reduced pressure, precipitation was obtained from DCM/hexane and subsequent

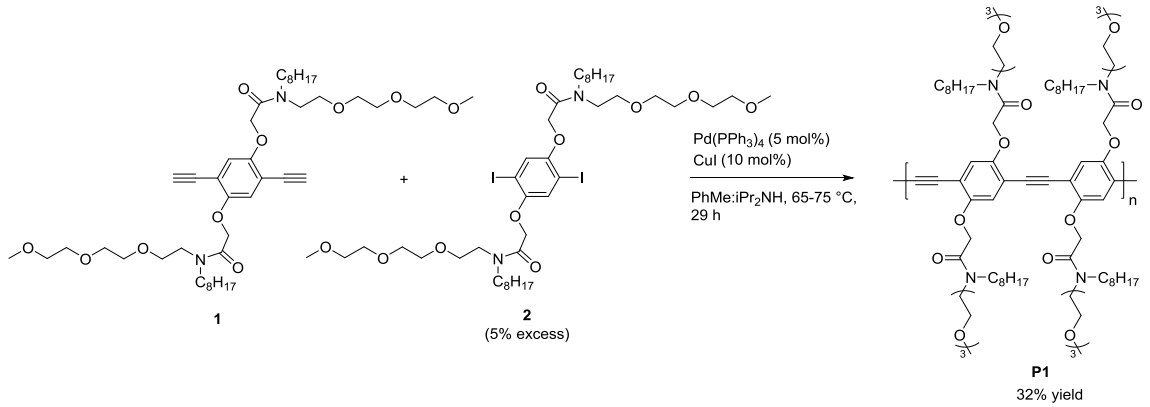

Scheme 2.1. Polymerization for **P1**.

centrifugation was carried out at 12,000 rcf for 10 min. Preparative GPC in THF was used to separate high molecular weight fraction of the solid product. The resulting fraction in THF was evaporated under reduced pressure, and further precipitation in DCM/hexane was carried out with the subsequent centrifugation at 12,000 rcf for 10 min. The product was dried in vacuo, affording a dark yellow rubbery solid (49 mg, 32 %). ^{1}H NMR (400 MHz, $CDCl_3$): δ = 7.13 (br, 2H), 4.88-4.84 (br, 4H), 3.60-3.33 (br, 34H), 1.55 (br, 4H), 1.25 (br, 20H), 0.86 (br, 6H). A complete ^{13}C NMR cannot be obtained as a result of insufficient solubility in solvents that would not obscure key signals such as chloroform or at high temperature (70–80 °C) 1,1,2,2-tetrachloroethane. We were also to detect the side chain resonances, which are ^{13}C NMR (101 MHz, $CDCl_2CDCl_2$, 70 °C): δ = 71.8, 70.3, 70.2, 58.5, 31.6, 29.1, 29.0, 22.4, 13.8. GPC (THF): Mn = 33 kDa (DP = 22), Đ = 1.40. The relatively short polymerization time could lead to the incompletion of the reaction and thus smaller degree of polymerization than the theoretical value (DP = 41). Anal. Calcd for $C_{84}H_{140}N_4O_{20}$ (repeat unit): C, 66.11; H, 9.25; N, 3.67; O, 20.97. Found: C, 62.73; H, 8.79; N, 3.44.

2.5 References

(1) Facchetti, A. *Chem. Mater.* **2011**, 23, 733.

(2) Guo, X.; Baumgarten, M.; Müllen, K. *Prog. Polym. Sci.* **2013**, 38, 1832.

(3) Bolinger, J. C.; Traub, M. C.; Brazard, J.; Adachi, T.; Barbara, P. F.; Vanden Bout, D. A. *Acc. Chem. Res.* **2012**, 45, 1992.

(4) Kline, R. J.; McGehee, M. D.; Kadnikova, E. N.; Liu, J.; Fréchet, J. M. J.; Toney, M. F. *Macromolecules* **2005**, 38, 3312.

(5) Hoeben, F. J. M.; Jonkheijm, P.; Meijer, E. W.; Schenning, A. P. H. J. *Chem. Rev.* **2005**, 105, 1491.

(6) Ariga, K.; Yamauchi, Y.; Mori, T.; Hill, J. P. *Adv. Mater.* **2013**, 25, 6477.

(7) Kim, J.; Swager, T. M. *Nature* **2001**, 411, 1030.

(8) Kim, J.; Levitsky, I. A.; McQuade, D. T.; Swager, T. M. *J. Am. Chem. Soc.* **2002**, 124, 7710.

(9) Lemmer, U.; Heun, S.; Mahrt, R. F.; Scherf, U.; Hopmeier, M.; Siegner, U.; Göbel, E. O.; Müllen, K.; Bässler, H. *Chem. Phys. Lett.* **1995**, 240, 373.

(10) Jenekhe, S. A.; Osaheni, J. A. *Science* **1994**, 265, 765.

(11) Levitsky, I. A.; Kim, J.; Swager, T. M. *J. Am. Chem. Soc.* **1999**, 121, 1466.

(12) Deans, R.; Kim, J.; Machacek, M. R.; Swager, T. M. *J. Am. Chem. Soc.* **2000**, 122, 8565.

(13) McQuade, D. T.; Kim, J.; Swager, T. M. *J. Am. Chem. Soc.* **2000**, 122, 5885.

(14) Birks, J. B. Photophysics of aromatic molecules; Wiley-Interscience: London, New York, 1970.

(15) Birks, J. B. *Rep. Prog. Phys.* **1975**, 38, 903.

(16) Mitschke, U.; Bauerle, P. *J. Mater. Chem.* **2000**, 10, 1471.

(17) Schwartz, B. J. *Annu. Rev. Phys. Chem.* **2003**, 54, 141.

(18) Yang, J.-S.; Swager, T. M. *J. Am. Chem. Soc.* **1998**, 120, 11864.

(19) Kline, R. J.; McGehee, M. D. *J. Macromol. Sci., Polym. Rev.* **2006**, 46, 27.

(20) Liu, X.-M.; He, C.; Hao, X.-T.; Tan, L.-W.; Li, Y.; Ong, K. S. *Macromolecules* **2004**, 37, 5965.

(21) Liu, Y.; Tao, X.; Wang, F.; Shi, J.; Sun, J.; Yu, W.; Ren, Y.; Zou, D.; Jiang, M. *J. Phys. Chem. C* **2007**, 111, 6544.

(22) Han, G.; Kim, D.; Park, Y.; Bouffard, J.; Kim, Y. *Angew. Chem. Int. Ed.* **2015**, 54, 3912.

(23) Although there was one report (Kim, Y.; Bouffard, J.; Kooi, S. E.; Swager, T. M. *J. Am. Chem. Soc.* **2005**, 127, 13726) discussing the emissive interpolymer excimers of PPE derivatives, the follow-up paper (Satrijo, A.; Kooi, S. E.; Swager, T. M. *Macromolecules* **2007**, 40, 8833) raised the possibility that anthracene defects may also be responsible for the new emission. Other reports of highly emissive aggregates of conjugated polymer have been observed in cyclophane (Deans, R.; Kim, J.; Machacek, M. R.; Swager, T. M. *J. Am. Chem. Soc.* **2000**, 122, 8565) and in chiral systems (Zahn, S.; Swager, T. M. *Angew. Chem. Int. Ed.* **2002**, 41, 4225). A report on intrapolymer emissive excimer in disubstituted polyacetylenes was previously reported through aggregation-induced emission mechanism (Qin, A.; Jim, C. K. W.; Tang, Y.; Lam, J. W. Y.; Liu, J.; Mahtab, F.; Gao, P.; Tang, B. Z. *J. Phys. Chem. B* **2008**, 112, 9281).

(24) Bouffard, J.; Swager, T. M. *Chem. Commun.* **2008**, 5387.

(25) Miteva, T.; Palmer, L.; Kloppenburg, L.; Neher, D.; Bunz, U. H. F. *Macromolecules* **2000**, 33, 652.

2.6 Appendix for Chapter 2

P1 (^{1}H NMR in $CDCl_3$)

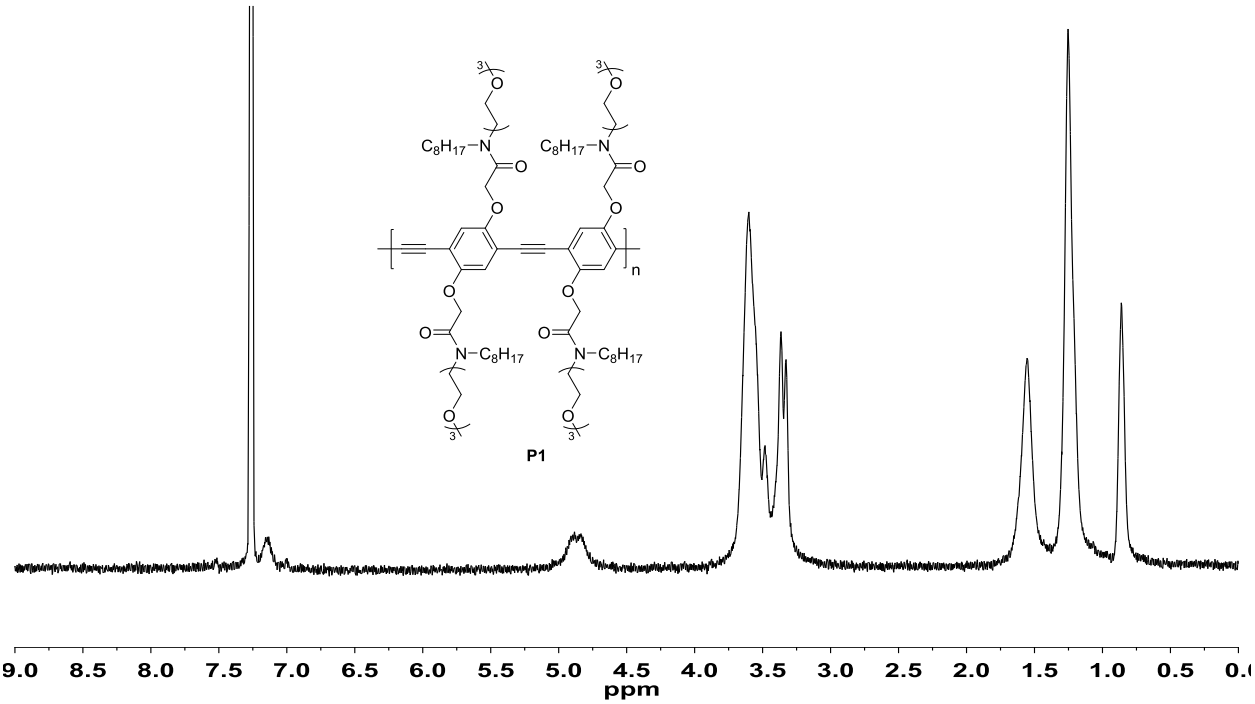

P1 (^{13}C NMR in 1,1,2,2-tetrachloroethane-d_2 at 70 °C)

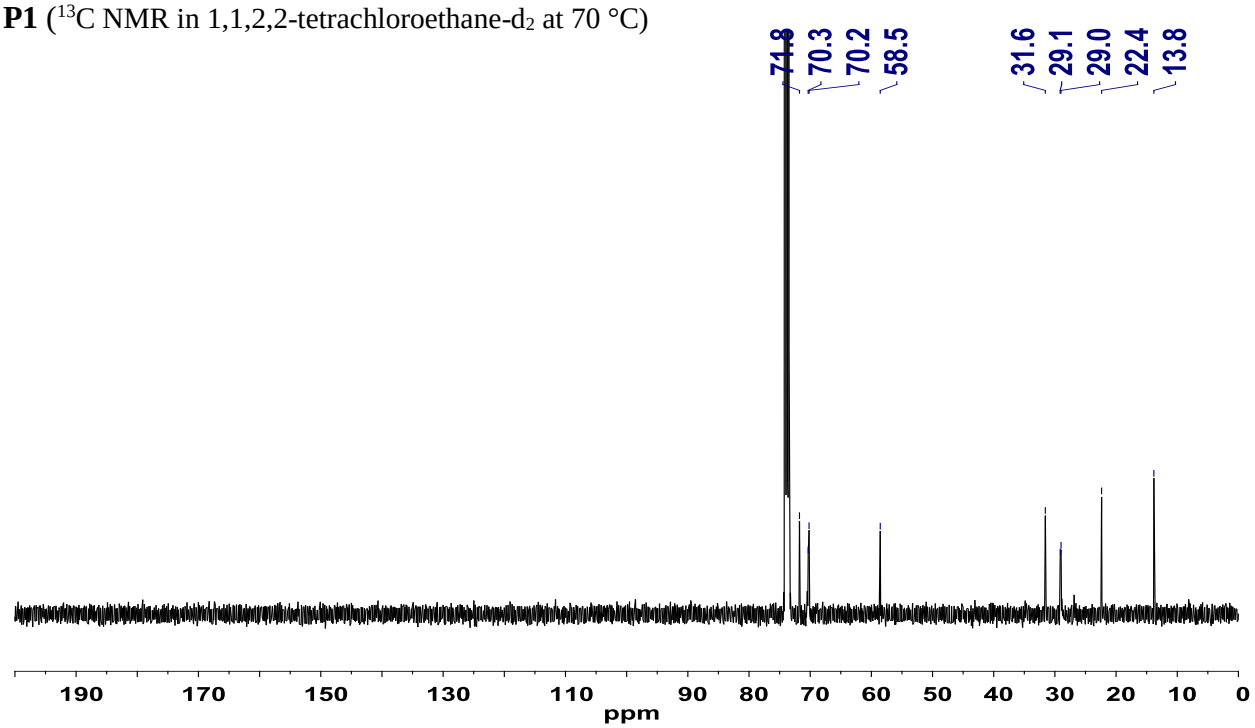

Chapter 3

Exciton Migration of Conjugated Polymers: Dual-Fluorescence at Water Interfaces

Abstract: Exciton migration to emissive defects in π-conjugated polymers is a robust signal amplification strategy for optoelectronic sensors. Herein we report endcapped conjugated polymers that show two distinct emissions as a function of interpolymer distances at the air-water and hydrocarbon-water interfaces. Amphiphilic poly(phenylene ethynylene)s (PPEs) endcapped with perylene monoimides display two distinct emission colors (cyan from PPE and red from perylene), the relative intensity of which depends on the surface pressure applied on the Langmuir monolayers. This behavior produces a ratiometric interfacial pressure indicator. Relative quantum yields are maintained at the different surface pressures and hence display no sign of self-quenching of the excitons in an aggregated state. These polymers can be organized at the micelle-water interface in lytropic liquid crystals, thereby paving the way for potential applications of endcapped amphiphilic conjugated polymers in biosensors and bioimaging.

Parts of this chapter were adapted and reprinted with permission from Koo, B.; Swager, T. M. "Interfacial Pressure/Area Sensing: Dual-Fluorescence of Amphiphilic Conjugated Polymers at Water Interfaces" *ACS Macro Lett.* **2017**, 6, 134.

3.1 Introduction

Understanding the optoelectronic properties of semiconductive polymers underpins technological advances in organic photovoltaics, organic light-emitting diodes, and many chemical sensors.[1-6] π-Conjugated polymers feature direct optical band gaps that produce large extinction coefficients and high fluorescence quantum yields,[7] and the delocalization of the π-orbitals facilitates efficient transport of charged carriers and excitons. In particular, exciton migration to low-energy sites in the solid-state of π-conjugated polymers has been recognized as a key mechanism for signal amplification of the sensory systems.[8,9] The higher dimensionality associated with interchain electronic couplings in solids is understood to enhance energy transfer. Specifically, the ability of excitons to undergo a 3D random walk (interchain) in films provides a statistical improvement, in contrast to 1D random walk (intrachain), wherein excitons revisit the same segments of the polymer backbone many times.[10]

The transport properties of exciton migration can be probed by using the Langmuir-Blodgett (LB) technique to create precise organizations. LB molecular processing can create highly aligned polymer films on substrates after sequential monolayer depositions. The thickness of multilayers can be precisely controlled, and in previous studies efficient intralayer and interlayer exciton migration in LB films was analyzed to determine the exciton diffusion length.[11] Additionally, vectorial energy transfer has been demonstrated in structured polymer films that create energy gradient.[12] In our present studies, we are exploiting the dynamic nature of the air-water and liquid-liquid interfaces. Given that energy transfer is enhanced by reducing interpolymer distances, we envision that compression and expansion of surfactant polymer monolayers with varying interfacial surface tension will modulate exciton migration to minority emitters and display two distinct fluorescences. To achieve these properties, we have produced specially

designed conjugated polymers with low-energy emissive traps. Changes in interfacial tension can then be translated to ratiometric fluorescent signals.

There are two general types of sensitive fluorescent sensors that make use of exciton migration. On-off sensors are systems wherein analytes trigger aggregations or electron transfer of π-conjugated polymers that cause fluorescence quenching.[13,14] In the case where less emissive aggregates are formed, excitons migrate through an efficient random walk and are trapped at weakly emissive lower energy trapping sites. Such response can be produced, for example, by potassium ion sandwich complexation with crown-ether functionalized PPEs.[15] A second type of sensor makes use of exciton transfer to efficient low-energy emitters that are either proximate or covalently integrated in the polymer backbone. For example, polyanionic PPEs with a few percent of low bandgap emitters undergo blue-to-green fluorescence changes when aggregated by electrostatic assembly with multicationic amines.[16] These dual-fluorescence systems potentially have broader appeal owing to the ability to tune emission colors by incorporating a variety of dyes (green, red, and even near-infrared) to meet specific applications. Building upon this methodology, we herein report surfactant poly(phenylene ethynylene)s with low bandgap emissive end-groups that display enhanced energy transfer at the air-water interface upon compression (Figure 3.1). The quantum yields remain relatively constant over this process and we achieve a dual-fluorescence interfacial pressure indicator with high color contrast. We further demonstrate this energy transfer scheme at micelle-water interfaces, suggesting potential applications in bioimaging and biosensors.

The choice of the amphiphilic PPE is critical to promote the proper organizations. Although energy transfer is efficient in the solid state, aggregation-induced quenching of singlet excitons is notoriously common and can lower the exciton diffusion lengths, giving diminished fluorescence quantum yields.[13,16] We previously showed that PPEs having amphiphilic side chains displayed

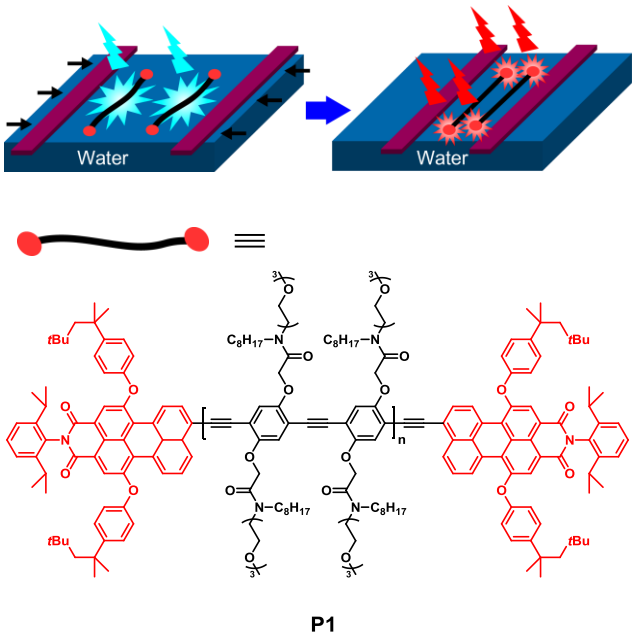

Figure 3.1. Schematic illustration of enhanced energy transfer to red end-caps in conjugated polymers upon applied surface pressure (top). The structure of the PPE **P1** (bottom).

novel behavior wherein the compressed monolayers at the air-water interface formed highly emissive excimers with the increase in relative quantum yields compared to non-compressed states.[17] Therefore, we have targeted this system for further applications by functionalization with low-energy emissive perylene dye endgroups (Figure 3.1). The perylene has emission bands (~575 nm) that do not overlap the PPE peaks at 475 nm (0-0) and 510 nm (0-1), thereby allowing for straightforward analysis of the ratiometric responses.

3.2 Results and Discussion

3.2.1 Synthesis of P1

We produced perylene monoimide-endcapped PPEs (**P1**, Figure 3.1) with amphiphilic side chains by Pd-catalyzed Sonogashira-type couplings (Figure 3.2a and see the Chapter 3.4 Experimental Details for detailed synthetic procedures). In this process we added a 5% excess of

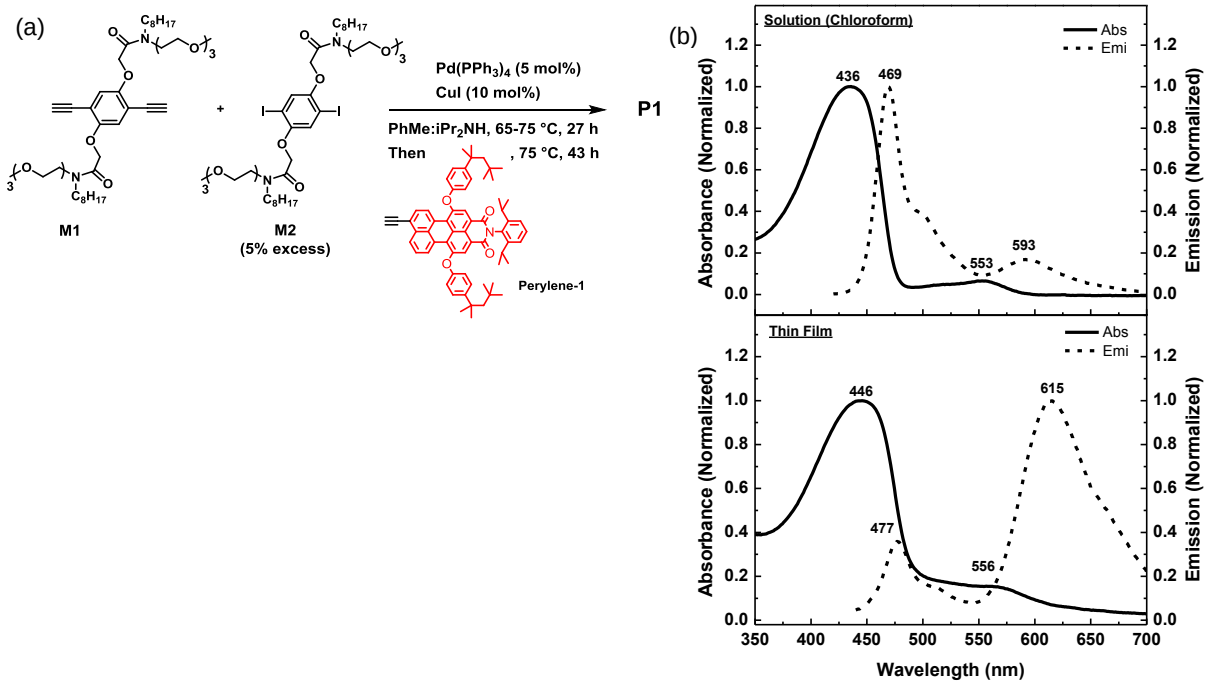

Figure 3.2. (a) Synthesis of **P1** using **M1** and **M2** (5% excess) with sequential *in situ* endgroup functionalization. Yield 71%, M_n = 27 kDa, and Đ 1.38. (b) Absorption and emission spectra of **P1** in solution (top) and spin-coated films (bottom).

diiodide monomer (**M2**) with the expectation that after monomer consumption there are Ar-Pd-I endgroups, which will react with a sequentially added perylene monoimide bearing a terminal acetylene (**Perylene-1**). The resulting polymers have a M_n of 27 kDa (degree of polymerization (n) = 18) and Đ of 1.38. The theoretical degree of polymerization on this composition of monomers is 41. The lower n may be related to incomplete polycondensation and/or also attributed to Glaser-type acetylene-acetylene linkages that are often present in PPEs, which effectively change the stoichiometry by depleting the alkynes. The degree of **Perylene-1** incorporation was analyzed by ^{1}H NMR spectrum (Figure 3.3). The perylene-associated signal at 8.27 ppm (2H per **Perylene-1**) is compared with the 4.85 ppm peak of the monomers (8H per repeat unit). With a degree of polymerization of 18, one polymer chain has 144 protons at 4.85 ppm. With this number, the integration at 8.27 ppm shows 1.38 protons and thus assuming 18 repeating units each polymer

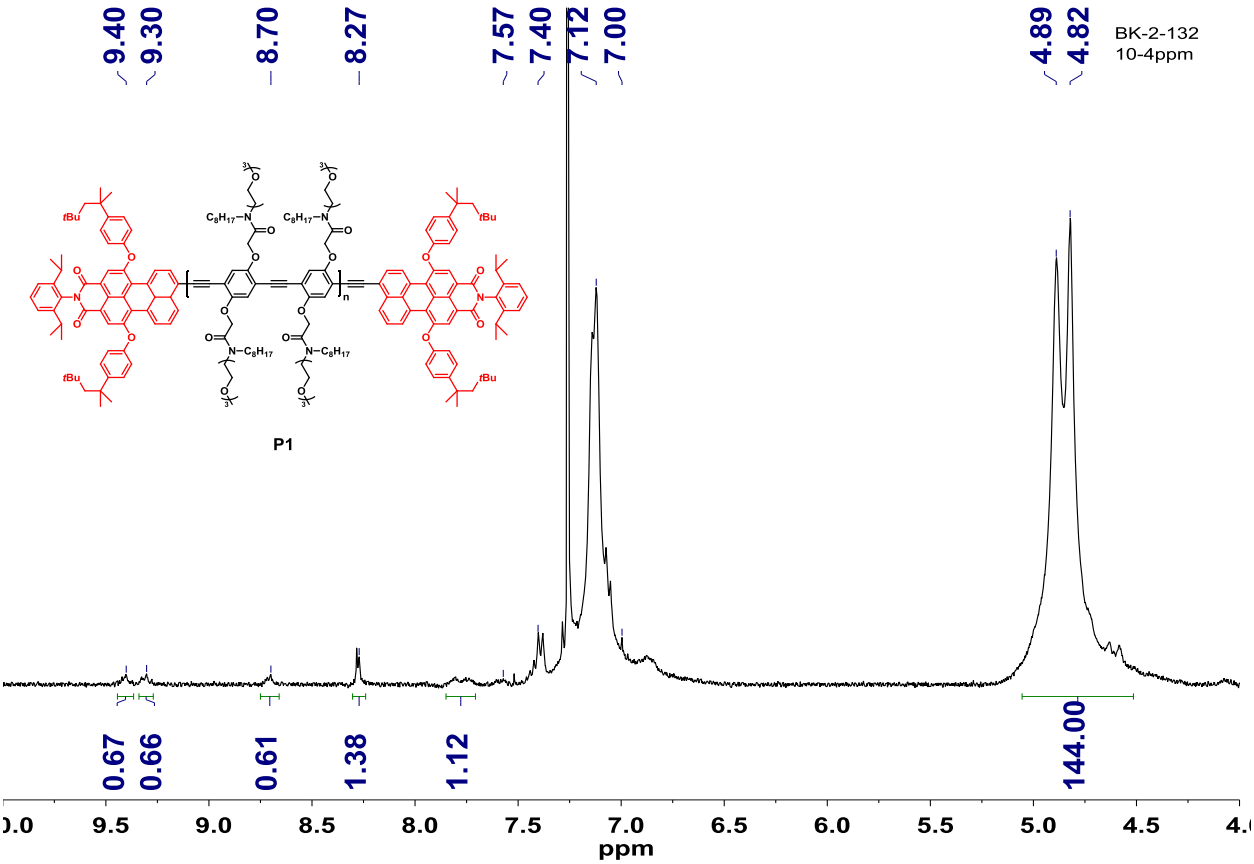

Figure 3.3. Partial NMR spectrum of **P1**. Full spectrum is shown in the Chapter 3.6.

chain has an average of 0.69 **Perylene-1** or about one for every 26 repeating units. The lowered incorporation of **Perylene-1** can be attributed to homocouplings between two **Perylene-1** (confirmed by preparative GPC), or the fact that the Ar-PdX endgroups decompose prior to coupling with **Perylene-1**. Assuming that the decomposition was problematic, we shortened the polymerization time before adding **Perylene-1**. However, the lowered polymerization times did not show increased endgroup incorporation (condition 2 in Figure 3.4). Combining the monomers and endgroups at the same time (condition 3 in Figure 3.4) was also ineffective and oligomers with endcaps were removed during the work-up. As a consequence this latter one-step strategy produced polymers with fewer endgroups. It is also important to note that the small integrations

(a)

Cond'n	Polymerization time before end-group	M2 Added (equiv)	End-group Added (%)	Mn	DP	End-group per repeat unit	End-group per chain (max. 2)
1	**27** h (65-75 °C)	1.05	15% (stoic. 10%)	27 kDa	17.7	0.038	**0.69**
2	**2** h (65 °C)	1.01	10% (stoic. 2%)	5.1 kDa	3.3	0.042	**0.14**
3	**0** h (65 °C)	1.01	3% (stoic. 2%)	11 kDa	7.2	0.026	**0.19**

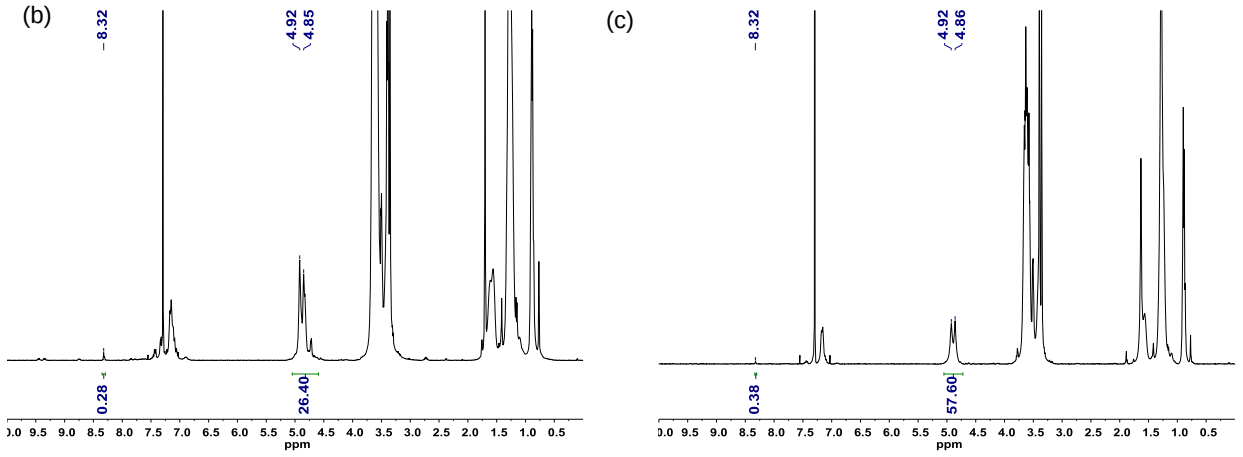

Figure 3.4. (a) Different polymerization conditions to optimize the extent of end-group incorporation. (b) NMR spectrum from condition 2. (c) NMR spectrum from condition 3. We attempted different polymerization conditions to optimize the extent of end-group (**Perylene-1**) incorporation. The condition 1 is described in Figure 3.2, synthesizing **P1**. In condition 2 and 3, we shortened the polymerization time before adding **Perylene-1**. In the "End-group Added (%)" column, the stoichiometric amount (abbreviated as stoic.) means the mol% of **Perylene-1** needed by considering the theoretical degree of polymerization (DP). 15 mol% in Condition 1 therefore means that 1.5 times more of Perylene-1 was added. In all conditions, the excess amounts of endgroups are added. The end-groups per chain are indicated in the last column. The NMR spectra of the polymers synthesized from the condition 2 and 3 are shown in (b) and (c), respectively.

of the NMR introduce errors and the n is perhaps overestimated in rigid-rod polymers[18] (the GPC calibrated with polystyrene). Although the endcapping reaction is not perfect, as will become apparent (vide infra) the concentration of the perylene endgroups is sufficient for our applications.

3.2.2 Pressure-Area Isotherms and Photophysics

The absorption and emission spectra of **P1** in solution and thin films are shown in Figure 3.2b. The absorption spectrum in spin-coated films is red-shifted relative to that of solution, reflecting increased planarization of the backbone in the solid state. We observe larger differences in emission between solution and thin films. In solution, the emission primarily originates from the backbone at 469 nm ($I_{backbone}$: I_{endcap} = 1 : 0.24), whereas in thin films the red endgroup emission at 615 nm is dominant ($I_{backbone}$: I_{endcap} = 1 : 7.1). The 30-fold increase in the relative endgroup emission intensity is not necessarily the result of higher exciton diffusion lengths in the solid state for this case. The analysis is complicated by the fact that the quantum yield of the thin films is 2.7%, which is substantially decreased from its solution quantum yield, 72%.[19] This decrease is likely the result of the lack of organization and thus inevitable cofacial contacts between polymer backbones or endgroup-polymer contacts, resulting in aggregation-induced quenching. The perylene endgroups are known to have near unity quantum yields in solution, so the reduced quantum yield is not the result of intrinsic photophysical properties.

We investigated **P1** monolayers over multiple compression-expansion cycles at the air-water interface on Langmuir trough. Previous studies revealed that conformations of surfactant-type PPEs deposited at the air-water interface include face-on, incline-stack, zipper, and edge-on organi-zations.[17,20] Additionally, the recently identified incline-stack assembly shows emissive aggregates with weak π-π overlap that can form bright excimers,[17] facilitating energy transfer studies in the aggregated state. The pressure-area isotherm and in situ absorption and emission spectra of **P1** monolayers are displayed in Figure 3.5. From the pressure-area isotherm, the extrapolated area to 0 mN/m is estimated to be ca. 150 $Å^2$ per one Ph-CC unit (half of repeat unit), corresponding to the typical face-on conformation in the uncompressed state.[20] We observed an

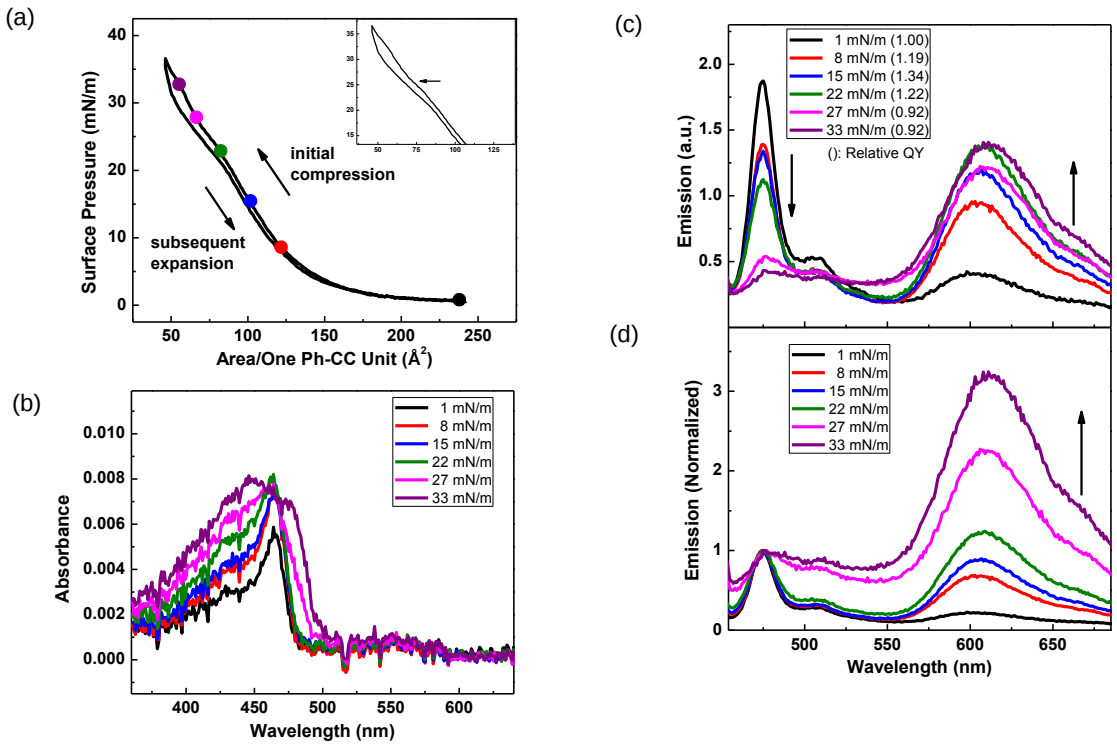

Figure 3.5. (a) Pressure-area isotherm of **P1**. The extrapolated area per one Ph-CC unit is ca. 150 Å^2, indicative of face-on conformation below 25 mN/m. The inflection point at 25 mN/m (the arrow in inset) indicates the transition from face-on to incline-stack conformation. (b) In situ absorption spectra of **P1**. A new peak (planarization) at 477 nm is observed above 25 mN/m. (c) In situ emission spectra (raw data) of **P1** and (d) its normalized spectra. The varying relative intensity of backbone to perylene depending on the surface pressure suggests **P1** as an interfacial pressure indicator.

inflection point at 25 mN/m, which indicates the transformation from face-on to incline-stack assembly. The in situ absorption spectra show the emergence of the red-shifted peak (~477 nm at > 25 mN/m) associated with a more ordered polymer backbone, which was also observed in the polymer lacking endgroups.[17] At 1 mN/m, the emission intensity from the perylene is minor (Figure 3.5c and 3.5d, black curve), and this feature increases dramatically upon compression (8–22 mN/m). The relative quantum yields increased by ca. 20–35% upon increasing the pressure, which could be attributed to facile intra- and inter-chain energy transfer. Above 25 mN/m, the

polymer has incline-stack conformation and broad excimer bands at 500-650 nm, which potentially are a radiative decay pathway in competition with energy transfer to the perylene endgroups. The relative quantum yields in highly compressed states are maintained as compared to films at 1 mN/m (parentheses in Figure 3.5c) as a result of the absence of cofacial π-π stacking.[17] Overall, the fluorescence spectra varying from 1 mN/m to 33 mN/m are similar to the that obtained solution and thin films, respectively (Figure 3.2b). However, the relative quantum yields are largely constant at the air-water interface due to the organization. Figure 3.5d shows the varying red emissions as a function of surface pressure, relative to the polymer backbone emissions at 475 nm. This behavior constitutes a fluorescence-based ratiometric interfacial pressure indicator.

3.2.3 Exciton Migration in Lytropic Liquid Crystals (LLCs)

This energy transfer scheme with dual-color photoluminescence at the air-water interface can also be applied to micelle(hydrophobic)-water interface in aqueous solution. Localization of surfactant fluorescent polymers/molecules at cell-like environments (lipid bilayers) is central to many biological imaging applications with visible[21,22] and near-infrared emission.[23] As a proof-of-concept, we fabricated nonspherical anisotropic micelles (lyotropic liquid crystals, or LLCs) composed of water/potassium dodecanate/1-decanol according to the literature procedure.[24] We have previously found that structurally similar surfactant polymers without endgroups showed the localization and planarization at the micelle-water interface in LLCs.[25] Based upon our results at the air-water interface, we expect that changes in the interfacial density of **P1** chains in the micelle will modulate the interpolymer distance (Figure 3.6a) and produce changes in the polymer-to-endgroup fluorescence signals. The absorption spectra in Figure 3.6b display largely red-shifted sharp peak at 468 nm, indicative of highly planar and rigid conformation at the micelle-water interface. This red-shifted absorption is comparable to the LB experiments (464 nm). The emission

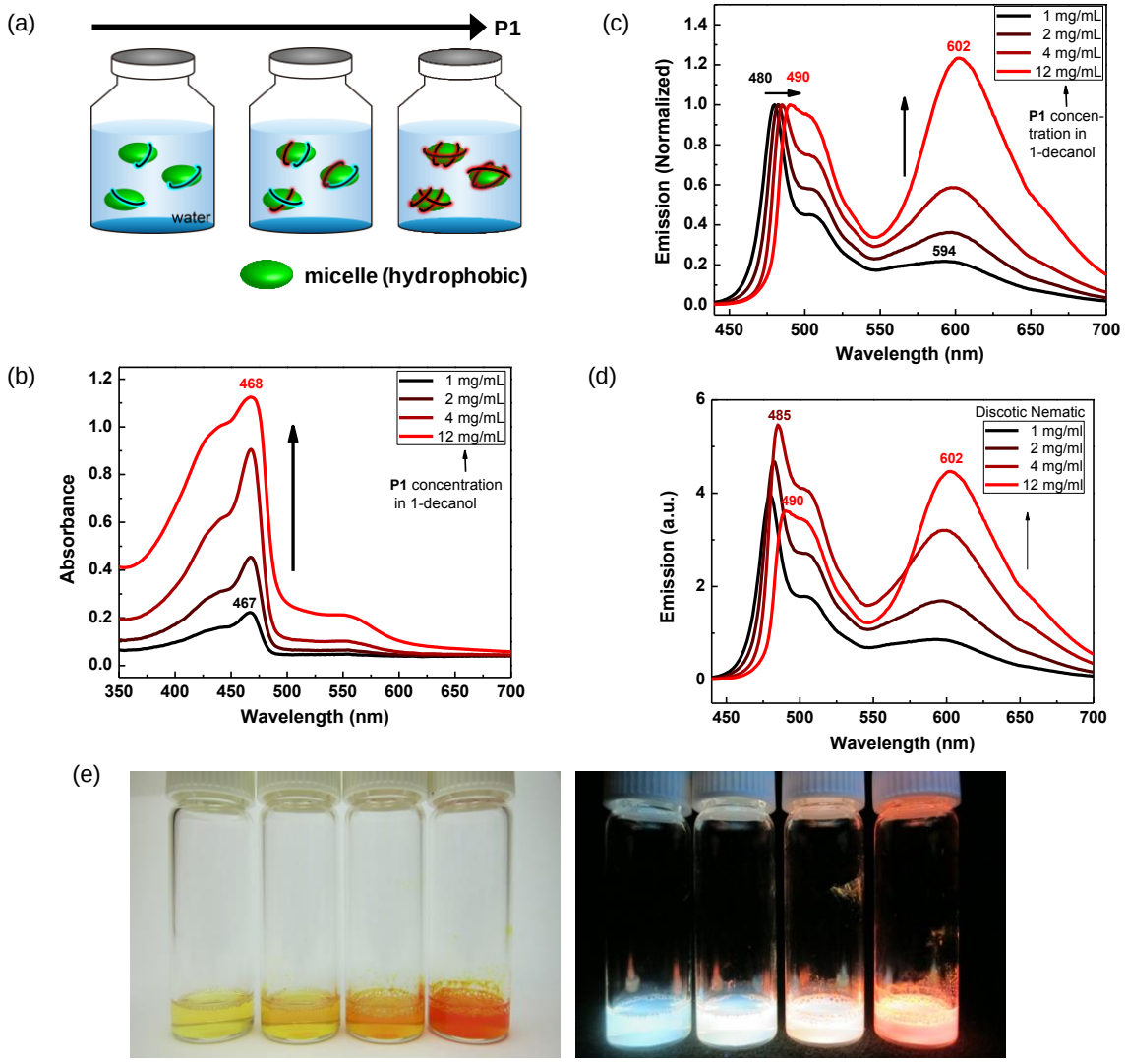

Figure 3.6. (a) Schemes of energy transfer in aqueous solution. More polymers are localized at the micelle-water interface with the increased **P1** concentration, resulting in enhanced energy transfer to perylene. (b) Absorption and (c: normalized; d: raw) emission spectra of LLCs with different concentrations of **P1**. Planarization of the polymers at the micelle-water interface results in the red-shifted sharp absorption shapes with clear vibronic transitions. Owing to energy transfer, the relative perylene emission is enhanced. (e) The LLC solutions are transparent (left) and their fluorescence is highly emissive with varying colors (right).

spectra shown in Figure 3.6c (normalized) and Figure 3.6d (raw) exhibit the backbone emission maximum at 480–490 nm, which is similarly red-shifted from those obtained in solution (469 nm)

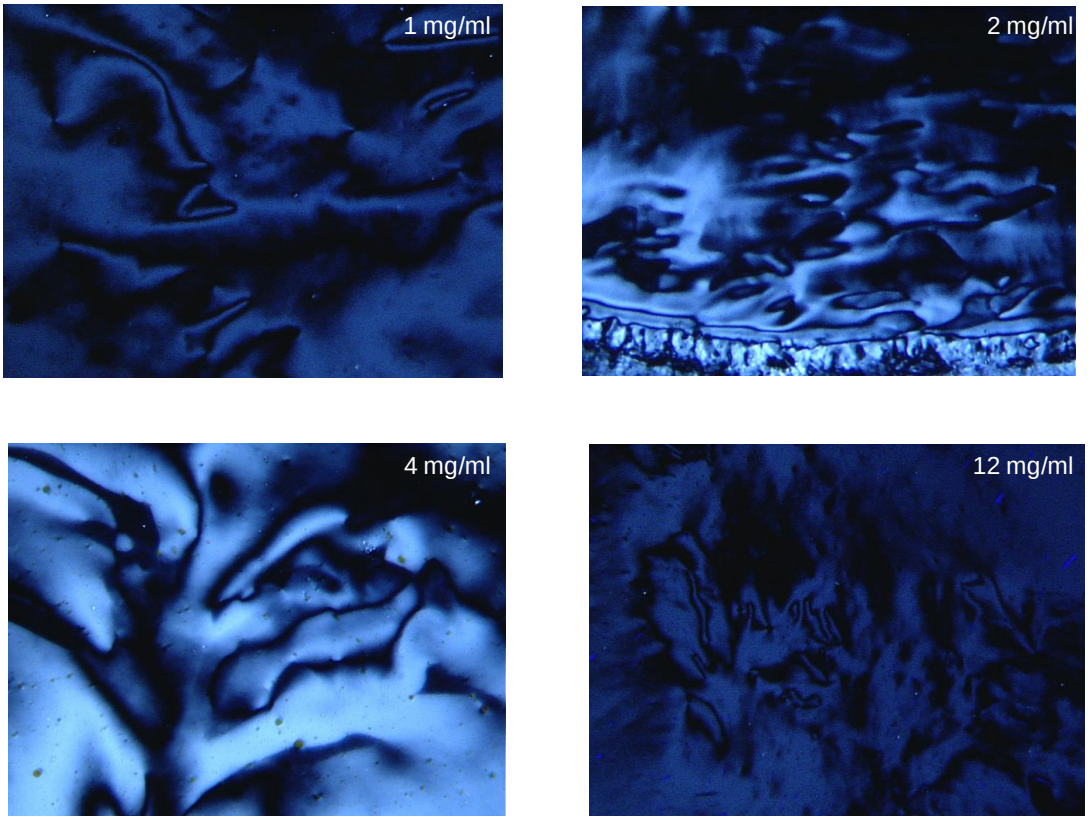

Figure 3.7. Images of lyotropic liquid crystals under an optical microscope with cross-polarizers.

and thin film (477 nm), and are even slightly lower energy than that obtained in the LB monolayers (475 nm). With increasing **P1** concentrations, we observe a concurrent increase in the red emission, demonstrating enhanced energy transfer to the perylene endgroup. Observation of the LLCs with an optical microscope equipped with cross-polarizers (Figure 3.7) gives optical textures characteristic of a nematic phase. The aqueous solutions of all concentrations are relatively transparent (Figure 3.6e, left) and their fluorescence is highly emissive with varying colors from cyan to red (Figure 3.6e, right). We also note that the **P1** appears to have some aggregation-induced quenching in these experiments with 12 mg/mL having a relative quantum yield 32% of the 1 mg/mL LLC compositions.

3.2.4 Mechanism Studies on Exciton Migration

The fundamental of this pressure indicator is based on the energy transfer process, and it is of primary interest to consider whether intra- or interchain energy transfer is facile upon applied surface pressure. However, disclosing which mechanism is dominant is not an easy task. Instead of providing firm conclusions, a few possible experiments and data analysis will be attempted as a future contribution in this field. We design an experiment outlined in Figure 3.8. The key objective in the experiment is to systematically vary the number of perylene end-caps in the Langmuir monolayer with the constant number of polymer chains by mixing **P1** with a homopolymer without end-groups (M_n = 33 kDa, Đ 1.40) and to monitor the relative emission intensity of the perylene to the backbone. Qualitatively speaking, if the interchain energy transfer is efficient, excitons generated at the backbone would like to visit different segments on the

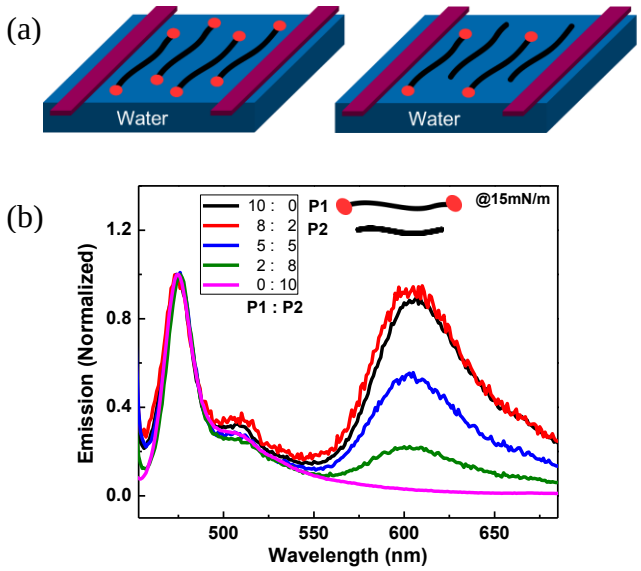

Figure 3.8. (a) The experimental design to distinguish intra- and interchain energy transfer. The number of the perylene end-caps is systematically varied; for example, the left and right schemes exhibit the monolayers composed only from **P1** (black curve in Figure 3.8b) and from **P1** : **P2** = 1 : 1 (blue curve in Figure 3.8b), respectively. (b) Comparison of emission spectra at 15 mN/m. Overall, the decrease in the number of end-groups shows the lower end-group emission, indicative of efficient intrachain and relatively inefficient interchain energy transfer.

monolayers to effectively find the low-energy sites, and the red emission intensity would still be comparable to the high amount of end-groups. In contrast, if interchain energy transfer is not efficient and intrachain energy transfer is facile, the red emission would be largely dependent on the number of red end-groups. Note that in this experimental design, it is assumed that the number of excitons generated on the backbone are identical. With this plan, Langmuir monolayers composed of the varying amount of end-groups are deposited from the mixture solution of **P1** and homopolymer of **P1** without end-groups (referred as **P2** herein). Figure 3.8b exhibits the normalized emission of the monolayers at 15 mN/m. The interchain distance at this pressure is about 15.5 Å, based on the area per repeat units of 102 $Å^2$ divided by the calculated repeat unit length (-PhCC-) of 6.6 Å. The interchain distance of 15.5 Å is close enough for the Förster energy transfer to occur since the typical Förster radius of most organic molecules is 20–60 Å.[10] The black and pink curves in Figure 3.8b are obtained from the monolayers made purely from the solution of **P1** and **P2**, respectively. The red, blue, and green curves are emission of monolayers deposited from the mixture of **P1** : **P2** = 8 : 2, 5 : 5, and 2 : 8, respectively. Although there might be some miniscule interchain energy transfer from the comparable emission intensity between black and red curves, overall, it is found that the red emission is highly dependent on the number of end-groups, indicative of relatively inefficient interchain energy transfer. Again, note that we cannot exclude efficient interpolymer energy transfer by considering black and red curves in Figure 3.8b. Therefore, it is concluded that the enhanced energy transfer with improved quantum yields could be attributed to the facile intra-chain energy transfer, presumably resulting from the enhanced wavefunction overlap in the Dexter energy transfer upon compression of monolayers. Previously, improved Dexter process with increased quantum yields was reported upon the planarization of

the PPE backbone in the liquid crystalline solution,[30] and analogous underlying physics could operate in the monolayers.

3.3 Conclusions

We synthesize surfactant PPEs endcapped with perylene monoimide which show dual emission colors (cyan/red) depending on the applied surface pressure in Langmuir monolayers, creating an interfacial pressure indicator. The enhanced energy transfer may originate from both intrachain (planarization) and interchain (3D) exciton migration, where both Förster and Dexter mechanism take effect. However, the mechanism studies imply that intrachain exciton migration may be more effective in this case. Application of the energy transfer scheme at the micelle-water interface in aqueous solution is demonstrated, significantly expanding the potential applications of the dual-fluorescent surfactant polymer probes in biosensors and bioimaging.

3.4 Experimental Details

3.4.1 General

Chemicals were purchased from Aldrich, Alfa Aesar, and TCI America without further purification unless noted otherwise. All reactions were carried out under argon with standard Schlenk techniques. Monomer **M1** and **M2** were synthesized by following the literature procedures or slight modifications thereof.[25] All ^{1}H NMR and ^{13}C NMR spectra are reported in ppm on a Bruker Avance-400. ^{1}H NMR is referenced to a chloroform peak (δ = 7.26 ppm). The multiplicity is reported as follows: s = singlet, d = doublet, dd = doublet of doublet, t = triplet, m = multiplet or unresolved, br = broad. Coupling constants J are reported in Hz. ^{13}C NMR is referenced to a chloroform peak (δ = 77.16 ppm). High-resolution mass spectra (HRMS) were obtained at the MIT

DCIF (Department of Chemistry Instrumentation Facility) using electrospray ionization (ESI) or direct analysis in real time (DART).

THF Gel Permeation Chromatography (GPC) was performed with a concentration of 0.5 mg/ml on an Agilent 1260 Infinity system equipped with three PLgel columns (10^3, 10^4, 10^5 Å) in series, calibrated with monodisperse polystyrene standards. UV-vis spectra were recorded on Agilent Cary 4000 spectrometer at room temperature. Fluorescence measurements were performed at room temperature with a Horiba Jobin Yvon SPEX Fluorolog-τ3 fluorimeter (model FL-321, 450 W Xenon lamp) using right-angle conformation for solution and Langmuir monolayers and front-face conformation for thin films. For sample preparations of photophysics measurements, the solutions were prepared in chloroform with 10^{-5} M – 10^{-6} M. The solid-state films were prepared on glass by spin-coating 1000–3000 rpm for 60 seconds from the solution in chloroform (1–5 mg/ml) and annealed at 70 °C for 15 min in ambient atmosphere.

The in situ UV/PL measurements on Langmuir monolayers were carried out with fiber optic cables that are connected with the Agilent spectrometer and the Horiba fluorimeter. The Langmuir monolayers were prepared from the polymer in chloroform solution (1 mg/mL) on 102 M trough from NIMA Technology equipped with a fused quartz window, using purified water with > 18 MΩ·cm as subphase. After drying the chloroform for ca. 15 min, the monolayers were mechanically annealed with 3 compression-expansion cycles and then photophysics data were recorded.

Lyotropic liquid crystals with discotic phases are fabricated with the mass ratio of D2O/potassium dodecanate/1-decanol (0.690/0.248/0.062). 1-Decanol dissolves **P1** with different concentrations: 1, 2, 4, and 12 mg/ml. 12 mg/ml is close to the saturation concentration and no higher concentration was attained. After adding D2O/potassium dodecanate/1-decanol to vials, the

mixtures were stirred with the aid of vortex for a few minutes and stabilized for 24 hours, after which all the measurements were taken. For spectroscopic measurements, a fused quartz cell with a narrow optical path (0.1 cm) was used. Absorption spectra were baseline-corrected by the LLC composition without **P1**. LLC textures were obtained by an optical microscope equipped with cross-polarizers. The tiny drops of LLC samples were placed between a microscope glass slide and a thin glass coverslip.

3.4.2 Polymerization for P1

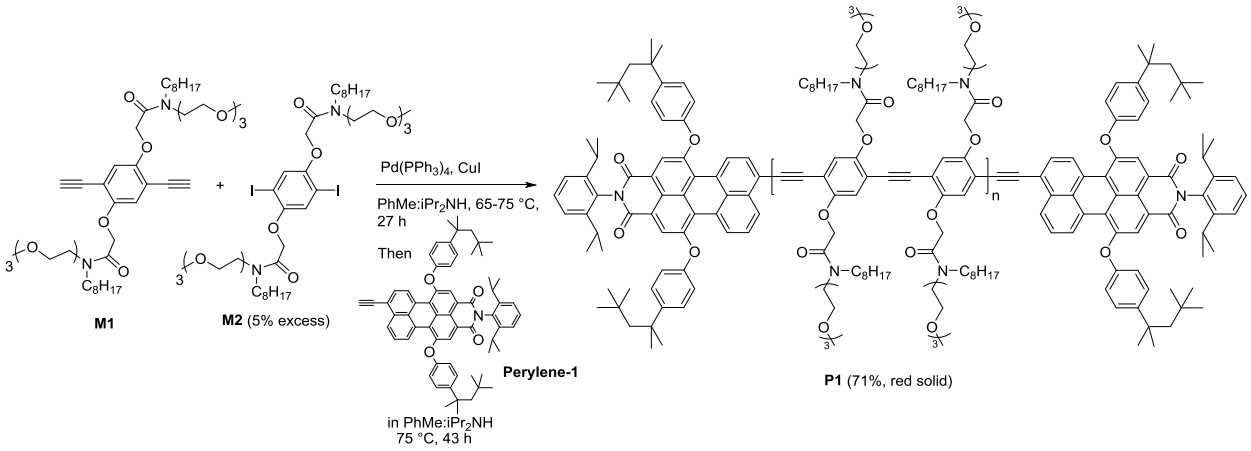

Scheme 3.1. Polymerization procedure for **P1**.

To the flame-dried Schlenk flask, **M1** (79 mg, 0.100 mmol, 1.00 equiv), **M2** (104.4 mg, 0.105 mmol, 1.05 equiv), $Pd(PPh_3)_4$ (5.8 mg, 0.005 mmol, 5 mol%), and CuI (2 mg, 0.010 mmol, 10 mol%) were added. The flask containing reagents was evacuated and back-filled with argon for 5 times. The mixture of dry toluene:diisopropylamine (3:1 v/v) was degassed with nitrogen for 30 min. 4 mL of the mixture was added to the flask. The reaction mixture was stirred for 30 min at room temperature to completely dissolve all the materials, followed by stirring at 65 °C for 11 hours and then at 75 °C for 16 hours. After cooling down to room temperature, **Perylene-1** (13.7 mg, 0.015 mmol, 15 mol%) dissolved in the degassed solvent mixture (toluene:diisopropylamine

3:1 v/v, 1.2 mL) was added, and the reaction mixture was further stirred at 75 °C for 43 hours. The crude mixture was concentrated in vacuo, diluted with DCM, filtered through a short plug (1–2 cm) of silica gel twice. After concentrated in vacuo, the crude mixture was precipitated in DCM/hexane, centrifuged 14,000 rcf for 10 min. Preparative GPC in THF was used to separate high molecular weight fraction of the solid product. The resulting fraction in THF was evaporated under reduced pressure, and further precipitation in DCM/hexane was carried out with the subsequent centrifugation at 14,000 rcf for 10 min. The product was dried in vacuo, affording a red rubbery solid (117 mg, 71 %). ^{1}H NMR (400 MHz, $CDCl_3$) δ 7.14 – 7.12 (br, 4H), 4.89 – 4.82 (br, 8H), 3.61 – 3.31 (br, 68H), 1.59 – 1.53 (br, 8H), 1.36 – 1.10 (br, 40H), 0.90 – 0.80 (br, 12H). Proton numbers only in the repeat unit are indicated. For small end-group peaks and integrations, see Figure 3.3. GPC (THF): Mn = 27 kDa, Đ = 1.38.

3.4.3 Synthesis of Perylene-1

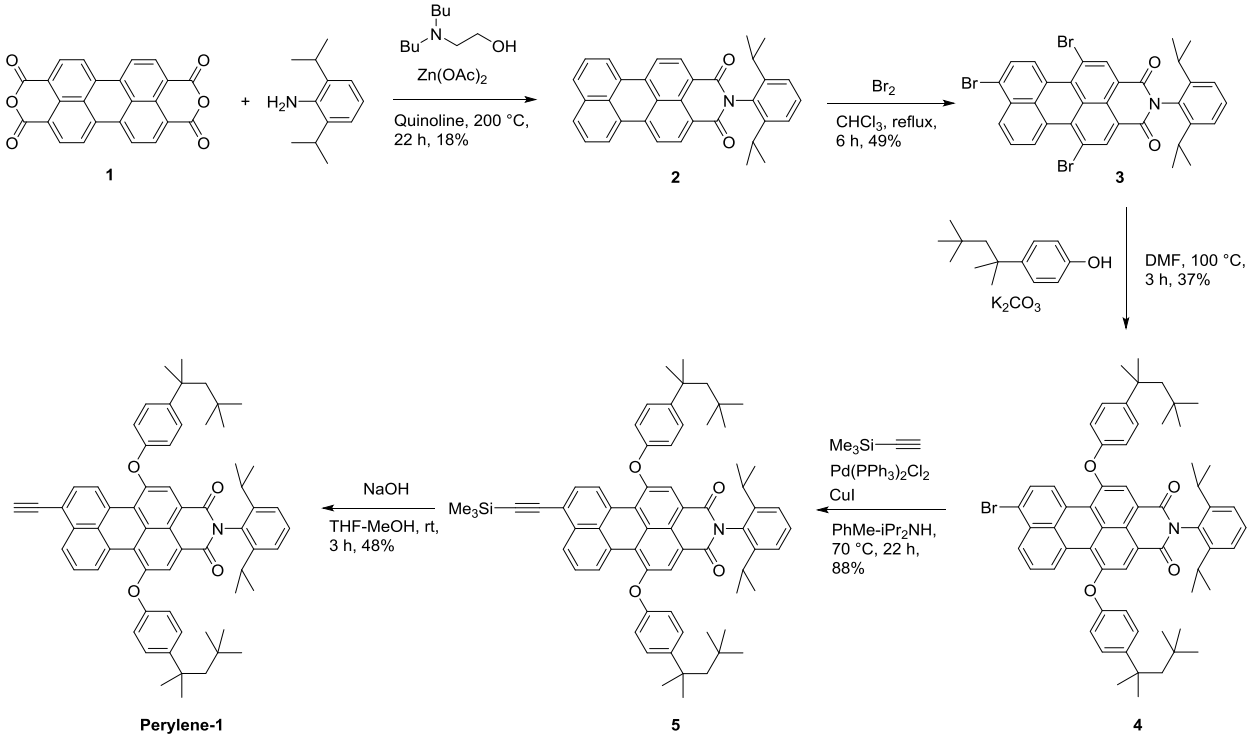

Scheme 3.2. Synthetic procedures for **Perynene-1**.

***N*-(2,6-Diisopropylphenyl)perylene-3,4-dicarboximide (2).** The modified procedure from the literature[26] was carried out. To the flame-dried Schlenk flask, perylene-3,4,9,10-tetracarboxylic dianhydride **1** (1.96 g, 5 mmol, 1 equiv), 2,6-diisopropylaniline (2.83 mL, 15 mmol, 3 equiv), 2-(dibutylamino)ethanol (1.21 mL, 6 mmol, 1.2 equiv), zinc acetate (1.65 g, 9 mmol, 1.8 equiv), and quinolone (7.5 mL) were added. The mixture was stirred at 200 °C for 22 hours. Cooling to room temperature, the mixture was diluted with dichloromethane (DCM), washed with 1.5 M HCl (aq), $NaHCO_3$ (aq), and brine. The organic phase was dried over $MgSO_4$, filtered, and concentrated. The crude material was purified by column chromatography (hexane:EtOAc:DCM = 6:1:0.2 to 3:1:0) and recrystallization in DCM/hexane. 18% yield (440 mg). ^{1}H NMR (400 MHz, $CDCl_3$) δ 8.66 (d, J = 8.1 Hz, 2H), 8.47 (t, J = 7.4 Hz, 4H), 7.93 (d, J = 8.0 Hz, 2H), 7.66 (t, J = 7.8 Hz, 2H), 7.52 – 7.44 (m, 1H), 7.34 (d, J = 7.8 Hz, 2H), 2.83 – 2.71 (m, 2H), 1.18 (d, J = 6.9 Hz, 12H). ^{13}C NMR (101 MHz, $CDCl_3$) δ 164.11, 145.82, 137.58, 134.38, 132.08, 131.20, 131.04, 130.63, 129.57, 129.27, 128.05, 127.14, 127.09, 124.15, 123.92, 121.09, 120.26, 29.31, 24.18. HRMS (ESI) calculated for $C_{34}H_{28}NO_2$ ([M+H]+) 482.2115; found, 482.22.

1,6,9-tribromo-*N*-(2,6-diisopropylphenyl)-perylene-3,4-dicarboximide (3).[27,28] To the flame-dried Schlenk flask, the starting material **2** (440 mg, 0.91 mmol, 1 equiv) was dissolved in chloroform (65 mL). After dropwise addition of bromine (2.6 mL), the reaction mixture was refluxed for 6 hours. Cooling down to room temperature, the reaction was quenched with the addition of sodium thiosulfate (10% aq.) and KOH (10% aq). Organic layer was separated, and the aqueous phase was extracted with chloroform (x3). The combined organic phase was dried over $MgSO_4$, filtered, and concentrated. The crude material was purified by column chromatography (hexane:DCM = 1:1) to obtain bright red solid. 49% yield (320 mg). ^{1}H NMR (400 MHz, $CDCl_3$) δ 9.32 (dd, J = 7.7, 1.0 Hz, 1H), 9.11 (d, J = 8.3 Hz, 1H), 8.93 (d, J = 5.7 Hz, 2H), 8.45 (dd, J =

8.4, 1.0 Hz, 1H), 7.99 (d, J = 8.3 Hz, 1H), 7.80 (t, J = 8.1 Hz, 1H), 7.50 (t, J = 7.8 Hz, 1H), 7.35 (d, J = 7.8 Hz, 2H), 2.77 – 2.64 (m, 2H), 1.18 (d, J = 6.9 Hz, 12H). HRMS (DART) calculated for $C_{34}H_{25}Br_3NO_2$ ([M+H]+) 719.9389; found, 719.95.

9-Bromo-1,6-bis(4-(2,4,4-trimethylpentan-2-yl)phenoxy)-*N*-(2,6-diisopropylphenyl)-perylene-3,4-dicarboximide (4).[29] To the Schlenk flask containing the starting material **3** (320 mg, 0.45 mmol, 1 equiv), 4-(2,4,4-trimethylpentan-2-yl)phenol (193 mg, 2.1 equiv), K_2CO_3 (493 mg, 8 equiv) were added. After three cycles of vacuum-argon exchange, DMF (10 mL) was added. The reaction mixture was stirred at 100 °C for 3 hours. Cooing down to room temperature, the mixture was quenched by 1.5 M HCl (aq), extracted with EtOAc. The combined organic phase was washed with brine, dried over $MgSO_4$, and concentrated. The crude material was purified by column chromatography (hexane:EtOAc = 50:1 to 40:1) and the second column chromatography (hexane:DCM = 4:1) to obtain red solid. 37% yield (161 mg). ^{1}H NMR (400 MHz, $CDCl_3$) δ 9.39 (dd, J = 7.9, 1.1 Hz, 1H), 9.15 (d, J = 8.5 Hz, 1H), 8.35 (dd, J = 8.4, 1.1 Hz, 1H), 8.30 (d, J = 4.9 Hz, 2H), 7.88 (d, J = 8.5 Hz, 1H), 7.69 (t, J = 8.1 Hz, 1H), 7.44 (t, J = 7.8 Hz, 1H), 7.39 (d, J = 8.0 Hz, 4H), 7.29 (d, J = 7.8 Hz, 2H), 7.08 – 7.01 (m, 4H), 2.77 – 2.65 (m, 2H), 1.38 (s, 4H), 1.13 (d, J = 6.9 Hz, 12H), 0.89 (s, 30H). HRMS (ESI) calculated for $C_{62}H_{67}BrNO_4$ ([M+H]+) 970.4228; found, 970.44.

9-Trimethylsilylethynyl-1,6-bis(4-(2,4,4-trimethylpentan-2-yl)phenoxy)-*N*-(2,6-diisopropylphenyl)-perylene-3,4-dicarboximide (5).[29] To the Schlenk flask, the starting material **4** (161 mg, 0.166 mmol, 1 equiv), $Pd(PPh_3)_2Cl_2$ (5.8 mg, 0.0083 mmol, 5 mol%), CuI (1.6 mg, 0.0083 mmol, 5 mol%) were added. The mixture underwent three vacuum-argon exchange cycles. Toluene:diisopropylamine (3:1 v/v) mixture was degassed under nitrogen bubbling for 30 min and 2 mL of the mixture was added to the flask. Then ethynyltrimethylsilane (0.052 mL, 2.2 equiv)

was injected. The mixture was stirred at 70 °C for 20 hours. The crude mixture was concentrated in vacuo and purified by column chromatography (hexane:EtOAc = 30:1 to 20:1) to obtain red solid. 88% yield (145 mg). ^{1}H NMR (400 MHz, $CDCl_3$) δ 9.38 (dd, J = 7.9, 1.2 Hz, 1H), 9.24 (d, J = 8.2 Hz, 1H), 8.46 (dd, J = 8.2, 1.1 Hz, 1H), 8.30 (d, J = 1.7 Hz, 2H), 7.77 (d, J = 8.2 Hz, 1H), 7.68 (t, J = 8.1 Hz, 1H), 7.44 (t, J = 7.8 Hz, 1H), 7.41 – 7.35 (m, 4H), 7.29 (d, J = 7.8 Hz, 2H), 7.08 – 7.01 (m, 4H), 2.77 – 2.64 (m, 2H), 1.72 (two singlets, 4H), 1.38 (two singlets, 12H), 1.14 (d, J = 6.8 Hz, 12H), 0.73 (two singlets, 18H), 0.35 (s, 9H). ^{13}C NMR (101 MHz, $CDCl_3$) δ 163.22, 154.05, 154.00, 153.35, 153.30, 146.49, 146.43, 145.78, 133.58, 131.78, 131.59, 130.86, 129.58, 129.27, 128.63, 128.33, 128.05, 128.00, 127.51, 126.85, 124.52, 124.10, 123.20, 122.78, 122.03, 121.79, 118.45, 118.25, 103.16, 102.58, 57.30, 38.48, 32.53, 31.91, 31.63, 29.23, 24.13, 0.20. HRMS (ESI) calculated for $C_{67}H_{76}NO_4Si$ ([M+H]+) 986.5538; found, 986.58.

9-Ethynyl-1,6-bis(4-(2,4,4-trimethylpentan-2-yl)phenoxy)-*N*-(2,6-diisopropylphenyl)-perylene-3,4-dicarboximide (Perylene-1).[29] To the flask containing starting material **5** (145 mg, 0.147 mmol, 1 equiv), THF (4 mL, degassed with nitrogen for 30 min) and NaOH (50 mg in 0.5 mL of methanol) were added. The mixture was stirred at room temperature for 3 hours. The crude mixture was poured into saturated NH_4Cl (aq), extracted with DCM. The organic phase was dried over $MgSO_4$, concentrated, and purified by column chromatography (hexane:DCM = 3:1 to 2:1) to obtain red solid. 48% yield (64 mg). ^{1}H NMR (400 MHz, $CDCl_3$) δ 9.38 (dd, J = 7.8, 1.1 Hz, 1H), 9.26 (d, J = 8.2 Hz, 1H), 8.46 (dd, J = 8.3, 1.1 Hz, 1H), 8.30 (d, J = 4.5 Hz, 2H), 7.80 (d, J = 8.2 Hz, 1H), 7.67 (t, J = 8.1 Hz, 1H), 7.44 (t, J = 7.8 Hz, 1H), 7.42 – 7.37 (m, 4H), 7.30 (d, J = 7.7 Hz, 2H), 7.09 – 7.03 (m, 4H), 3.61 (s, 1H), 2.77 – 2.67 (m, 2H), 1.73 (s, 4H), 1.39 (s, 12H), 1.14 (d, J = 6.8 Hz, 12H), 0.74 (s, 18H). ^{13}C NMR (101 MHz, $CDCl_3$) δ 163.21, 154.28, 154.06, 153.31, 153.23, 146.59, 146.52, 145.77, 133.73, 131.93, 131.77, 130.83, 129.59,

129.33, 129.27, 128.72, 128.36, 128.10, 128.08, 128.06, 127.87, 127.60, 126.93, 126.51, 124.47, 124.30, 124.11, 123.09, 122.16, 121.87, 121.67, 118.45, 84.40, 81.93, 57.30, 38.49, 32.53, 31.91, 31.63, 29.23, 24.14. HRMS (ESI) calculated for $C_{64}H_{68}NO_4$ ([M+H]+) 914.5143; found, 914.5159.

3.5 References

(1) Thomas, S. W.; Joly, G. D.; Swager, T. M. *Chem. Rev.* **2007**, 107, 1339.

(2) Grimsdale, A. C.; Leok Chan, K.; Martin, R. E.; Jokisz, P. G.; Holmes, A. B. *Chem. Rev.* **2009**, 109, 897.

(3) Facchetti, A. *Chem. Mater.* **2011**, 23, 733.

(4) Guo, X.; Baumgarten, M.; Müllen, K. *Prog. Polym. Sci.* **2013**, 38, 1832.

(5) Rochat, S.; Swager, T. M. *ACS Appl. Mater. Interfaces* **2013**, 5, 4488.

(6) Huang, Y.; Kramer, E. J.; Heeger, A. J.; Bazan, G. C. *Chem. Rev.* **2014**, 114, 7006.

(7) McQuade, D. T.; Pullen, A. E.; Swager, T. M. *Chem. Rev.* **2000**, 100, 2537.

(8) Swager, T. M.; Gil, C. J.; Wrighton, M. S. *J. Phys. Chem.* **1995**, 99, 4886.

(9) Zhou, Q.; Swager, T. M. *J. Am. Chem. Soc.* **1995**, 117, 12593.

(10) Andrew, T. L.; Swager, T. M. *J. Polym. Sci. B Polym. Phys.* **2011**, 49, 476.

(11) Levitsky, I. A.; Kim, J.; Swager, T. M. *J. Am. Chem. Soc.* **1999**, 121, 1466.

(12) Kim, J.; McQuade, D. T.; Rose, A.; Zhu, Z.; Swager, T. M. *J. Am. Chem. Soc.* **2001**, 123, 11488.

(13) Yan, M.; Rothberg, L. J.; Kwock, E. W.; Miller, T. M. *Phys. Rev. Lett.* **1995**, 75, 1992.

(14) Kim, J. *Pure Appl. Chem.* **2002**, 74, 2031.

(15) Kim, J.; McQuade, D. T.; McHugh, S. K.; Swager, T. M. *Angew. Chem. Int. Ed.* **2000**, 39, 3868.

(16) Satrijo, A.; Swager, T. M. *J. Am. Chem. Soc.* **2007**, 129, 16020.

(17) Koo, B.; Swager, T. M. *ACS Macro Lett.* **2016**, 5, 889.

(18) Bunz, U. H. F. *Chem. Rev.* **2000**, 100, 1605.

(19) The quantum yields (QYs) of thin films and solution are calculated from 9,10-diphenylanthracene in PMMA (QY = 83%) and coumarin 6 in ethanol (QY = 78%), respectively.

(20) Kim, J.; Swager, T. M. *Nature* **2001**, 411, 1030.

(21) Herland, A.; Inganäs, O. *Macromol. Rapid Commun.* **2007**, 28, 1703.

(22) Terai, T.; Nagano, T. *Curr. Opin. Chem. Biol.* **2008**, 12, 515.

(23) Guo, Z.; Park, S.; Yoon, J.; Shin, I. *Chem. Soc. Rev.* **2014**, 43, 16.

(24) Hendrikx, V.; Charvolin, J.; Rawiso, M.; Liebert, L.; Holmes, M. *J. Phys. Chem.* **1983**, 87, 3991.

(25) Bouffard, J.; Swager, T. M. *Chem. Commun.* **2008**, 5387.

(26) Konemann, M.; Blaschka, P.; Reichelt H. Method for producing perylene-3,4-dicarboxylic acid imides. U.S. Patent, US 20080114170 A1, May 15, **2008**.

(27) Schlichting, P.; Duchscherer, B.; Seisenberger, G.; Basché, T.; Bräuchle, C.; Müllen, K. *Chem. Eur. J.* **1999**, 5, 2388.

(28) Rohr, U.; Kohl, C.; Müllen, K.; van de Craats, A.; Warman, J. *J. Mater. Chem.* **2001**, 11, 1789.

(29) Bouffard, J. Ph.D. Dissertation, Massachusetts Institute of Technology, MA, **2008**.

(30) Nesterov, E. E.; Zhu, Z.; Swager, T. M. *J. Am. Chem. Soc.* **2005**, 127, 10083.

3.6 Appendix for Chapter 3

P1 (^{1}H NMR in $CDCl_3$)

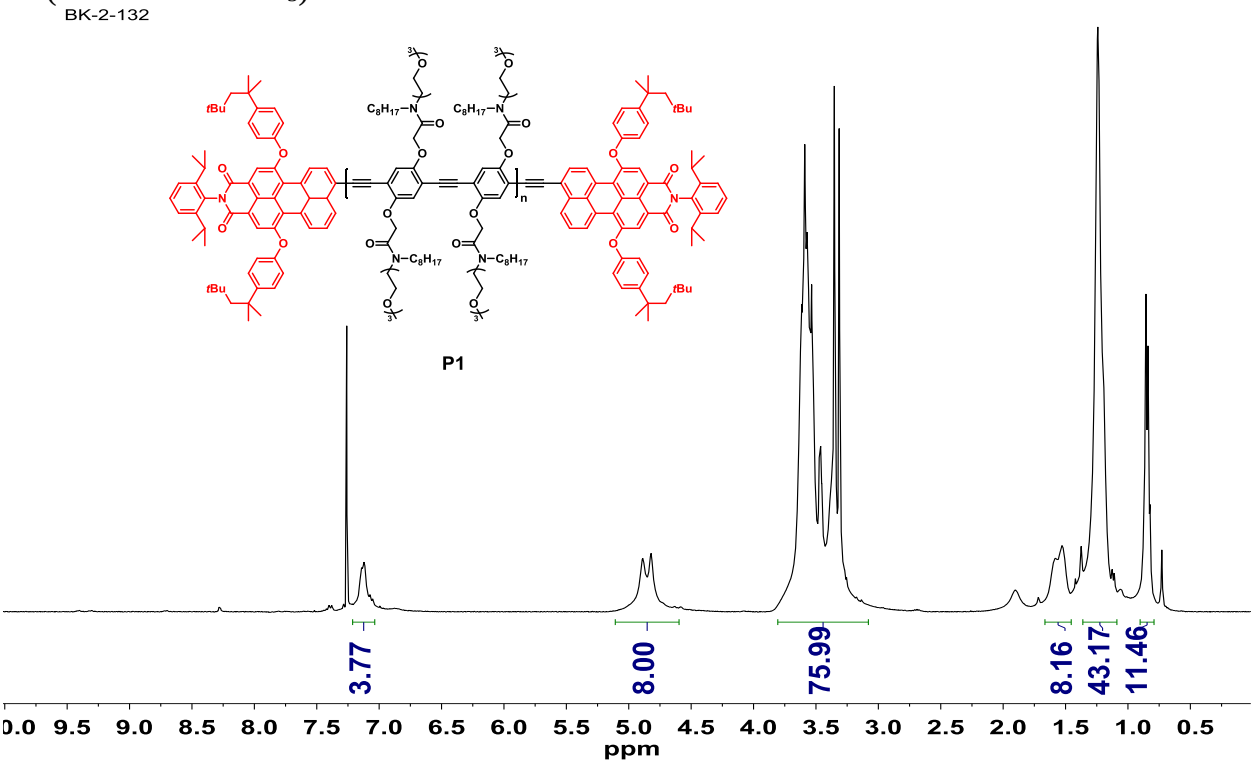

2 (^{1}H NMR in $CDCl_3$)

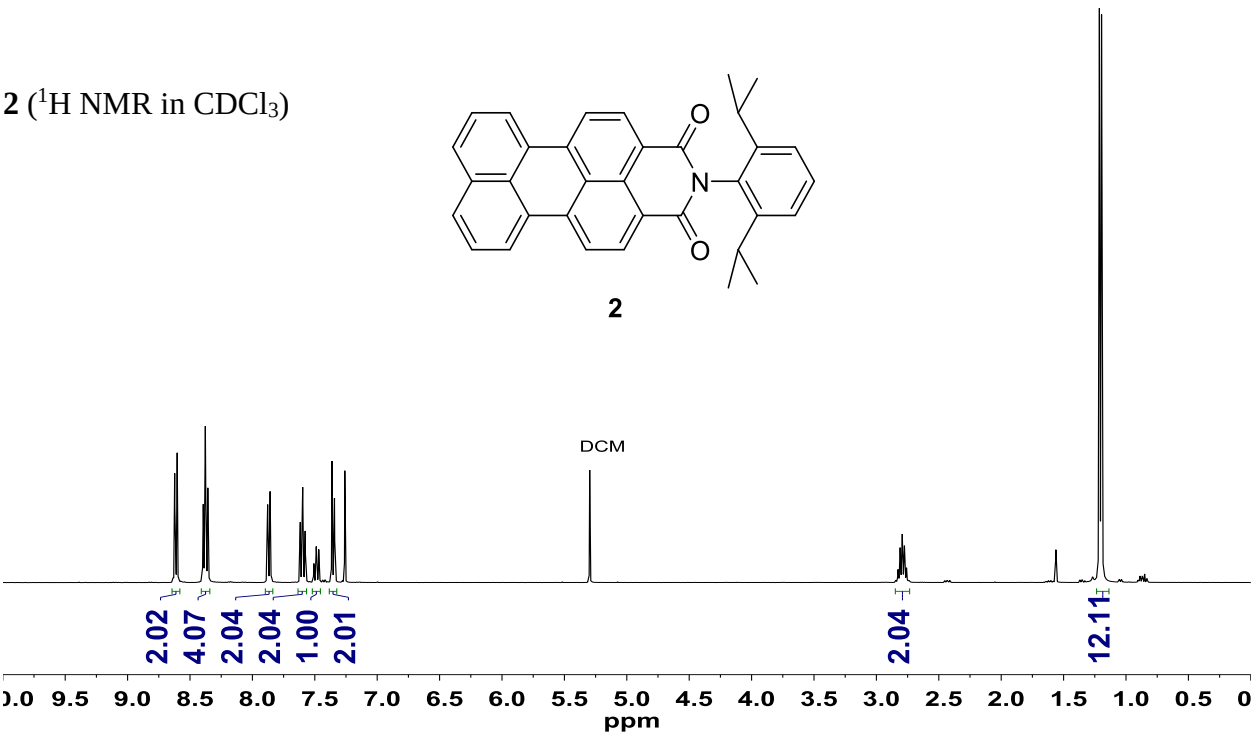

2 (^{13}C NMR in $CDCl_3$)

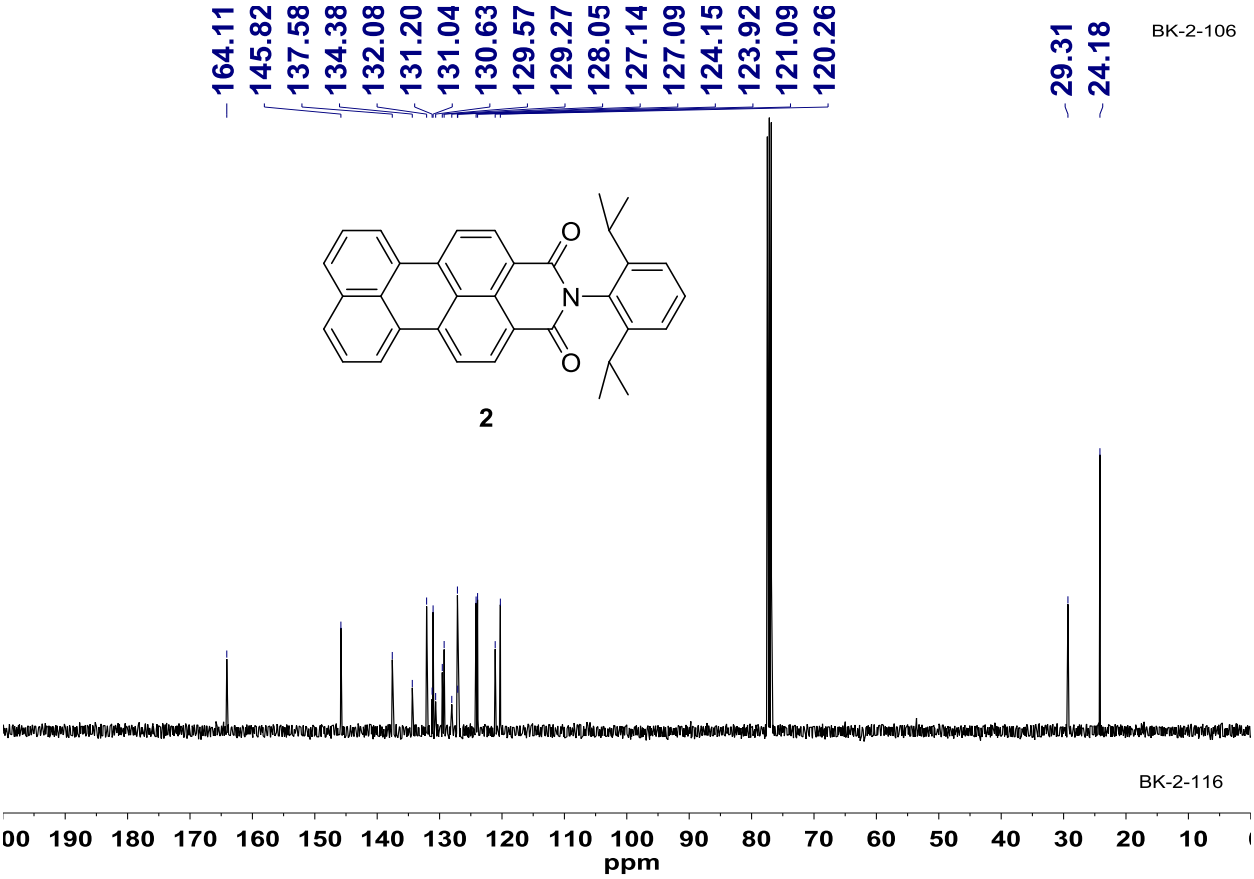

3 (^{1}H NMR in $CDCl_3$)

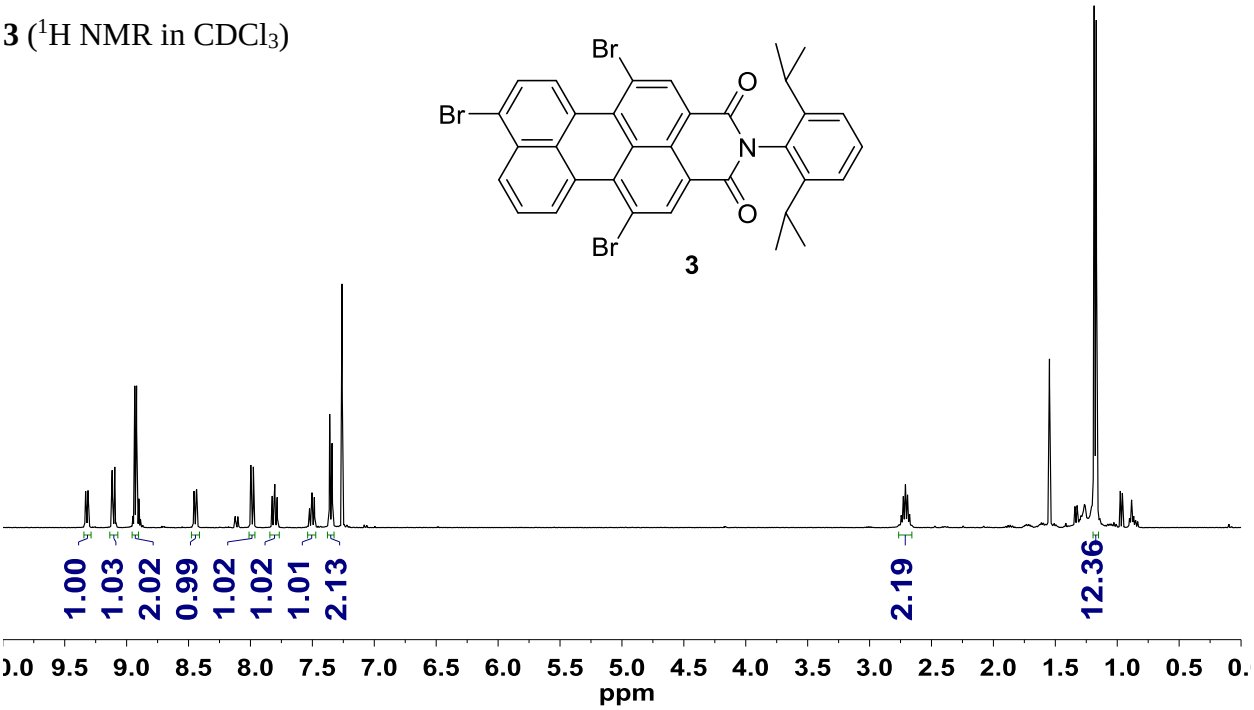

4 (^{1}H NMR in $CDCl_3$)

BK-2-122

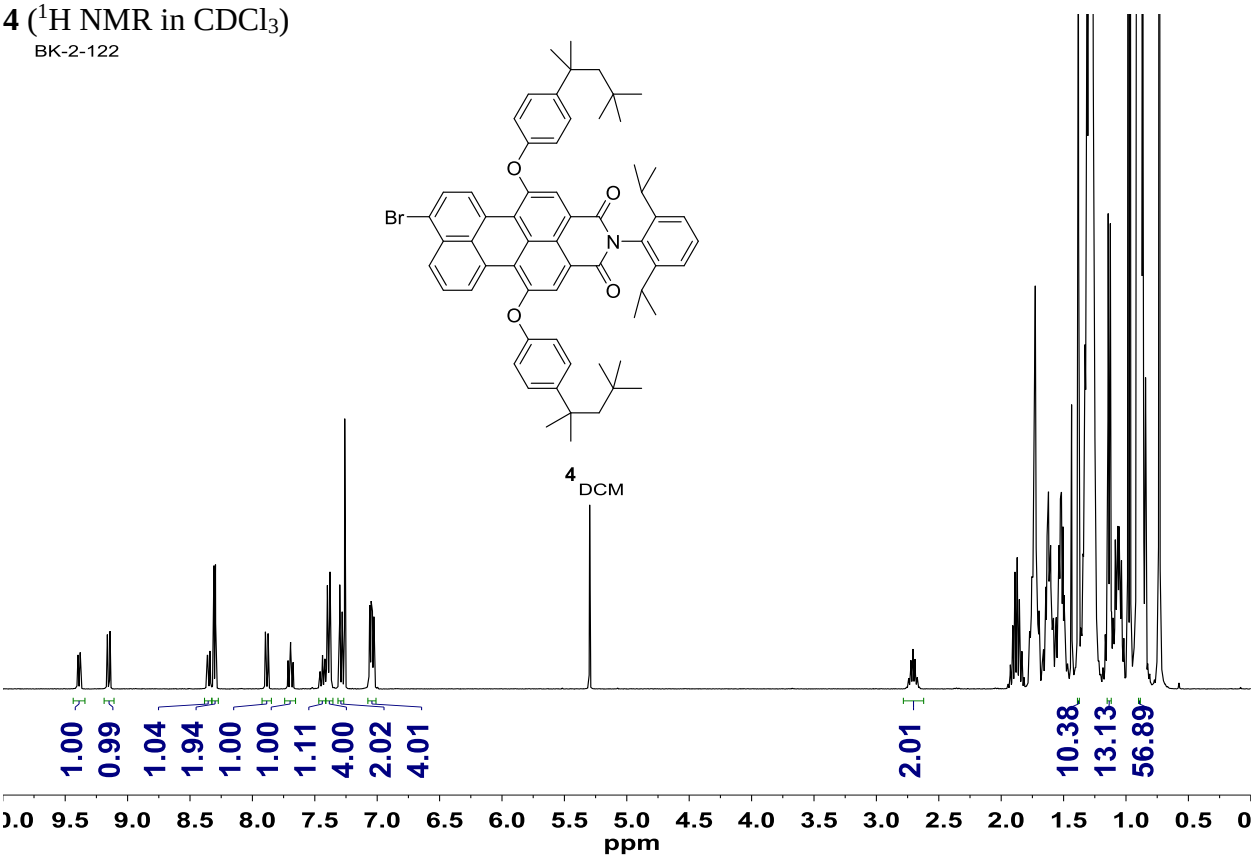

BK-2-126

5 (^{1}H NMR in $CDCl_3$)

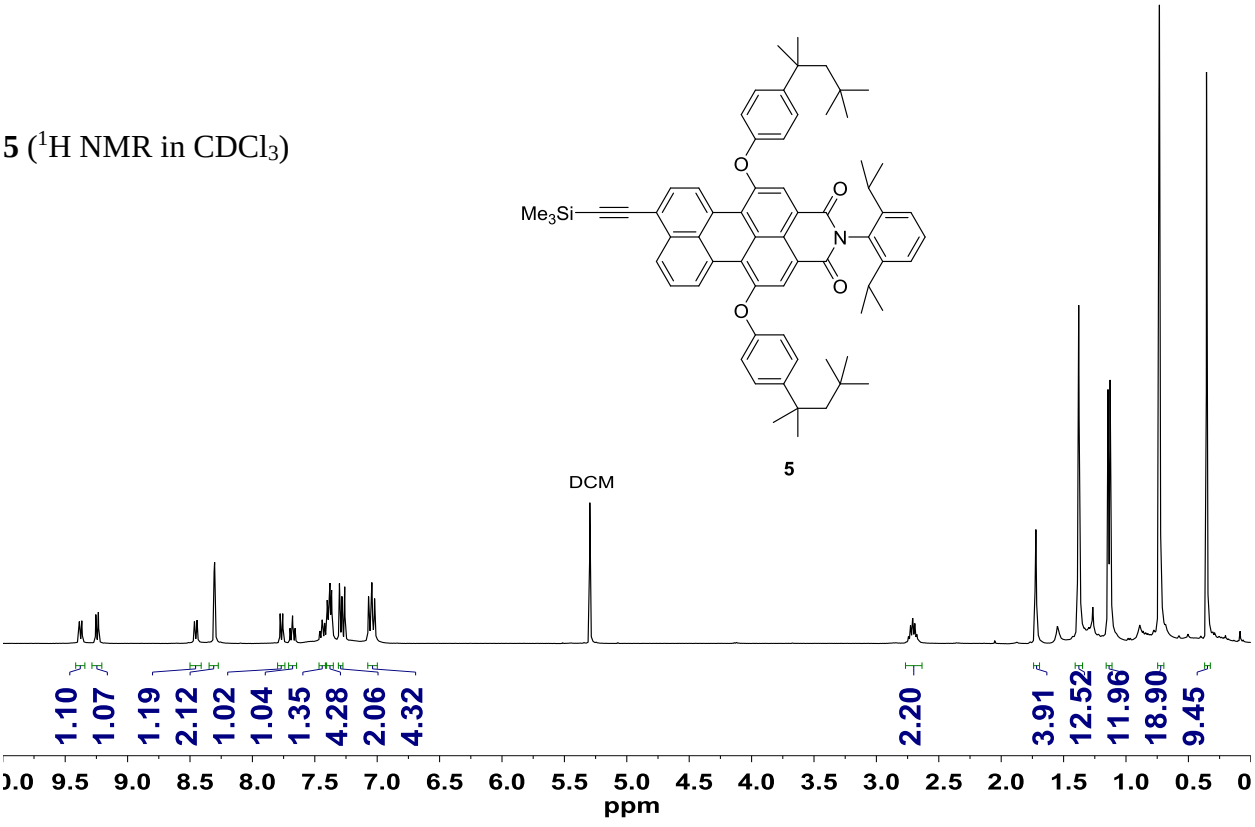

5 (^{13}C NMR in $CDCl_3$)

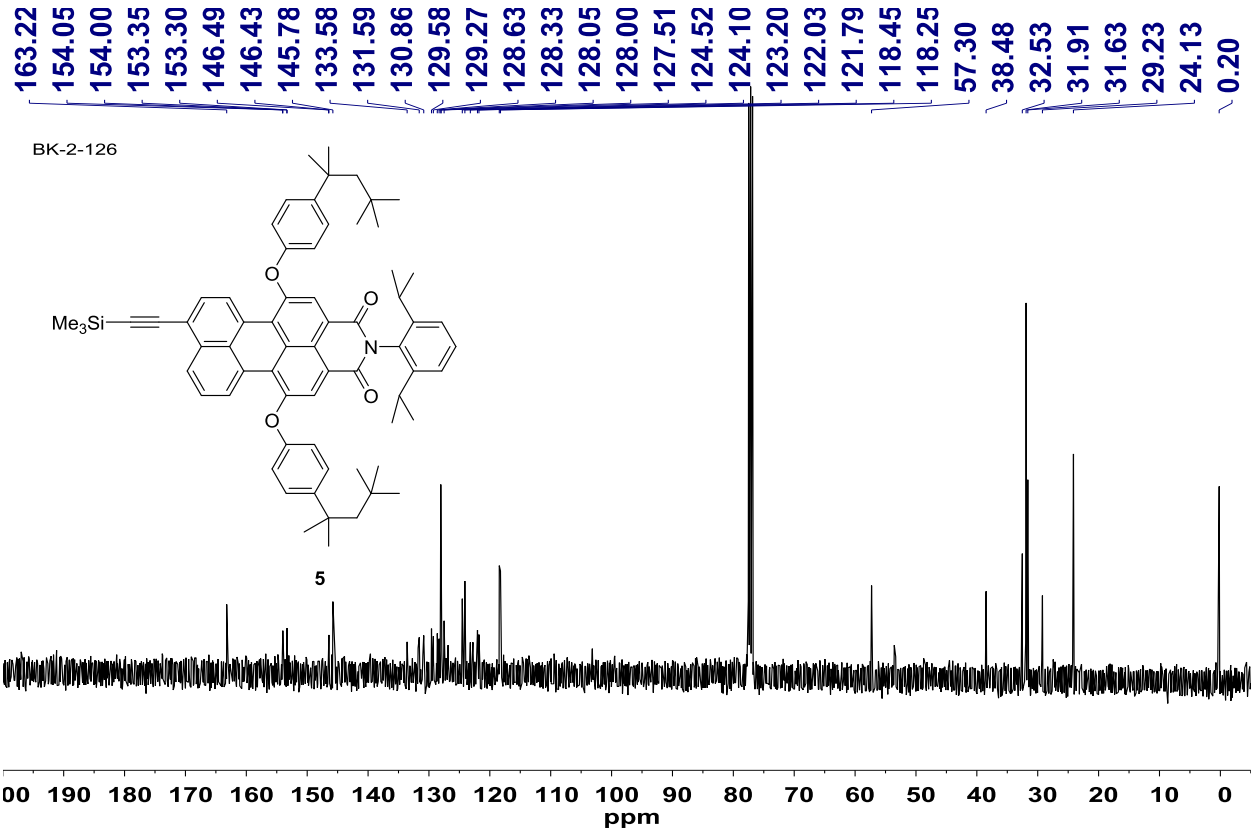

BK-2-130

Perylene-1 (^{1}H NMR in $CDCl_3$)

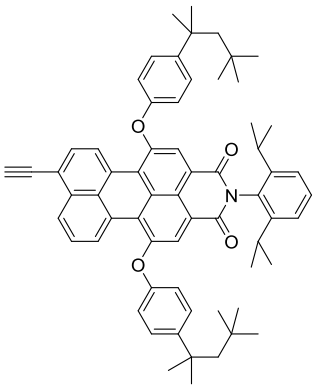

Perylene-1 (^{13}C NMR in $CDCl_3$)

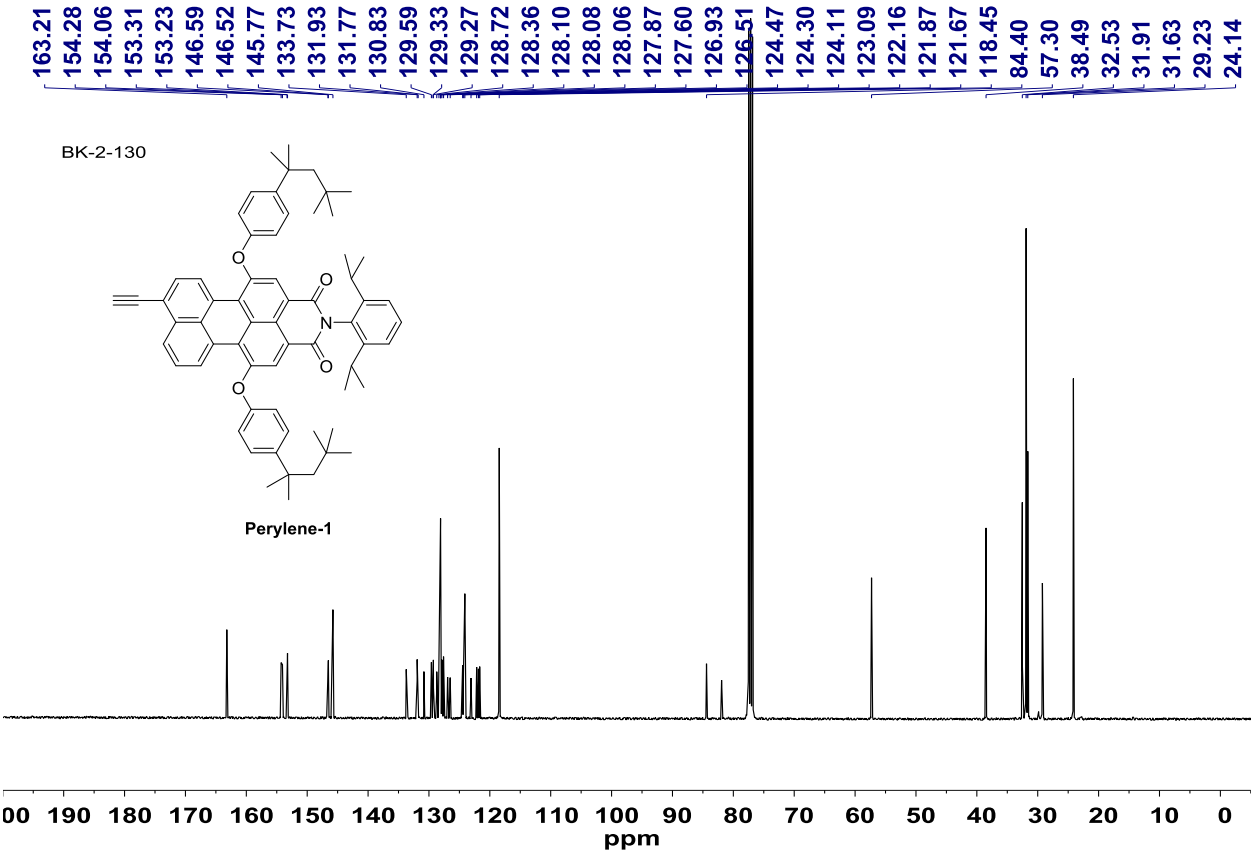

Chapter 4

Oil-in-Water Emulsions Stabilized by Conjugated Polymers

Abstract: This chapter describes the synthesis of surfactant-type poly(phenylene ethynylene)s with the primary applications in the emulsion fabrication. We first synthesize the PPEs with nonionic side chains. Tuning the structures of the side chains (hydrophilic/hydrophobic ratios) controls water solubility and the optimized PPE leads to efficient localization at the oil-water interfaces in emulsions and makes stable oil droplets. We analyze the localization via absorption and emission spectroscopy as well as confocal laser scanning microscopy. The exciton migration and dual-fluorescence of the polymers in different physical environments can provide a new concept of visualization methods in many amphiphilic colloidal systems and bioimaging.

Parts of this chapter were reprinted from Koo, B.; Swager, T. M. "Distinct Interfacial Fluorescence in Oil-in-Water Emulsions via Exciton Migration of Conjugated Polymers." *Submitted.*

4.1 Introduction

Emulsions are metastable colloids with two immiscible liquids,[1] where one phase is dispersed in a continuous phase. Typically, emulsions contain oil, water, and an emulsifier,[2] which is also referred as a surfactant. Surfactants reduce the interfacial tension between oil and water and make stable dispersion. Chemical structures of a surfactant are generally composed of a hydrophobic part (alkyl or aromatic groups) and a hydrophilic part (ionic or nonionic functional groups). In addition to their capability to stabilize interfaces, there have been general interests in synthesizing surfactants with other functions, such as fluorescence.[3] These functional surfactants can expand their utility in many applications wherein amphiphilic interfaces are present, such as emulsions and cell membranes. In this chapter, we are focusing on fluorescent surfactant-type conjugated polymers, poly(phenylene ethynylene)s, for their applications in the fabrication and visualization of oil droplets in water. We will mainly manipulate the chemical structures of side chains and relevant conformations of the polymers, which will lead to fluorescent transduction resulting from exciton migration.

Poly(phenylene ethynylene)s (PPEs), fluorescent conjugated polymers, have been extensively investigated as optoelectronic and fluorescent sensory materials.[4-6] They possess both high extinction coefficients and fluorescence quantum yields, resulting from direct band gap materials[7] as well as rigid butatriene-like excited state structures as introduced in Chapter 1. The strong brightness (extinction coefficient multiplied by quantum yield) makes them suitable materials as fluorescent dyes and leads to surfactant-type dyes by tuning their sidechain structures. One distinct feature of fluorescent PPEs as fluorescent probes, compared to conventional small molecular probes, is that their fluorescence can be switched depending on their conformations[8] and interpolymer distances.[9] We reported[9] that surfactant-type PPEs having low-energy emissive

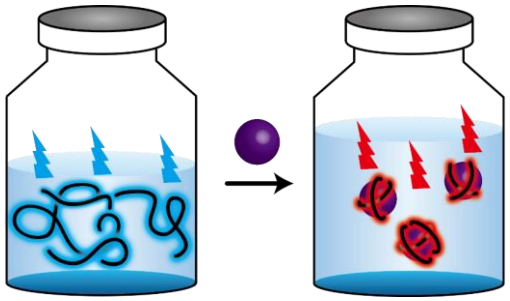

Figure 4.1. Schematics of exciton migration upon the formation of emulsions. In water (left), **P1** shows cyan fluorescence. At oil–water interfaces, **P1** shows red fluorescence owing to enhanced exciton migration to perylene endgroups.

endgroups can display dual-fluorescence, which is cyan (backbone) in solution and red (endgroup) in thin films at a single excitation wavelength. In their Langmuir monolayers, we could control interpolymer distances and show ratiometric fluorescence changes at the air–water interfaces. In this Chapter, we aim to extend this dual-fluorescence concept to more general amphiphilic colloidal systems, specifically emulsions. As a proof of concept, we choose oil-in-water emulsions that are stabilized by PPE surfactants. We found that PPEs show cyan fluorescence in water, which switches to red fluorescence in stable oil-in-water emulsions (Figure 4.1). The red results from the enhanced exciton migration of the PPE localized at the oil-water interface. We envision that this switchable fluorescence between bulk and interface can pave a novel way of high-contrast visualization techniques for many amphiphilic systems found in colloids and bioimaging.

4.2 Results and Discussion

4.2.1 Structure Optimizations

We first plan to synthesize several perylene end-capped water-soluble PPEs to make stable oil droplets in water. As introduced in Chapter 3, the perylene serving as low-energy emissive endgroups is functionalized with bulky groups at its bay area, designed to reduce π-π stacking and

aggregation-induced fluorescence quenching.[10] Regarding the side chains of the polymer backbone, we choose branched triethylene glycol monomethyl ether as one of the sidechains because of structural simplicity and the highest fluorescent quantum yield in water (QY = 43%) among the reported water-soluble PPEs.[11,12] The other type of the side chain is the amphiphilic one, a branched triethylene glycol with octyl, following the previous report.[13] Based on the combination of two types of sidechains, we synthesize three PPEs as shown in Scheme 4.1. The number ratio of triethylene glycol (TEG) to octyl per repeat unit is 6:2 (**P1**), 8:0 (**P2**), and 4:4 (**P3**). **P3** turns out to be not water-soluble and thus emulsion fabrication was not possible. **P3** could be an interesting polymer for reverse phase emulsions, that is, water-in-oil emulsions, although this is beyond the scope of this Chapter. **P1** and **P2** are water-soluble, and oil-in-water emulsions are fabricated. However, we will mainly focus on **P1** since **P2** does not show enhanced red emission in the emulsion. This is perhaps attributed to the fact that **P2** is too water-soluble and they tend to stay in water, not staying at the interface. **P1** is moderately water-soluble and we observe stable oil-in-water emulsions with the increased red fluorescence (vide infra).

We synthesize **P1** via Sonogashira cross-couplings with **M1** (diyne) and **M2** (diiodide) in the presence of $Pd(PPh_3)_4$, CuI, trime-thylamine (TEA), and tetrahydrofuran (THF) as a solvent (Scheme 4.2). The perylene with a terminal acetylene was added in situ to perform the endcapping reaction of the polymer. We also synthesize **P2** and **P3** in a similar way (see Chapter 4.4 Experimental Details). Figure 4.2 shows the photophysics of **P1** in water and thin films. The absorption spectra between solution and thin films are very similar with no sign of planarization. This indicates that π-π stacking in the solid state is absent presumably owing to sterically bulky branched side chains as well as bulky perylene endgroups. The absence of π-π interaction is desirable for our application since it will prevent aggregation-induced fluorescence quenching at

the oil-water interface. The emission spectra indicate a large difference between solution and thin films. In the solid state, excitons in the backbone migrate to the perylene via statistically improved

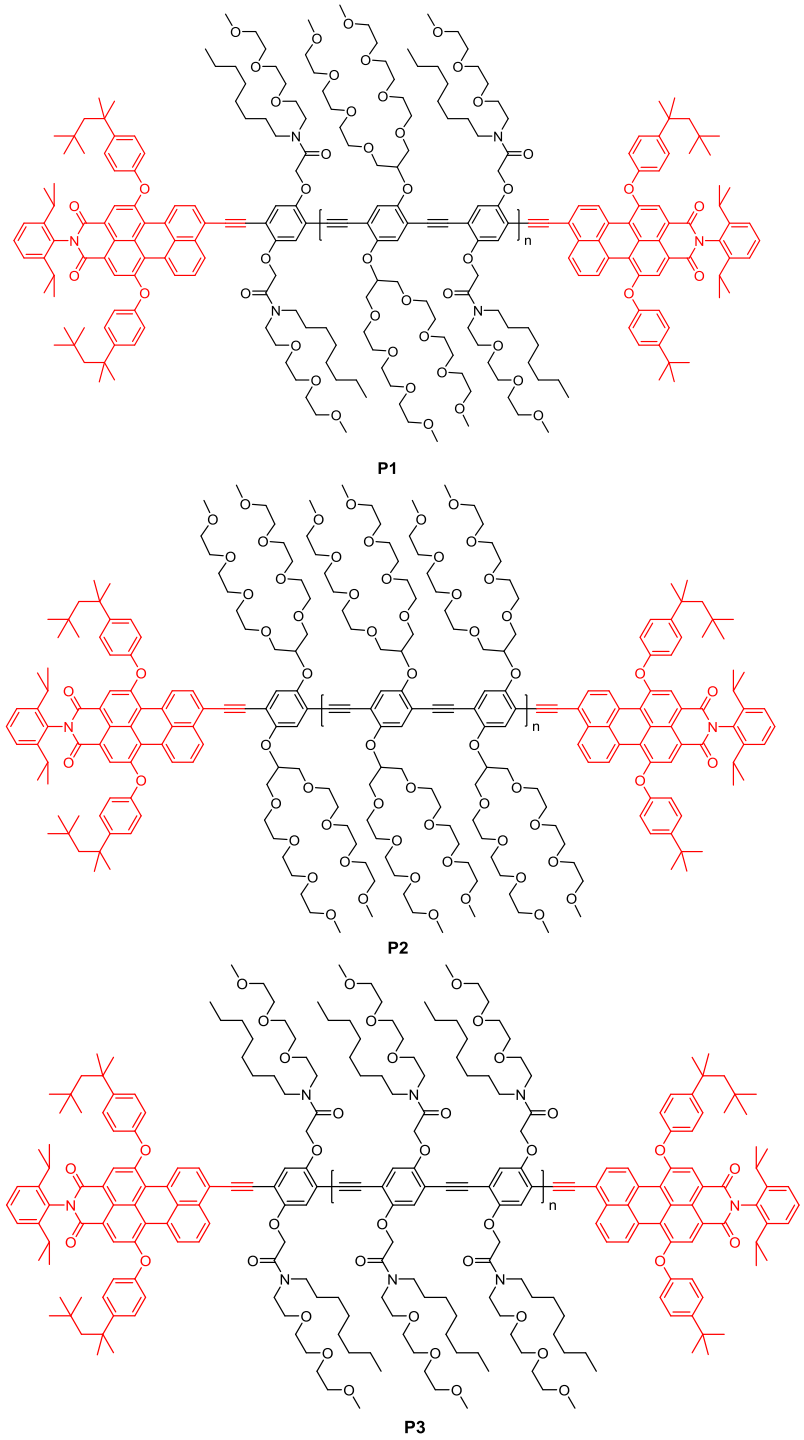

Scheme 4.1. Structures of endcapped surfactant-type PPE **P1** (moderately water-soluble), **P2** (highly water-soluble) and **P3** (non water-soluble).

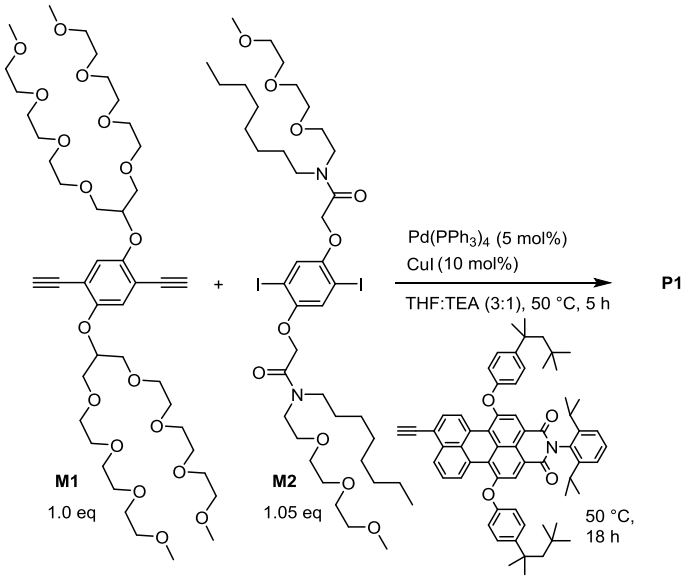

Scheme 4.2. Polymerization for **P1**. 1.05 equiv of **M2** is used to make Ar-Pd-I endgroups after polymerization, which further react in situ with acetylene-terminal perylene.

3D random walk, which is much faster than 1D intrachain exciton migration in solution.[14]

4.2.2 Fabrication of Emulsions

P1 can serve as surfactants that can stabilize oil-in-water emulsions. We dissolve **P1** in water with the concentration of 25 μg/ml. The solution is slightly cloudy and after overnight there

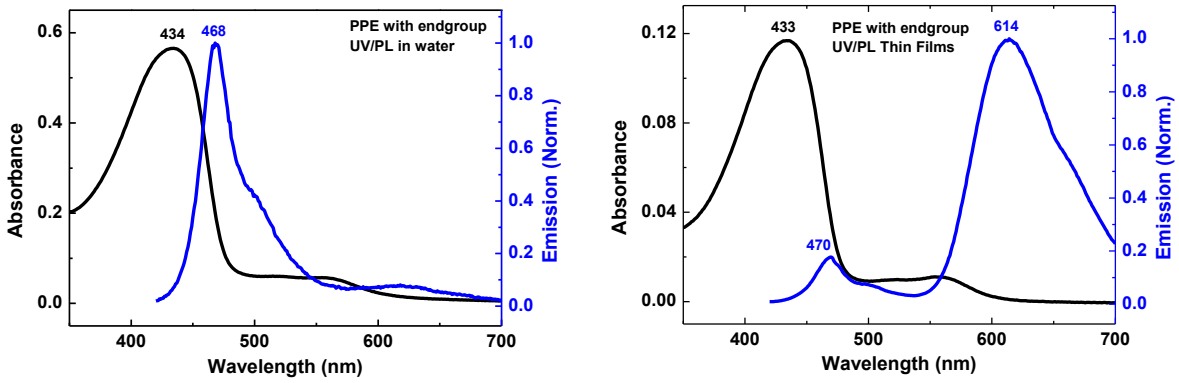

Figure 4.2. Absorption and emission spectra in water (left) and thin films (right). The absorption spectra are similar each other, whereas the emission spectra exhibit either backbone (solution) or end-group fluorescence (thin films) as a result of the exciton migration in the solid state.

were small amounts of tiny aggregates that settle down at the bottom of the vial. It is believed that they are micelles consisting of **P1**, which are typically beneficial in emulsion fabrication since they can be a reservoir of surfactants that can further stabilize oil-water interfaces upon the addition of an oil phase. From the aqueous **P1** solution, we made heptane-in-water and benzyl benzoate-in-water emulsions with 5 vol% of oil phases in both cases (Figure 4.3a). The use of two different oil phases are intended to compare the effect of **P1's** solubility in oil on exciton migration (heptane as a poor solvent and benzyl benzoate (BB) as a good solvent). Upon the addition of oil, there were bright red emission at the top (Figure 4.3a, heptane-in-water, heptane is lighter than water) and at the entire solution (Figure 4.3a, BB-in-water, BB is denser than water). In the latter case, the actual red emission come from the interface of droplets at the bottom (which will be discussed in the confocal laser scanning microscopy images in Figure 4.4), but the entire solution looks red because of red fluorescence scattering. The fluorescence spectra are presented in Figure 4.3b. In both cases, the relative intensity of red to cyan is increased compared to the **P1** solution spectrum and is still

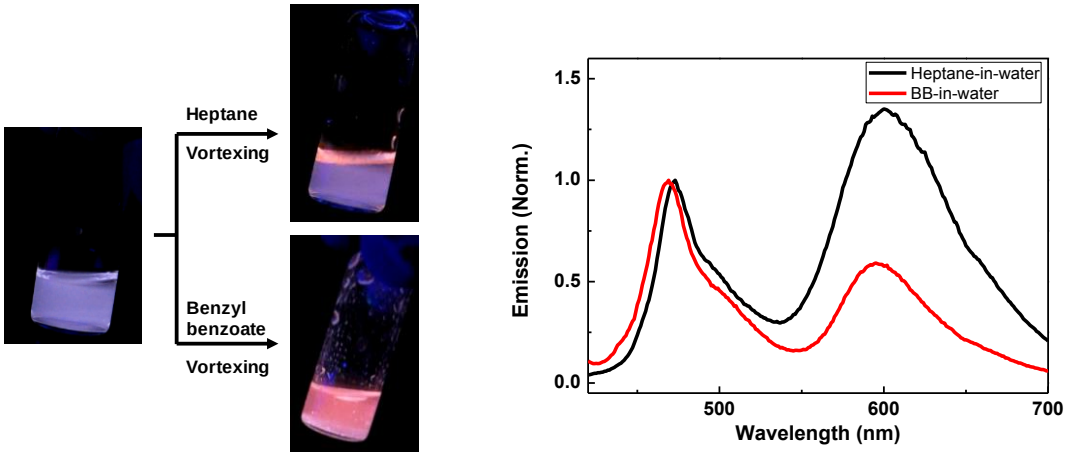

Figure 4.3. (a) Pictures of emulsions. To **P1** in water (left), heptane (top right) and benzyl benzoate (top bottom) are added and then vortexed. (b) Emission spectra of heptane-in-water (black) and BB-in-water (red) emulsions. Increased red emissions are observed in both cases after adding oil phases.

lower than the **P1** thin film spectrum. Heptane-in-water emulsion shows more red (more thin film-like) than BB-in-water emulsion (more solution-like, vide infra).

We collect confocal laser scanning microscopy (CLSM) images (Figure 4.4) in order to visualize the droplets and locate the origin of fluorescence. Figure 4.4a-c (and Figure 4.4d-f) shows the heptane-in-water (and BB-in-water) emulsions, where Figure 4.4a (and 4.4d), 4.4b (and 4.4e), 4.4c (and 4.4f) are from the mixed channels, green channel, and red channel, respectively. In all cases, the polymers are successfully localized at the interface and thus we observe the emission exclusively from the droplet interfaces. In heptane-in-water emulsion, the red emission intensity (Figure 4.4c) is much stronger than the green one (Figure 4.4b), whereas in BB-in-water emulsion

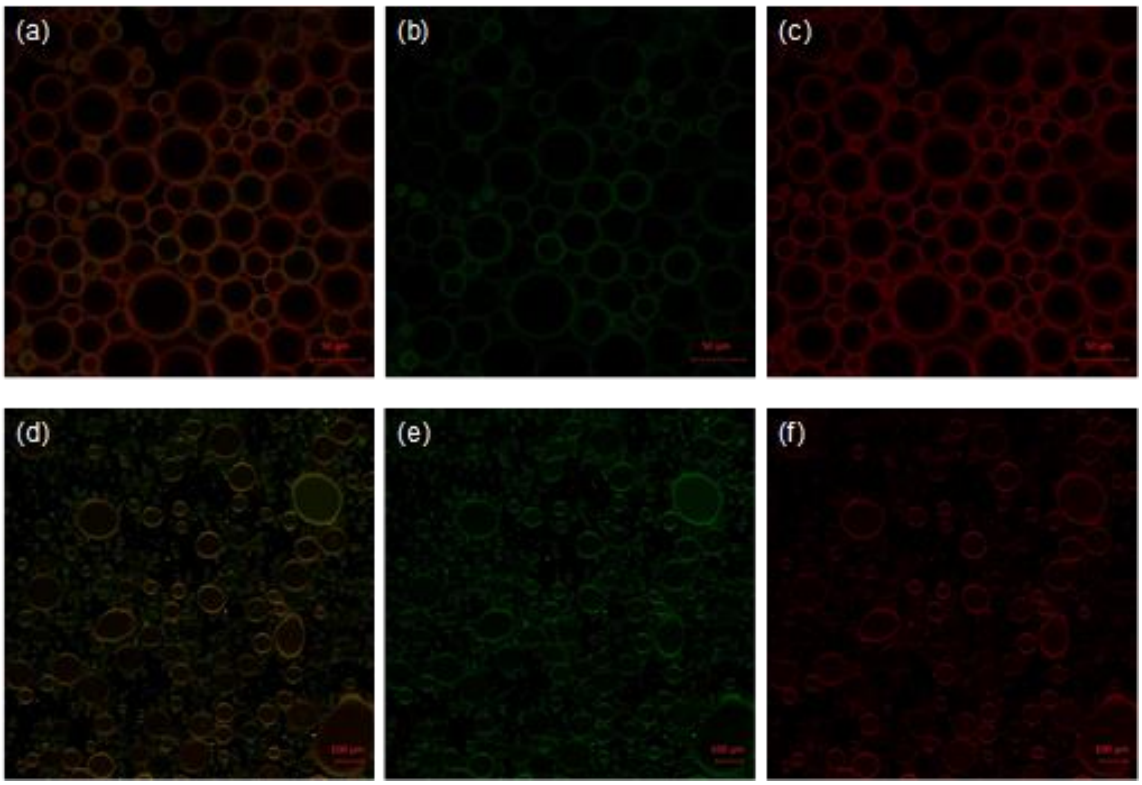

Figure 4.4. Confocal laser scanning microscopy images. (a-c) Heptane-in-water emulsions. Scale bar: 50 μm. Emission channels from (a) mixed (b) green and (c) red. (d-f) Benzyl benzoate-in-water emul-sions. Scale bar: 100μm. Emission channels from (d) mixed (e) green and (f) red. Excitation laser at 458 nm. Green emission (471–511 nm) and red emission (579–621 nm).

the red and green (Figure 4.4e and 4.4f) are similar, which is consistent with the spectroscopic results in Figure 4.3b. We hypothesize that this result is related to the local environment of interfaces. Since heptane is a poor solvent, the polymers are efficiently packed and thus the interpolymer distances are close, leading to effective exciton migration and thin film-like emission. Because BB is a good solvent, the interfacial polymer layers are not packed very well and could be interdigitated by BB molecules (or BB vapors near the interface). Thus, the exciton migration is not effective. In heptane-in-water emulsion, increasing concentration of the polymer solution to

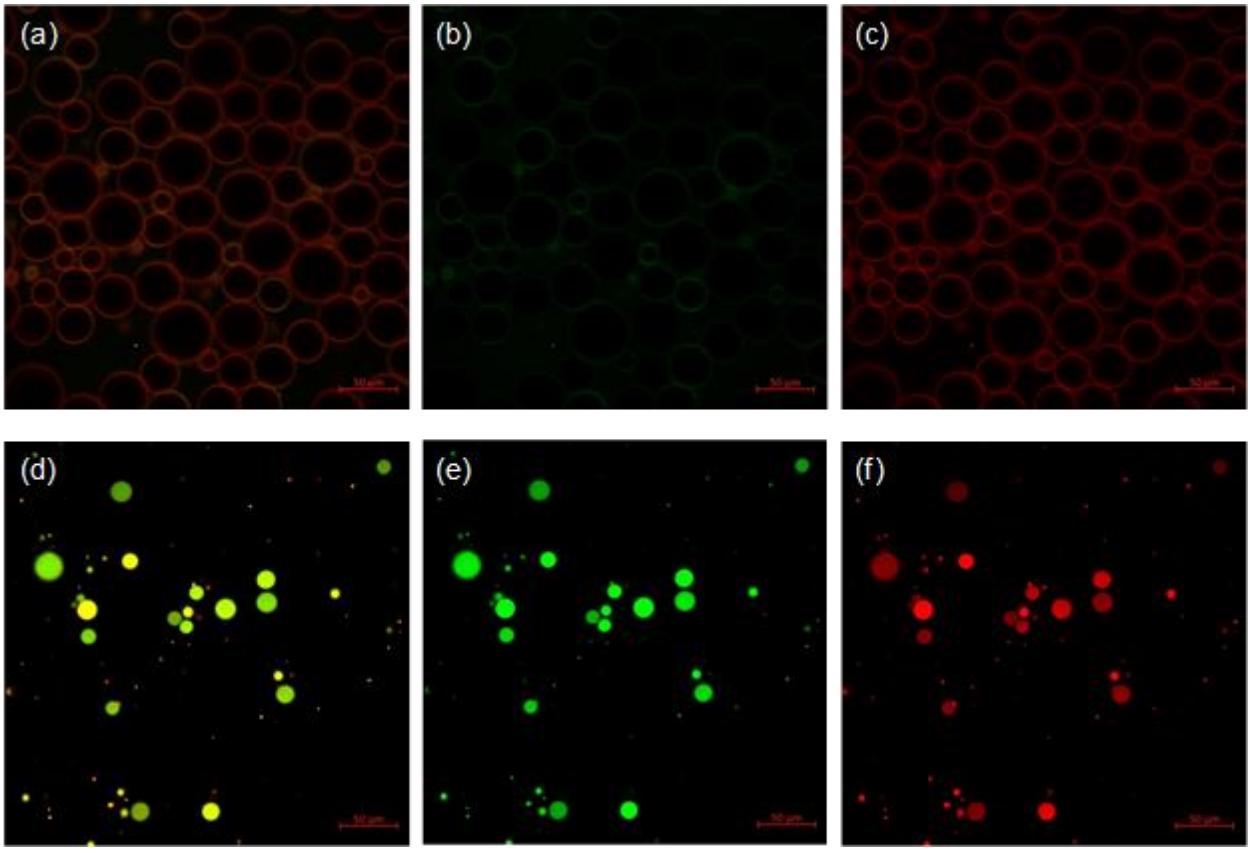

Figure 4.5. Confocal laser scanning microscopy images with higher concentration of **P1** in water (100 μg/mL). (a-c) Heptane-in-water emulsions. Scale bar: 50 μm. Emission channels from (a) mixed (b) green and (c) red. (d-f) Benzyl benzoate-in-water emulsions. Scale bar: 50 μm. Emission channels from (d) mixed (e) green and (f) red. Excitation laser at 458 nm. Green emission (471–511 nm) and red emission (579–621 nm).

100 μg/ml results in dense interfacial localization and much stronger red emission, whereas in BB-in-water emulsion, the polymers start being dissolved in the BB phase (Figure 4.5).

4.3 Conclusions

We synthesize surfactant-type fluorescent conjugated polymers that generate cyan (water) and red (interface) emissions depending on their locations in emulsions. **P1** has moderate solubility in water and it can be preferentially localized at the oil–water interface. This location-dependent fluorescence, which has never been observed from conventional small molecular dyes, results from the judicious design of surfactant-type PPEs and the enhanced exciton migration at the oil–water interface. The increased red fluorescence was confirmed by fluorescence spectroscopy and visualized by the confocal laser scanning microscopy. We believe that the tunable emissions can provide a rational design principle to make novel synthetic dyes in many other applications, for example, by the modification of the polymer backbone or endgroups (such as near infrared dyes) to meet specific needs. We are currently expanding this methodology to complex emulsions.

4.4 Experimental Details

4.4.1 General

Chemicals were purchased from Aldrich, Alfa Aesar, and TCI America without further purification unless noted otherwise. All reactions were carried out under argon with standard Schlenk techniques. **M2**,[15] **M3**,[16] and **P3**[9] were synthesized by following the literature procedures or slight modifications thereof. All ^{1}H NMR and ^{13}C NMR spectra are reported in ppm on a Bruker Avance-400. ^{1}H NMR is referenced to a chloroform peak (δ = 7.26 ppm). The multiplicity is reported as follows: s = singlet, d = doublet, t = triplet, q = quartet, quint = quintet, m = multiplet

or unresolved, dd = doublet of doublets, br = broad signal. Coupling constants J are reported in Hz. ^{13}C NMR is referenced to a chloroform peak (δ = 77.16 ppm). High-resolution mass spectra (HRMS) were obtained at the MIT DCIF (Department of Chemistry Instrumentation Facility) using electrospray ionization (ESI) or direct analysis in real time (DART).

THF Gel Permeation Chromatography (GPC) was performed with a concentration of 0.5 mg/ml on an Agilent 1260 Infinity system equipped with three PLgel columns (103, 104, 105 Å) in series, calibrated with monodisperse polystyrene standards. UV-vis spectra were recorded on Agilent Cary 4000 spectrometer at room temperature. Fluorescence measurements were performed at room temperature with a Horiba Jobin Yvon SPEX Fluorolog-τ3 fluorimeter (model FL-321, 450 W Xenon lamp) using right-angle conformation for solution and front-face conformation for thin films. For sample preparations of photophysics measurements, the solutions were prepared in water. The solid-state films were prepared on glass by spin-coating 3000 rpm for 30 seconds from the solution in THF and annealed at 70 °C for 15 min in ambient atmosphere.

Emulsions are made from distilled water and 5% of oil phases. Specifically, to the polymer solution in water (0.95 mL) is added heptane (0.05 mL) or benzyl benzoate (0.05 mL). The vial containing the mixture is shaken with the aid of vortex for 30–60 seconds. Confocal microscopy images are collected from the W. M. Keck Microscopy Facility at the Whitehead Institute. Zeiss 710 Laser Scanning Confocal Microcopy was used with the excitation lasers 405 or 458 nm. Photons are collected in two channels, one being green (ca. 460–510 nm) and the other being red (ca. 580–620 nm). The emulsion samples are placed between a cover slip and a microscope slide with double-sided tape, which creates a very thin gap where the samples can be loaded by capillary. The top droplets for heptane-in-water and the bottom droplets for benzyl benzoate-in-water are used.

4.4.2 Synthesis of Monomers

The synthetic scheme and procedures are as follows.

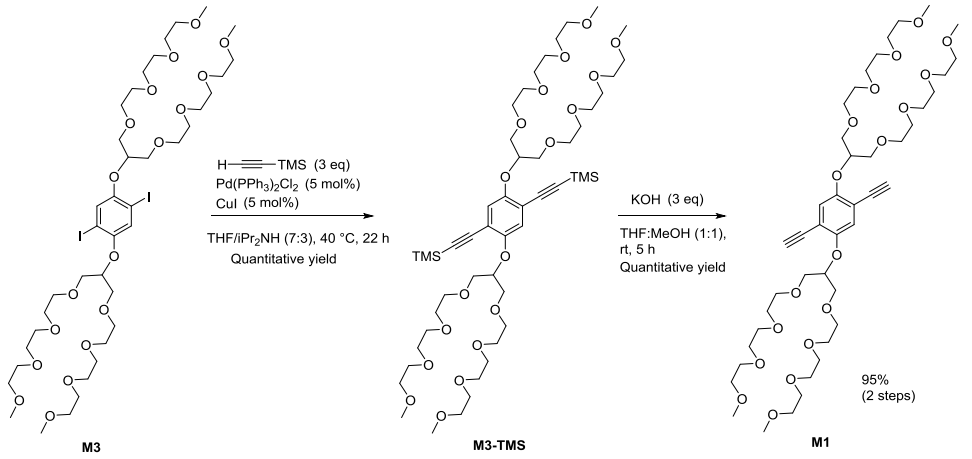

((2,5-bis((2,5,8,11,15,18,21,24-octaoxapentacosan-13-yl)oxy)-1,4-phenylene)bis(ethyne-2,1-diyl))bis(trimethylsilane) (M3-TMS). To the flame-dried Schlenk flask, **M3** (340 mg, 0.183 mmol, 1 equiv), $Pd(PPh_3)_2Cl_2$ (10.9 mg, 0.009 mmol, 5 mol%), and CuI (3.0 mg, 0.009 mmol, 5 mol%) were added, followed by three vacuum-argon exchange cycles. The mixture of THF:diisopropylamine (7:3 v/v) was degassed with N_2 for 30 min and 2 mL of the mixture was added to the flask. Ethynyltrimethylsilane (0.13 mL, 0.55 mmol, 3 equiv) were added. The mixture was stirred at 40 °C for 22 hours. After cooling down to room temperature, the solvents were evaporated in vacuo. The crude material was purified by column chromatography (hexane:CH_2Cl_2:EtOAc:MeOH = 5:3:2:1). Quantitative yield. ^{1}H NMR (400 MHz, $CDCl_3$) δ 7.06 (s, 2H), 4.42 (quint, *J* = 5.1 Hz, 2H), 3.74 – 3.61 (m, 48H), 3.56 – 3.52 (m, 8H), 3.37 (s, 12H), 0.23 (s, 18H).

13,13'-((2,5-diethynyl-1,4-phenylene)bis(oxy))bis(2',5',8',11',15',18',21',24'-octaoxapentacosane) (M1). The starting material **M3-TMS** (189 mg, 0.183 mmol, 1 equiv) was

placed in a vial, followed by three vacuum-argon exchange cycles. KOH (30.7 mg, 0.548 mmol, 3 equiv) was dissolved in MeOH with the concentration of 30.7 mg/1 mL. THF (1 mL) and KOH-MeOH solution (1 mL) were added to the vial (there may be a slight error in the amount of added KOH due to density change of KOH-MeOH solution, but it may not be significant). The mixture was stirred at room temperature for 5 hours, followed by evaporation in vacuo. The crude material was purified by column chromatography (EtOAc:MeOH = 10:1). Quantitative yield. ^{1}H NMR (400 MHz, $CDCl_3$) δ 7.15 (s, 2H), 4.43 (quint, *J* = 5.1 Hz, 2H), 3.76 – 3.60 (m, 48H), 3.56 – 3.51 (m, 8H), 3.37 (s, 12H), 3.31 (s, 2H). ^{13}C NMR (101 MHz, $CDCl_3$) δ 154.14, 121.50, 115.04, 82.75, 80.01, 79.71, 71.91, 71.15, 70.62, 70.60, 70.55, 70.49, 59.01. HRMS (DART) calculated for $C_{44}H_{75}O_{18}$ ($[M+H]^+$) 891.4948; found, 891.4977.

4.4.3 Polymerizations

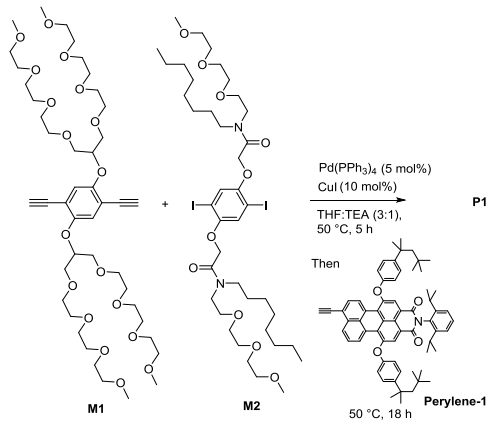

P1. To the flame-dried Schlenk flask, **M1** (30 mg, 0.0337 mmol, 1.00 equiv), **M2** (35.1 mg, 0.0354 mmol, 1.05 equiv), $Pd(PPh_3)_4$ (2.0 mg, 0.0017 mmol, 5 mol%), and CuI (0.64 mg, 0.0034 mmol, 10 mol%) were added. The flask containing reagents was evacuated and back-filled with argon for 3 times. The mixture of dry THF:triethylamine (3:1 v/v) was degassed with nitrogen for 30 min, and 1.5 mL was added to the flask. The reaction mixture was stirred for 30 min at room temperature

to completely dissolve all the materials, followed by stirring at 50 °C for 5 hours. **Perylene-1** (2.3 mg, 0.0025 mmol, 0.075 equiv) dissolved in dry THF (0.5 mL) was added and further stirred at 50 °C for 18 hours. The crude mixture was concentrated in vacuo, diluted with DCM, filtered through a short plug (1–2 cm) of silica gel. After concentrated in vacuo, preparative GPC in THF was used to separate high molecular weight fraction of the solid product. The resulting fraction in THF was evaporated under reduced pressure, and the product was dried in vacuo, affording a red rubbery solid (43 mg). 78% yield (yield does not consider endgroup since it is a very small amount). ^{1}H NMR (400 MHz, $CDCl_3$) δ 7.18 (s, 2H), 7.05 (s, 2H), 4.85 (br, 4H), 4.54 (br, 2H), 3.76 – 3.52 (br, 84H), 3.35 (s, 18H), 1.53 (br, 4H), 1.25 (br, 20H), 0.86 (br, 6H), where the proton integrations are based on the repeat unit. GPC (THF): M_n = 9.5 kDa, Đ = 1.36.

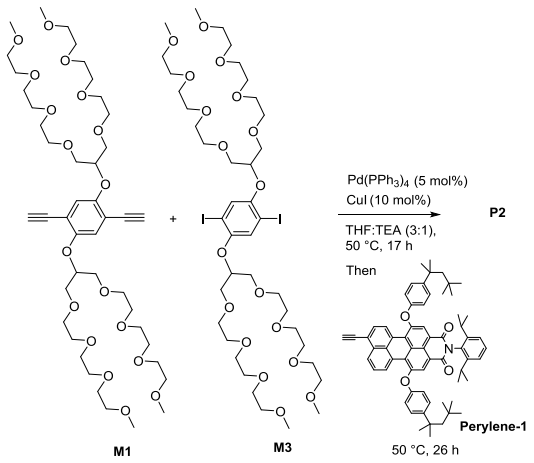

P2. To the flame-dried Schlenk flask, **M1** (50.0 mg, 0.0561 mmol, 1.00 equiv), **M3** (64.5 mg, 0.0589 mmol, 1.05 equiv), $Pd(PPh_3)_4$ (3.2 mg, 0.0028 mmol, 5 mol%), and CuI (1.1 mg, 0.0056 mmol, 10 mol%) were added. The flask containing reagents was evacuated and back-filled with argon for 3 times. The mixture of dry THF:triethylamine (3:1 v/v) was degassed with nitrogen for

30 min, and 2 mL was added to the flask. The reaction mixture was stirred for 30 min at room temperature to completely dissolve all the materials, followed by stirring at 50 °C for 17 hours. **Perylene-1** (6.0 mg, 0.0066 mmol, 0.012 equiv) dissolved in dry THF (0.5 mL) was added and further stirred at 50 °C for 26 hours. The crude mixture was concentrated in vacuo, diluted with DCM, filtered through a short plug (1–2 cm) of silica gel. After concentrated in vacuo, preparative GPC in THF was used to separate high molecular weight fraction of the solid product. The resulting fraction in THF was evaporated under reduced pressure, and the product was dried in vacuo, affording a red rubbery solid (80 mg). 82% yield (yield does not consider endgroup since it is a very small amount). ^{1}H NMR (400 MHz, $CDCl_3$) δ 7.14 (s, 4H), 4.51 (br, 4H), 3.76 – 3.50 (br, 112H), 3.34 (s, 24H), where the proton integrations are based on the repeat unit. GPC (THF): M_n = 14 kDa, Đ = 1.69.

4.5 References

(1) Bibette, J.; Calderon, F. L.; Poulin, P. *Rep. Prog. Phys.* **1999**, *62*, 969.

(2) Gupta, A.; Eral, H. B.; Hatton, T. A.; Doyle, P. S. *Soft Matter* **2016**, *12*, 2826.

(3) Yao, H.-W.; Zhu, X.-Y.; Guo, X.-F.; Wang, H. *Anal. Chem.* **2016**, *88*, 9014.

(4) Bunz, U. H. F. *Chem. Rev.* **2000**, *100*, 1605.

(5) Thomas, S. W.; Joly, G. D.; Swager, T. M. *Chem. Rev.* **2007**, *107*, 1339.

(6) Rochat, S.; Swager, T. M. *ACS Appl. Mater. Interfaces* **2013**, *5*, 4488.

(7) McQuade, D. T.; Pullen, A. E.; Swager, T. M. *Chem. Rev.* **2000**, *100*, 2537.

(8) Nesterov, E. E.; Zhu, Z.; Swager, T. M. *J. Am. Chem. Soc.* **2005**, *127*, 10083.

(9) Koo, B.; Swager, T. M. *ACS Macro Lett.* **2017**, *6*, 134.

(10) Yan, M.; Rothberg, L. J.; Kwock, E. W.; Miller, T. M. *Phys. Rev. Lett.* **1995**, *75*, 1992.

(11) Khan, A.; Muller, S.; Hecht, S. *Chem. Commun.* **2005**, 584.

(12) Bunz, U. H. F.; Seehafer, K.; Bender, M.; Porz, M. *Chem. Soc. Rev.* **2015**, *44*, 4322.

(13) Koo, B.; Swager, T. M. *ACS Macro Lett.* **2016**, *5*, 889.

(14) Andrew, T. L.; Swager, T. M. *J. Polym. Sci. B Polym. Phys.* **2011**, *49*, 476.

(15) Bouffard, J.; Swager, T. M. *Chem. Commun.* **2008**, 5387.

(16) Freudenberg, J.; Kumpf, J.; Schäfer, V.; Sauter, E.; Wörner, S. J.; Brödner, K.; Dreuw, A.; Bunz, U. H. F. *J. Org. Chem.* **2013**, *78*, 4949.

4.6 Appendix for Chapter 4

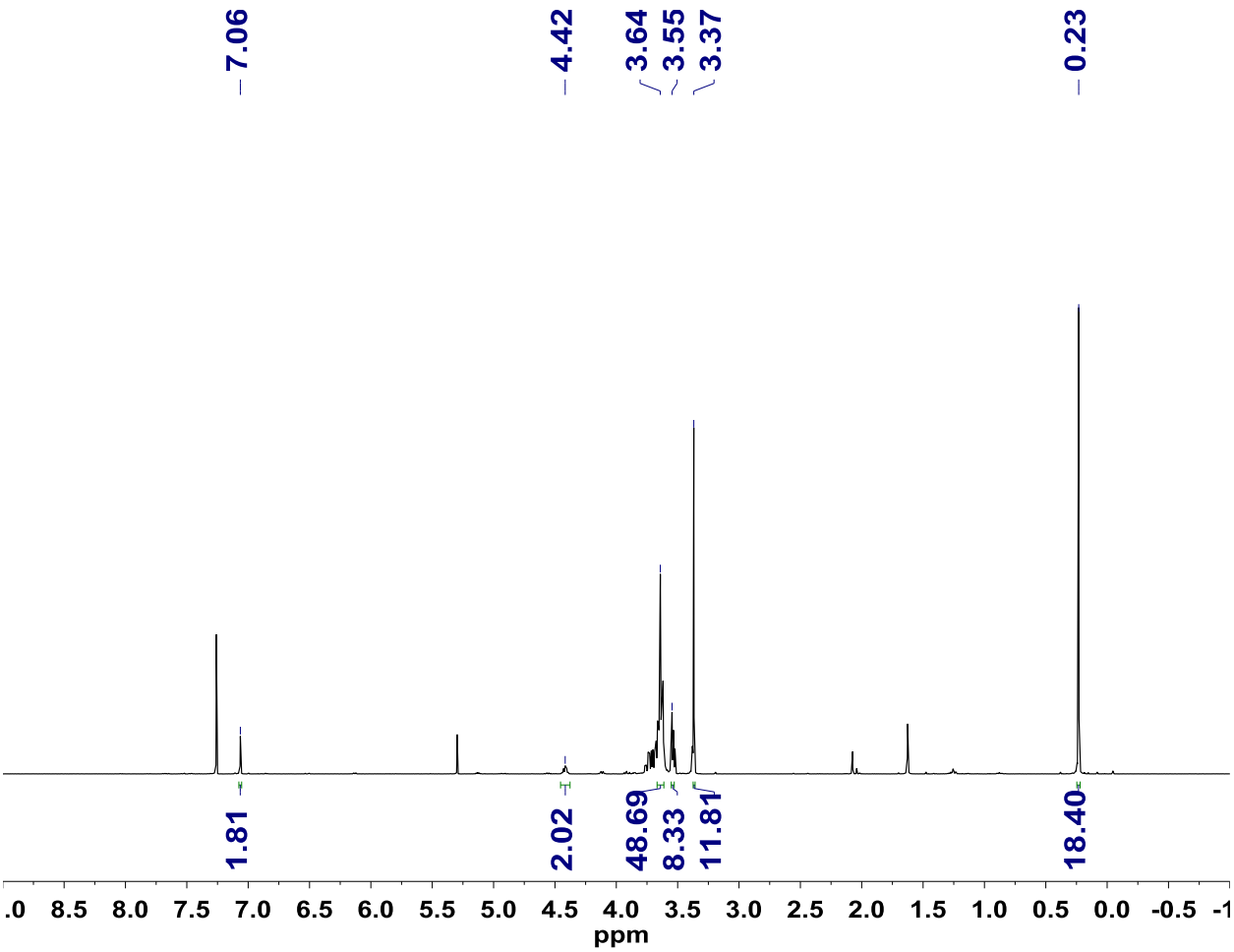

M3-TMS ^{1}H NMR spectrum in $CDCl_3$.

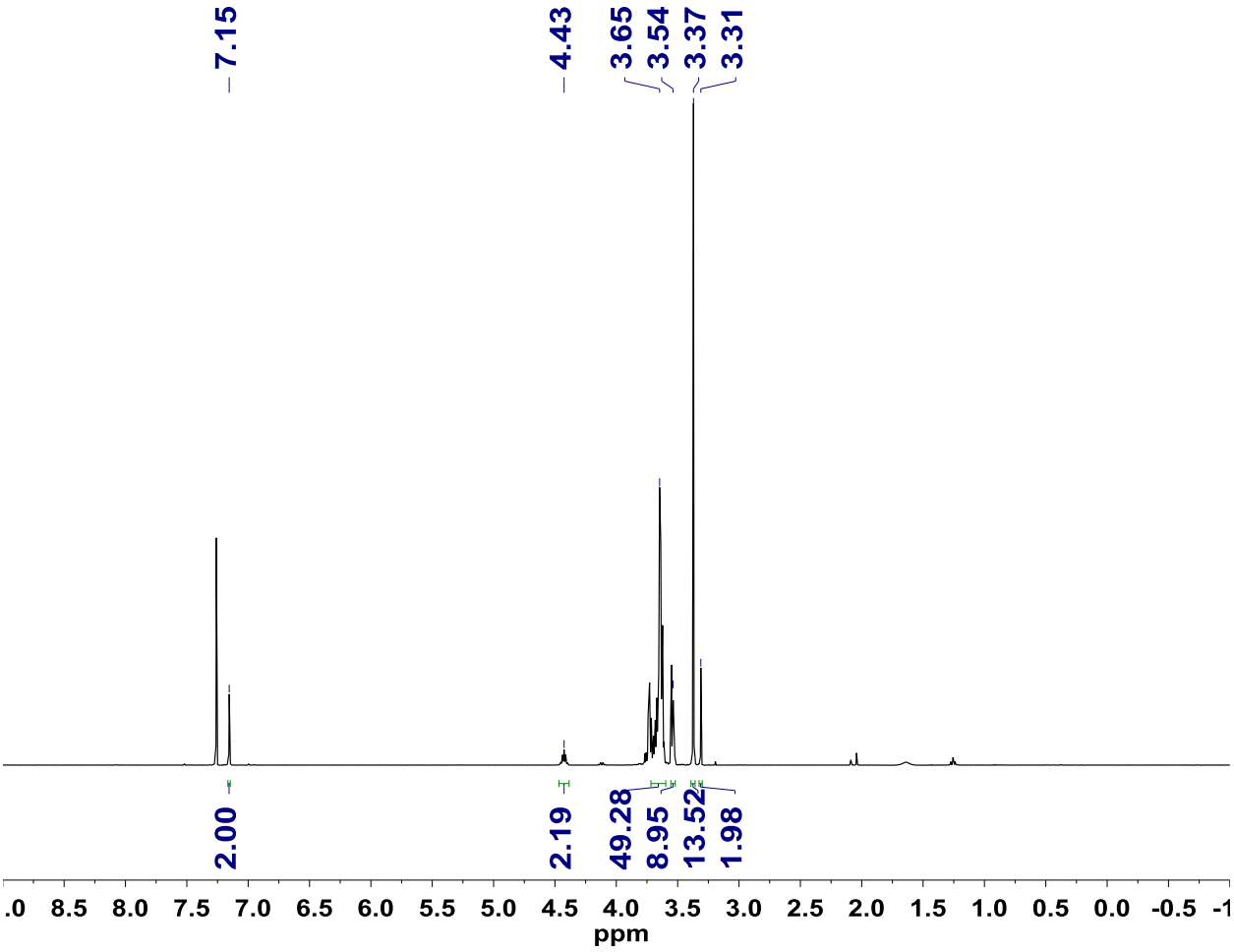

M1 ^{1}H NMR spectrum in $CDCl_3$.

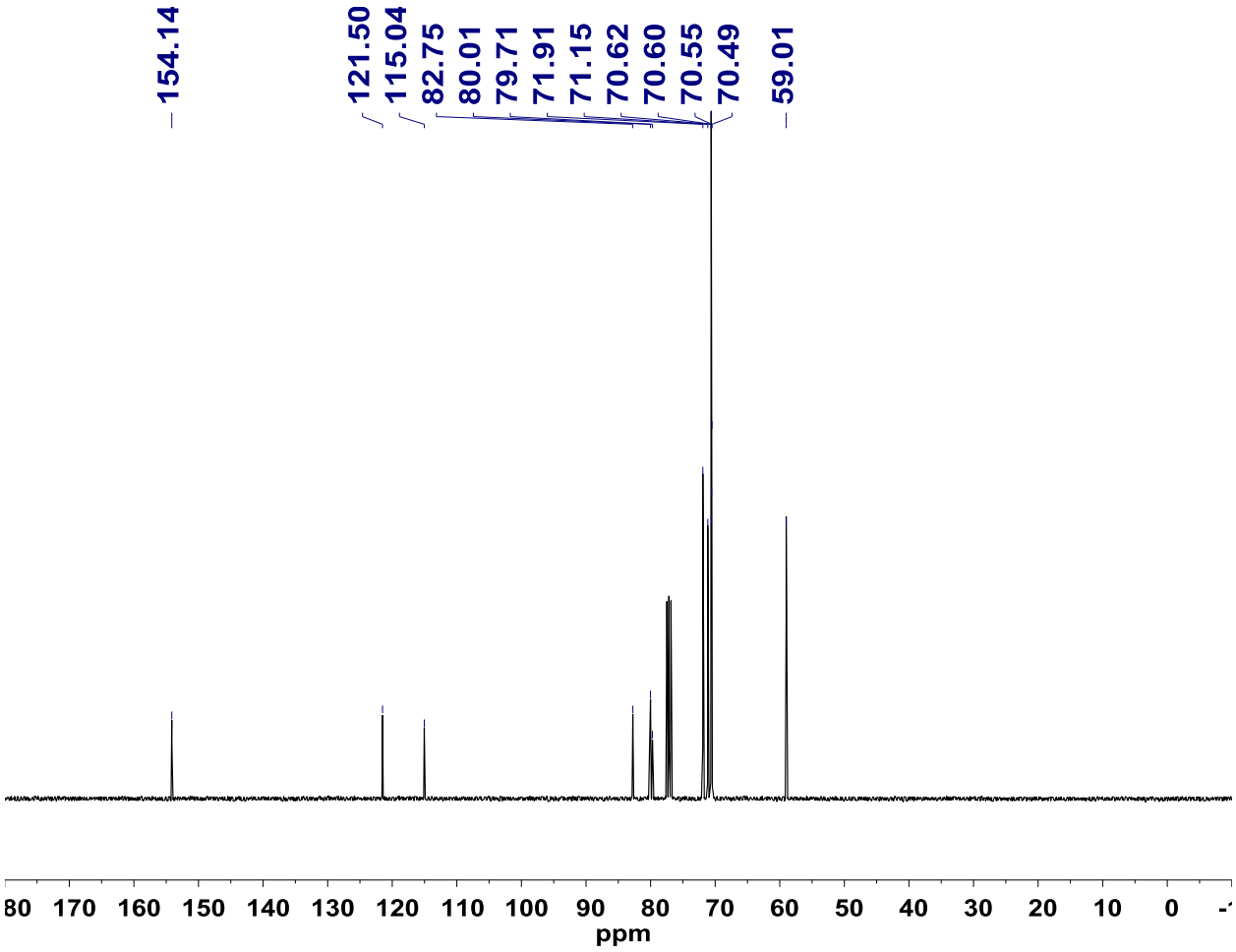

M1 ^{13}C NMR spectrum in $CDCl_3$.

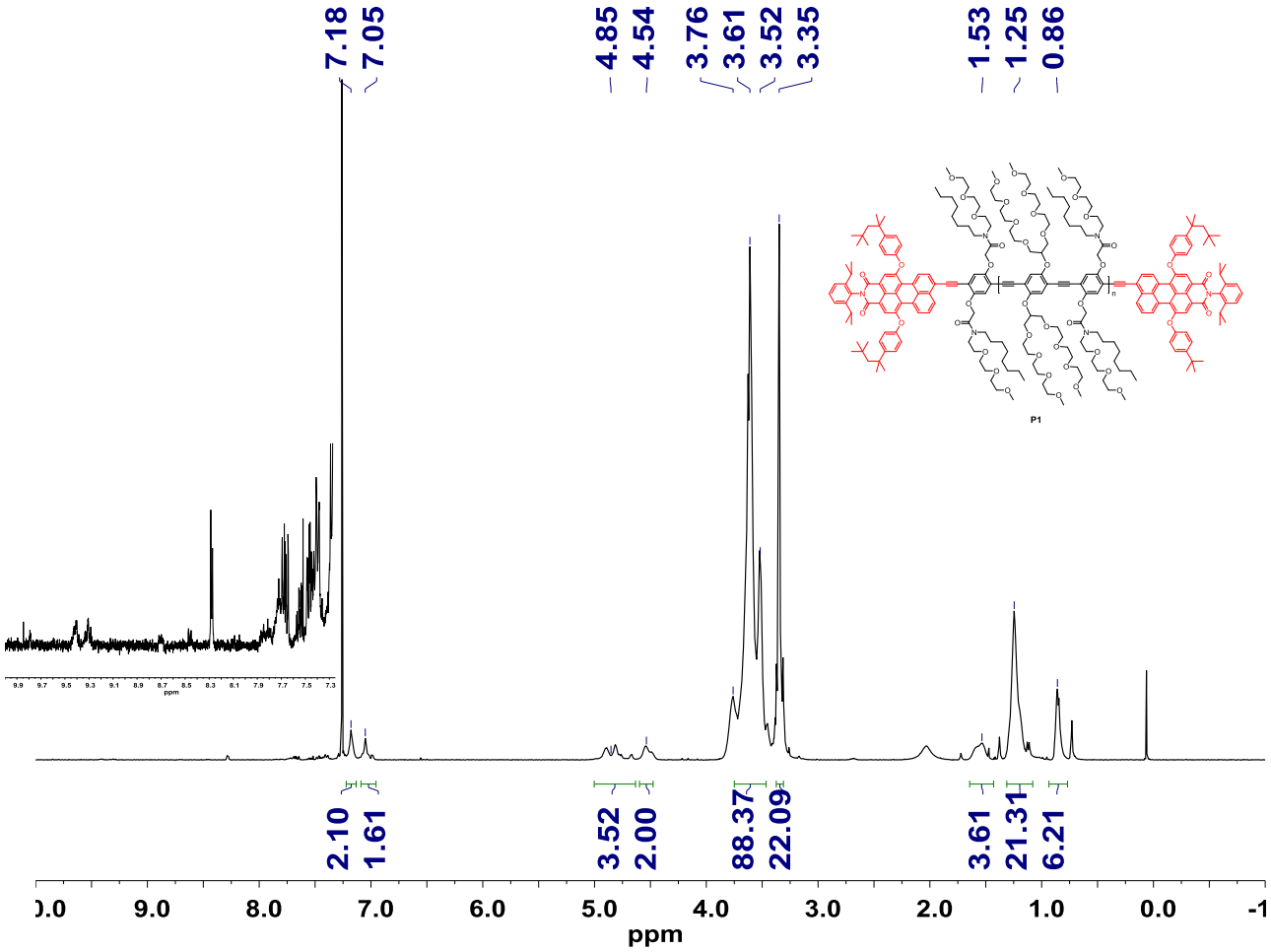

^{1}H NMR spectrum of **P1** in $CDCl_3$. Inset is the enlarged area (7.3 – 10 ppm), showing the perylene endgroup signals.

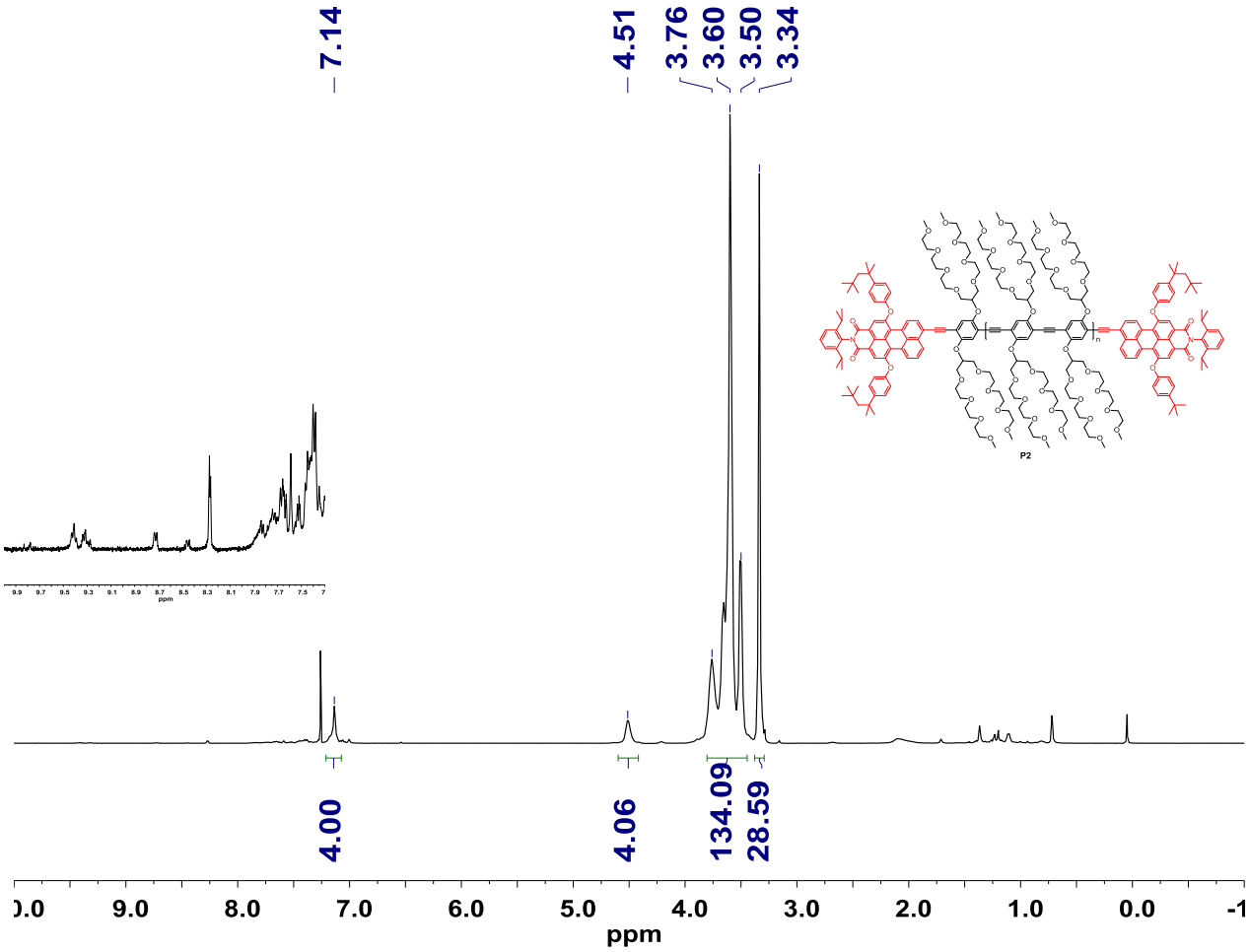

^{1}H NMR spectrum of **P2** in $CDCl_3$. Inset is the enlarged area (7.3 – 10 ppm), showing the perylene endgroup signals.

Chapter 5

Chemistry of Poly(3-hexylthiophene)s: 4-Position Functionalizations for Conformational Studies and New Functional Materials

Abstract: Poly(3-hexylthiophene) (P3HT) is one of the most investigated conjugated polymers and has been employed as the active material in many devices including field-effect transistors, organic photovoltaics and sensors. As a result, methods to further tune the properties of P3HT and analysis of their conformations are desirable for specific applications. In this chapter, we report a facile postpolymerization modification strategy to functionalize the 4-position of commercially available P3HT in two simple steps – bromination of the 4-position of P3HT (Br-P3HT) followed by lithium-halogen exchange and quenching with an electrophile. Specifically, we achieved near quantitative lithium-bromine exchange with Br-P3HT, which requires over 100 thienyl lithiates to be present on a single polymer chain. The lithiated-P3HT is readily combined with functional electrophiles, resulting in P3HT derivatives with ketones, secondary alcohols, trimethylsilyl (TMS) group, fluorine, or an azide at the 4-position. A primary focus of this chapter will be on the conformational analysis of the polymers using absorption and emission spectroscopy. Particularly, we utilize the selected functionalized polymers to analyze how the substituents can change the polymer conformations. The sizes of 4-position substituents alter polymer conformations such as highly planar, moderately twisted, or largely twisted.

Parts of this chapter were adapted and reprinted with permission from Koo, B.; Sletten, E. M.; Swager, T. M. "Functionalized Poly(3-hexylthiophene)s via Lithium–Bromine Exchange" *Macromolecules*, **2015**, 48, 229.

5.1 Introduction

Polythiophenes (PTs) are the most widely studied conjugated polymers in organic electronics, and are currently employed in field-effect transistors,[1,2] light-emitting diodes,[3] and organic photovoltaics.[4-6] Unsubstituted PT is highly crystalline and thus insoluble, hampering its processability; however, 3-hexyl substitution overcomes these limitations. The synthesis of poly(3-hexylthiophene) (P3HT) has been studied extensively over the last few decades. Grignard metathesis (GRIM) polymerization is a particularly powerful approach and allows for the large-scale preparation of highly regioregular P3HT at non-cryogenic reaction temperatures.[7-10]

In order to enhance and fully exploit the properties of PTs, facile chemical modification of PTs is necessary. In particular, the tailoring of PT properties has largely focused on the addition of alkyl or functional side chains to the 3- and/or 4-positions in order to expand their structure-property relationships for improved utility in optoelectronic devices.[11-19] For example, Ueda and co-workers reported regioregular PTs with phenyl and pyridyl side chains, which have resulted in decreased band-gaps as a result of extended π-conjugation.[11] Ludwigs and co-workers reported that head-to-tail PTs having an alkylthiophene side chain display a 30% increase in open circuit voltage (V_{oc}) in solar cells, which was attributed to a lowered highest occupied molecular orbital (HOMO).[12] Our group has reported pentafluorophenoxy-containing analogues of regioregular P3HT behave as surfactants at the bulk heterojunction interfaces, and the addition of only a small amount of these materials yielded a 30% increase in power conversion efficiency (PCE) as compared to a P3HT:PCBM standard.[13] In addition to solar cells, functionalized PTs play a pivotal role in designing chemoresistive sensors when used to wrap carbon nanotubes (CNTs). Using this scheme, customized, receptor-functionalized PTs were used to create selective detection schemes for chemical warfare agents[14] and were able to distinguish between structural isomers of xylene.[15]

Methods to prepare functionalized PTs generally integrate the side-chains or functional groups at the monomer stage. A clear advantage of this approach is that 100% of the thiophene repeating units can be reliably functionalized. However, this method is not universally applicable, and in particular, GRIM polymerization conditions are not compatible with many functional groups. As a result, post-polymerization modification[20] can offer an alternative, efficient strategy to functionalize PTs. For example, current methods to modify PTs via post-polymerization modification include the GRIM polymerization of protected terminal alkyne[21] or alkyl-bromide thiophene monomers,[22] which can be modified after polymerization through Cu-mediated Huisgen 1,3-dipolar cycloaddition[23,24] or nucleophilic substitution, respectively. These approaches allow for the installation of functional groups which could not be employed in a GRIM polymerization; however, these examples still entailed preparation of specialized monomers.

A more attractive approach is the direct modification of commercially available regioregular P3HT. Previously, Holdcroft and co-workers have achieved efficient, direct modification of the 4-position of P3HT through electrophilic bromination with *N*-bromosuccinimide (NBS).[25] The brominated P3HT (Br-P3HT) then served as a cross-coupling substrate to introduce functionality to the 4-position of P3HT[26] via Suzuki-Miyaura,[27] Stille,[28] and Heck reactions.[29] Others have extended these cross-coupling strategies to introduce fullerene derivatives,[30,31] pyrene,[32] perylene bisimide,[33] and copolymers.[34-36] Herein, we expand the utility of Br-P3HT and demonstrate that near-quantitative lithium-halogen exchange occurs at the 4-position and can be quenched with a variety of electrophiles to yield new 4-position functionalized P3HTs (Scheme 5.1). This methodology diversifies the portfolio of functionalized P3HTs with an efficient synthetic procedure.

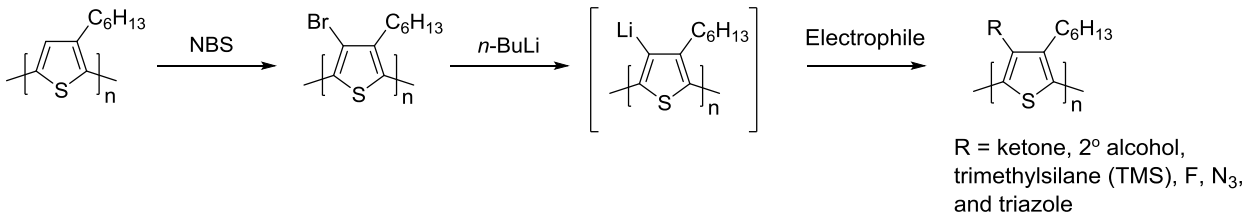

Scheme 5.1. Post-polymerization modification via Li-Br exchange and subsequent quenching with functional electrophiles.

The analysis of photophysics demonstrates that the conformations of polythiophenes are affected by 4-position substituents. Among the functionalized polymers, we choose hydrogen-, fluorine-, and bromine-substitutions at the 4-position of polythiophenes, and show how the different sizes can affect the planarity of polymer backbones.

5.2 Results and Discussion

5.2.1 Formation of Poly(3-Hexyl-4-Thienyllithium)s

Lithium-bromine exchange is an extensively utilized chemical transformation, and most aryl or vinyl bromides react with alkyllithium reagents to form new organolithiates. These aryl- and vinyl-lithium species are highly reactive intermediates and readily react with electrophiles. This strategy is widely employed in small-molecule chemistry; however, its extension to polymer chemistry has been limited, most likely as a result of concerns over polyanion formation. Specifically, it is well-accepted that generating a second anion within the same molecule is much more difficult to form than the first.[39] Extrapolating this to a polymer chain, the $(n+1)^{th}$ anion should be more difficult to form than the n^{th} anion. To explore the limits of lithium-halogen exchange and utility in polymer systems, we initiated a thorough analysis of the lithium-halogen exchange on Br-P3HT.

To test the efficiency of polyanion formation from Br-P3HT (**1**), we subjected **1** to varying amounts of *n*-butyllithium (*n*-BuLi), followed by quenching with excess methanol and examined the conversion back to P3HT (Scheme 5.2). We characterized the magnitude of the lithium-bromine exchange by comparing the NMR spectrum integration values of the thiophene 4-H (6.98 ppm, Figure 5.1) with the α-methylene of the hexyl chain (2.81 ppm, Figure 5.1) in addition to analyzing the weight percent of bromine as determined by elemental analysis (EA). The results are summarized in Table 5.1 and the NMR spectra are shown in Figure 5.1, where x and y represent monomers containing proton and bromine at the 4-position, respectively. Gratifyingly, our results indicated we were indeed able to achieve near-quantitative lithium-bromine exchange on P3HT. Standard small-molecule conditions for lithium-halogen exchange often employ 1.2 equivalents of butyl lithium. Using analogous conditions, we found that 73% lithiation was observed (**3a**).

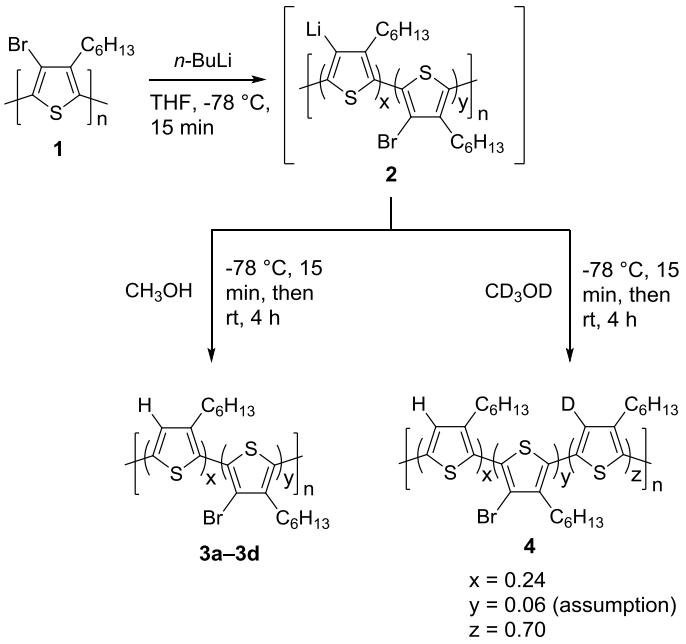

Scheme 5.2. Analysis of the lithium-bromine exchange.

Entry	*n*-BuLi (eq.)	NMR		EA		Yields
		x	y	X	y	
3a	1.25	0.73	0.27	0.852	0.148	62%
3b	2.5	0.92	0.08	0.978	0.022	78%
3c	5	0.94	0.06	0.987	0.013	86%
3d	10	>0.95	0.05<	0.991	0.009	91%

Table 5.1. Relationship between equivalents of *n*-BuLi and degree of lithium-bromine exchange. NMR indicates conversions determined by ^{1}H NMR integration, and EA indicates conversions determined by elemental analysis.

Upon increasing the amount of *n*-BuLi (**3b**–**3d**), more than 95% lithium-bromine exchange was achieved. The EA data for **3a**–**3d** also display analogous trends to the NMR spectra. From Table 5.1, it is evident that as the amount of *n*-BuLi is increased, the recovered yields also increase. This relationship appears to be the result of more efficient precipitation of the polymers from methanol

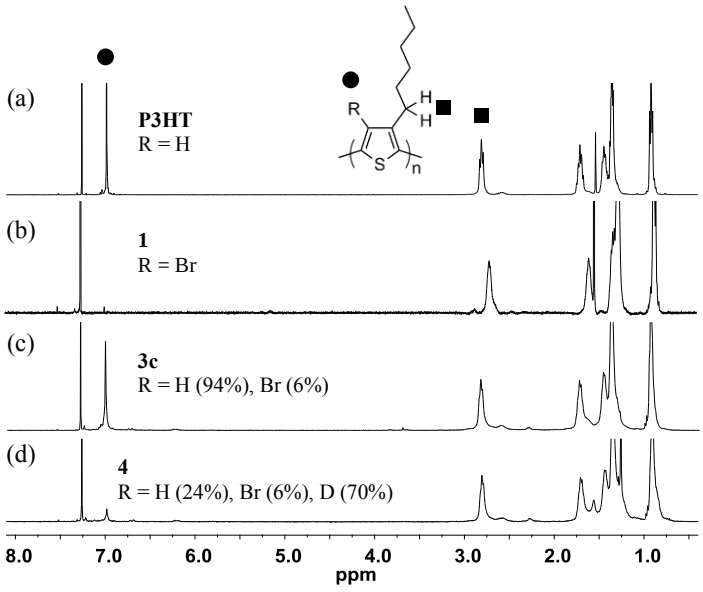

Figure 5.1. ^{1}H NMR spectra of the polymers: (a) P3HT, (b) **1** (Br-P3HT), (c) **3c**, and (d) **4**. The sharp peak at 6.98 ppm from 4-position proton (●) enables the estimation of the Li-Br exchange by comparison to the peak at 2.81 ppm from α–methylene (■) of the hexyl chain. For detailed integration values and peak locations, please refer to the Chapter 5.6 Appendix.

due to the higher salt concentration (lithium salt) in the reaction mixture. The salt weakens the solvation of the polymer by interacting with THF and thus facilitate polymer aggregation. The dispersity of **3a**–**3d** is increased during the reaction from the corresponding Br-P3HT starting polymer (26 kDa, M_w/M_n = 1.80) to **3a** (15 kDa, M_w/M_n = 3.01), **3b** (28 kDa, M_w/M_n = 9.43), **3c** (41 kDa, M_w/M_n = 7.39), and **3d** (24 kDa, M_w/M_n = 13.4). The GPC traces of these polymers (Chapter 5.6 Appendix) show that new peaks at higher molecular weight portions (such as 100 kDa and 550 kDa) emerged, suggesting some oligomerization and/or crosslinking. The exact nature of these high molecular weight species has not been determined. Considering the above results, we choose to develop a new PT modification methodology using 5 equivalents of *n*-BuLi.

Before proceeding with the introduction of electrophiles to the lithiated P3HT (Chapter 5.2.2 Scope), we further investigated the origin of the 4-position proton in our methanol quenching experiments. In light of the high basicity of the polylithium intermediate **2**, a portion of the recovered 4-position proton could originate from undesired proton impurities such as deprotonation of the α-methylene on the hexyl chain or the solvent, tetrahydrofuran (THF). To assay this, under rigorously dry conditions, Br-P3HT was combined with 5 equivalents of *n*-BuLi and quenched with deuterated methanol (CD_3OD), yielding **4** (Scheme 5.2). The NMR spectrum of polymer **4** (Figure 5.1d) showed 24% recovery of the 4-position thiophene proton at 6.98 ppm. By assuming that residual bromine content of **4** is the same as the contents of **3c** (that is, 6%), 70% of the monomers contained a deuteron (z = 0.70, Scheme 5.2). This result demonstrates that with this methodology P3HTs with up to 70% modification at the 4-position can be achieved. It should be noted that lower degrees of functionalization can also be achieved by controlling the levels of bromination.[40]

The possible avenue for introduction of the recovered 4-position proton in **4** could be E2 elimination of *n*-butyl bromide formed in situ by Li-Br exchange. However, the direct introduction of *n*-butyl bromide did not increase the recovered 4-position proton. As described in Figure 5.2a, we added 10 equiv of *n*-BuBr after Li-Br has occurred and before quenching with deuterated methanol. The *n*-BuBr used here was purified by stirring it for 4 hours under K_2CO_3, followed by distillation in order to remove any proton impurities. Our hypothesis is that if E2 elimination would occur, there could be more protons back at the 4-position than 24% which is without *n*-BuBr addition. Two independent reactions with the identical reaction condition were carried out in order to best assess whether E2 elimination would occur or not. The two NMR spectra are shown in Figure 5.2a and 5.2b. The recovered 4-position protons appeared at 6.98 ppm, and after subtracting ^{13}C-^{1}H coupling satellite overlapped with the 4-position proton peak, we have seen that 25%

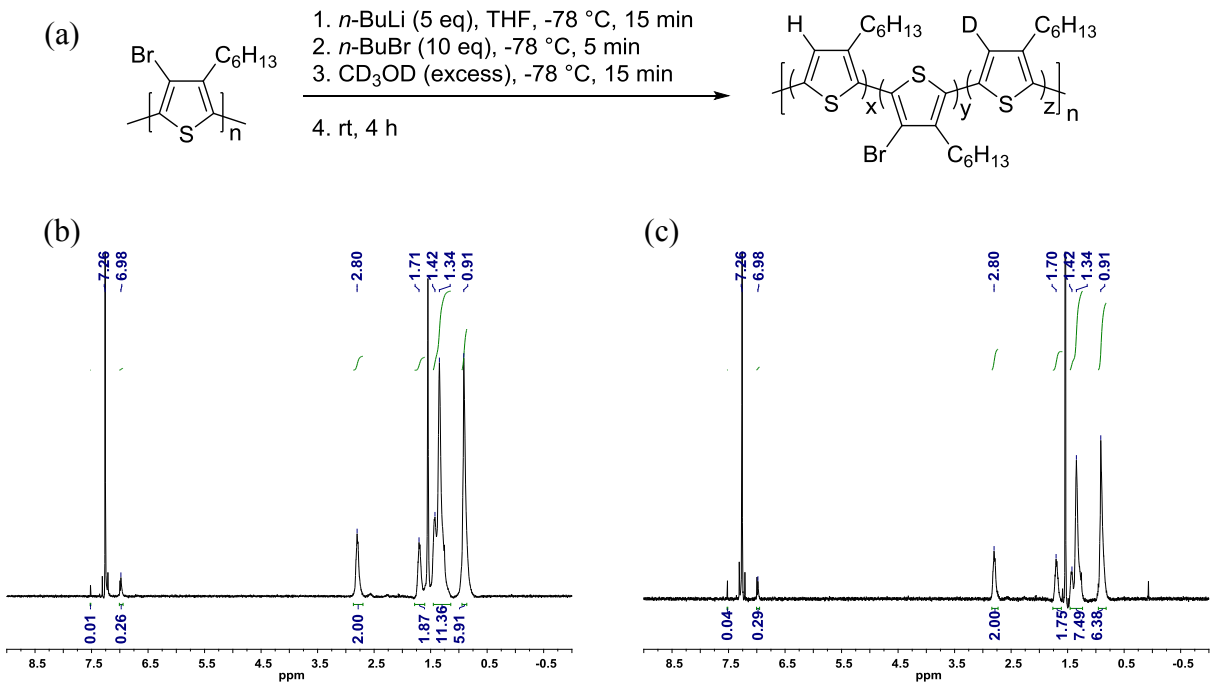

Figure 5.2. Control experiments with *n*-butyl bromide. (a) Reaction scheme. *n*-butyl bromide is added after Li-Br has occurred and before quenching with methanol. (b, c) Two NMR spectra obtained from two independent experiments.

protons are back in both independent experiments. This 25% is almost identical to the reaction in Figure 5.1d (24%) without the addition of *n*-butyl bromide, suggesting E2 elimination with *n*-butyl bromide is not a significant source of recovered proton.

5.2.2 Scope of Functional P3HTs: Quenching with Electrophiles

The efficient lithiation and quenching suggested that this methodology could be a versatile, efficient approach for the synthesis of 4-position functionalized P3HT by introducing lithiated intermediate **2** to a variety of electrophiles. We first applied this methodology to the synthesis of ketone-functionalized P3HTs (**5**–**11** in Scheme 5.3) by the introduction of anhydrides to **2**. We found that short, long, and bulky alkyl ketones (**5**–**7**), trifluoromethyl ketone (**8**), and aryls with different substituents (**9**–**11**) can all be appended to P3HT. The conversions (z values in Scheme 5.3) range from 47–65% as determined by NMR spectroscopy. Infrared (IR) spectroscopy confirms the appearance of distinct ketone peaks at around 1650-1800 cm^{-1} for all cases (**5**–**11**, see the Chapter 5.6 Appendix). Secondary alcohol P3HT derivatives (**12**–**14**) were obtained by quenching the intermediate **2** with the corresponding aldehydes. Despite being weaker electrophiles than anhydrides, similar conversions were achieved (51–63%). Trimethylsilyl (TMS) functionalized P3HT (**15**) was synthesized by quenching the lithiated P3HT with TMS chloride to result in 59% incorporation of TMS groups. Fluoride and azide moieties could also be installed at the 4-position using *N*-fluorobenzenesulfonimide (NFSI) and tosyl azide as electrophiles, respectively (vide infra). The dispersity of most of the synthesized polymers is increased during the chemical transformation as shown in the GPC traces (SI). Although there could be multiple interpolymer coupling in the ketone-functionalized P3HTs, it is most likely that the increased dispersity is primarily due to the lithium-bromine exchange, since **3a**–**3d** have already possessed the increased dispersity.

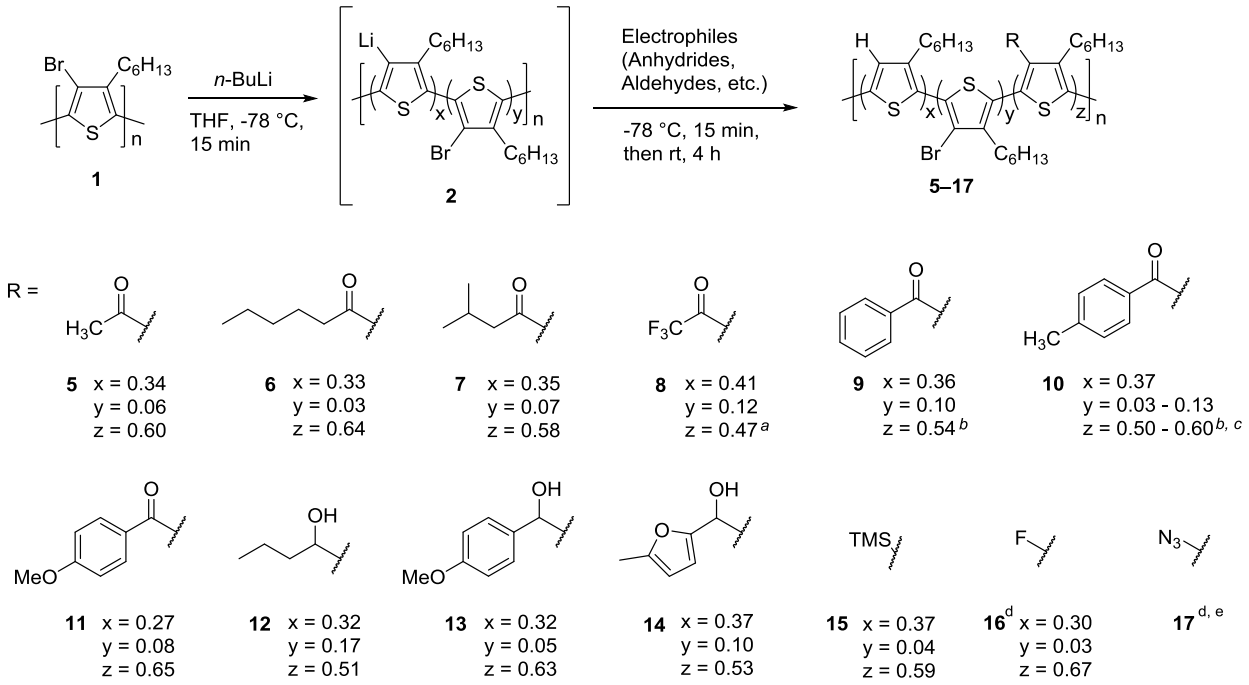

a. The conversion determined by ^{19}F NMR with trifluorotoluene as an internal standard in NMR solvent. EA showed 46% conversion (See SI).

b. The conversion is slightly overestimated due to overlapped peaks in the aryl region of the ^{1}H NMR spectra with CDCl3.

c. The conversion cannot be calculated with a single value due to the overlapped peaks of α-CH_2 of hexyl chain with Ar-Me.

d. Slightly different reaction contions are employed. Please see below and SI for detailed conditions.

e. The conversion was not available due to the insolubility of the product.

Scheme 5.3. The scope of this methodology: ketone (**5**–**11**), secondary alcohol (**12**–**14**), TMS (**15**), F (**16**), and azide (**17**) functionalized P3HTs.

5.2.3 Conformational Studies of P3HT: The Effects of 4-Position Sizes

Roncali and coworkers[41] have proposed 4-fluoro-P3HT (F-P3HT, **16**) as an advantageous material for organic photovoltaics due to the combination of its high electronegativity and small size that will lower the HOMO and LUMO levels yet not significantly alter the crystal packing. Despite attempts to synthesize F-P3HT with a fluorine atom at each 4-position through a monomer-modification approach, Roncali's efforts were unable to surpass 33% fluorination of PT using a monofluorinated terthiophene as the monomer unit. Our new lithium-halogen exchange methodology facilitated regioregular F-P3HT with higher percent fluorine in fewer steps. Upon

subjecting lithiated P3HT to NFSI (Figure 5.3a), the introduction of fluorine atoms onto the 4-position was immediately evident by the broad singlet at -123.60 ppm in the ^{19}F NMR spectrum (Chapter 5.6 Appendix). The conversion was calculated by determining the amount of 4-position proton by ^{1}H NMR spectroscopy and 4-position residual bromine by EA. From these values, the amount of 4-position fluorine was inferred to be 67%, twice as much as previously possible by the monomer-modification approach. We further investigated the electronic properties of the F-P3HT and compared it to P3HT and Br-P3HT through absorption spectroscopy, photoluminescence spectroscopy, and cyclic voltammetry (CV) (Figure 5.3 and Chapter 5.6 Appendix). As predicted by Roncali and coworkers, the small size of the fluorine atom resulted in minimal twisting of the backbone and thus longer conjugation lengths as compared to Br-P3HT, although P3HT still appeared to have a superior conjugation length as indicated by solution spectra (Figure 5.3b, chloroform) and thin films (Figure 5.3c). The optical bandgap of F-P3HT (1.97 eV), measured from absorption spectra in the thin film (Figure 5.3c), is similar to P3HT (1.90 eV), but much smaller than Br-P3HT (2.80 eV). The HOMO is measured by carrying out cyclic voltammetry in 0.1 M tetrabutylammonium hexafluorophosphate in acetonitrile as an electrolyte, along with spin-coated polymer film on ITO-coated glass, Pt wire, and Ag/AgCl electrode as a working, counter, and reference electrode, respectively. Ferrocene/ferrocenium redox couple was used as an internal standard, assuming its redox positioned at -4.8 eV from vacuum level. CV analysis (Figure 5.3e) revealed that the HOMO of F-P3HT is at -5.38 eV, which is 0.51 eV lower than P3HT (-4.87 eV), indicating increased oxidative stability in atmosphere. Br-P3HT did not show any significant current peak, indicative of its non-conductive nature and absence of π-π stacked polymer backbone. P3HT and F-P3HT thin films exhibit bathochromic shifts as compared to solution (451 to 530 nm for P3HT; 419 to 491 nm for F-P3HT) as a result of a planarization of the polymer main chain in

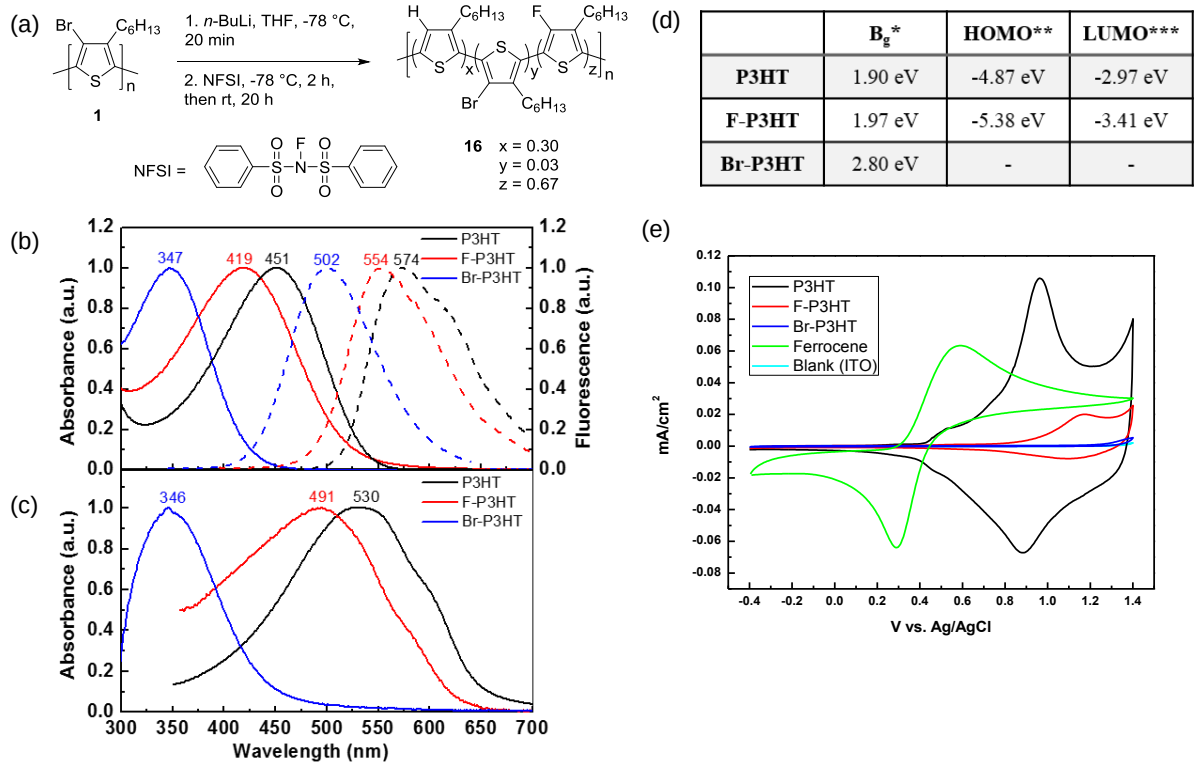

(d)

	B_g*	HOMO**	LUMO***
P3HT	1.90 eV	-4.87 eV	-2.97 eV
F-P3HT	1.97 eV	-5.38 eV	-3.41 eV
Br-P3HT	2.80 eV	-	-

Figure 5.3. (a) Synthesis of F-P3HT (**16**). NFSI = *N*-fluorobenzenesulfonimide. (b) Absorption (solid line) and photoluminescence (dotted line) spectra of P3HT (black), F-P3HT (red), and Br-P3HT (blue) in $CHCl_3$. Excitation at 400 nm (P3HT), 380 nm (F-P3HT), and 330 nm (Br-P3HT). (c) Absorption spectra of thin films of each polymer. The films are fabricated on glass by spin-coating each polymer from a chlorobenzene solution. (d) Electronic properties of P3HT, F-P3HT, and Br-P3HT obtained from photophysics and cyclic voltammetry measurements. *Optical bandgap (B_g) was measured by onset (drawing a tangent line) of the absorption spectra in thin film. **HOMO = e$(-E_{polymer}^{onset,oxidation} + E_{Fc}^{onset,oxidation} - 4.8\,V)$. *** LUMO = HOMO + B_g. (e) Cyclic voltammetry curves of P3HT (black), F-P3HT (red), Br-P3HT (blue), ferrocene (light green), and blank measured on bare ITO (light blue).

the solid state. Thin film spectra also show shoulder signals at 600 nm for P3HT and 574 nm for F-P3HT that are well-defined vibronic transitions[42,43] from the planarized π-π stacked (partially crystalline) polymer backbone. As expected in the case of Br-P3HT, no bathochromic shift or shoulder peak is observed, indicating that the steric bulk of the bromine atoms result in a twisted

backbone and thus no π-π stacking is present in the Br-P3HT film. These results are consistent with the CV data.

5.2.4 Azide-Alkyne Click Reactions on Azido-P3HT

To expand our methodology, we installed an azide group at the 4-position, which could be further modified through copper-catalyzed[23,24] or strained-promoted copper-free[44] cycloaddition reactions with alkynes[45]. We were able to synthesize poly(3-azido-4-hexylthiophene) (N_3-P3HT, **17**) by the addition of tosyl azide to lithiate **2**, followed by the addition of an acid, such as glacial acetic acid or hydrochloric acid (Figure 5.4a). Acidic workup is intended for preventing decomposition pathways in the basic condition, such as the formation of amines from 1,3-disubstituted triazenes.[46] The strong azide peak in the IR spectrum at 2105 cm^{-1} (Figure 5.4b)

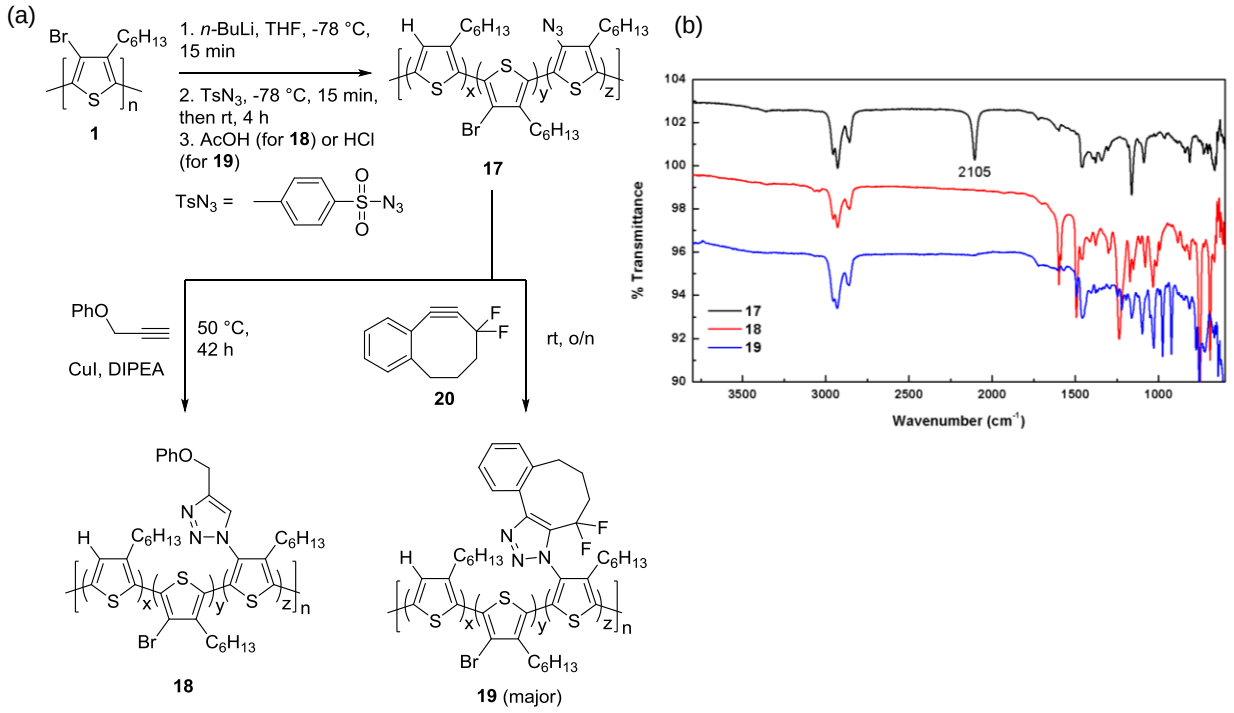

Figure 5.4. (a) Click reactions with azido-P3HT (**17**) in the Cu-catalyzed (**18**) and strain-promoted Cu-free (**19**) conditions. (b) Comparison of IR of **17** (black), **18** (red), and **19** (blue). **17** was made from HCl quenching and resulted in a strong azide peak at 2105 cm^{-1}. Quenching with AcOH produced the same azide peak. In both **18** and **19**, complete disappearance of the azide peak was observed.

indicated the presence of azide moieties. Next, we modified **17** through click reactions with alkynes. As a result of the insolubility of azido-P3HT after precipitation in methanol, we took measures to avoid precipitation (see the Chapter 5.4 Experimental Details) and performed an in situ click reaction on a crude solution (suspension) of **17**. A Cu-catalyzed click reaction in the presence of copper iodide (CuI), diisopropylethylamine (DIPEA),[21] and phenyl propargyl ether was carried out to synthesize **18**. The IR spectrum of **18** (Figure 5.4b) reveals the disappearance of the azide peak, associated with the emergence of characteristic triazole (1599 cm^{-1}) and phenyl (1494 cm^{-1}) signals. We also modified N_3-P3HT through a strain-promoted cycloaddition with difluorobenzocyclooctyne **20**.[37] The resulting triazole-containing P3HT (**19**) was soluble in common organic solvents, and ^1H NMR spectroscopy, ^{19}F NMR spectroscopy, as well as the disappearance of the azido group in the IR spectrum (Figure 5.4b) confirmed that the cycloaddition had occurred on the polymer. The analysis of ^{19}F NMR spectrum indicated that **19** is the major regioisomer. The ability to easily synthesize N_3-P3HT and its click reaction offer a plethora of opportunities for custom P3HT derivatives to be prepared from commercially available P3HT.

5.3 Conclusions

A variety of functionalized P3HTs were synthesized in a simple two-step approach, and the conformations of selected functionalized polymers are analyzed. In contrast to the conventional belief that the generation of multiple reactive anions on one molecule is not favorable,[39] we observed nearly quantitative lithium-bromine exchange on ca. 30 kDa Br-P3HT (more than 100 thiophene repeat units). The multi-lithiated P3HT is highly reactive, yet stable enough to undergo the next reaction in situ with functional electrophiles, resulting in an array of modified P3HTs. We successfully prepared ketone-, secondary alcohol-, TMS-, F-, and N_3-containing P3HTs, many of

which could not be synthesized by direct GRIM polymerization. The optical spectra of F-P3HT in solution and thin films as well as cyclic voltammetry were investigated to infer the electronic properties, chain configuration, and solid state behavior in comparison to P3HT and Br-P3HT. This conformational analysis will provide a novel design principle to tune the optical and electronic properties of polymers. Additionally, we demonstrated that N_3-P3HT could be further derivatized with alkynes using click chemistry. This novel, efficient methodology, and more generally the ability to generate polyanions through lithium-halogen exchange, will allow for the synthesis of many new functional polymers.

5.4 Experimental Details

5.4.1 General

Chemicals were purchased from Aldrich, Alfa Aesar, and TCI America without further purification unless noted otherwise. Acetic acid and methanol were purchased from Macron Fine Chemicals. Methanol-d_4 "100%" (D, 99.95%) in ampule were purchased from Cambridge Isotope Laboratories, Inc. Butylaldehyde and 4-methoxybenzaldehyde were distilled before use. Regioregular P3HT was purchased from Aldrich. All reactions were carried out under argon with standard Schlenk techniques. Anhydrous tetrahydrofuran (THF) was obtained from Sigma-Aldrich dry solvent kegs and kept in a Schlenk flask with molecular sieves (3 Å). Difluorobenzocyclooctyne (**20**) was synthesized by the literature procedure with the use of tetrabutylammonium fluoride (TBAF), instead of CsF.[37] All ^{1}H, and ^{19}F NMR spectra were collected on a Bruker Avance-400 and data is reported in ppm. ^{1}H NMR spectroscopy is referenced to solvent peaks, and ^{19}F NMR spectroscopy is referenced to trifluorotoluene (δ = -62.72 ppm). The multiplicity is reported as follows: s = singlet, d = doublet, t = triplet, m = multiplet or

unresolved, br = broad, bs = broad singlet, and bm = broad multiplet. Coupling constants J are reported in Hz. Elemental analyses were carried out by Robertson Microlit Laboratories, Ledgewood NJ (USA). UV-vis spectra were recorded on an Agilent Cary 4000 spectrometer at room temperature. The solutions were prepared in dichloromethane or chloroform with concentrations between 10^{-4} M and 10^{-6} M. Thin films were prepared on glass by spin-coating 3500 rpm for 30 seconds from a solution of functionalized P3HT in chlorobenzene (1 mg/ml, F-P3HT is not completely soluble in this concentration, and undissolved polymers are syringe-filtered). Fluorescence measurements were performed at room temperature with a Horiba Jobin Yvon SPEX Fluorolog-τ3 fluorimeter (model FL-321, 450 W Xenon lamp) using right-angle conformation. Infrared (IR) spectra were measured on a Thermo Scientific Nicolet 6700 Fourier Transform Infrared Spectrometer using the Attenuated Total Reflectance (ATR) mode on a germanium crystal. THF Gel Permeation Chromatography (GPC) was performed (0.5 mg/ml) on an Agilent 1260 Infinity system, calibrated with polystyrene standards. Cyclic voltammetry was carried out with an AUTOLAB PGSTAT 10 potentiostat (Eco Chemie) on three electrode system: polymer film on indium tin oxide (ITO)-coated glass (1.2 cm x 1.2 cm) as a working electrode, Pt wire as a counter electrode, and Ag/AgCl as a reference electrode. Polymer films on ITO-coated glass were prepared by spin-coating a solution of PT in chloroform (2 mg/ml, F-P3HT was sonicated to dissolve it for about 1 hour) with 2000 rpm for 30 seconds. The film was dried and annealed at 70 °C for 15 min. The area of 1.2 cm x 0.7 cm was immersed in the electrolyte (0.1 M tetrabutylammonium hexafluorophosphate in anhydrous acetonitrile) during measurement. The ferrocene/ferrocenium redox couple was used as an internal standard.

5.4.2 Synthetic Procedures for Polymers

Br-P3HT (1): Br-P3HT was synthesized as previously reported.[25] Briefly, to a stirring solution of commercial P3HT (300 mg, 1.80 mmol in terms of repeat unit) in chloroform (20 mL), NBS (386 mg, 2.16 mmol) was added portionwise. The reaction mixture was stirred for 12 h at room temperature. The temperature was elevated to 50 °C for 2 h, then the mixture was poured into a saturated $NaHCO_3$ solution (50 mL). The organic layer was washed with water five times and dried over $MgSO_4$. The mixture was precipitated in methanol. The precipitates were filtered and dried overnight under vacuum at room temperature, resulting in yellow polymer (441.6 mg, 1.80 mmol in terms of repeat unit, 99% yield based on 100% bromination). Four different batches of Br-P3HTs were used throughout the paper. #1 (33,000 g/mol, M_w/M_n = 2.05, starting from commercial P3HT with 41,000 g/mol, M_w/M_n = 2.16), #2 (27,000 g/mol, M_w/M_n = 1.82, starting from commercial P3HT with 28,000 g/mol, M_w/M_n = 1.86), #3 (26,000 g/mol, M_w/M_n = 1.80, starting from commercial P3HT with 28,000 g/mol, M_w/M_n = 1.86), and #4 (39,000 g/mol, M_w/M_n = 1.99, starting from commercial P3HT with 33,000 g/mol, M_w/M_n = 2.03)). Anal. Calcd for $C_{10}H_{13}BrS$ (#4): C, 48.99; H, 5.34; Br, 32.59; S, 13.08. Found: C, 48.38; H, 5.09; N, 0.38; Br, 33.40; S, 12.35.

General procedures for the synthesis of the functionalized P3HT (3–15): To a stirring solution of Br-P3HT (30 mg, 0.122 mmol in terms of repeat units) in THF (6 mL) at -78 °C, *n*-BuLi (0.612 mmol, 5 equiv, 1.6 M in hexane, 0.38 mL) was added dropwise. After 15 min of stirring, an electrophile (1.22 mmol, 10 eq.) was added to the mixture. Stirring continues for another 15 min. The temperature was increased to room temperature, and the resulting mixture was stirred for 4 h. Methanol (50 mL) was poured and stirring continued until precipitate was generated. The precipitated solution was filtered, and the polymer was dried overnight under vacuum at 50 °C.

Poly[(3-hexylthiophene)-*ran*-(3-bromo-4-hexylthiophene)] (3a). Following the general procedure with Br-P3HT #3 (30 mg, M_n 26,000 g/mol, M_w/M_n = 1.80) and methanol (excess) as an electrophile, **3a** was obtained (14.4 mg, average repeat unit molecular weight 187.58 g/mol, 62 % yield). GPC: M_n 15,000 g/mol, M_w/M_n = 3.01; ^{1}H NMR (400 MHz, $CDCl_3$): δ 7.04–6.98 (m, 0.73H), 2.86–2.62 (bm, 2H), 1.69 (bm, 2H), 1.43–1.28 (bm, 6H), 0.91 (bm, 3H); IR (cm^{-1}): 1726 (C-Br), 1458 (thiophene); Anal. Calcd for $C_{10}H_{14}S$: C, 72.23; H, 8.49; S, 19.28. Calcd for $C_{10}H_{13}BrS$: C, 48.99; H, 5.34; Br, 32.59; S, 13.08. Found: C, 66.33; H, 7.43; N, 0.39; Br, 6.65; S, 16.69.

Poly[(3-hexylthiophene)-*ran*-(3-bromo-4-hexylthiophene)] (3b). Following the general procedure with Br-P3HT #3 (30 mg, Mn 26,000 g/mol, M_w/M_n = 1.80) and methanol (excess) as an electrophile, **3b** was obtained (16.5 mg, average repeat unit molecular weight 172.59 g/mol, 78 % yield). GPC: M_n 28,000 g/mol, M_w/M_n = 9.43; ^{1}H NMR (400 MHz, $CDCl_3$): δ 6.98 (s, 0.92H), 2.81–2.57 (bm, 2H), 1.71 (bm, 2H), 1.44–1.35 (bm, 6H), 0.91 (bm, 3H); IR (cm^{-1}): 1725 (C-Br), 1463 (thiophene); Anal. Calcd for $C_{10}H_{14}S$: C, 72.23; H, 8.49; S, 19.28. Calcd for $C_{10}H_{13}BrS$: C, 48.99; H, 5.34; Br, 32.59; S, 13.08. Found: C, 71.06; H, 8.33; N, 0.27; Br, 1.02; S, 16.92.

Poly[(3-hexylthiophene)-*ran*-(3-bromo-4-hexylthiophene)] (3c). Following the general procedure with Br-P3HT #3 (30 mg, Mn 26,000 g/mol, M_w/M_n = 1.80) and methanol (excess) as an electrophile, **3c** was obtained (17.9 mg, average repeat unit molecular weight 171.01 g/mol, 86 % yield). GPC: M_n 41,000 g/mol, M_w/M_n = 7.39; 1H NMR (400 MHz, $CDCl_3$): δ 6.98 (s, 0.94H), 2.81–2.57 (bm, 2H), 1.71 (bm, 2H), 1.44–1.35 (bm, 6H), 0.91 (bm, 3H); IR (cm^{-1}): 1725 (C-Br), 1464 (thiophene); Anal. Calcd for $C_{10}H_{14}S$: C, 72.23; H, 8.49; S, 19.28. Calcd for $C_{10}H_{13}BrS$: C, 48.99; H, 5.34; Br, 32.59; S, 13.08. Found: C, 71.57; H, 8.59; N, < 0.02; Br, 0.64; S, 17.53.

Poly[(3-hexylthiophene)-*ran*-(3-bromo-4-hexylthiophene)] (3d). Following the general procedure with Br-P3HT #3 (30 mg, M_n 26,000 g/mol, M_w/M_n = 1.80) and methanol (excess) as an electrophile, **3d** was obtained (18.9 mg, average repeat unit molecular weight 169.44 g/mol, 91 % yield). GPC: M_n 24,000 g/mol, M_w/M_n = 13.4; ^{1}H NMR (400 MHz, $CDCl_3$): δ 6.98 (s, 0.96H), 2.81–2.57 (bm, 2H), 1.71 (bm, 2H), 1.44–1.35 (bm, 6H), 0.91 (bm, 3H); IR (cm^{-1}): 1726 (C-Br), 1464 (thiophene); Anal. Calcd for $C_{10}H_{14}S$: C, 72.23; H, 8.49; S, 19.28. Calcd for $C_{10}H_{13}BrS$: C, 48.99; H, 5.34; Br, 32.59; S, 13.08. Found: C, 71.53; H, 8.27; N, 0.39; Br, 0.42; S, 17.38.

Poly[(3-hexylthiophene)-*ran*-(3-bromo-4-hexylthiophene)-*ran*-(3-hexylthiophene-4-d)] (4). Following the general procedure with Br-P3HT #2 (30 mg, M_n 27,000 g/mol, M_w/M_n = 1.82) and methanol-d4 (excess) as an electrophile, **4** was obtained (average repeat unit molecular weight 171.72 g/mol). ^{1}H NMR (400 MHz, $CDCl_3$): δ 6.98 (s, 0.24H), 2.81–2.57 (bm, 2H), 1.71 (bm, 2H), 1.44–1.35 (bm, 6H), 0.92 (bm, 3H).

Poly[(3-hexylthiophene)-*ran*-(3-bromo-4-hexylthiophene)-*ran*-(1-(4-hexylthiophen-3-yl)ethan-1-one)] (5). Following the general procedure with Br-P3HT #2 (30 mg, M_n 27,000 g/mol, M_w/M_n = 1.82) and acetic anhydride (10 eq., 0.116 mL) as an electrophile, **5** was obtained (26.0 mg, average repeat unit molecular weight 196.24 g/mol, quantitative yield). GPC: M_n 22,000 g/mol, M_w/M_n = 3.86; ^{1}H NMR (400 MHz, $CDCl_3$): δ 7.06–7.00 (bm, 0.34H), 2.81–2.56 (bm, 2H), 2.21 (bs, 1.81H), 1.68 (bm, 2H), 1.41–1.31 (bm, 6H), 0.87 (bm, 3H); IR (cm^{-1}):1686 (carbonyl), 1458 (thiophene); UV-vis (CH_2Cl_2): λ_{max} 277, 379 nm; Fluorescence (CH_2Cl_2): λ_{max} 549 nm (Ex. 350 nm).

Poly[(3-hexylthiophene)-*ran*-(3-bromo-4-hexylthiophene)-*ran*-(1-(4-hexylthiophen-3-yl)hexan-1-one)] (6). Following the general procedure with Br-P3HT #1 (30 mg, M_n 33,000 g/mol, M_w/M_n = 2.05) and hexanoic anhydride (10 eq., 0.28 mL) as an electrophile, **6** was obtained (27.7

mg, average repeat unit molecular weight 231.46 g/mol, 98% yield). GPC: M_n 64,000 g/mol, M_w/M_n = 3.13; ^{1}H NMR (400 MHz, $CDCl_3$): δ 7.04–6.98 (bm, 0.33H), 2.78–2.56 (bm, 2H), 2.44–2.28 (bm, 1.28H), 1.68–1.54 (bm), 1.39–1.28 (bm), 0.87–0.86 (bm); IR (cm^{-1}): 1688 (carbonyl), 1464 (thiophene); UV-vis (CH_2Cl_2): λ_{max} 256, 386 nm; Fluorescence (CH_2Cl_2): λ_{max} 551 nm (Ex. 350 nm).

Poly[(3-hexylthiophene)-*ran*-(3-bromo-4-hexylthiophene)-*ran*-(1-(4-hexylthiophen-3-yl)-3-methylbutan-1-one)] (7). Following the general procedure with Br-P3HT #1 (30 mg, M_n 33,000 g/mol, M_w/M_n = 2.05) and isovaleric anhydride (10 eq., 0.245 mL) as an electrophile, **7** was obtained (27.3 mg, average repeat unit molecular weight 220.59 g/mol, quantitative yield). GPC: M_n 64,000 g/mol, M_w/M_n = 2.35; ^{1}H NMR (400 MHz, $CDCl_3$): δ 7.04–6.98 (bm, 0.35H), 2.77–2.60 (bm, 2H), 2.34–2.33 (bm, 1.16H), 2.10 (bm), 1.68–1.58 (bm, 2H), 1.42–1.27 (bm), 0.85–0.83 (bm); IR (cm^{-1}): 1688 (carbonyl), 1465 (thiophene); UV-vis (CH_2Cl_2): λ_{max} 387 nm; Fluorescence (CH_2Cl_2): λ_{max} 554 nm (Ex. 350 nm).

Poly[(3-hexylthiophene)-*ran*-(3-bromo-4-hexylthiophene)-*ran*-(2,2,2-trifluoro-1-(4-hexylthiophen-3-yl)ethan-1-one)] (8). Following the general procedure with Br-P3HT #1 (31.1 mg, M_n 33,000 g/mol, M_w/M_n = 2.05) and trifluoroacetic anhydride (10 eq., 0.176 mL) as an electrophile, **8** was obtained (28.7 mg, average repeat unit molecular weight 220.87 g/mol, quantitative yield). GPC: M_n 33,000 g/mol, M_w/M_n = 5.50; ^{1}H NMR (400 MHz, $CDCl_3$): δ 7.07–6.99 (bm, 0.41H), 2.76–2.60 (bm, 2H), 1.68–1.60 (bm, 2H), 1.41–1.29 (bm, 6H), 0.88 (bm, 3H); ^{19}F NMR (376 MHz, $CDCl_3$): δ -74.38 (bm); IR (cm^{-1}): 1798 (carbonyl), 1202 (CF_3), 1157 (CF_3); UV-vis (CH_2Cl_2): λ_{max} 278, 387 nm; Fluorescence (CH_2Cl_2): λ_{max} 576 nm (Ex. 350 nm); Anal. Calcd for $C_{10}H_{14}S$: C, 72.23; H, 8.49; S, 19.28. Calcd for $C_{10}H_{13}BrS$: C, 48.99; H, 5.34; Br, 32.59;

S, 13.08. Calcd for $C_{12}H_{13}F_3OS$: C, 54.95; H, 5.00; F, 21.73; O, 6.10; S, 12.22. Found: C, 59.88; H, 6.12; N, < 0.02; Br, 3.55; F, 11.67; S, 13.62.

Poly[(3-hexylthiophene)-*ran*-(3-bromo-4-hexylthiophene)-*ran*-((4-hexylthiophen-3-yl)(phenyl)methanone)] (9). Following the general procedure with Br-P3HT #1 (30 mg, M_n 33,000 g/mol, M_w/M_n = 2.05) and benzoic anhydride (10 eq., 277 mg pre-dissolved in 1 mL THF) as an electrophile, **9** was obtained (25.6 mg, average repeat unit molecular weight 230.39 g/mol, 91% yield). GPC: M_n 55,000 g/mol, M_w/M_n = 2.04; ^{1}H NMR (400 MHz, $CDCl_3$): δ 7.78–7.32 (bm, 2.69H), 6.98–6.73 (bm, 0.36H), 2.80–2.29 (bm, 2H), 1.68–1.51 (bm, 2H), 1.40−1.19 (bm, 6H), 0.90–0.82 (bm, 3H); IR (cm^{-1}): 1663 (carbonyl), 1597 (phenyl), 1449 (thiophene); UV-vis (CH_2Cl_2): λ_{max} 250, 279, 397 nm; Fluorescence (CH_2Cl_2): λ_{max} 562 nm (Ex. 360 nm).

Poly[(3-hexylthiophene)-*ran*-(3-bromo-4-hexylthiophene)-*ran*-((4-hexylthiophen-3-yl)(p-tolyl)methanone)] (10). Following the general procedure with Br-P3HT #1 (30 mg, M_n 33,000 g/mol, M_w/M_n = 2.05) and 4-methylbenzoic anhydride (10 eq., 311 mg pre-dissolved in 1 mL THF) as an electrophile, **10** was obtained (30.5 mg, average repeat unit molecular weight 238.35 g/mol based on x = 0.37, y = 0.06, z = 0.57, quantitative yield). GPC: M_n 62,000 g/mol, M_w/M_n = 1.83; ^{1}H NMR (400 MHz, $CDCl_3$): δ 7.68–7.05 (bm), 6.98–6.75 (bm, 0.37H), 2.79–2.33 (bm), 1.70–1.10 (bm, 8H), 0.90–0.81 (bm, 3H); IR (cm^{-1}): 1660 (carbonyl), 1605 (phenyl), 1457 (thiophene); UV-vis (CH_2Cl_2): λ_{max} 266, 390 nm; Fluorescence (CH_2Cl_2): λ_{max} 566 nm (Ex. 360 nm).

Poly[(3-hexylthiophene)-*ran*-(3-bromo-4-hexylthiophene)-*ran*-((4-hexylthiophen-3-yl)(4-methoxyphenyl)methanone)] (11). Following the general procedure with Br-P3HT #1 (30 mg, M_n 33,000 g/mol, M_w/M_n = 2.05) and 4-methoxybenzoic anhydride (10eq., 350 mg pre-dissolved in 1 mL THF) as an electrophile, **11** was obtained (31.1 mg, average repeat unit

molecular weight 259.78 g/mol, 98% yield). GPC: M_n 63,000 g/mol, M_w/M_n = 1.84; ^{1}H NMR (400 MHz, $CDCl_3$): δ 7.78 (bm, 0.65H), 7.41 (bm, 0.65H), 6.97 (bm, 0.27H), 6.80 (bm, 1.30H), 3.82 (bs, 1.94H), 2.79–2.33 (bm, 2H), 1.68–1.17 (bm, 8H), 0.89–0.81 (bm, 3H); IR (cm^{-1}): 1655 (carbonyl), 1598 (methoxy phenyl), 1509 (methoxy phenyl), 1460 (thiophene); UV-vis (CH_2Cl_2): λ_{max} 286, 397 nm; Fluorescence (CH_2Cl_2): λ_{max} 557 nm (Ex. 365 nm).

Poly[(3-hexylthiophene)-*ran*-(3-bromo-4-hexylthiophene)-*ran*-(1-(4-hexylthiophen-3-yl)butan-1-ol)] (12). Following the general procedure with Br-P3HT #2 (30 mg, M_n 27,000 g/mol, M_w/M_n = 1.82) and butyraldehyde (10eq., 0.11 mL) as an electrophile, **12** was obtained (22.5 mg, average repeat unit molecular weight 216.47 g/mol, 85% yield). GPC: M_n 18,000 g/mol, M_w/M_n = 4.19; ^{1}H NMR (400 MHz, $CDCl_3$): δ 7.03 (bm, 0.32H), 4.78 (bm, 0.51H), 2.92–2.54 (bm, 2H), 1.88 (bm, 1.02H), 1.69–1.31 (bm, 9.02H), 0.88 (bm, 4.53H); IR (cm^{-1}): 3436 (hydroxyl), 1464 (thiophene); UV-vis ($CHCl_3$): λ_{max} 258, 360 nm; Fluorescence ($CHCl_3$): λ_{max} 536 nm (Ex. 330 nm).

Poly[(3-hexylthiophene)-*ran*-(3-bromo-4-hexylthiophene)-*ran*-((4-hexylthiophen-3-yl)(4-methoxyphenyl)methanol)] (13). Following the general procedure with Br-P3HT #1 (30 mg, Mn 33,000 g/mol, Mw/Mn = 2.05) and 4-methoxybenzaldehyde (10 eq., 0.15 mL) as an electrophile, **13** was obtained (26.6 mg, average repeat unit molecular weight 256.00 g/mol, 85% yield). GPC: M_n 57,000 g/mol, M_w/M_n = 4.24; ^{1}H NMR (400 MHz, $CDCl_3$): δ 7.20 (bm), 6.97 (bm, 0.32H), 6.82 (bm), 5.94 (bs), 3.84 (bs), 3.77 (bm), 2.75–2.27 (bm, 2H), 1.65–1.04 (bm, 8H), 0.86–0.81 (bm, 3H); IR (cm-1): 3497 (hydroxyl), 1599 (methoxy phenyl), 1510 (methoxy phenyl), 1463 (thiophene); UV-vis (CH_2Cl_2): λ_{max} 276, 297, 349 nm; Fluorescence (CH_2Cl_2): λ_{max} 532 nm (Ex. 335 nm).

Poly[(3-hexylthiophene)-*ran*-(3-bromo-4-hexylthiophene)-*ran*-((4-hexylthiophen-3-yl)(5-methylfuran-2-yl)methanol)] (14). Following the general procedure with Br-P3HT #2 (30

mg, M_n 27,000 g/mol, M_w/M_n = 1.82) and 5-methylfurfural (10 eq., 0.12 mL) as an electrophile, **14** was obtained (31 mg, average repeat unit molecular weight 232.53 g/mol, quantitative yield). GPC: M_n 14,000 g/mol, M_w/M_n = 1.99; ^{1}H NMR (400 MHz, $CDCl_3$): δ 6.98–6.88 (bm, 0.37H), 6.04–5.59 (bm), 2.79–2.35 (bm, 2H), 2.26 (bs), 1.67–1.24 (bm, 8H), 0.86 (bm, 3H); IR (cm^{-1}): 3445 (hydroxyl), 1684 (furan), 1511 (furan), 1458 (thiophene).

Poly[(3-hexylthiophene)-ran-(3-bromo-4-hexylthiophene)-ran-((4-hexylthiophen-3-yl)trimethylsilane)] (15). Following the general procedure with Br-P3HT #1 (30 mg, M_n 33,000 g/mol, M_w/M_n = 2.05) and trimethylsilyl chloride (10 eq., 0.155 mL) as an electrophile, **15** was obtained (20.8 mg, average repeat unit molecular weight 212.02 g/mol, 80% yield). GPC: M_n 32,000 g/mol, M_w/M_n = 5.83; ^{1}H NMR (400 MHz, $CDCl_3$): δ 6.96 (bs, 0.37H), 2.85–2.50 (bm, 2H), 1.68–1.58 (bm, 2H), 1.41–1.28 (bm, 6H), 0.87 (bm, 3H), 0.16 (bm); IR (cm^{-1}): 1465 (thiophene), 837 (Si-C).

Poly[(3-hexylthiophene)-*ran*-(3-bromo-4-hexylthiophene)-*ran*-(3-fluoro-4-hexylthiophene)] (16).): To a stirring solution of Br-P3HT #3 (30 mg, M_n 26,000 g/mol, M_w/M_n = 1.80, 0.122 mmol in terms of repeat units) in THF (6 mL) at -78 °C, *n*-BuLi (0.612 mmol, 5 equiv, 1.6 M in hexane, 0.38 mL) was added dropwise. After 20 min of stirring, *N*-fluorobenzenesulfonimide (1.22 mmol, 10 eq., 0.386 mg) dissolved in THF (2 mL) was added. The mixture was stirred for 2 h, at which point the temperature was increased to room temperature and the solution was further stirred for 20 h. Methanol (50 mL) was added to precipitate the polymer. F-P3HT **16** was collected by filtration, washed with methanol and acetone, and dried under vacuum at 50 °C overnight. Yield: 99% (22 mg, average repeat unit molecular weight 180.70 g/mol); GPC: M_n 17,000 g/mol, M_w/M_n = 1.47; ^{1}H NMR (400 MHz, $CDCl_3$): δ 7.02 (bm, 0.30H), 2.79–2.59 (bm, 2H), 1.65 (bm, 2H), 1.40–1.33 (bm, 6H), 0.90 (bm, 3H); ^{19}F NMR (376 MHz,

$CDCl_3$): δ -123.60 (bs); IR (cm^{-1}): 1464 (thiophene); UV-vis ($CHCl_3$): λ_{max} 266, 419 nm; UV-vis (thin film): λ_{max} 491 nm; Fluorescence ($CHCl_3$): λ_{max} 554 nm (Ex. 380 nm); Anal. Calcd for $C_{10}H_{14}S$: C, 72.23; H, 8.49; S, 19.28. Calcd for $C_{10}H_{13}BrS$: C, 48.99; H, 5.34; Br, 32.59; S, 13.08. Calcd for $C_{10}H_{13}FS$: C, 65.18; H, 7.11; F, 10.31; S, 17.40. Found: C, 60.19; H, 6.56; N, 0.64; Br, 1.11; F, 8.81; S, 14.57.

Poly[(3-hexylthiophene)-*ran*-(3-bromo-4-hexylthiophene)-*ran*-(3-azido-4-hexylthiophene)] (17). The procedure is the same as the general procedure until the quenching step (4 h stirring at room temperature). Starting from Br-P3HT #2 (30 mg, M_n 27,000 g/mol, M_w/M_n = 1.82) and using *p*-toluenesulfonyl azide solution (11-15 % (w/w) in toluene, 10 eq., 2.06 mL added based on the assumption of 13 % (w/w) in toluene) as an electrophile, the reaction was was further quenched by either glacial acetic acid (1.22 mmol, 10 equiv, 0.068 mL) or hydrochloric acid (1.22 mmol, 10 equiv, 3 M, 0.4 mL) and then the mixture was stirred for 30 – 60 min. Methanol (50 ml) was poured and stirring continued until precipitate was generated. The precipitated solution was filtered, and the polymer was dried overnight under vacuum at 50 °C. **17** was obtained (29.1 mg from HCl quenching). IR (cm^{-1}): 2105 (azide), 1457 (thiophene). As a result of acidic workup and excess tosyl azide, hydrazoic acid might be formed, and thus, cautions need to be taken. When a large reaction scale needs to be performed, aqueous workup can also be carried out, according to the literature (Gavenonis, J.; Tilley, T. D. *Organometallics* **2002**, 21, 5549-5563). Due to insolubility after precipitation, the crude mixture prior to methanol-induced precipitation was used for the next click reaction.

Poly[(3-hexylthiophene)-*ran*-(3-bromo-4-hexylthiophene)-*ran*-(1-(4-hexylthiophen-3-yl)-4-(phenoxymethyl)-1H-1,2,3-triazole)] (18). To the mixture **17** (12.7 mg) containing acetic acid, phenyl propargyl ether (12 equiv, 0.094 ml), DIPEA (50 equiv, 0.54 ml), and CuI (14 mg, 10

mol% of the acetylene) were added. The mixture was heated at 50 ºC and stirred for 42 h. Methanol was added to precipitate the polymer, and the polymer was collected by centrifugation (11k rcf[38], 10 min), washed with acetone:ethyl acetate (1:1), and dried under vacuum at 50 ºC overnight. **18** was obtained (24 mg). IR (cm^{-1}): 1599 (triazole), 1494 (phenyl), 1457 (thiophene).

Poly[(3-hexylthiophene)-*ran*-(3-bromo-4-hexylthiophene)-*ran*-(4,4-difluoro-3-(4-hexylthiophen-3-yl)-4,5,6,7-tetrahydro-3H-benzo[3,4]cycloocta[1,2-d][1,2,3]triazole)] (19). Starting from Br-P3HT #2 (30 mg, M_n 27,000 g/mol, M_w/M_n = 1.82), the crude mixture of **17** was obtained. The mixture **17** containing HCl was neutralized with NaOH (aq, 10%), and difluorobenzocyclooctyne (**20**)[37] (1.47 mmol, 12 equiv, 282 mg) in THF was added. The resulting mixture was stirred at room temperature overnight. The polymer was precipitated with methanol (50 mL), collected by filtration, washed with methanol, and dried overnight under vacuum at 50 °C, resulting in obtaining **19** (39 mg). GPC: M_n 13,000 g/mol, M_w/M_n = 2.59; ^{1}H NMR (400 MHz, $CDCl_3$): δ 7.86 (bm), 7.40 (bm), 6.98 (bm), 6.77 (bm), 2.79–2.41 (bm), 2.06 (bm), 1.66–1.30 (bm), 0.86 (bm); ^{19}F NMR (376 MHz, $CDCl_3$): δ -71.58 (bm), -90.06 (bm); IR (cm^{-1}): 1611–1570 (triazole), 1493 (phenyl), 1458 (thiophene).

Procedure for difluorobenzocyclooctyne (20): This compound was synthesized in a similar method to the literature.[37] 7,7-difluoro-5-(trimethylsilyl)-7,8,9,10-tetrahydrobenzo[8]annulen-6-yl triflate[37] (700 mg, 1.69 mmol) was dissolved in THF (3 mL). To this mixture, tetrabutylammonium fluoride solution (1 M in THF, 1.1 eq., 1.86 mL) was added, and the reaction mixture was stirred at room temperature for 10 min. This crude mixture was used in the synthesis of the polymer **19**.

5.5 References

(1) Tsumura, A.; Koezuka, H.; Ando, T. *Appl. Phys. Lett.* **1986**, 49, 1210.

(2) Sirringhaus, H.; Tessler, N.; Friend, R. H. *Science* **1998**, 280, 1741.

(3) Ohmori, Y.; Uchida, M.; Muro, K.; Yoshino, K. *Jpn. J. Appl. Phys. 2* **1991**, 30, L1938.

(4) Padinger, F.; Rittberger, R. S.; Sariciftci, N. S. *Adv. Funct. Mater.* **2003**, 13, 85.

(5) Yu, G.; Gao, J.; Hummelen, J. C.; Wudl, F.; Heeger, A. J. *Science* **1995**, 270, 1789.

(6) Günes, S.; Neugebauer, H.; Sariciftci, N. S. *Chem. Rev.* **2007**, 107, 1324.

(7) McCullough, R. D.; Lowe, R. D. *J. Chem. Soc., Chem. Commun.* **1992**, 70.

(8) Chen, T. A.; Rieke, R. D. *J. Am. Chem. Soc.* **1992**, 114, 10087.

(9) Loewe, R. S.; Khersonsky, S. M.; McCullough, R. D. *Adv. Mater.* **1999**, 11, 250.

(10) Loewe, R. S.; Ewbank, P. C.; Liu, J.; Zhai, L.; McCullough, R. D. *Macromolecules* **2001**, 34, 4324.

(11) Ohshimizu, K.; Takahashi, A.; Rho, Y.; Higashihara, T.; Ree, M.; Ueda, M. *Macromolecules* **2011**, 44, 719.

(12) Richter, T. V.; Braun, C. H.; Link, S.; Scheuble, M.; Crossland, E. J. W.; Stelzl, F.; Würfel, U.; Ludwigs, S. *Macromolecules* **2012**, 45, 5782.

(13) Lobez, J. M.; Andrew, T. L.; Bulović, V.; Swager, T. M. *ACS Nano* **2012**, 6, 3044.

(14) Wang, F.; Gu, H.; Swager, T. M. *J. Am. Chem. Soc.* **2008**, 130, 5392.

(15) Wang, F.; Yang, Y.; Swager, T. M. *Angew. Chem. Int. Ed.* **2008**, 47, 8394.

(16) Yao, K.; Chen, L.; Chen, Y.; Li, F.; Wang, P. *J. Mater. Chem.* **2011**, 21, 13780.

(17) Miyanishi, S.; Tajima, K.; Hashimoto, K. *Macromolecules* **2009**, 42, 1610.

(18) Osaka, I.; McCullough, R. D. *Acc. Chem. Res.* **2008**, 41, 1202.

(19) Holcombe, T. W.; Woo, C. H.; Kavulak, D. F. J.; Thompson, B. C.; Fréchet, J. M. J. *J. Am. Chem. Soc.* **2009**, 131, 14160.

(20) Gauthier, M. A.; Gibson, M. I.; Klok, H.-A. *Angew. Chem. Int. Ed.* **2009**, 48, 48.

(21) Benanti, T. L.; Kalaydjian, A.; Venkataraman, D. *Macromolecules* **2008**, 41, 8312.

(22) Zhai, L.; Pilston, R. L.; Zaiger, K. L.; Stokes, K. K.; McCullough, R. D. *Macromolecules* **2003**, 36, 61.

(23) Rostovtsev, V. V.; Green, L. G.; Fokin, V. V.; Sharpless, K. B. *Angew. Chem. Int. Ed.* **2002**, 41, 2596.

(24) Tornøe, C. W.; Christensen, C.; Meldal, M. *J. Org. Chem.* **2002**, 67, 3057.

(25) Li, Y.; Vamvounis, G.; Holdcroft, S. *Macromolecules* **2001**, 34, 141.

(26) Li, Y.; Vamvounis, G.; Yu, J.; Holdcroft, S. *Macromolecules* **2001**, 34, 3130.

(27) Miyaura, N.; Suzuki, A. *Chem. Rev.* **1995**, 95, 2457.

(28) Stille, J. K. *Angew. Chem. Int. Ed.* **1986**, 25, 508.

(29) Beletskaya, I. P.; Cheprakov, A. V. *Chem. Rev.* **2000**, 100, 3009.

(30) Li, M. H.; Xu, P.; Yang, J. G.; Yang, S. F. *J. Mater. Chem.* **2010**, 20, 3953.

(31) Chen, M. Q.; Li, M. H.; Wang, H. T.; Qu, S. X.; Zhao, X. M.; Xie, L. X.; Yang, S. F. *Polym. Chem.* **2013**, 4, 550.

(32) Li, M. H.; Xu, P.; Yang, J. G.; Ying, H.; Haubner, K.; Dunsch, L.; Yang, S. F. *J. Phys. Chem. C* **2011**, 115, 4584.

(33) Zhou, Z. Y.; Brusso, J. L.; Holdcroft, S. *Chem. Mater.* **2010**, 22, 2287.

(34) Chen, X. W.; Gholamkhass, B.; Han, X.; Vamvounis, G.; Holdcroft, S. *Macromol. Rapid Commun.* **2007**, 28, 1792.

(35) Economopoulos, S. P.; Chochos, C. L.; Gregoriou, V. G.; Kallitsis, J. K.; Barrau, S.; Hadziioannou, G. *Macromolecules* **2007**, 40, 921.

(36) Zhou, Z. Y.; Chen, X. W.; Holdcroft, S. *J. Am. Chem. Soc.* **2008**, 130, 11711.

(37) Sletten, E. M.; Nakamura, H.; Jewett, J. C.; Bertozzi, C. R. *J. Am. Chem. Soc.* **2010**, 132, 11799.

(38) rcf = 1.1 * 10^{-5} * r (cm) * rpm^2, where r is the rotor radius.

(39) Thompson, C. M.; Green, D. L. C. *Tetrahedron* **1991**, 47, 4223.

(40) With 0.1 equivalent of NBS, 10% of repeat units on P3HT were brominated, and the resulting polymer underwent Li-Br exchange followed by quenching with tosyl azide to append a few % of azide group on P3HT. This polymer was more soluble than **17** due to fewer azide groups on P3HT.

(41) Gohier, F.; Frère, P.; Roncali, J. *J. Org. Chem.* **2013**, 78, 1497.

(42) Crossland, E. J. W.; Rahimi, K.; Reiter, G.; Steiner, U.; Ludwigs, S. *Adv. Funct. Mater.* **2011**, 21, 518.

(43) Kim, J.; Swager, T. M. *Nature* **2001**, 411, 1030.

(44) Agard, N. J.; Prescher, J. A.; Bertozzi, C. R. *J. Am. Chem. Soc.* **2004**, 126, 15046.

(45) Palermo, E. F.; Darling, S. B.; McNeil, A. J. *J. Mater. Chem. C* **2014**, 2, 3401.

(46) Smith, P. A. S.; Rowe, C. D.; Bruner, L. B. *J. Org. Chem.* **1969**, 34, 3430.

5.6 Appendix for Chapter 5

Gel Permeation Chromatography Traces

All the Gel Permeation Chromatography (GPC) traces are plotted here. First, Br-P3HT from batch #1 to batch #4 is shown below. All Br-P3HT traces exhibit similar shape. Number-averaged molecular weights of a few peaks are indicated.

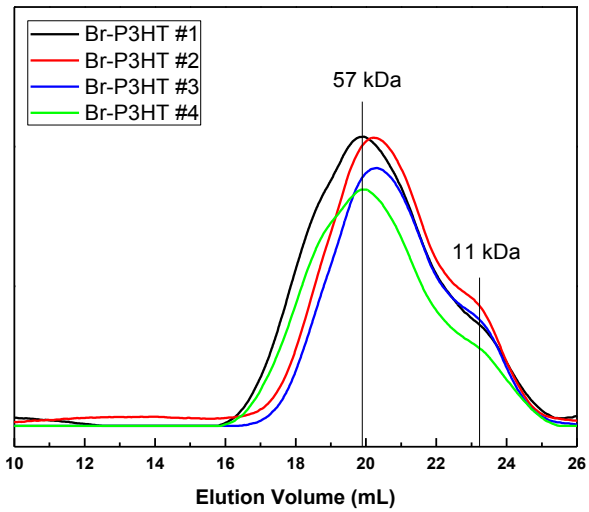

The GPC traces of compound **3a** – **3d** are plotted below. Their starting Br-P3HT #3 is also shown together. Number-averaged molecular weights of a few peaks are indicated.

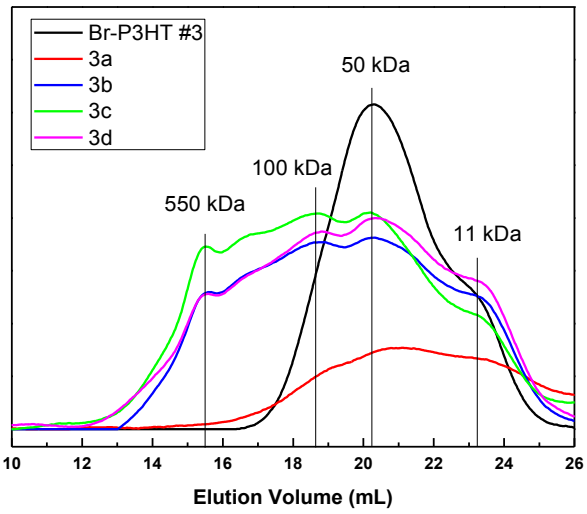

The GPC traces of ketone-functionalized P3HT (**5** – **11**) are shown below. The most frequently used Br-P3HT (#1 for ketone-functionalized P3HT) is plotted together for comparison. Number-averaged molecular weights of a few peaks are indicated.

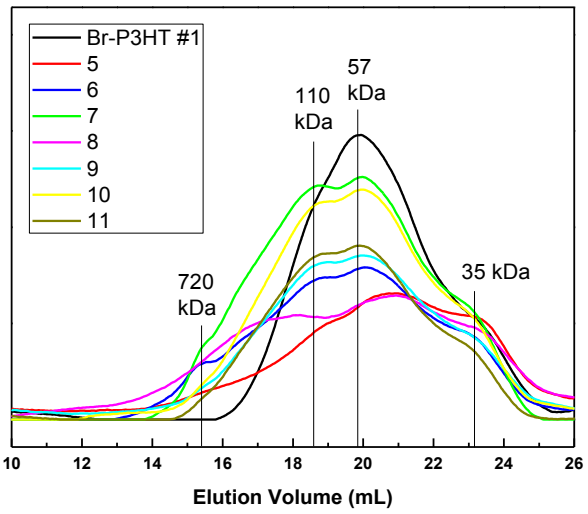

The GPC traces of secondary alcohol-functionalized P3HT (**12** – **14**) are shown below. The most frequently used Br-P3HT (#2 for secondary alcohol-functionalized P3HT) is plotted together for comparison. Number-averaged molecular weights of a few peaks are indicated.

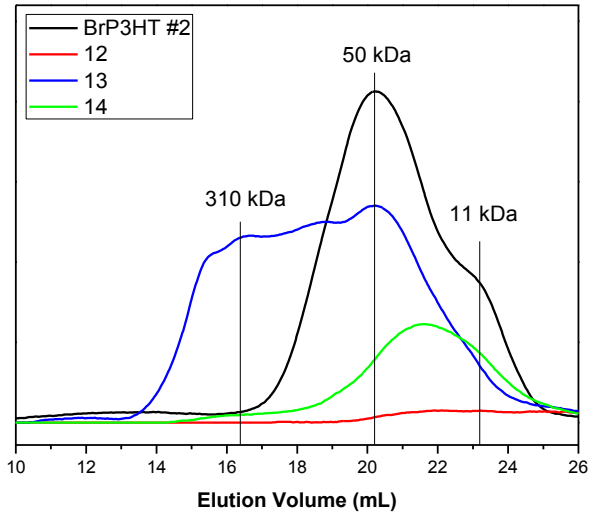

The GPC traces of **15**, **16**, and **19** are plotted below with their corresponding starting polymer Br-P3HT.

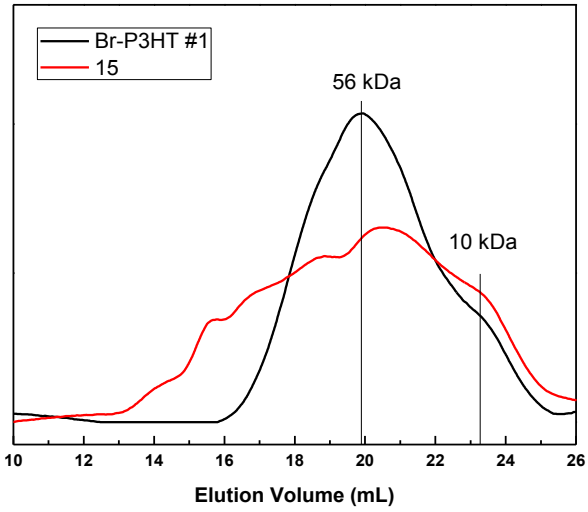

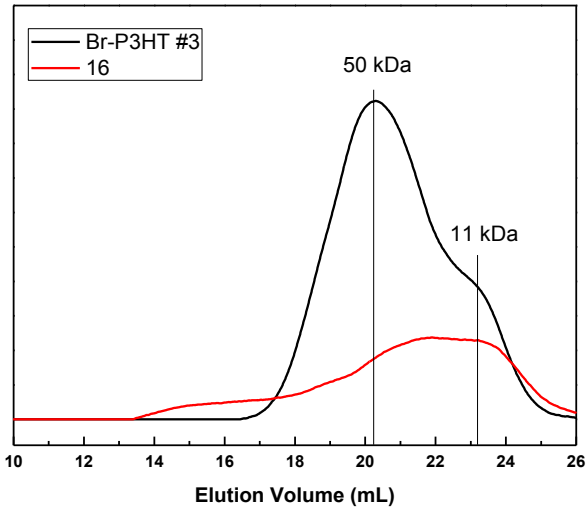
Br-P3HT #3
16
50 kDa
11 kDa
10
12
14
16
18
20
22
24
26
Elution Volume (mL)

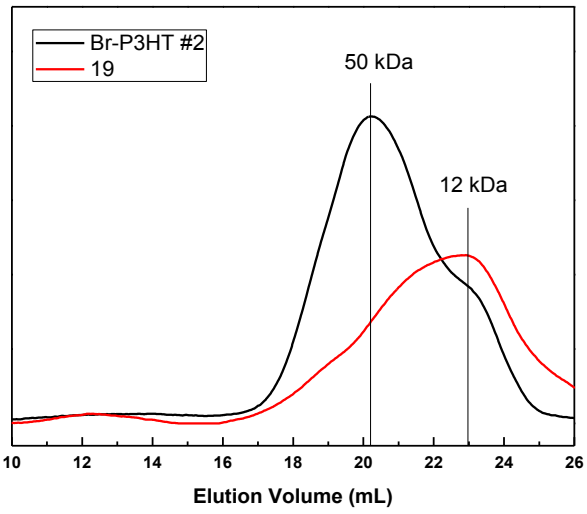
Br-P3HT #2
19
50 kDa
12 kDa
10
12
14
16
18
20
22
24
26
Elution Volume (mL)

^{1}H and ^{19}F NMR Spectra

3a (^{1}H NMR)

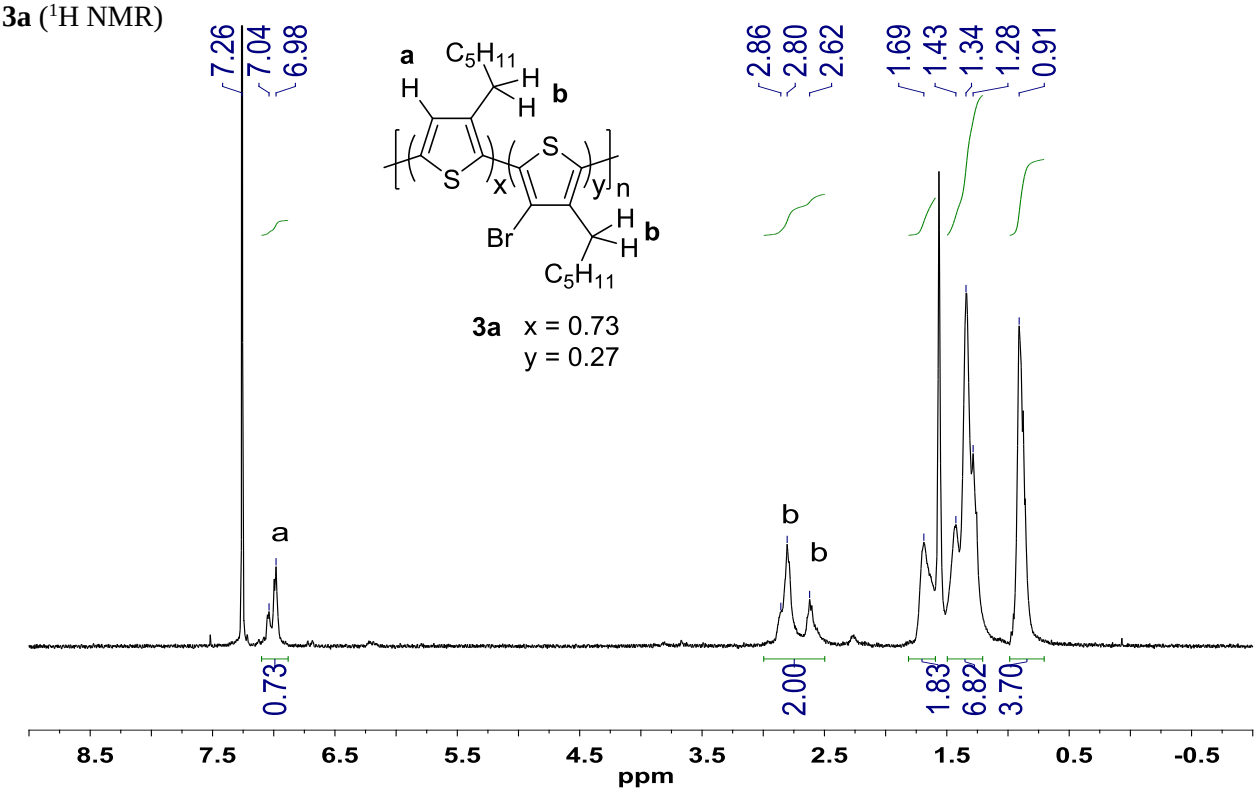

3a x = 0.73
y = 0.27

3b (^{1}H NMR)

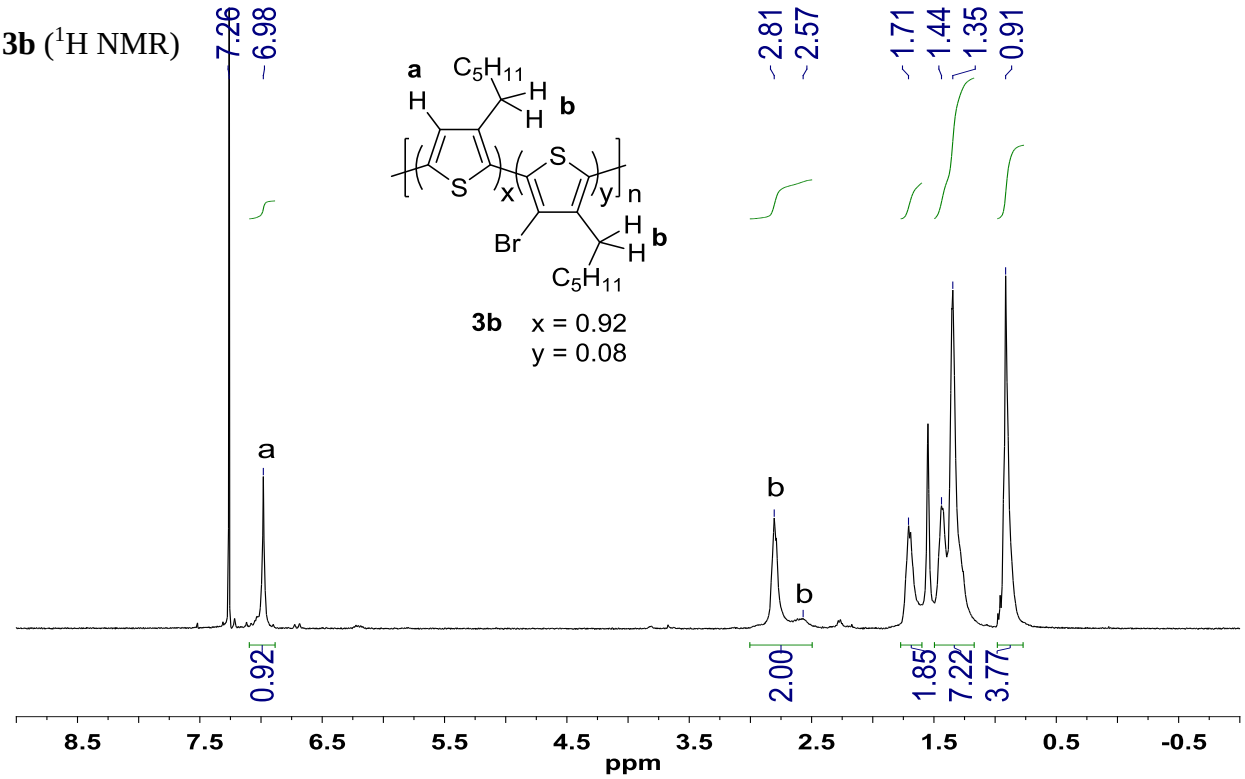

3b x = 0.92
y = 0.08

3c (^{1}H NMR)

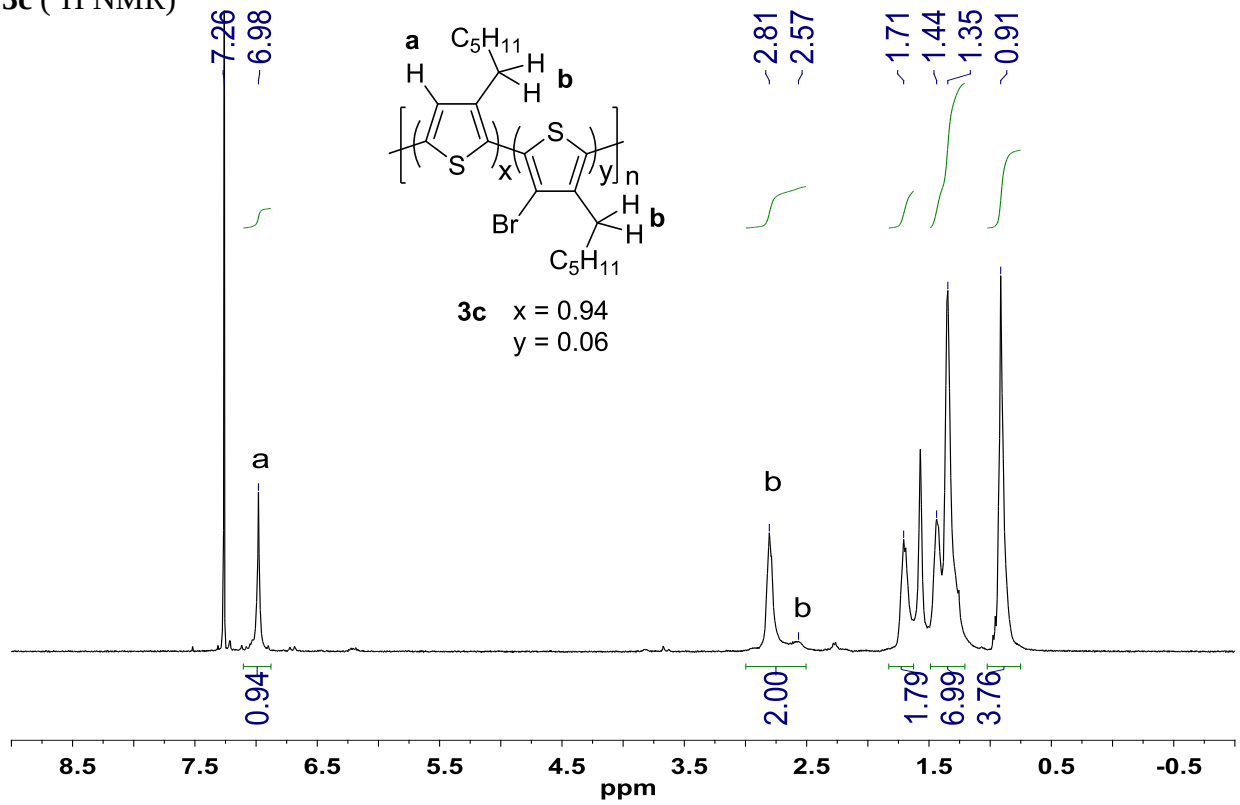

3c x = 0.94
y = 0.06

3d (^{1}H NMR)

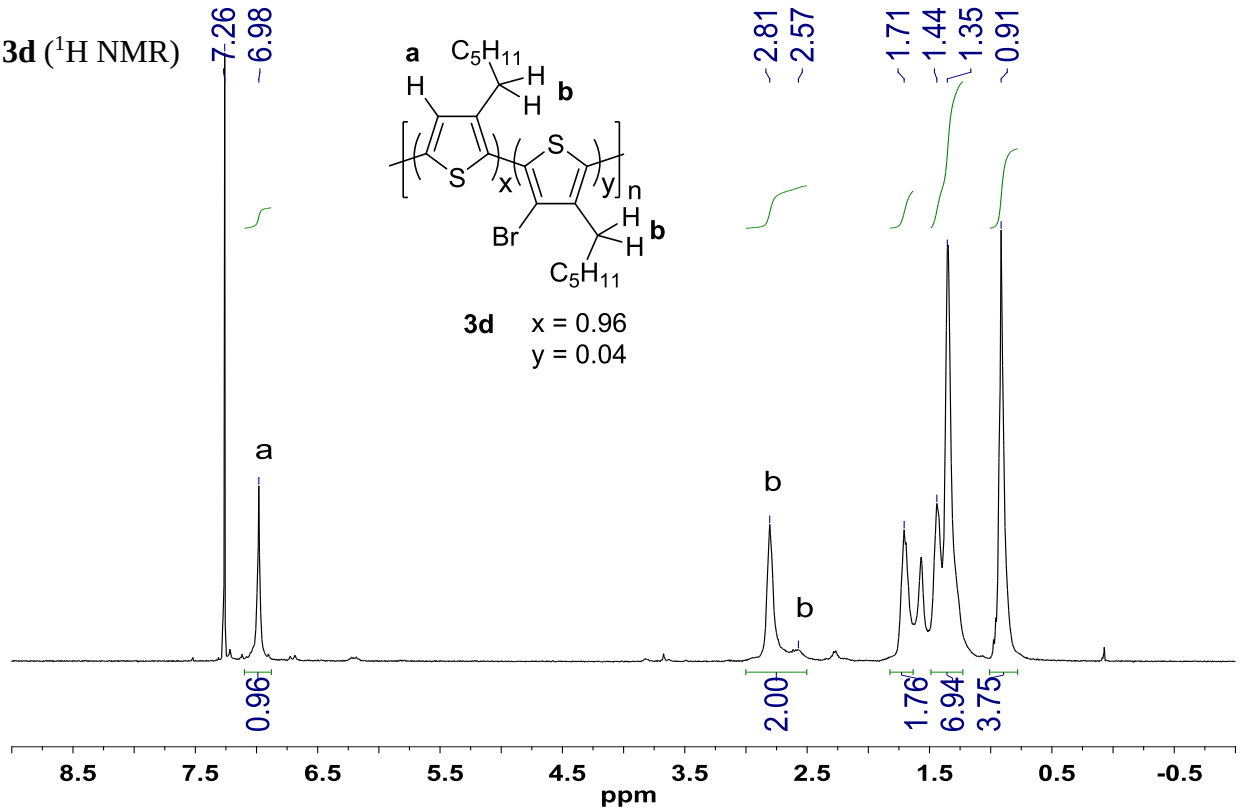

3d x = 0.96
y = 0.04

4 (^{1}H NMR)

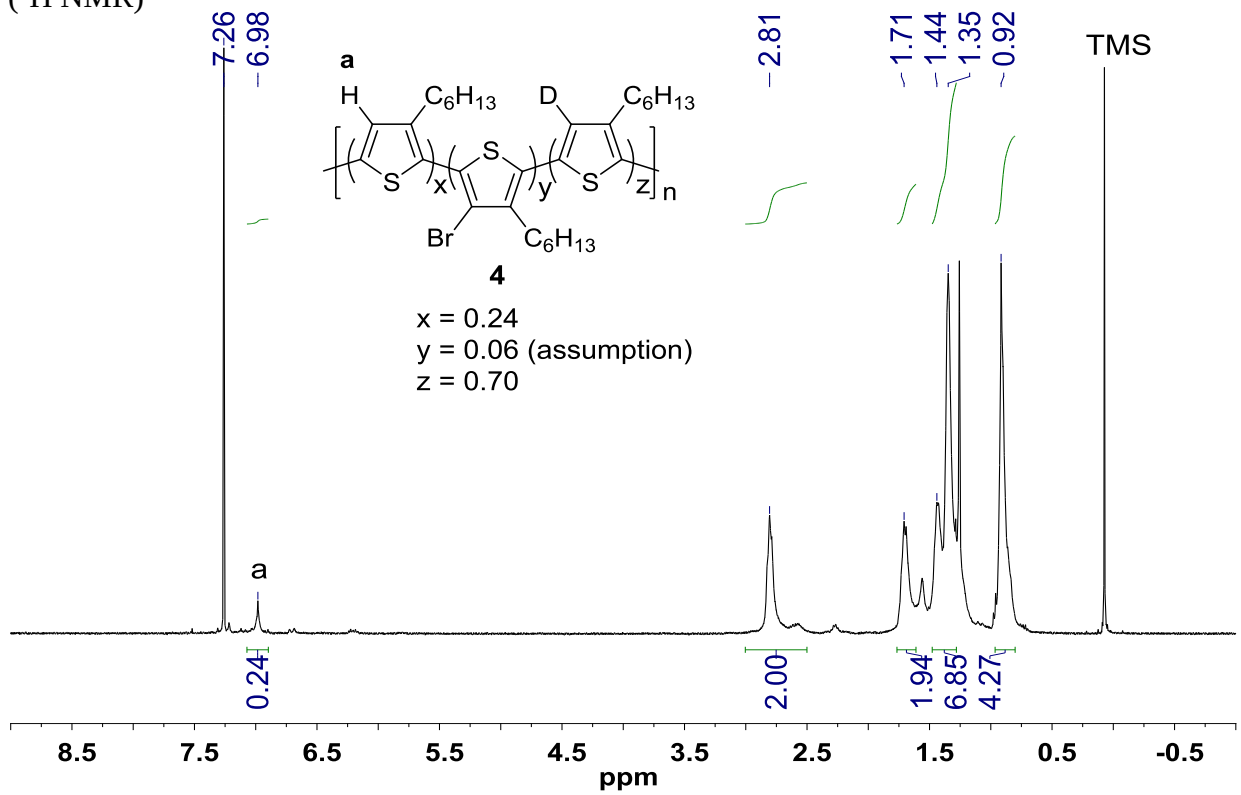

5 (^{1}H NMR)

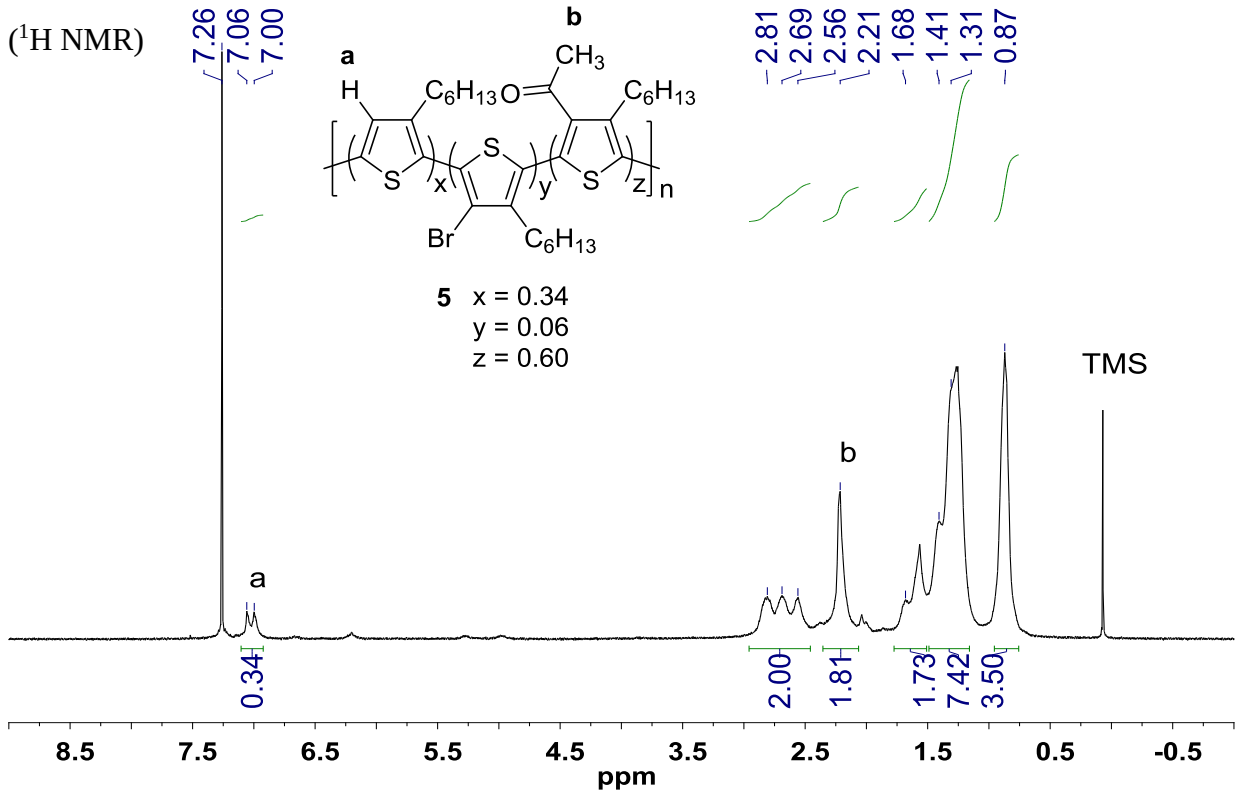

6 (^{1}H NMR)

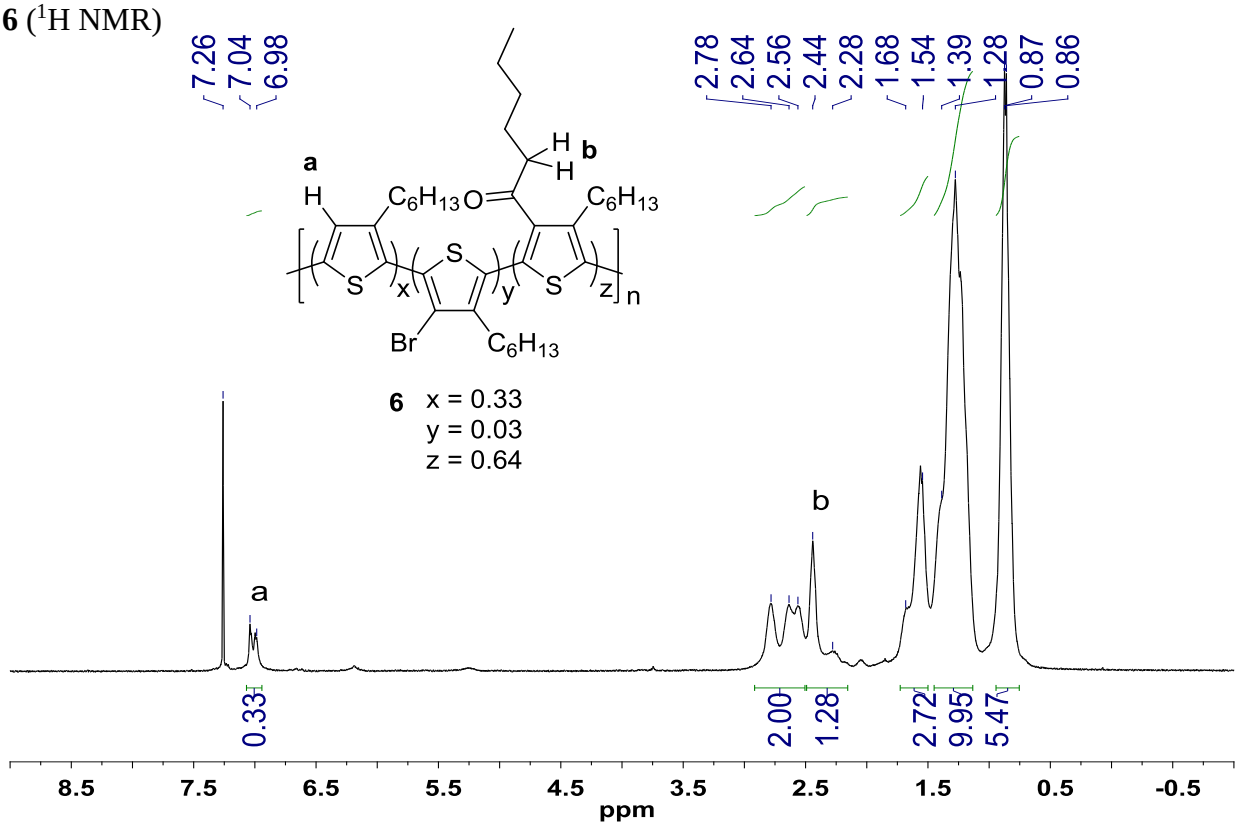

7 (^{1}H NMR)

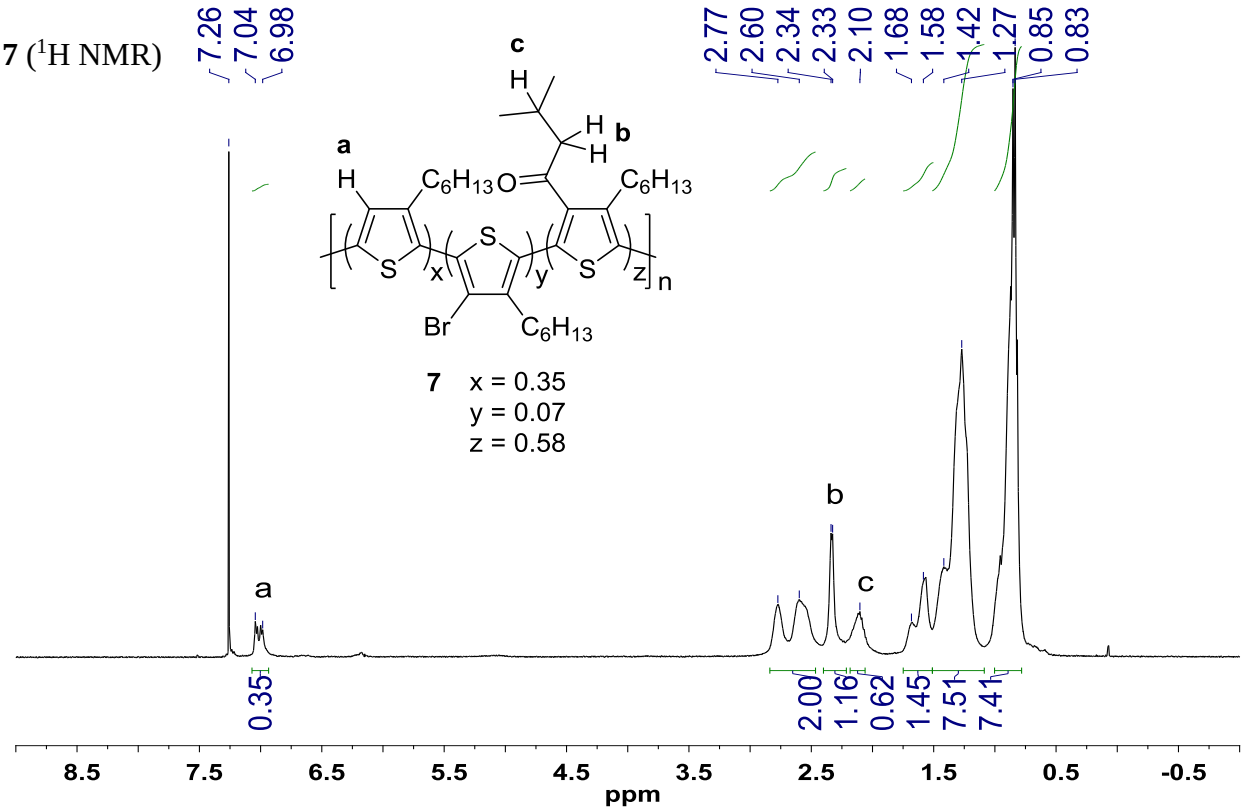

8 (^{1}H NMR)

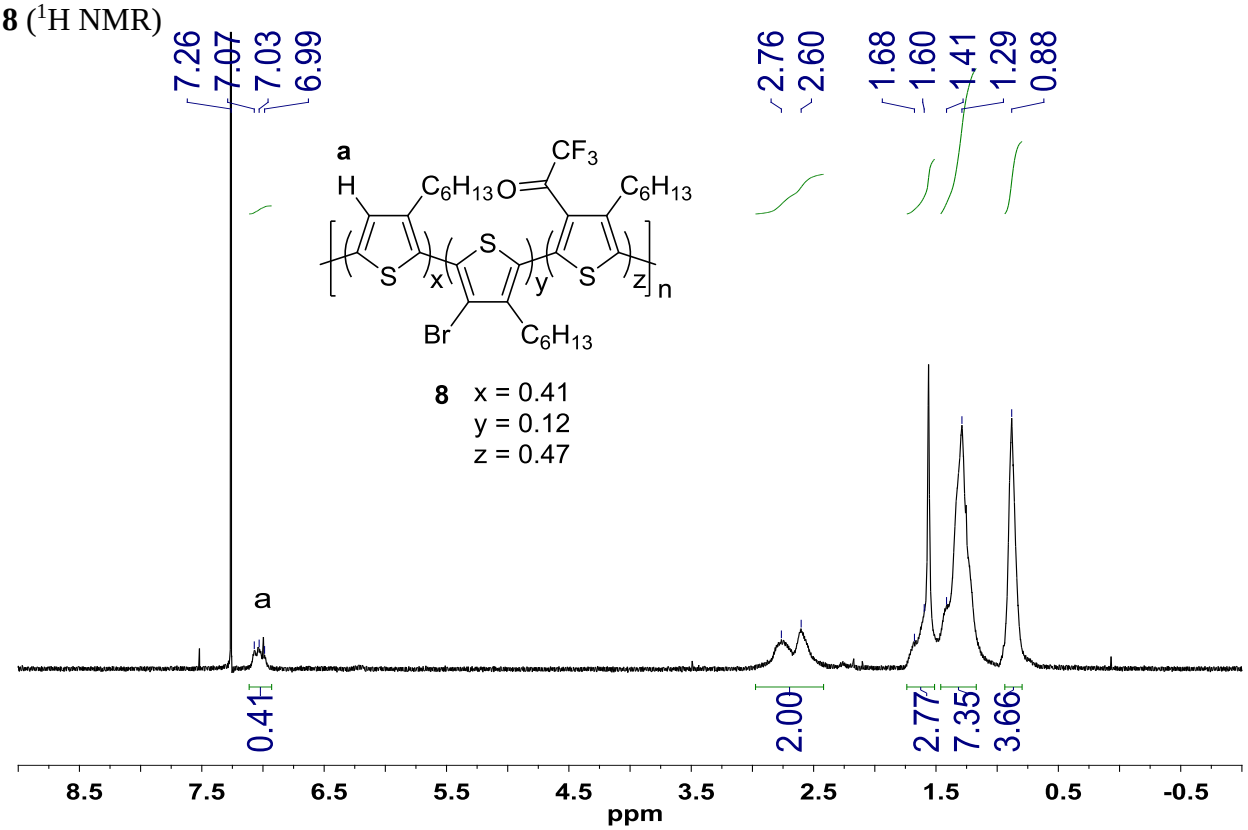

8 (^{19}F NMR)

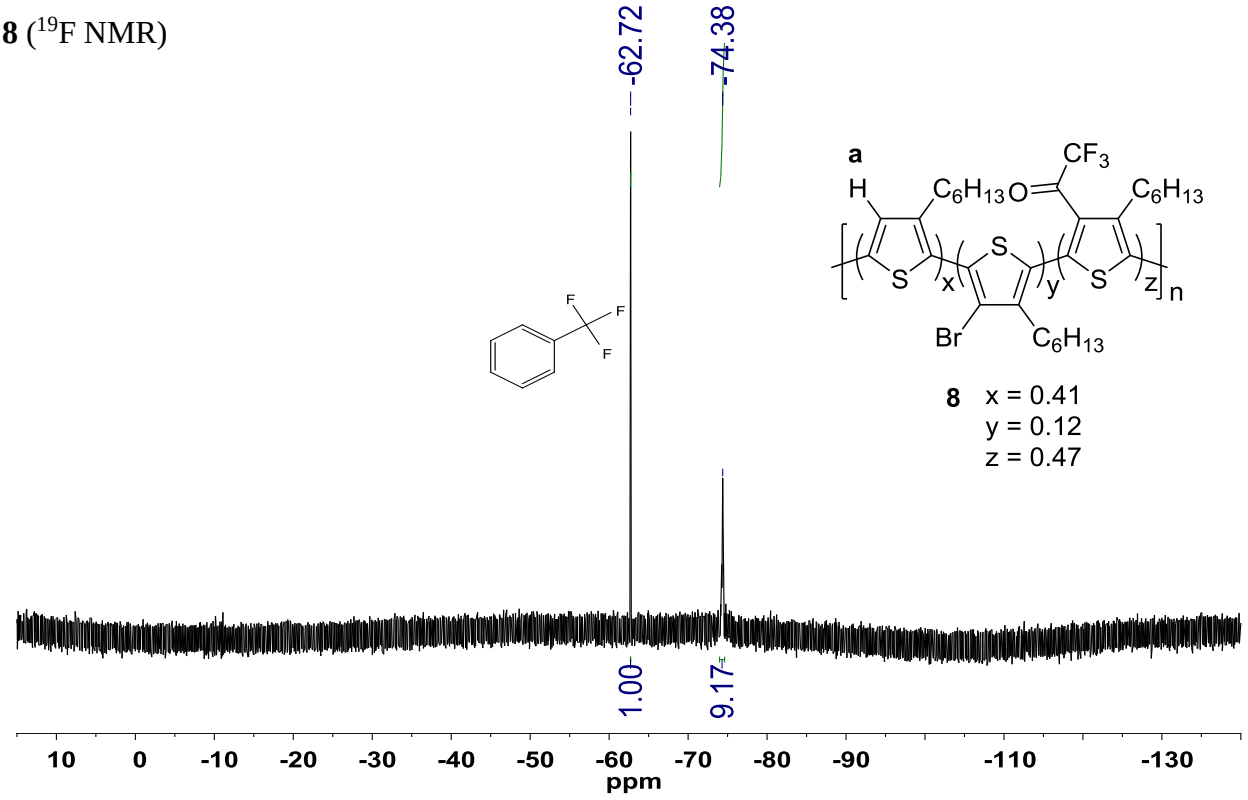

9 (^{1}H NMR)

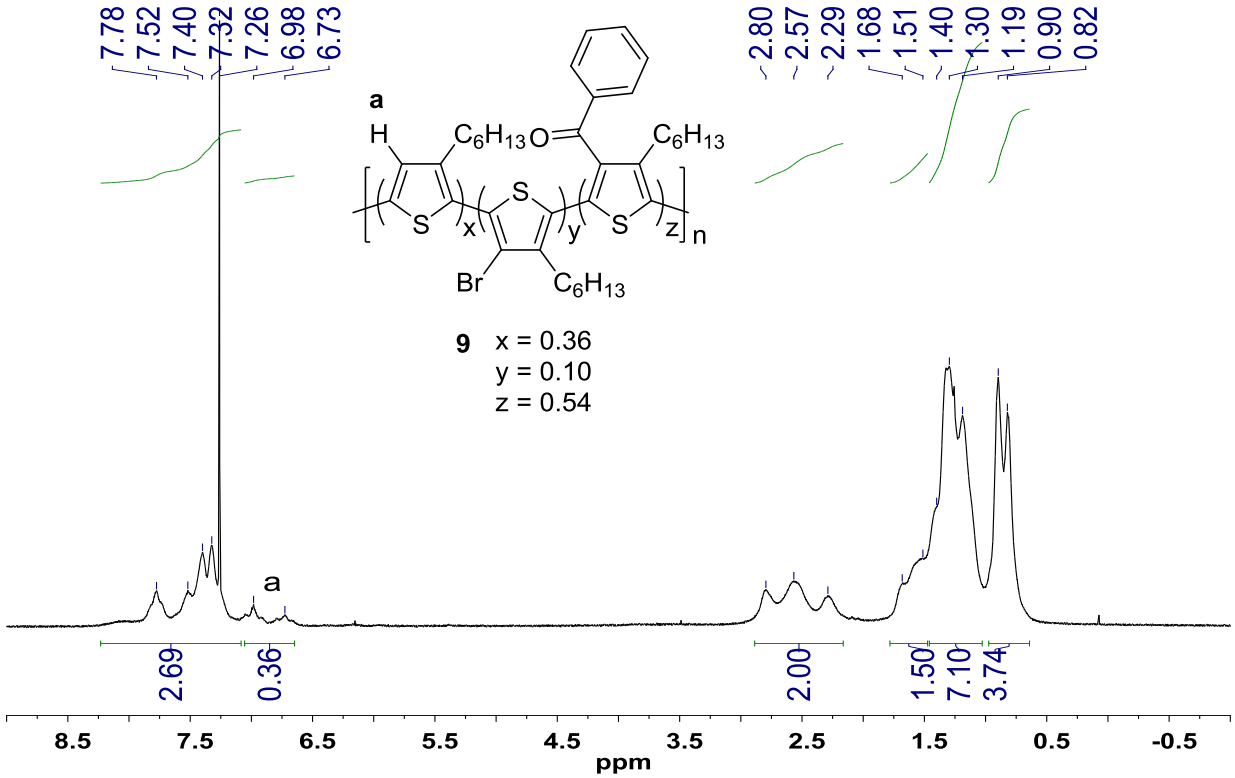

10 (^{1}H NMR, integration value based on 57 % conversion)

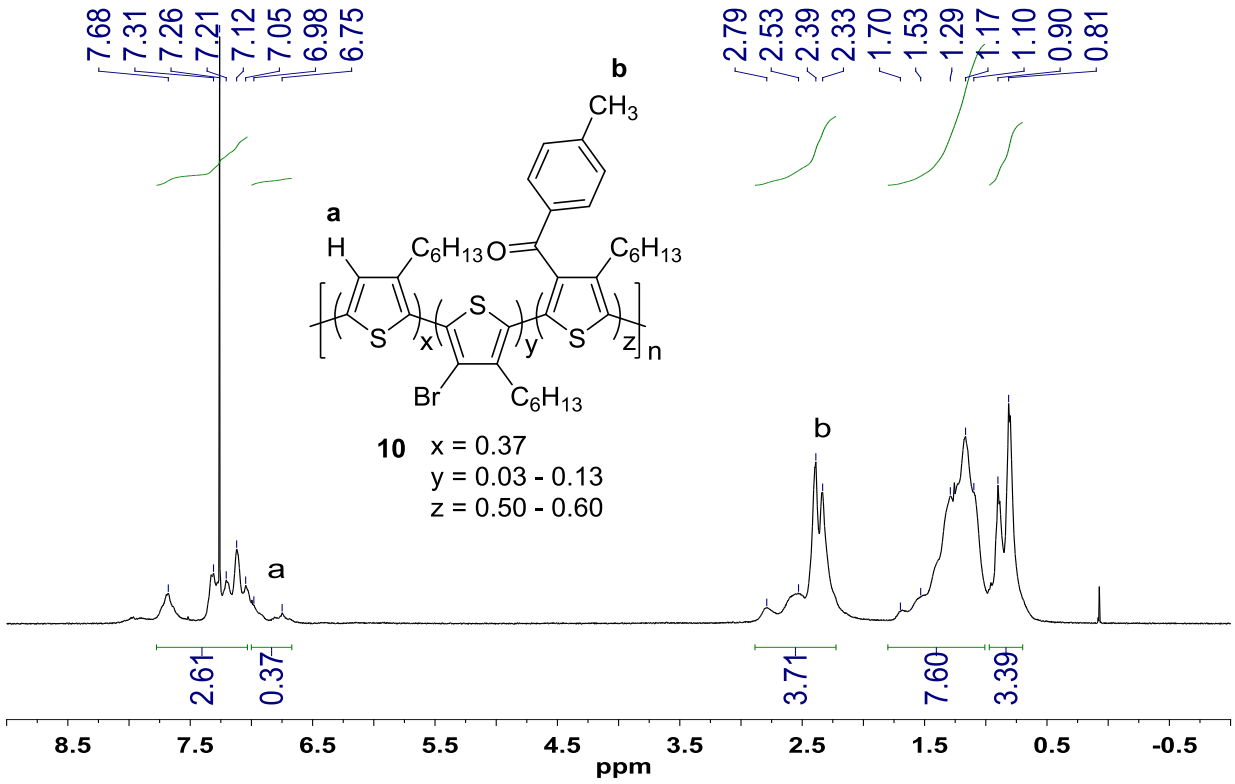

11 (^{1}H NMR)

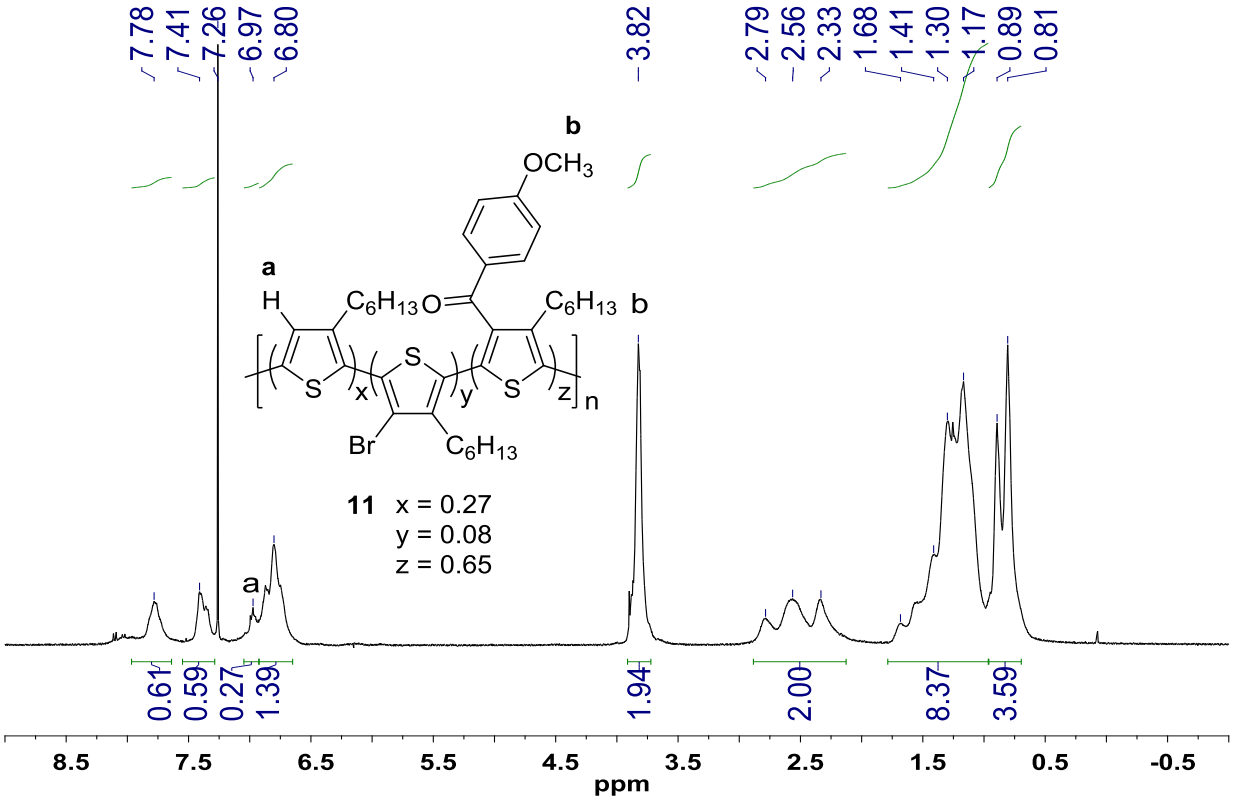

12 (^{1}H NMR)

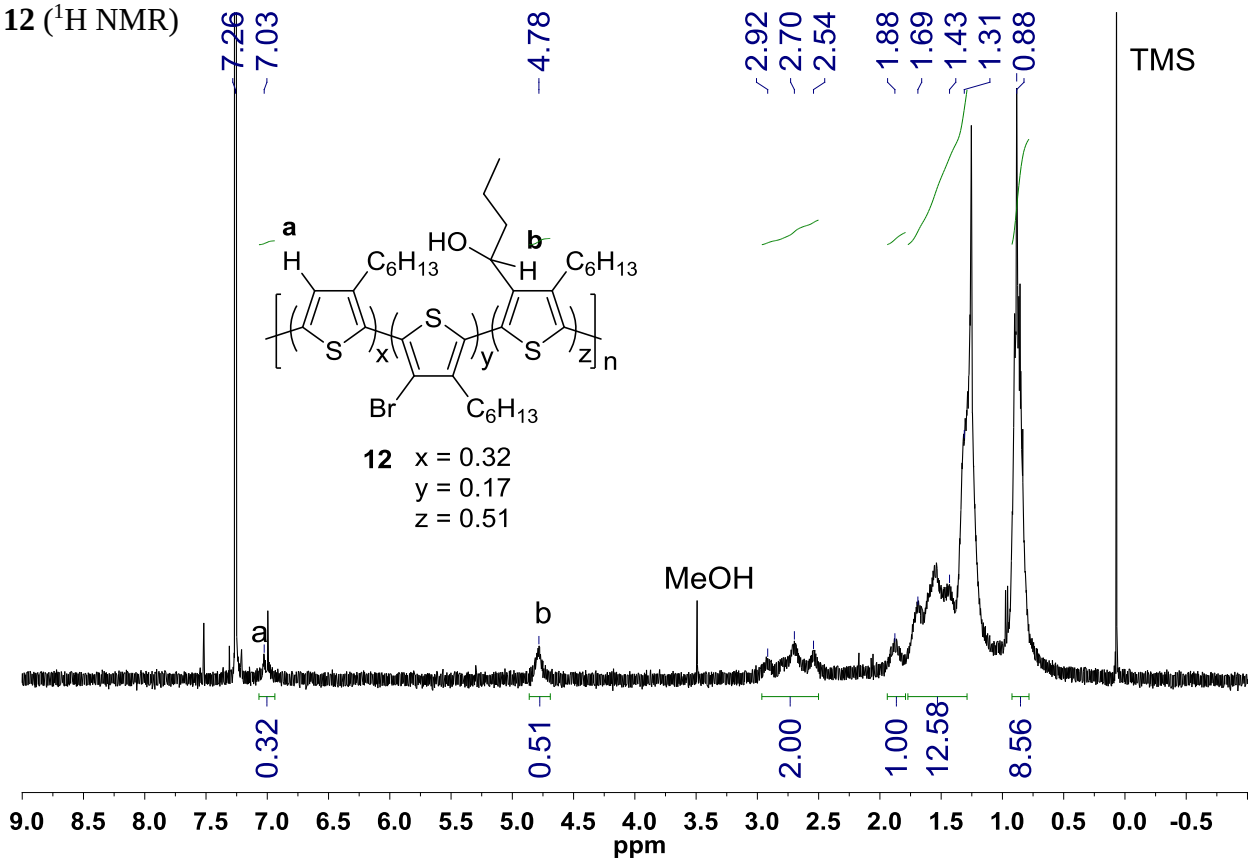

13 (^{1}H NMR)

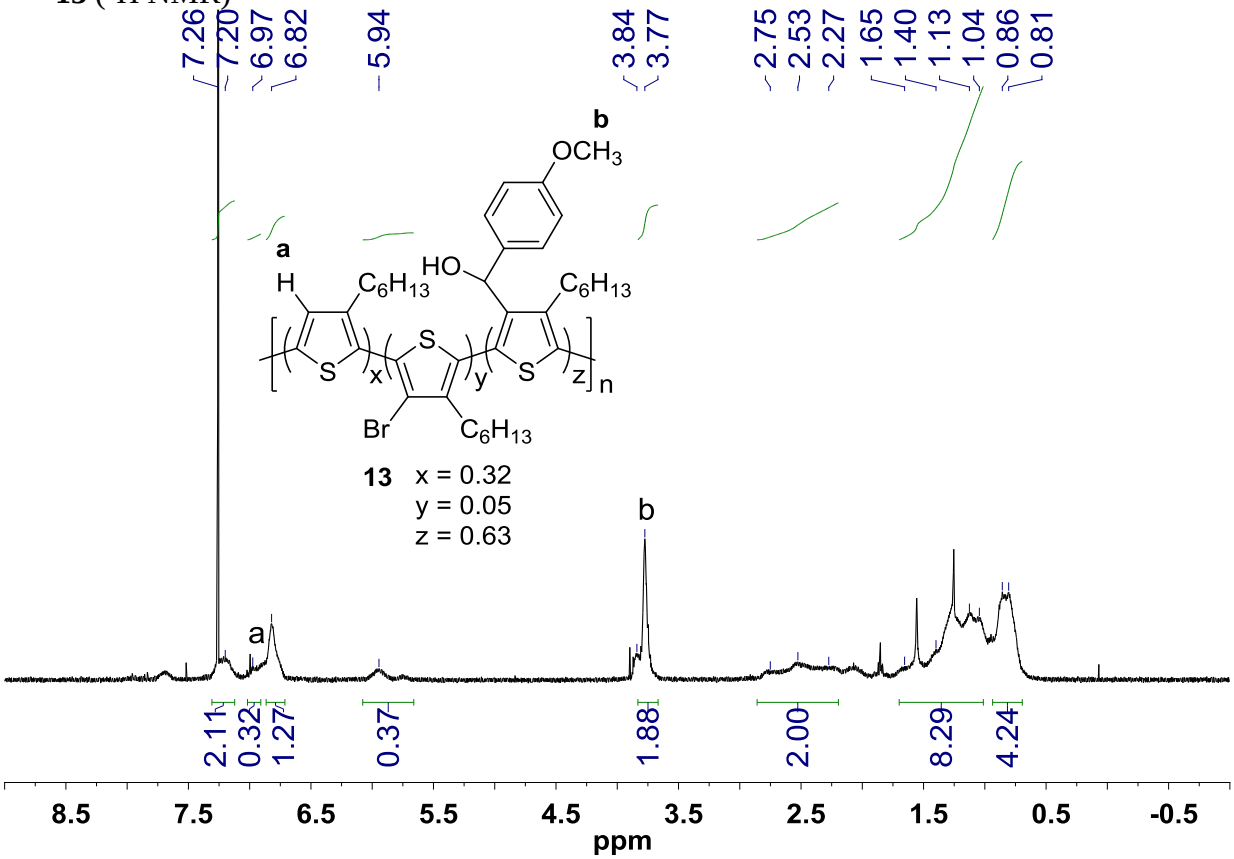

14 (^{1}H NMR)

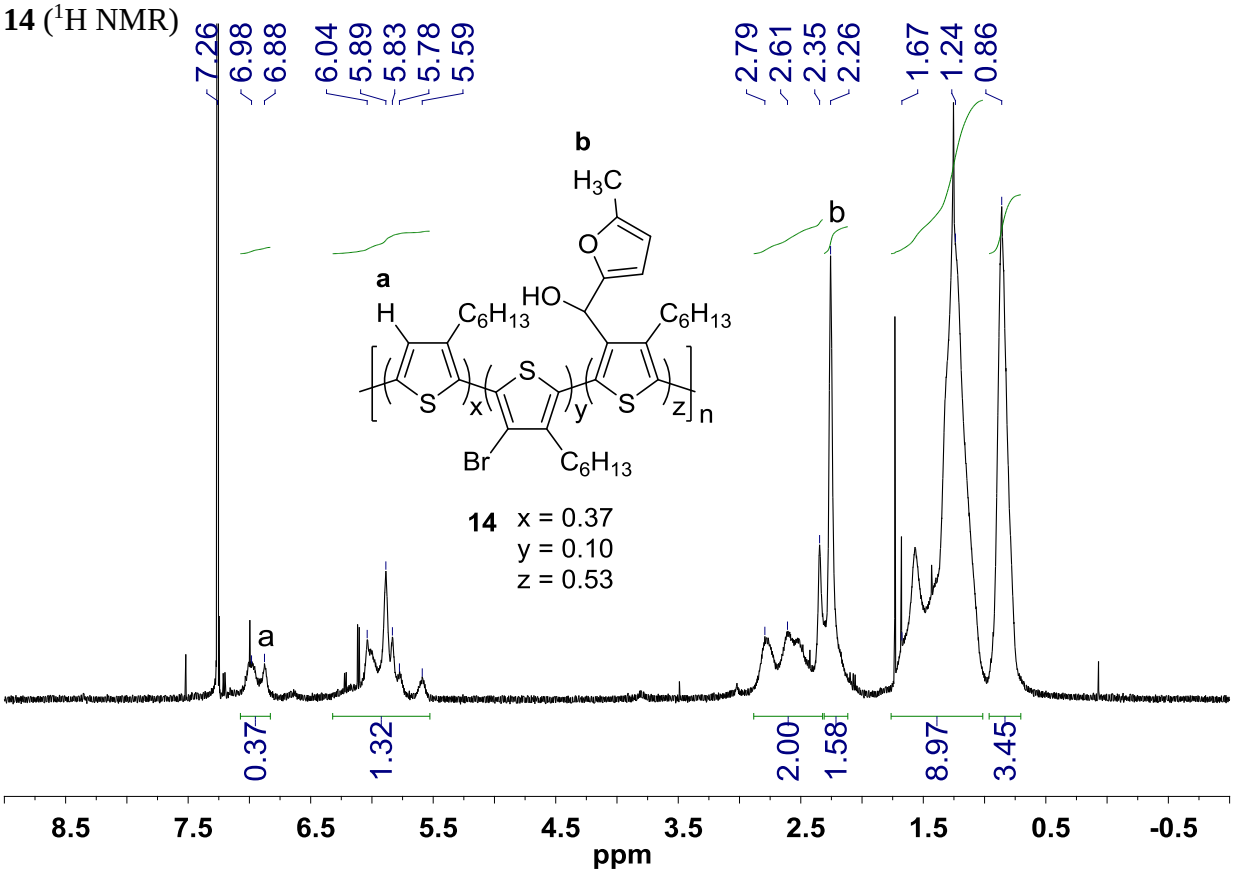

15 (^{1}H NMR)

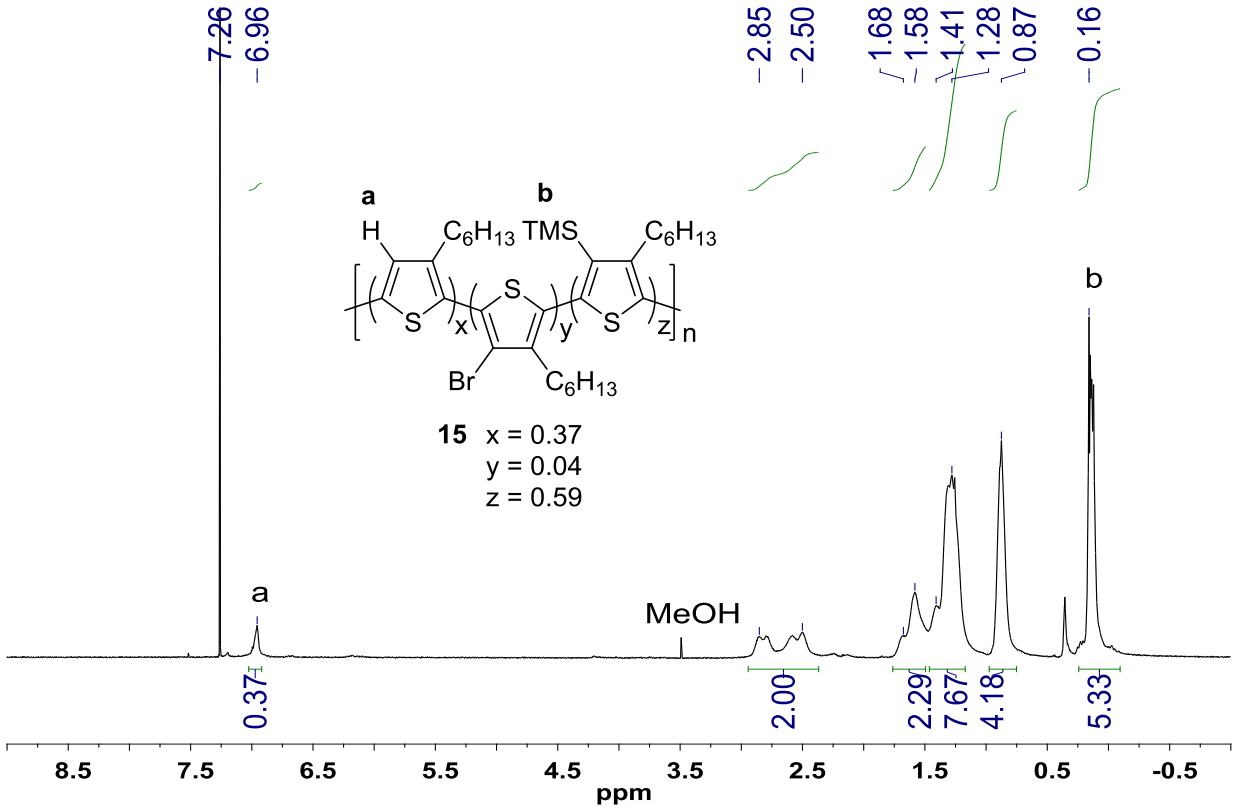

16 (^{1}H NMR)

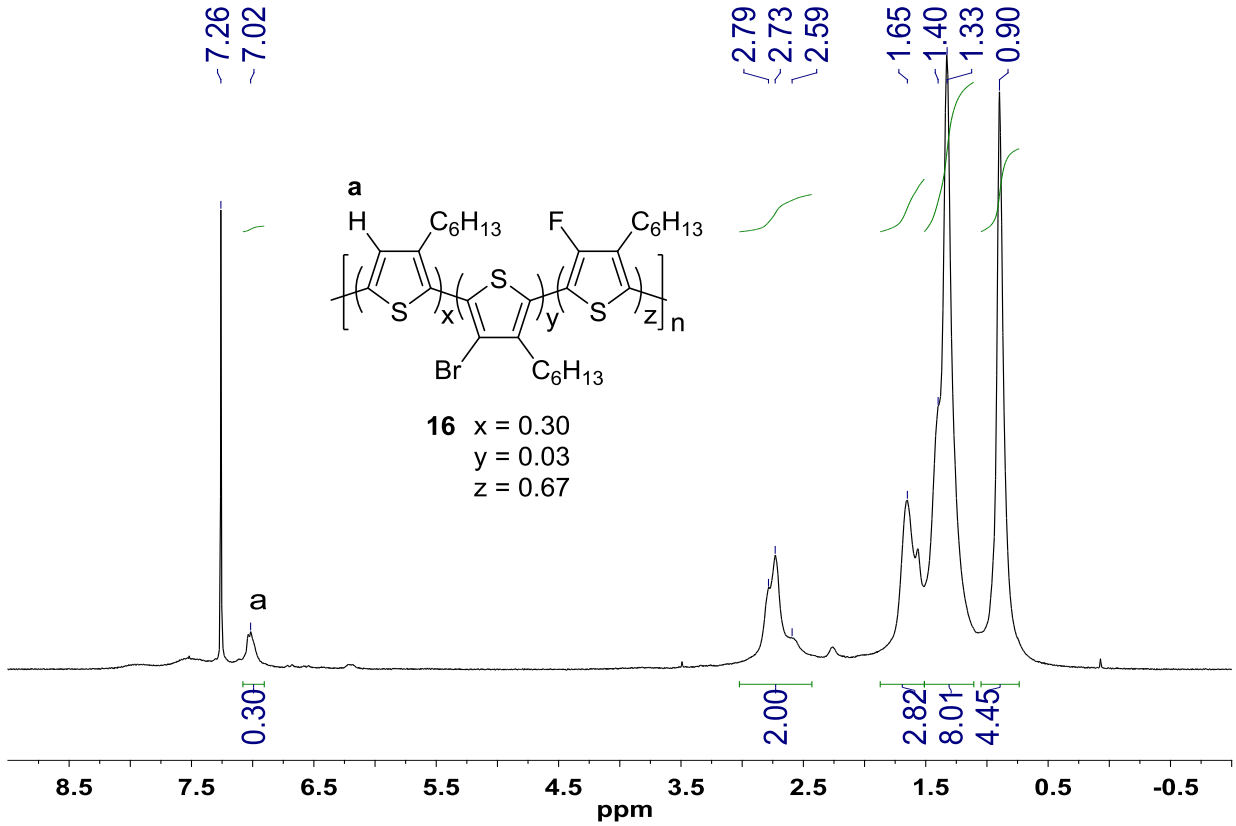

16 (^{19}F NMR)

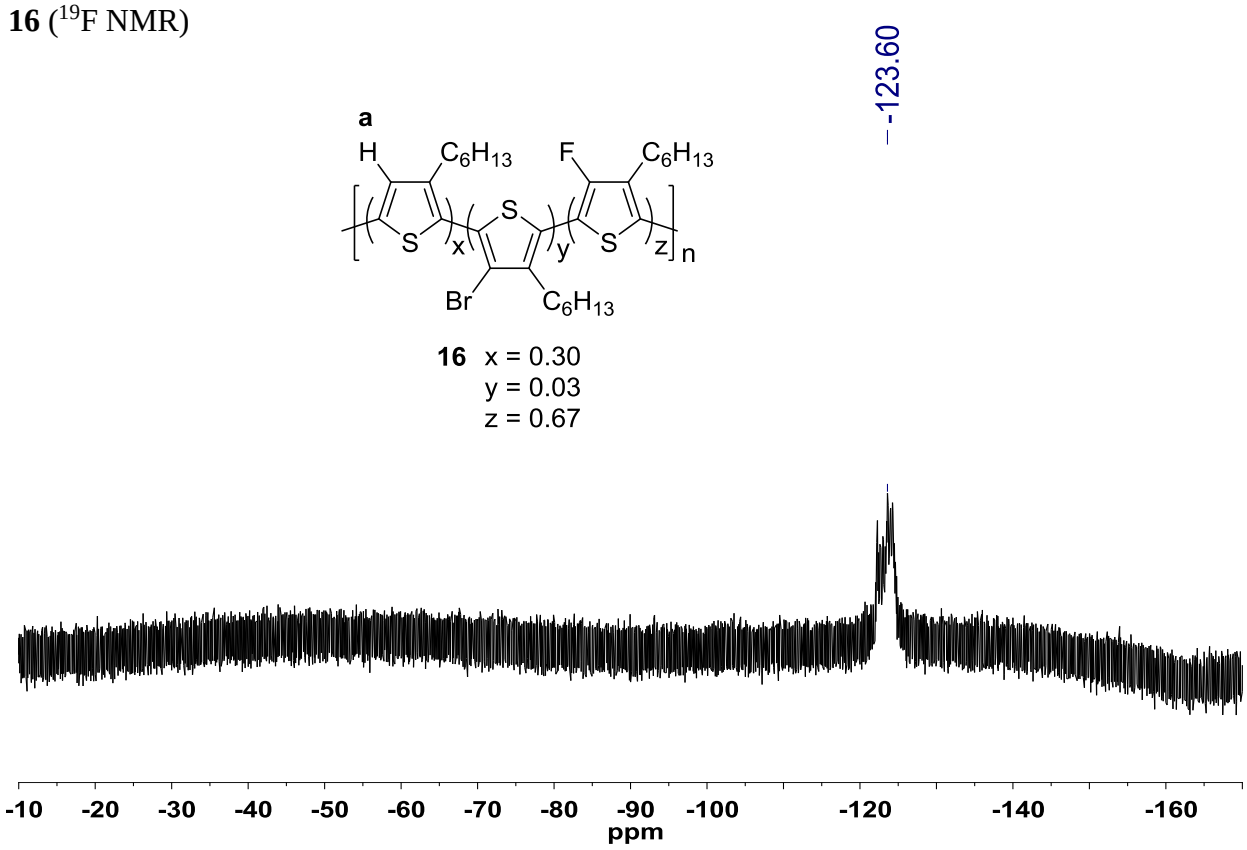

19 (^{1}H NMR)

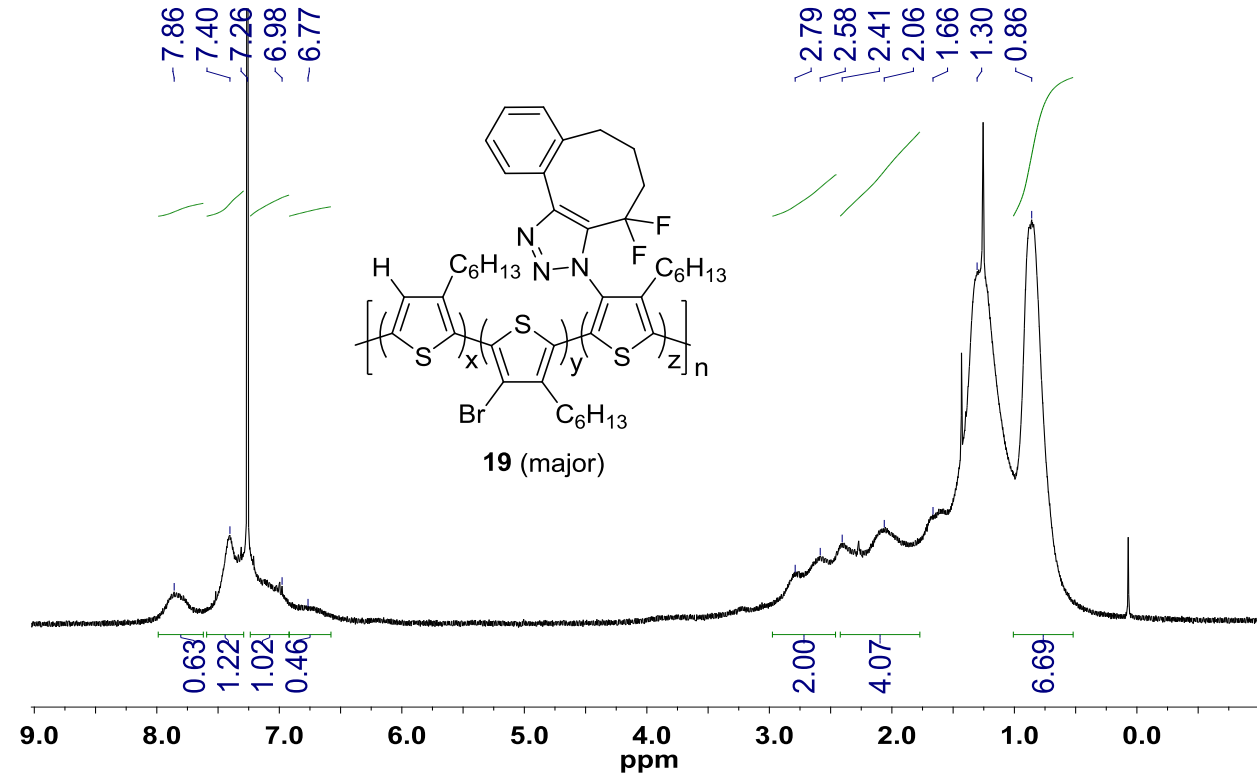

19 (^{19}F NMR)

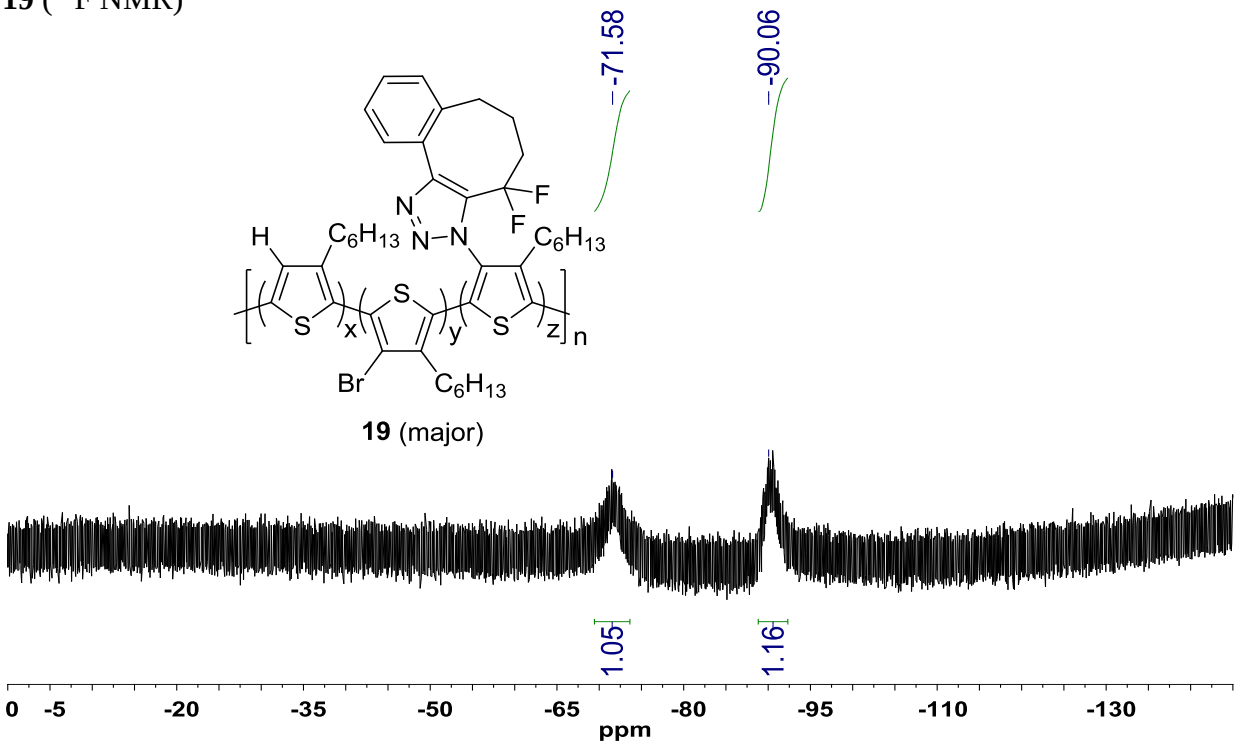
-71.58
-90.06
F
F
N
N–N
H
C6H13
C6H13
S
S
S
x
y
z
n
Br
C6H13
19 (major)
1.05
1.16
0
-5
-20
-35
-50
-65
-80
-95
-110
-130
ppm

IR Spectra

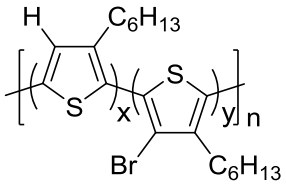

3a x = 0.73
y = 0.27

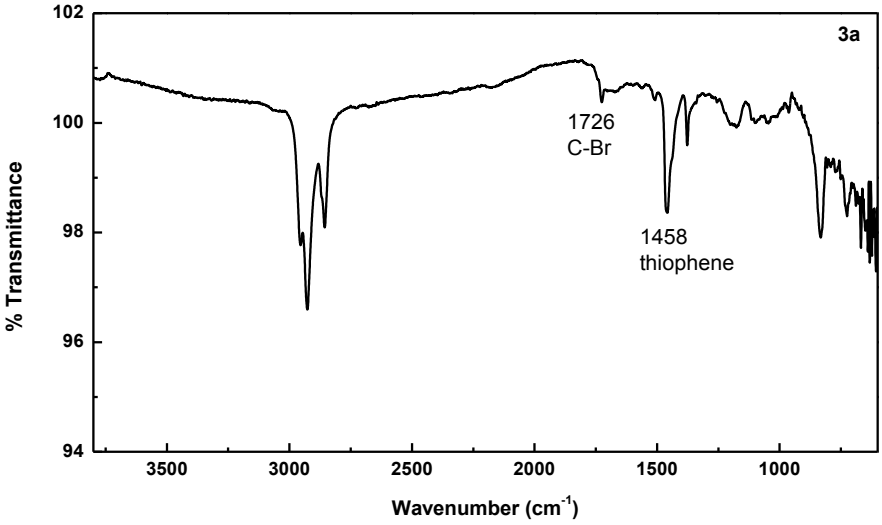

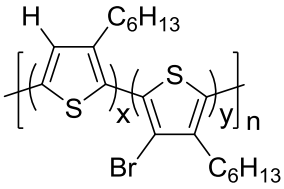

3b x = 0.92
y = 0.08

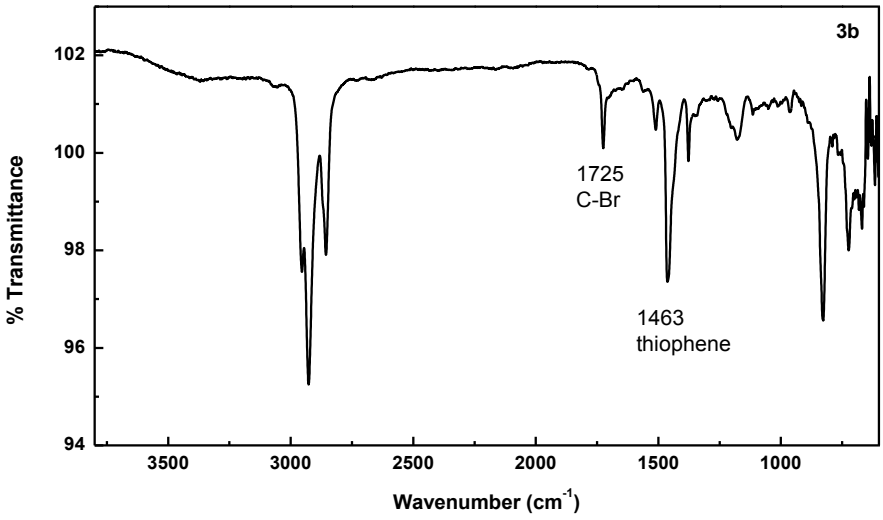

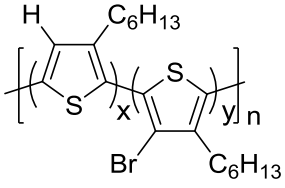

3c x = 0.94
y = 0.06

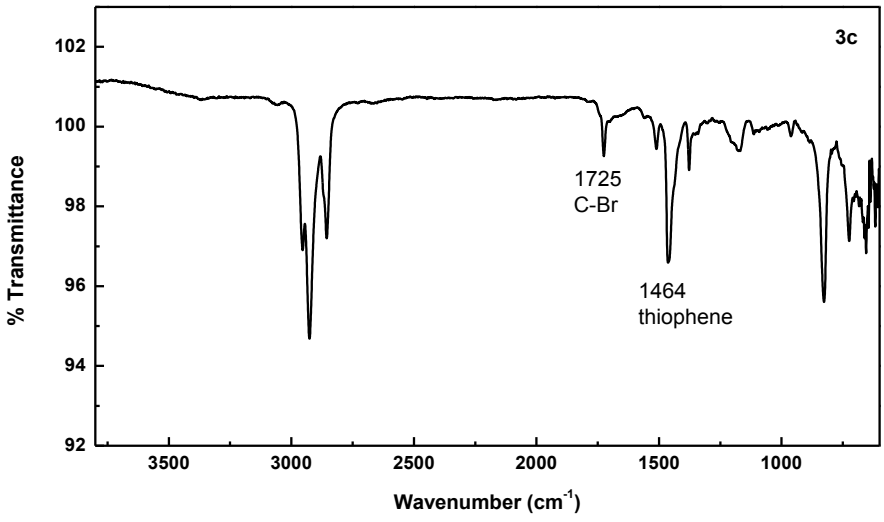

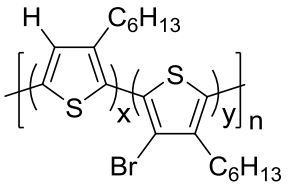

3d x = 0.96
y = 0.04

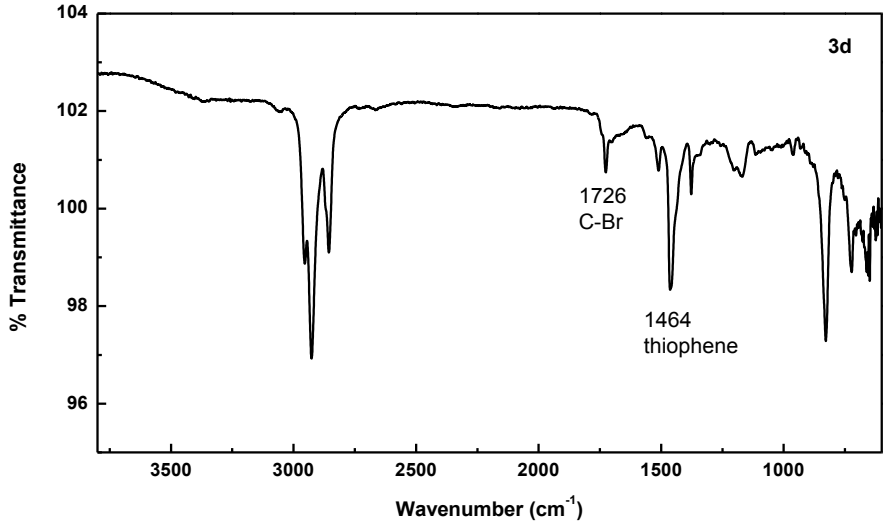

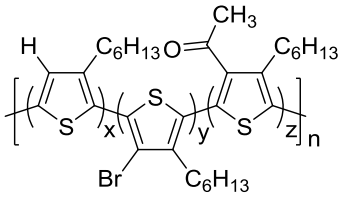

5 x = 0.34
y = 0.06
z = 0.60

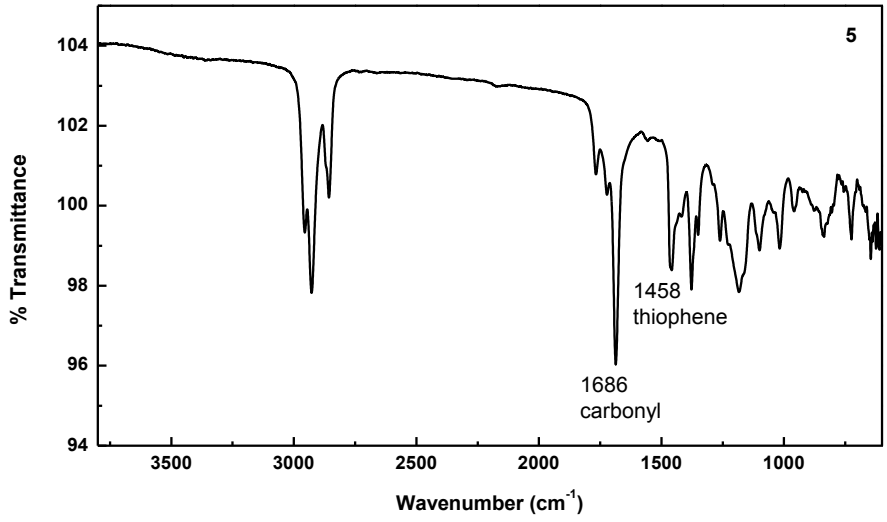

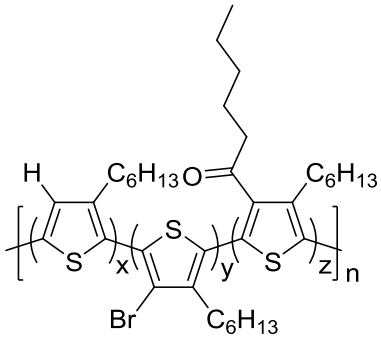

6 x = 0.33
y = 0.03
z = 0.64

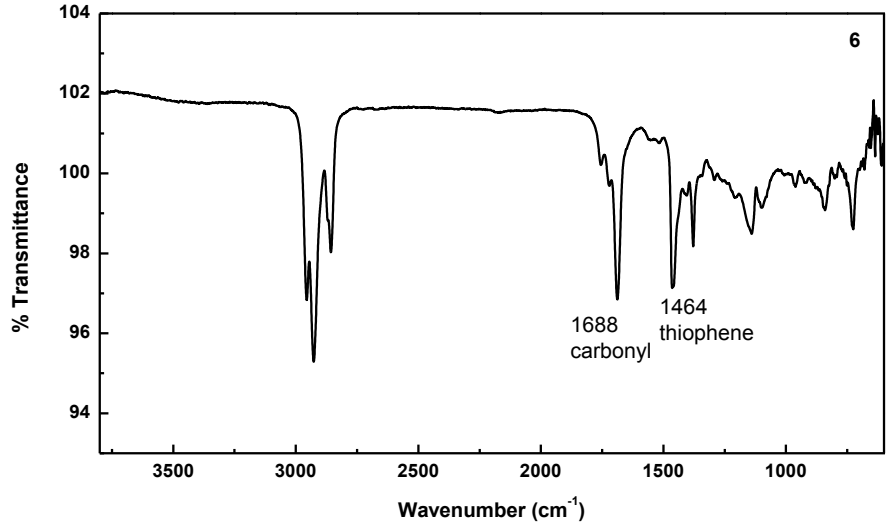

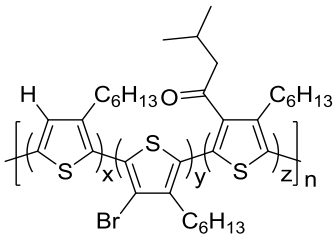

7 x = 0.35
y = 0.07
z = 0.58

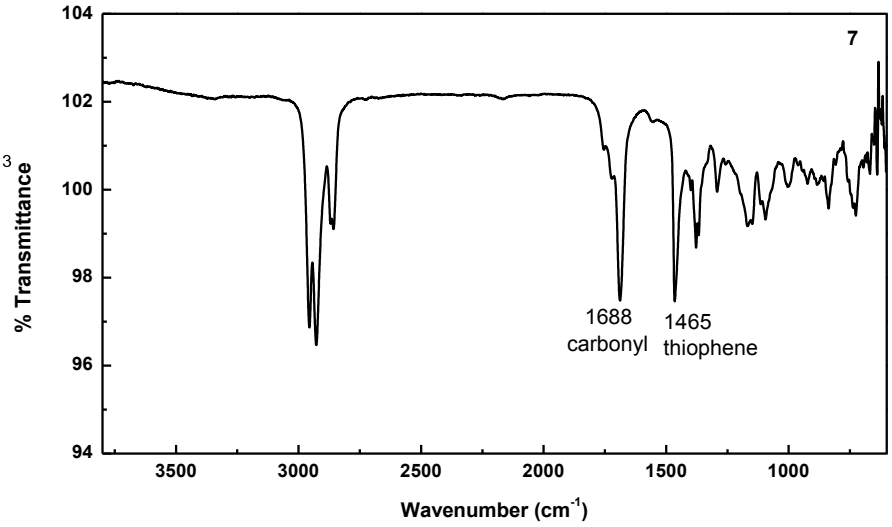

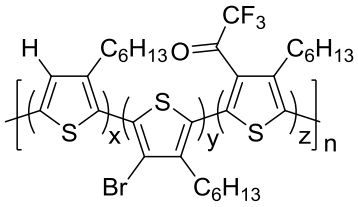

8 x = 0.41
y = 0.12
z = 0.47

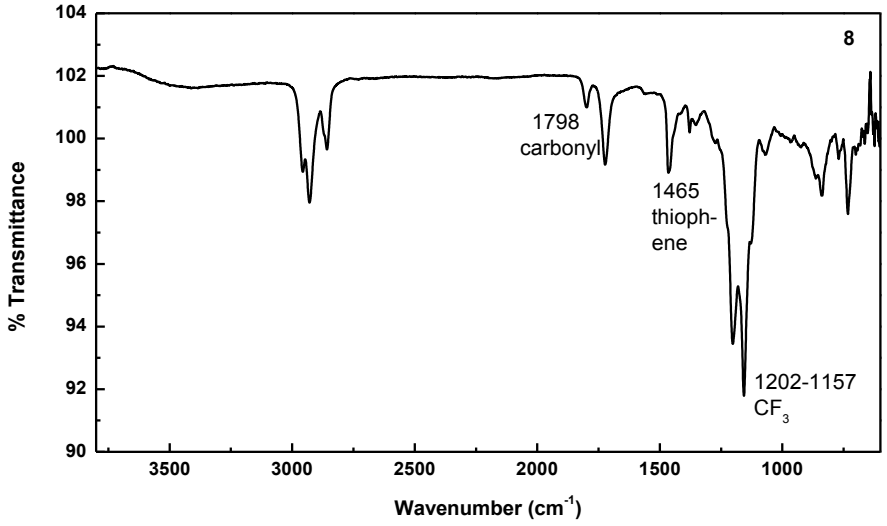

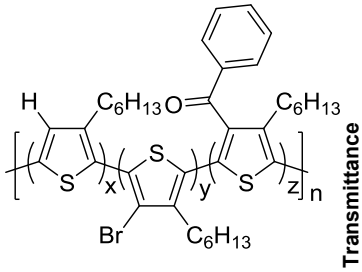

9 x = 0.36
y = 0.10
z = 0.54

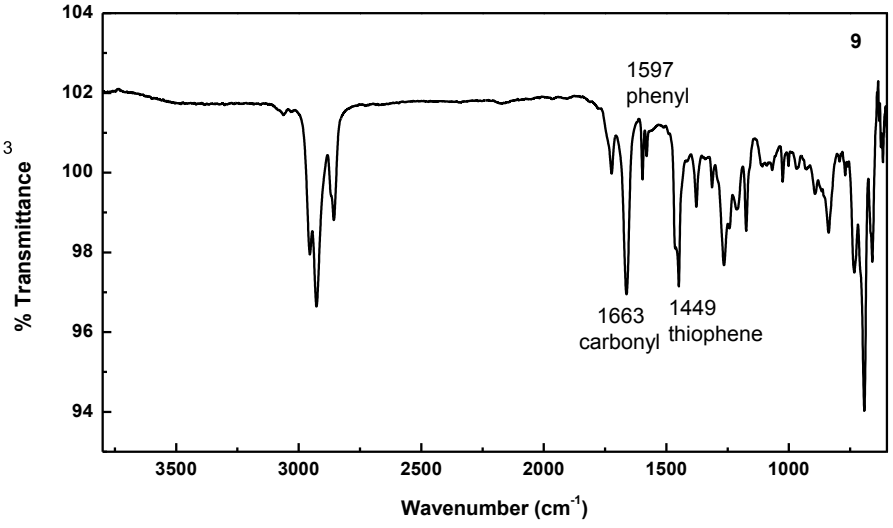

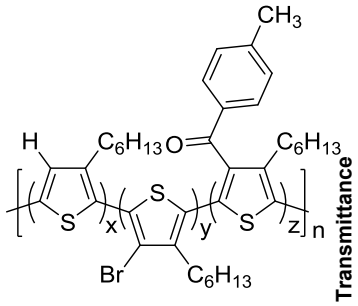

10 x = 0.37
y = 0.03 - 0.13
z = 0.50 - 0.60

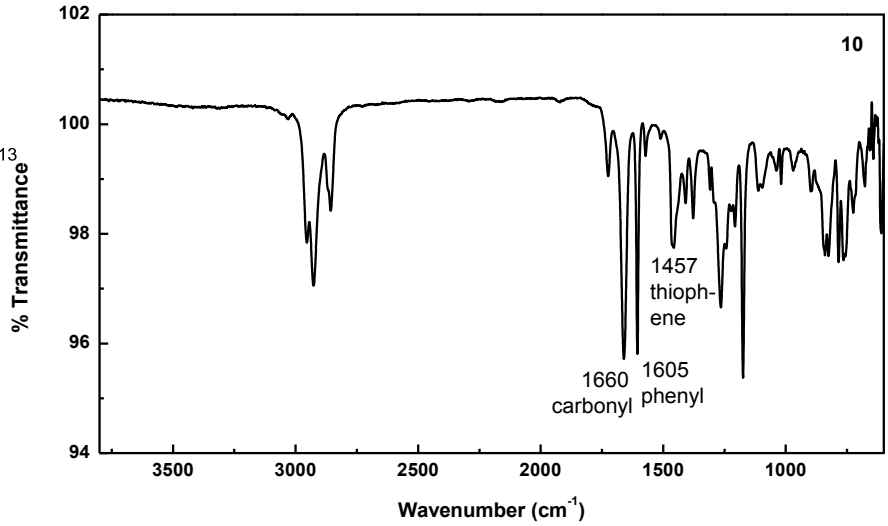

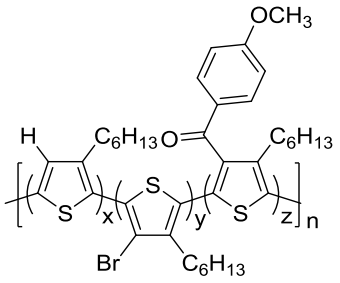

11 x = 0.27
y = 0.08
z = 0.65

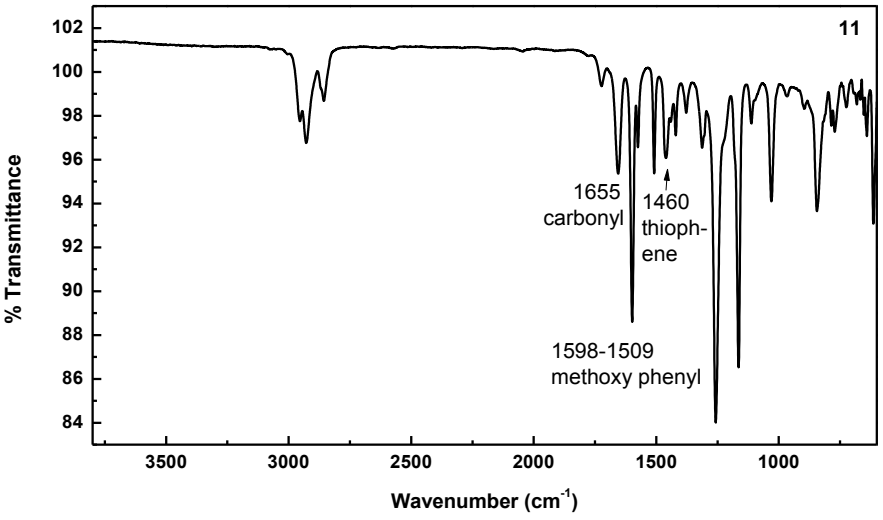

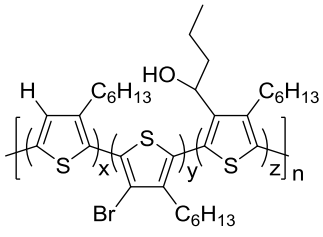

12 x = 0.32
y = 0.17
z = 0.51

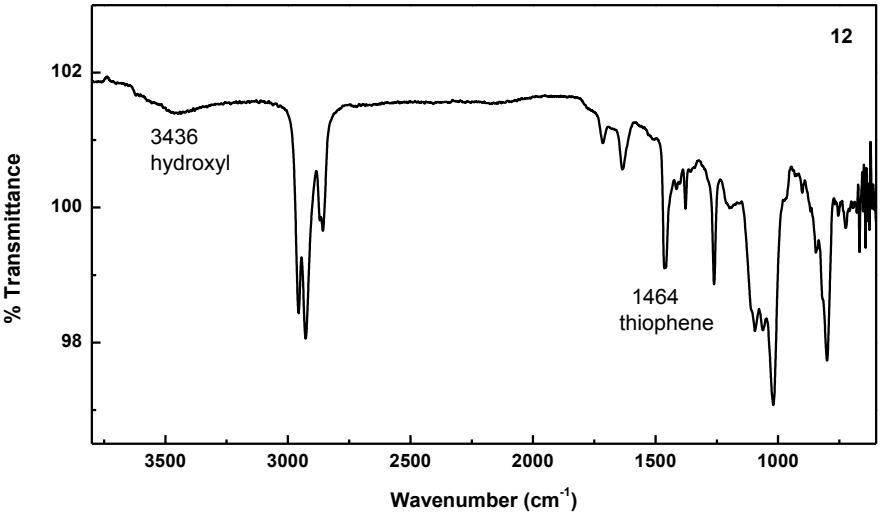

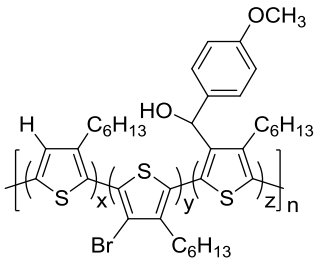

13 x = 0.32
y = 0.05
z = 0.63

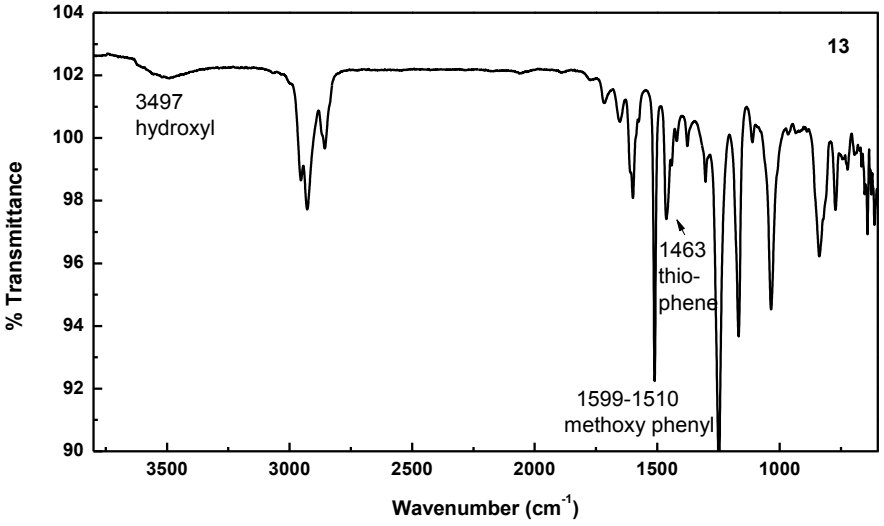

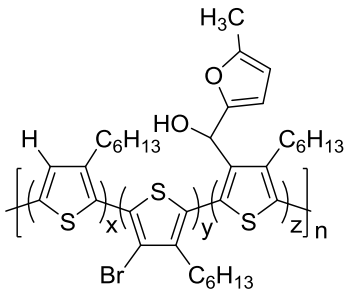

14 x = 0.37
y = 0.10
z = 0.53

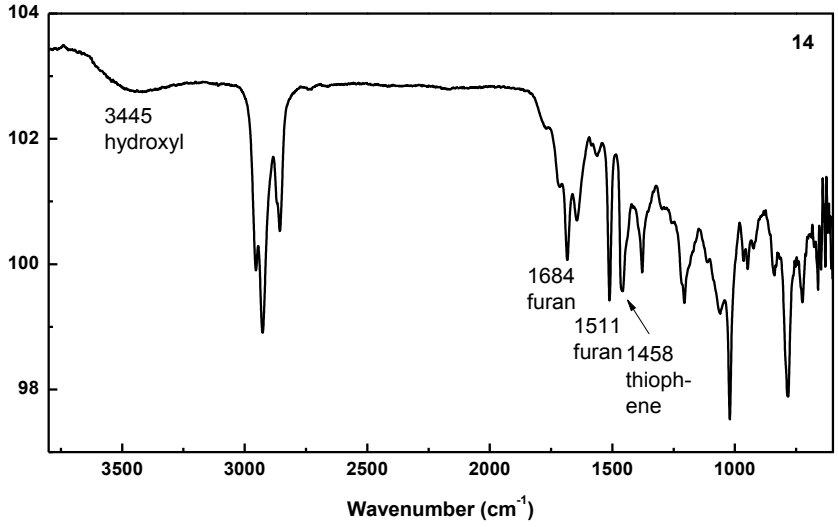

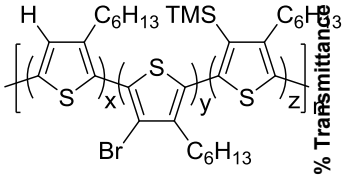

15 x = 0.37
y = 0.04
z = 0.59

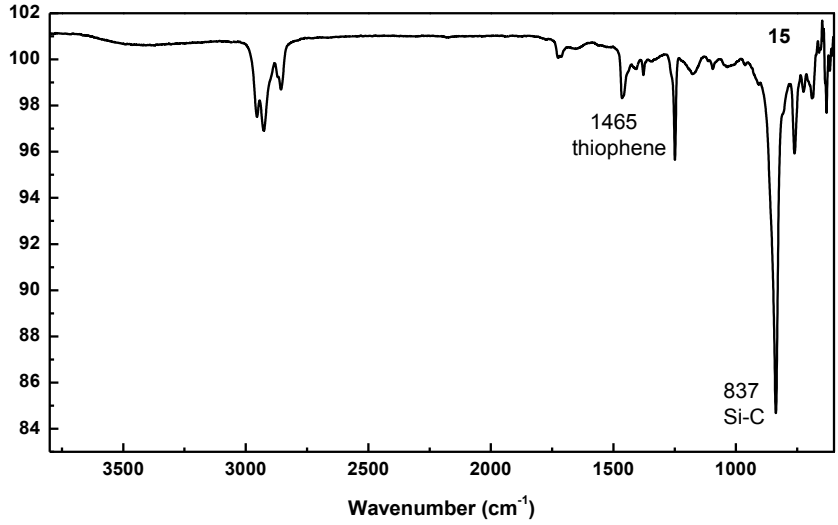

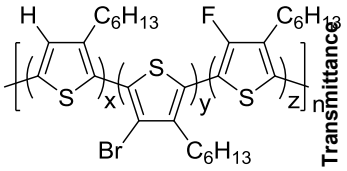

16 x = 0.30
y = 0.03
z = 0.67

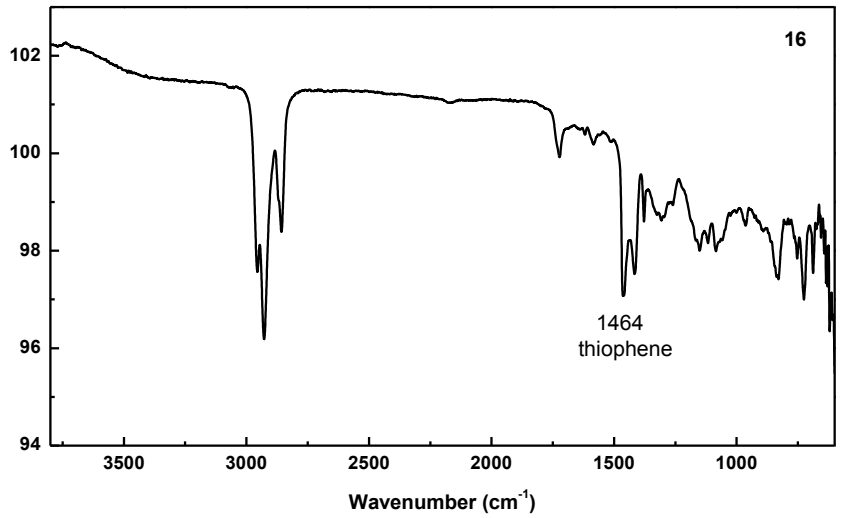

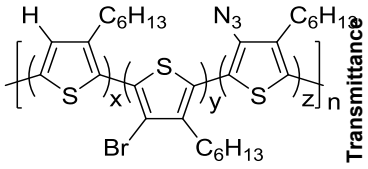

17

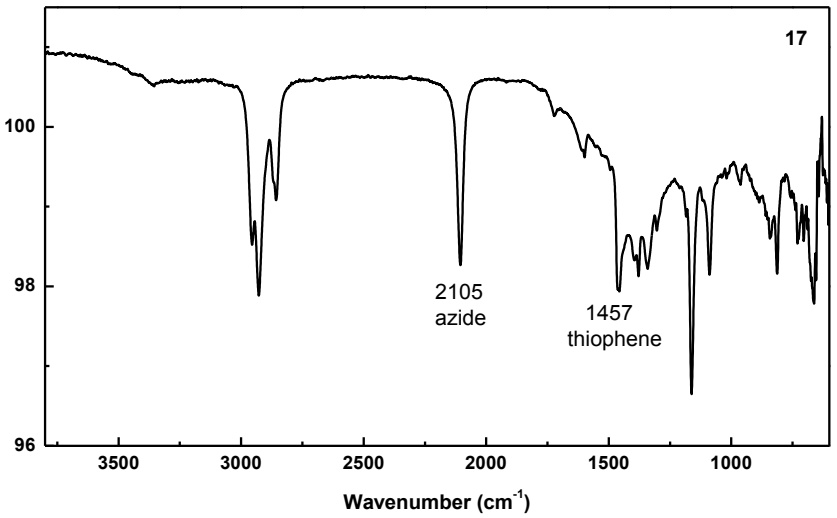

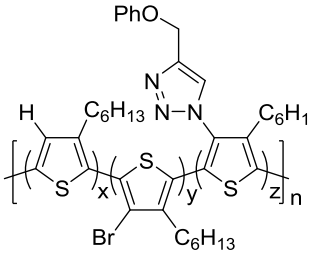

18

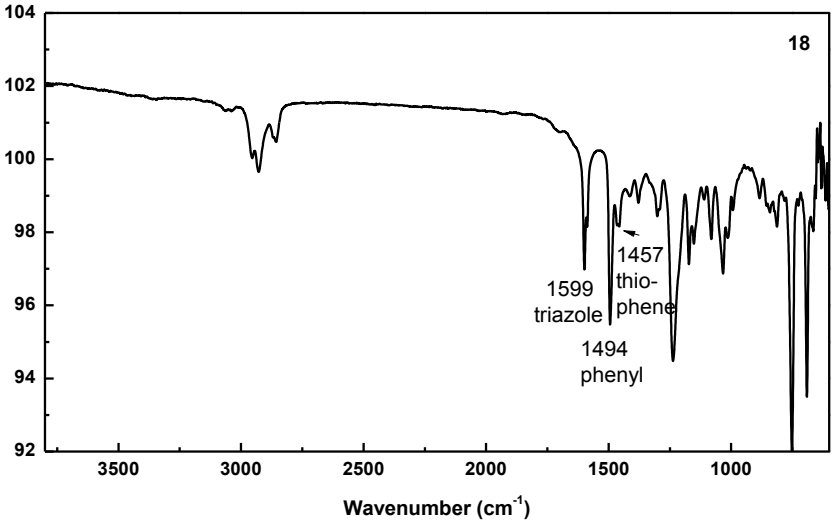

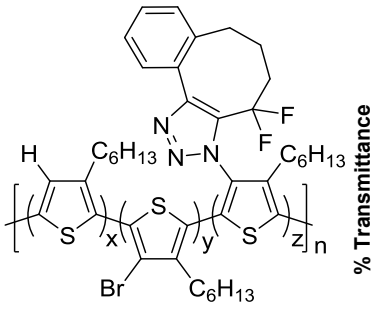
H
C6H13
N
N–N
F
F
C6H13
S
x
S
y
S
z
n
Br
C6H13

19 (major)

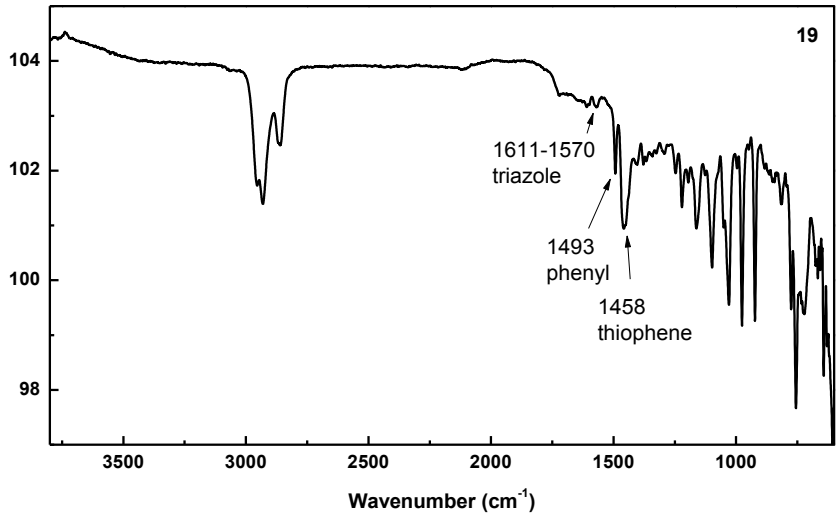
19
% Transmittance
104
102
100
98
1611-1570
triazole
1493
phenyl
1458
thiophene
3500
3000
2500
2000
1500
1000
Wavenumber (cm-1)

Acknowledgements

The journey for my Ph.D. would have been impossible if I had not received considerable guidance and support from many people. My foremost gratitude goes to my research advisor, Prof. Timothy M. Swager. Tim is a brilliant scientist and provided ingenious ideas and directions on my research. I learn a lot from his creativity, chemical instincts, and persistent eagerness. I thank him for giving me freedom to pursue my research and his belief in me. Owing to his freedom and trust, I was able to come up with many research ideas and became an independent researcher. I appreciate his continuing support for my future career as well. It was a great honor to become his student, and working with him for 4.5 years will be unforgettable. I also would like to thank my thesis committee members, Prof. Michael F. Rubner and Prof. Alfredo Alexander-Katz, for their excellent guidance and career support. I was sometimes obsessed with trivial details, but their guidance conferred me a broader perspective on my research.

Performing research in the Swager group is remarkably seamless due to our hard-working lab managers. Brian Pretti and Dr. Joseph Walish make my life substantially easier, and I especially thank Kathy Sweeney for her assistance on administrative works.

I want to convey my profound thanks to my many co-workers and collaborators. The first person I thank should undoubtedly be Dr. Ellen Sletten who was my mentor when I joined the group. She is an amazing, creative, and innovative scientist. As a materials science major, I did not have any background in chemical synthesis. I learned the ABCs of chemistry from her, including basic skills such as running TLCs and flash columns. She was very patient and supportive, and answered my endless questions. She was a nice collaborator as well, and with her help and insight, I was able to publish my very first, first-author paper with her as a co-author. I will never forget her support. I am also especially grateful to Dr. Yanchuan Zhao for his excellent guidance. Yanchuan is an intelligent chemist, and after Ellen left, he helped me solve countless synthetic problems. Many of my syntheses could have never been achieved without his advice.

There are of course more people who I want to show my deep gratitude. Dr. Julia Kalow was my GPC steward mate and I appreciate her instruction on GPC, synthesis, and my career development. Particularly for my postdoc search, I genuinely thank Dr. Myles Herbert, Dr. Julia Kalow, and Dr. Graham Sazama for their advice. They helped me how to initiate my postdoc application. Therefore, I was able to find my future advisor about one year before my graduation. Myles revised many of my writings. I appreciate Lionel's help, particularly for his support on PPSM (Program in Polymers and Soft Matter) qualifying exams at MIT. He and other PPSM senior students grilled me so I was able to pass the written and oral exams. My last project in Chapter 4 about emulsion fabrication was assisted by Qifan who is an expert in colloids. She improved my understanding on emulsions, and I appreciate her help. I thank Wendy Salmon (Whitehead Institute) for her confocal images in Chapter 4. I thank Jon W. and Balta for their chemistry instructions, Greg for photophysics guidance, Cagatay and Pan for helping me solve GPC issues, Wen and Markrete for great research discussion and enjoyable chats. I appreciate others for their support on my science and becoming nice colleagues in the basement: Jens R., Jens E., Duncan, Joe. A., Kelvin, Silvia, Derik, Intak, Liz, Sarah, Tran, Yifan, Suchol, Elisabeth, Bora, Grace, John F., Georgios, Henry, Vera, Maggie, Sibo, Constantin, Sophie, Kathleen, Kazu, Tomo, Hiro, Lukas, Kosuke, Soichi, Mason, and Yoshi. Most of them are in the Synthesis Subgroup. The weekly subgroup meetings were one of the core part for my scientific growth. I also served as the captain of the subgroup which was a great opportunity to learn how to manage people and schedules. I

appreciate the previous captain's guidance from Jon W. and Sophie, along with Kathleen who was willing to take over my duty.

I appreciate the Korean community at MIT and the Korean Catholic church. I sometimes miss my country and feel homesick, and owing to their warmhearted support, I was able to push myself through difficulties. I thank my roommate, Reginald, for making our graduate residence apartment comfortable, quiet, and clean. He was my first roommate ever, and I am not convinced that I could meet such a great roommate in the future. We have fruitful conversation in our monthly dinner. Also, most importantly, the Samsung scholarship as my financial supporter should be thanked. Without them, I could not have come to the U.S. for my graduate school.

I also want to thank myself for getting through the Ph.D. course. I hate praising myself because I do not deserve it, but it seems the time and space to do so. Doing research is fun but frequently I need to struggle with failures. I felt lots of stress. However, my Ph.D. is finally approaching because I overcame those obstacles. I think this Ph.D. is awarded because of not only my growth in science, but also my broadened perspective on life itself, as the name stands for, Doctor of Philosophy.

I would like to finish the Acknowledgements with my heartfelt gratitude to the most significant people, my family. I am greatly indebted to my family for their unconditional love and persistent support. I thank Hyunjoo Koo, my older sister, for her support for me and her care to my parents. Because I live too far from my country, I cannot take care of my parents well. However, because of her dedication, I have been able to concentrate on my studies. My genuine gratitude now goes to my father, Kyungsool Koo, and mother, Chaesoon Kim. My hardworking nature is inherited from my parents who work for a long time everyday without taking weekends off. They work harder than me so I feel ashamed that I am still lazier than my parents. They are my role models. The reason why I live a life and study is for my parents and sister. I dedicate this thesis to my loving family from the bottom of my heart.